THE SYNTHESIS AND PROPERTIES OF THREE NEW NETWORK POLYMERS

THE SYNTHESIS AND PROPERTIES OF THREE NEW NETWORK POLYMERS STUDIED BY CALORIMETRIC, DIELECTRIC AND MECHANICAL RELAXATION METHODS

By

DWAYNE ANDREW WASYLYSHYN, B.ENG.

A Thesis

Submitted to the School of Graduate Studies

in Partial Fulfilment of the Requirements

for the Degree

Master of Engineering

McMaster University

MASTER OF ENGINEERING (1995) McMASTER UNIVERSITY
(Materials Science and Engineering) Hamilton, Ontario

TITLE: The Synthesis and Properties of Three New Network Polymers Studied by Calorimetric, Dielectric and Mechanical Relaxation Methods

AUTHOR: Dwayne Andrew Wasylyshyn, B.Eng. (McMaster University)

SUPERVISOR: Professor G.P. Johari

NUMBER OF PAGES: xxiv, 217

Abstract

This thesis is based on the studies of cross-linked network polymerization by measurements of dielectric permittivity and a study of the polymers formed by dynamic mechanical analysis. The network polymers are formed by reacting a trifunctional epoxy with three primary amines, namely, aniline, 3-chloroaniline and 4-chloroaniline. The manner in which the dielectric permittivity changes on polymerization was followed from the monomeric to the ultimately polymeric state, and the relaxation time and the distribution of reaction times was followed with reaction time. Isothermal measurements of the heat evolved during the reaction led to a determination of the number of covalent bonds formed at any instant of reaction time, thus the dielectric relaxation time was related to the number of covalent bonds formed during polymerization. The relaxation time increased progressively more rapidly with the increase in the number of covalent bonds formed under isothermal conditions as the reaction progressed towards completion. As the number of covalent bonds increased, a high-frequency, or low-temperature, relaxation process emerged. This was observed for both the time-variant (fixed frequency) and time-invariant (dielectric spectra) dielectric data.

The extent of reaction at the gelation time deduced from the irreversible decrease in the dc conductivity on polymerization was 50% lower than anticipated from Flory-Stockmayer theory, but, the extent of reaction at the point of singularity agreed with the theory. As polymerization reactions occurred, both the static and high-frequency dielectric permittivities decreased with time. Data simulated for the dielectric behaviour for a fixed frequency during the course of polymerization were analyzed to confirm that the two analysis procedures (time-invariant and time-variant) yield the same parameters within 2-3%.

The three, new, network polymers thus produced had unrelaxed and relaxed moduli that were in the ranges of 1.35-1.51GPa and 6.6-10.6MPa, respectively. G_U of the three polymers decreased with increasing temperature and G_R increased. The former effect has been attributed to mainly a decrease in the G_R of the low-temperature, or high-frequency, β-relaxation process, and the latter to the increase in the temperature, and consequently, the increase in the entropy, as discussed in the entropy theories of the rubber modulus. The spectrum of the shear modulus cannot be superposed by shifting the spectra along the frequency scale alone. The three reasons discussed are; (1) G_U and G_R change with temperature, therefore the spectra differ in magnitude for each measurement temperature, (2) the presence of a temperature-dependent, frequency-independent background loss changes the magnitude of tanϕ with the temperature, and (3) the influence of secondary-, β-, or Johari-Goldstein relaxations causes deviations in the shape of the spectrum such that they cannot be superposed. It was determined that none of the three effects described contribute significantly to the changes in the isothermal spectra, and hence, the principle of the time-temperature superposition does not apply to the three polymers in this study. The three polymers produced have a mechanical loss peak at room temperature that is attributed to the β-relaxation process and whose magnitude is greater than that of polycarbonates. This suggests that the three new polymers produced here can absorb more energy at room temperature than the polycarbonates.

ACKNOWLEDGEMENTS

Firstly, I would like to thank Dr. G.P. Johari for the guidance and patience that allowed me to complete this work, which could not have been accomplished without his comments, suggestions and support. Under his supervision, I learned to critically examine and question concepts in a manner which I hope to retain for all my future undertakings.

I would also like to thank past and present colleagues; W. Pascheto, M.G. Parthun, Dr. T. Xiao and Dr. G. Sartor. These individuals taught me to use the various instruments effectively, and also provided me with many discussions on the results and related concepts.

I want to thank my family and friends, who supported and encouraged me during my work. Lastly, I would like to thank the Orefices for lending me their new printer, which enabled me to complete this work.

TABLE OF CONTENTS

LIST OF FIGURES

LIST OF TABLES

LIST OF SYMBOLS

$\alpha(t)$	the extent of conversion for a reacting mixture
β	the stretched exponential parameter for time-invariant states
γ	the stretched exponential parameter for time-variant states
ε^*	the complex dynamic dielectric permittivity
ε''	the dielectric loss (the imaginary component of ε^*)
ε'	the permittivity (the real component of ε^*)
$\varepsilon'(t\rightarrow 0)$	the limiting permittivity at reaction times approaching 0 seconds
$\varepsilon'(t\rightarrow \infty)$	the limiting permittivity at long reaction times
ε_s	the limiting low frequency permittivity
ε_∞	the limiting high frequency permittivity
τ	the relaxation time of a time-dependent property
υ	the measurement frequency (Hz)
$\phi(t)$	the relaxation distribution function of a time-dependent property
ω	the angular frequency ($2\pi\upsilon$)
G^*	the complex dynamic shear modulus
G''	the loss modulus (the imaginary component of G^*)
G'	the shear storage modulus (the real component of G^*)
G_R	the relaxed storage modulus (high temperature or low frequency)
G_U	the unrelaxed storage modulus (low temperature or high frequency)

$N(t)$	the number of covalent bonds formed at reaction time t
q	the heating rate (K/min)
T	the measurement temperature (K)
T_g	the glass transition temperature (K)

CHAPTER I

INTRODUCTION AND BACKGROUND INFORMATION

1.1 Introduction

Thermosetting polymers are commonly used as structural materials, coatings of various types, tooling in the automobile and aerospace industries, concrete bonding and repair, microelectronics encapsulations and a variety of composites. In most such technologies, the solid polymer is formed as a result of additive chemical reactions between two dissimilar liquid substances, and it acts as an adhesive to either one surface, for example as coatings on substrates, or several surfaces as with laminated materials or composites. In a variety of other applications, the polymer ultimately formed is used in a shape obtained by a suitable moulding procedure.

The term 'epoxy resin' is used to describe a specific component that is used in the making of most thermosetting polymers. It contains at least two reactive epoxy groups, R-CH-CH_2, hence the name. In the polymerized products, all of the reactive groups may have reacted, so that although they no longer contain epoxy groups, the polymerized product is still called an epoxy resin. Ellis (1993) has provided a figure for the sale of epoxy resins as 195 million tonnes in the year 1991, which was used for the production of the thermosetting polymers. Several monographs and collected works (McCrum, Read

and Williams 1970, Neilsen 1974, May 1988, Ellis 1993) have summarized the technical importance of epoxy thermosets.

Scientific studies of the properties of thermosetting epoxy polymers and of their long term durability have gained importance during the last decade. All such studies have focussed on the nature and the physical properties of the polymer formed after a certain time, temperature, processing procedure, and, in some cases, have lead to the development of phase diagrams (Enns and Gillham 1983) in which an irreversible transformation occurs from an initially liquid state to a gelled, rubber-like, or vitreous state.

The liquid epoxy resin is converted to a hard, insoluble and infusible state by forming a molecular network structure using another component called the cross-linking agent. These cross-linkers, hardeners or curing agents, as they are widely known, react with the epoxy groups of the resin molecules by exchanging a proton for a covalent bond. Most such curing agents therefore contain amine or hydroxyl groups that are capable of donating protons. The larger the number of epoxy groups per molecule in a resin or the larger the number of protons available in the molecule of the cross-linking agent, the more compact is the network structure formed, i.e. the chemical functionality, or, functionality, of the epoxy and cross-linking molecules determines the properties of the ultimately formed polymer. Thus the overall properties of a thermosetting epoxy polymer are determined by the chemical nature of the components used, and, for the same components, by the time-temperature profile for processing.

Recent studies by Johari and Pascheto (1995) and Parthun and Johari (1995a,

1995b) have shown that thermosetting polymers are not as a rule infusible cross-linked structures. They have experimentally demonstrated that when difunctional epoxies are reacted with monoamines, i.e. those molecules that contain only one amine group ($-NH_2$), the reaction produces a linear chain structure rather than a cross-linked structure. This linear chain structure, like all thermoplastics, can be fused by raising its temperature and vitrified on cooling in a reversible manner. This means that it can be recycled like a thermoplastic, although in a strict sense it is a thermoset polymer because it is produced by a spontaneous reaction between a diepoxide and a monoamine. Their work has put into question the original definition of the thermoset polymers which was based on thermal characteristics.

The experimental work of this thesis was done for three purposes; The first was to prepare new polymers using a triepoxide resin and monoamines as a cross-linking agent in which steric hindrances to molecular motions that determine the electrical and mechanical characteristics of the ultimately formed polymer can be modified by a suitable choice of the main group to which the $-NH_2$ group is attached. Towards this end, pure aniline and two isomeric states of chloroanilines, namely 3-chloroaniline and 4-chloroaniline were used to cross-link the resin molecules containing the epoxide groups. The dynamic mechanical properties of the new polymers thus formed may then be studied. The second purpose was to study how the process of synthesis itself, which occurs spontaneously, is altered by isomeric substitution of the linking molecules, namely, the amines.

The third purpose was a scientific one for which experimental observations were needed. This purpose is discussed as follows: The irreversible growth in the size of a macromolecule during the course of an additive reaction slows the rate of the very chemical reactions by which the macromolecules grow. This concept has been developed by Johari and co-workers (Johari and Mangion 1991, Parthun and Johari 1992c, Johari 1994) in a number of recent papers and is termed as negative feedback between two processes, specifically, the molecular diffusion and the chemical reactions during the course of a macromolecule's growth. Johari and co-workers have also developed the formalisms, and tested them by experiments. They studied molecular diffusion by using Brillouin light scattering (Mangion et al. 1991), dielectric relaxation (Mangion and Johari 1990b), mechanical relaxation (Cavaillé et al. 1989), ultrasonic relaxation (Alig et al. 1992), absolute heat capacity (Cassettari, Salvetti, Tombari, Veronsi and Johari 1993) and the dynamic heat capacity (Ferrari et al. 1995) of a liquid as the liquid's viscosity increased during polymerization, or growth of a macromolecule.

The phenomenon of this negative feed back may be briefly stated as follows; during the growth of a macromolecule by step-addition reactions, the rate of the chemical reactions by which this growth occurs is ultimately controlled by the diffusion rate of the reacting species. As the size of the molecule grows, the diffusion rate decreases which then slows the rate of the step-addition reaction or the rate of growth of a macromolecule. Thus the growth itself slows the rate at which it occurs. Nevertheless, the ideal macromolecule ultimately formed when the chain ends and the cross-link ends have

remained reactive would correspond to a chemical structure with the number of covalent bonds determined from the functionality or the number of reaction sites of the two monomers. A cyclic and completely bonded network structure therefore would be the ultimate product of the addition reactions. Although possible in principle, such structures, as Johari (1994) has discussed, do not form in practice, as the rate of molecular diffusion becomes imperceptibly slow before the reaction has reached completion. The molecular diffusion rate thus becomes unobservable over a time period of several hours and, when that has occurred, the substance, which was initially a fluid, is said to have vitrified. It becomes rigid under isothermal conditions. The physical and chemical properties of the material do remain time-variant in an irreversible manner because its chemical, configurational and vibrational states all change continuously with time, albeit at a progressively slower rate.

When the step-addition reactions first produce a virtually infinite connected network within the sample's volume, the sample acts mechanically as a gel-structure. Further reactions increase the number of cross-links, thus leading ultimately to its vitrification. Earlier experimental studies have left a number of features of this gel formation and vitrification unresolved in a conclusive manner. In particular, the gelation of the material that occurred prior to vitrification was described in terms of the percolation theory (DeGennes 1979, Djabourov 1988), according to which the dc conductivity is expected to decrease towards zero at the time of gelation. An alternative equation given by Mangion and Johari (1991a,b,c) showed that even without gelation, the

conductivity may approach a singularity. This equation also described the decrease in conductivity towards zero for network formation in a number of polymers where gelation had occurred (Parthun and Johari 1992c). To examine the relative merits of the two equations, studies of polymerization of a triepoxide with monoamines were necessary so that the results obtained could be compared to the results obtained from studies of polymerization of a diepoxide with the same or other monoamines, as done by Johari (1993a), Johari and Pascheto (1995) and Parthun and Johari (1995b). In the former case, step-addition reactions produce a network structure and gelation occurs; in the latter case the reaction produces linear chains and gelation does not occur.

One more aspect of the theory and the procedure had remained unresolved in previous studies. This was whether or not the distribution of dielectric relaxation times represented by a stretched exponential relaxation function, β, is equivalent to the reaction parameter, γ (Mangion and Johari 1990b), within the approximations made. Also, it remained to be seen whether or not reliable values of the relaxation time could be obtained by single frequency measurements. To study this in detail, multifrequency measurements were needed and the dielectric spectra was to be obtained so that β and γ could be compared directly.

This thesis is divided into six chapters. This chapter has introduced general concepts of a macromolecule's growth under isothermal conditions, time dependence of the properties and technological importance of such macromolecules. It has also given an outline of the concepts involved and the purpose of this study. In the section to

follow, a brief review of the literature, general aspects of polymerization and the chemical structures of the materials used are given.

In Chapter II, theories of dielectric and mechanical relaxation and experimental details of calorimetry, dielectric spectroscopy and dynamic-mechanical spectroscopy, which are the techniques used in this study, are presented. The chapter also includes a description of the procedures for preparing the substances which ultimately and spontaneously converted into polymers.

The data obtained during the course of the synthesis of three new polymers from monomer components are given in Chapter III. Further, the data obtained from calorimetry and dielectric spectroscopy are analyzed and the results thus deduced are given. In this chapter a computer simulation and the subsequent analysis of the time variant and time-invariant states is given to show whether the analysis of data for time-variant states obtained from single frequency measurements provide essentially the same information as the dielectric spectrum of the time-invariant states.

In Chapter IV the results of the analyses are discussed, and interpreted in terms of the concepts developed earlier by Johari (1993a), and the formalism for the increase in the relaxation time with increase in the number of covalent bonds in the polymers formed during their growth is given. These observations are then contrasted, in quantitative terms, against those obtained from studies of network polymerization in which a diepoxide and diamines were used as reactants, and of linear chain polymerization in which instead monoamines were used as reactants.

The equilibrium and dynamic mechanical behaviours of the three new network polymers are described in Chapter V, where the glass transition characteristics of the polymers are also given. These properties are then discussed in terms of the distribution of relaxation times, secondary relaxations and the time-temperature superposition, and the effect of the cross-links types in the network structure.

The conclusions of the thesis are given in Chapter VI. To avoid repetition of the text, a section containing a comprehensive literature review is not given. Instead, the literature review and related references are given in the pertinent places in Chapters II through V.

Since May 1993, when this study was begun, a number of papers on the calorimetric, mechanical, electrical and ultrasonic studies of the thermosetting polymers have appeared in the literature. References to these papers are collected in a block at the end of the reference section. Two Gordon Conferences have been held on this subject and several workshop sessions were held at the Annual meetings of the Material Research Society, The American Physical Society and the American Chemical Society during the years 1993-1995, and at the 3rd International Conference on Relaxations in Complex Systems held from June 29 to July 10 in Alicante, Spain. Part of this work was presented at the 1994 Gordon Research Conference on Dielectric Phenomena by the author. It therefore seemed necessary to submit an account of this study for publication in scientific journals prior to writing this thesis. Consequently, one paper on the analysis of dielectric relaxation data has been published in the Journal Chemical Society, Faraday Transactions

90, pp2065-2070 (1994) (The work reported in this paper is excluded from this thesis). Two additional papers entitled, (1) Comparing the Time-Invariant and Time-Variant Dielectric Relaxation Data Simulated For a Macromolecules Growth, and (2) Physics of Linear-Chain and Network Polymerization by Dielectric Spectroscopy, are scheduled to appear in the special volume of the Journal of Molecular Liquids to be issued in the honour of the work of Professor B.K.P. Scaife. The last two papers, which are co-authored with my colleague M.G. Parthun, provide a comparison between the growth behaviours of linear chain and network macromolecules.

1.2 Literature Review

There is an overwhelmingly large number of studies on polymeric materials that utilize thermodynamic measurements and dielectric mechanical spectroscopy as investigative techniques. Since techniques of calorimetry, dielectric spectroscopy and mechanical spectroscopy are used for our study, a comprehensive literature review of both the use of these techniques and a discussion of the measurements on various polymers is required. A review of the pertaining literature and of the related discussion is provided in the text of this thesis where it was needed. In the following is presented a general review of the studies in the literature concerning certain aspects of dielectric and dynamic mechanical spectroscopy.

Dielectric measurements for monitoring polymerization have been used since the

1930s (Kienle and Race 1934, Aukward et al. 1958, Delmonte 1959) and continues to expand due in part to the better theoretical understanding of the dielectric phenomenon, and in part to the ease of data acquisition that is offered by most present-day computer automated dielectric measurement assemblies. As the polymerization progresses, the macromolecules grow by addition reaction, which in turn alters irreversibly the dipole moments and their diffusion times, leading to dielectric properties that irreversibly vary as the polymerization progresses. During the resulting growth of the macromolecule, different processes contribute to the overall dielectric properties observed, and separation of these contributions and subsequent analyses are possible. A variety of empirical relationships have been proposed for describing the dielectric and mechanical relaxation behaviour of a material (Wagner 1913, Whitehead and Banos 1932, Yeager, 1936, Fuoss and Kirkwood 1941, Cole and Cole 1941, Davidson and Cole 1950, Havriliak and Negami 1966, Williams and Watts 1970), and while they seem sufficient for describing the data, they don't necessarily offer useful insight to the molecular dynamics associated with the irreversible physical and chemical changes during the polymerization.

One of the most widely used empirical equations for describing the asymmetric distribution times was given by Kohlrausch (1854), Douglas (1963, 1966), Williams and Watts (1970) and Majumdar (1971). Referred to also as the KWW function, it is used to discuss the relaxation behaviour of physically and chemically stable materials. This function has also been adapted to describe the time-dependent relaxation behaviour during polymerization, or a macromolecule's growth, by Mangion and Johari (1990b), and its

parameter, termed the reaction parameter, γ, since it describes the result of chemical reactions on the distribution of diffusion times as the reactions occurs. Further work by Mangion and Johari (1991a,b,c), Johari and Mangion (1991), Parthun and Johari (1992a,c) and Johari (1993a) has described the time-dependent electrical properties during the polymerization of several epoxy polymers, and discussed the significance of the parameter γ. They also described the conductivity of the initial monomeric liquid as containing contributions from the diffusion of impurity ions, such as Na^+ and Cl^- remaining in the epoxide as a result of its processing, as well as from proton transfer along hydrogen-bonds formed between the amine molecules. They found that during polymerization, the conductivity decreases towards zero, and they pointed out that this is due to at least two effects; firstly, the increasing density and viscosity of the reacting liquid which slows the diffusion of impurity ions, and secondly, the H-bonded network, that existed prior to the reaction, is consumed in favour of covalent bonds formed between the epoxy molecules and the curing agent molecules.

Studies of the relationship between the structure and the mechanical properties of polymers are of particular importance for technological applications, and as a reflection of this, the literature contains a variety of studies of the relaxation processes of polymeric materials (McCrum, Read and Williams 1967, Charlesworth 1988a,b, and references therein). The main relaxation process, or α-relaxation, which is observed at or above the glass-transition temperature, T_g, as well as secondary relaxation processes (β-relaxation), which are usually observed below T_g, have been studied under several different conditions

in order to understand the molecular dynamics of the polymer (McCrum, Read, and Williams 1967, Charlesworth 1988a,b, Muzeau et. al 1991). In particular, it is known that the variation of the cross-link density has a profound effect on both the strength and temperatures of the α and β-relaxations as well as on the rubber modulus at temperatures above the glass transition temperature (Fox and Loshaek 1955, DiMarzio 1955, Katz and.Tobolsky 1962, Charlesworth 1988a,b, Muzeau et al. 1991). Controlled studies of the molecular structure of polymers, in which the degree of cross-linking was varied, therefore have been performed in order to associate the molecular structure to the relaxation processes observed. In such cases mathematical models to describe the behaviour observed were formulated in terms of the average network parameters and its thermodynamics, since the entropy of the entire network is an important factor in determining both T_g and the magnitude of the rubber modulus. Charlesworth (1988a) has argued that such a broad treatment of mathematical models cannot be made for the secondary relaxation processes, for which local motions of segment groups are seen to be responsible for the relaxation behaviour. He pointed out that, due to these localized motions, neighbouring groups may interact with the relaxing units and any particular method of varying the cross-link density may produce, in addition, its own characteristic change in the physical properties.

Cavaillé, Mikolajczak and Johari (1987) have studied the effects of a second inert phase material on the properties of polymers such as glass-fibre polymer composites. They observed a decrease in the mechanical modulus of the matrix of the composite as

compared to the pure polymer of the same chemical compositions. Using a statistical analysis originally given by DiMarzio (1964), they determined the decrease in cross-link density that would have to change the mechanical properties of the polymer matrix in the composite. Mikolajczak, Cavaillé, and Johari (1987) studied also the effect of the processing technique of epoxy resins on the final properties of the polymer. They dissolved and reacted the monomeric starting material in a solvent to compare the mechanical properties with that of a polymer produced without the use of the solvent. Their results showed that the polymers prepared from the solvent mixture had a lower mechanical modulus compared to the polymer prepared without it.

Mechanical spectroscopy has been used also to study the polymerization of epoxy polymers by Gillham and coworkers (see Aronhime and Gillham 1986, for a comprehensive review). Instead of the pure bulk state, they used impregnated thin-wire braids with epoxy resins, and thereafter monitored the changes that occur in the mechanical properties measured in the torsional oscillation, as the reaction approached completion. By studying the isothermal mechanical spectra and assigning stages of cure to its various features, such as gelation and vitrification, they constructed 'isothermal time-temperature-transformation' (TTT) diagrams that displayed the regions of various chemical and physical states as functions of reaction temperatures and reaction times. Choy and Plazek (1986) have studied instead the mechanical creep, and have deduced a general pattern of the physical changes that occur during the cure of an epoxy resin with diamines. Specifically, as an epoxy ring opens up to form one OH group upon reacting

and bonding with the nitrogen atom of the curing agent, the viscosity increases such that ultimately the original liquid, or sol, state is converted to the gel state of an infinitely connected macromolecule of modulus less than 1MPa. Although viscosity approaches a formally infinite value, molecular motions, including those of the reactants, still persist and the cross-link density further increases. Thus the polymer network's mechanical modulus increases irreversibly, and approaches that of a vitreous material, approximately 10 GPa.

Prolonged polymerization has two effects on a vitrified material. The first is the result of continued reactions when the reacting species diffuse at an extremely slow rate. This further increases the cross-link density, the bulk density of the polymer and the glass transition temperature, all of which slow the reaction itself. The second effect is a spontaneous densification that occurs without chemical reactions as a high-energy, kinetically metastable amorphous material tends towards a lower energy, thermodynamically metastable structure. This is known as structural relaxation and is described in depth in a monograph by Scherer (1986). Sidebottom and Johari (1991) have discussed the effects of both these effects on the dielectric relaxation of an epoxy-diamine network thermoset.

1.3 Polymerization of a Thermosetting Mixture

Thermoset polymers are obtained from the chemical reaction of two or more relatively low molecular weight monomeric materials. During the reaction, the functional

groups of one type of monomer react with the other and form covalently bonded cross-links, resulting in a two or three dimensional continuous growth of the macromolecule. This step-wise addition reaction, referred to as the curing of the polymer, occurs through two types of chemical reactions for a di-epoxy resin reacting with a di-functional amine, which acts as a cross-linking agent.

In the first reaction step illustrated in Figure 1.1, the primary amine of the $-NH_2$ functional group chemically reacts with the epoxide ring group of the epoxy molecule, breaking the ring open to form a hydroxyl-OH group, and its nitrogen atom covalently bonding with the terminal atom of the epoxy molecule. Thus the primary amine now becomes the secondary amine, with a functionality of one. The secondary amine similarly reacts with the epoxide ring of another epoxy molecule resulting in a branched tertiary amine, which now serves as a cross-link between the two epoxy molecules, as illustrated in Figure 1.1. The degree of molecular branching in the polymer depends on both the nature of the monomeric species and the temperature used for the cure, since the rates of reaction of the primary and secondary amines are not equal (Horie et al. 1970, Ryan and Dutta 1979, Dušek 1985). Thus, the cure, or polymerization, involves an additive reaction with a single product, and as a consequence, the molecular network continues to grow until the reaction has reached completion, or arrested on an experimenter's time scale as a result of increased viscosity. Ultimately, the liquid monomeric mixture becomes a densely cross-linked polymeric solid under isothermal conditions.

To facilitate the chemical reactions, the chemical species must diffuse towards one

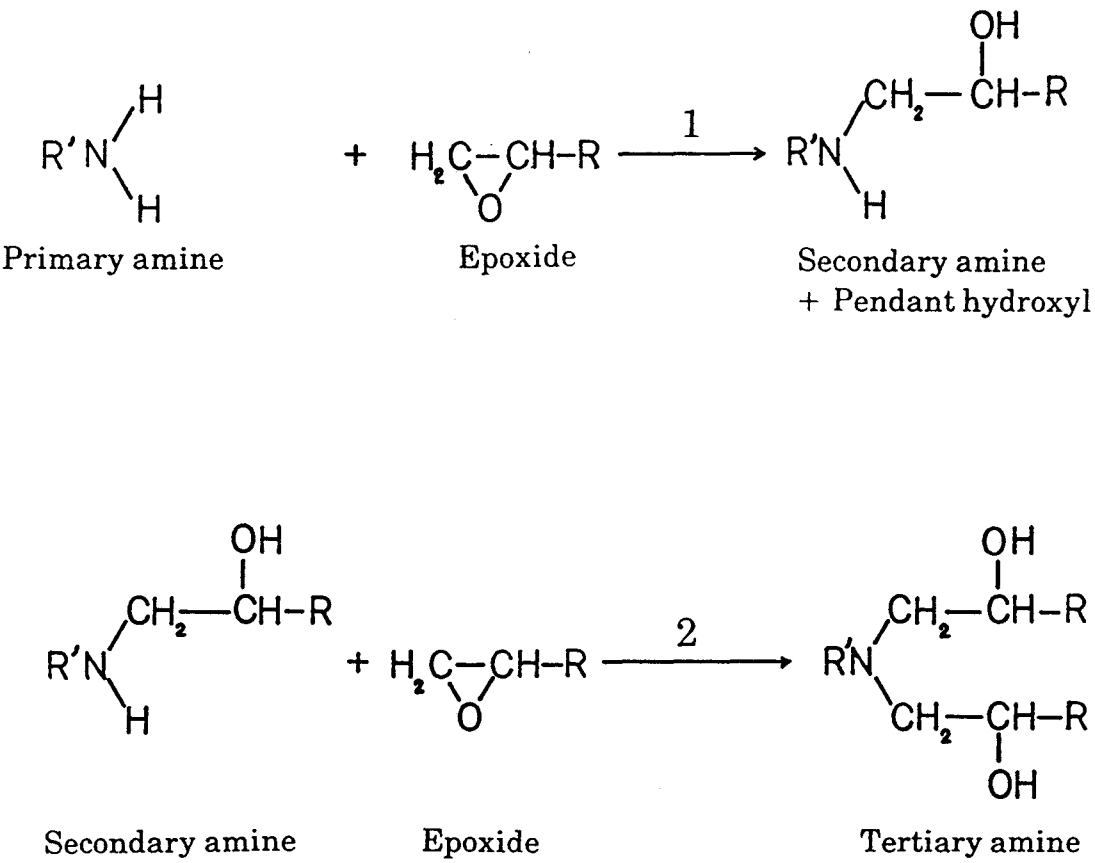

Figure 1.1: The two reaction steps that occur for the reaction between an epoxy and amine molecule.

another, therefore the reaction rate depends on the diffusion rate of the reactive groups of the species towards each other. The chemical reactions cause the viscosity of the product to increase as the molecular network grows, thereby slowing the diffusion rate of the reacting groups towards one another, which in turn slows the rate of chemical reaction. Thus the process involves a negative feedback between chemical reactions and molecular diffusion that ultimately vitrifies the liquid (Johari and Mangion 1991). As the molecular network spontaneously grows during the polymerization by the negative feedback mechanism under isothermal conditions, there is an associated decrease in the volume of the liquid as the longer Van der Waals interactions are replaced by the shorter covalent bonds. With this decrease in volume, there is an increase in the glass transition temperature, T_g, of the partially polymerized mixture. During the polymerization the T_g can increase only up to the reaction temperature, and the liquid becomes vitrified at that isothermal temperature.

At the time during the reaction when the growing molecular network extends continuously over the whole volume of the liquid, the viscous liquid is said to have formed a gel-like solid. This phenomenon is called gelation and it usually occurs before vitrification. Hence the unreacted molecules or molecular segments in the thermoset, although giving a solid-like character to the material after gelation, still have a sufficiently high local diffusivity to allow the mutual diffusion of unreacted species or groups towards each other over an experimental time scale. Gelation is found to occur at 55%-80% consumption of epoxide groups during the reaction of epoxides with curing agents in

stoichiometric amounts (Flory 1941, 1953, Stockmayer 1943). As the chemical reaction progresses in the gelled state, the microscopic viscosity and T_g of the gelled state increase. When T_g has increased to the temperature of the isothermal cure, the state of the polymer changes from that of a mechanically low modulus gel (about 10^6Pa) to a high modulus, vitreous solid (about 10^9Pa). Associated with this state is an extremely low diffusivity that slows the rate of chemical reactions until they become unobservable.

1.4 Chemical Structures

The chemical structures of the materials used for preparing the thermoset polymers in this study are shown in Figure 1.2, where the tris(hydroxyphenyl) methane-based epoxy is the epoxide resin and aniline, 3-chloroaniline and 4-chloroaniline are the three curing agents. The reaction mechanism is shown in Figure 1.1. One hydrogen atom from the primary amine dissociates and reacts with the O atom of the broken epoxide ring, and the nitrogen atom of the amine group reacts with the carbon atom of the $-CH_2$ group to form $R'-CH(OH)-CH_2-NH(RNH_2)$. This occurs until all the hydrogen atoms of the aniline have combined with the O atoms to form the OH groups, and each amine has formed two covalent bonds with two epoxide molecules or, in a less likely case, with two epoxide groups of the same epoxide molecule.

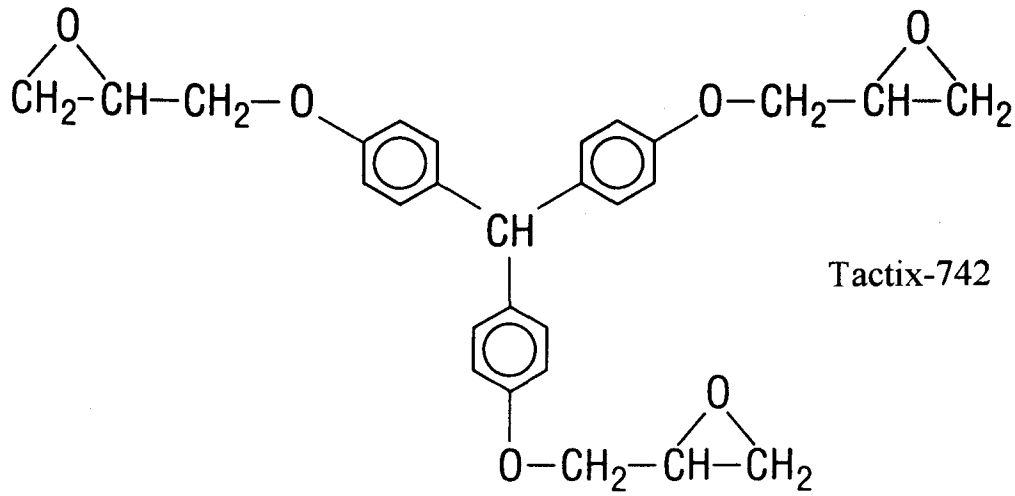

Tactix-742

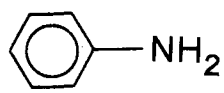

Aniline

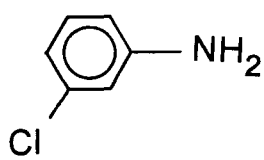

3-Chloroaniline

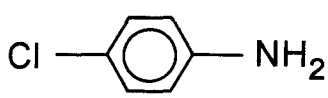

4-Chloroaniline

Figure 1.2: The chemical structures of Tactix-742, aniline, 3-chloroaniline and 4-chloroaniline as used in this study.

CHAPTER II

THEORIES OF RELAXATION AND EXPERIMENTAL METHODS

2.1 Theories of Relaxation

2.1.1 Dielectric Relaxation

Generally, dielectric measurements are made by placing a sample between two capacitor plates to which a fixed (or sinusoidal) electric field is applied. The dielectric sample, devoid of free electrons, undergoes preferential alignment of molecular and ionic dipoles within its bulk, causing instantaneous and time-dependent charge build-up on the capacitor plates. The build-up of surface charge per unit surface area is called the polarization of a dielectric material. The time-dependent electrical polarization, P(t), of the dielectric sample can therefore be expressed as,

$$P(t) = P_{\infty} + P_o\left(1 - \phi_D(t)\right) \qquad (2.1)$$

where P_∞ is the instantaneous polarization associated with the electronic transitions and atomic vibrations, and P_o is the time-dependent dipolar polarization. $\phi_D(t)$ is a relaxation function that describes the time-dependent approach of the polarization from P_∞ to $(P_\infty+P_o)$, its equilibrium value. The polarization and charge displacement, D(t), for a constant electric field, E_o, are related through the expression;

$$D(t) = \varepsilon_s E(t) + P(t) = \varepsilon(t)\varepsilon_s E(t) \qquad (2.2)$$

where ε_o is the permittivity of vacuum (8.854pF/m), $\varepsilon(t)$ is the time-dependent permittivity of the dielectric sample under the boundary conditions $\varepsilon(t\rightarrow 0) = \varepsilon_\infty$ (or $\omega\rightarrow\infty$) and $\varepsilon(t\rightarrow\infty) = \varepsilon_s$ (or $\omega\rightarrow 0$). ε_∞ and ε_s are the limiting high frequency and static (low frequency) permittivities respectively. In a similar manner to Equation (2.2), $\varepsilon(t)$ can be related to $\phi_D(t)$ through the equation,

$$\varepsilon(t) = \varepsilon_\infty + (\varepsilon_s - \varepsilon_\infty)(1 - \phi_D(t)) \qquad (2.3)$$

When the electric field is not constant, but applied by incremental amounts, the Boltzmann superposition principle (Hopkinson 1877, Curie 1888) is applied. The charge displacement, D(t), at any time, t, due to an applied electric field, E(t), history becomes the sum of displacements, dD(t), arising from the incremental field, dE(t), applied at previous times, μ, when $\mu \leq t$. This is expressed as,

$$\frac{D(t)}{\varepsilon_o} = \int_{-\infty}^{t} \frac{\partial E(\mu)}{\partial \mu}\varepsilon(t-\mu)d\mu \qquad (2.4)$$

where ε_o is the permittivity of free space (=8.854pF/m). By substituting $a = t - \mu$ and integrating Equation (2.4) by parts, one obtains,

$$\frac{D(t)}{\varepsilon_o} = \varepsilon_\infty E(t) + \int_0^\infty E(t-a)\frac{\partial \varepsilon(a)}{\partial a}da \qquad (2.5)$$

Substituting Equation (2.3) into Equation (2.5) gives,

$$\frac{D(t)}{\varepsilon_o} = \varepsilon_\infty E(t) + (\varepsilon_s - \varepsilon_\infty)\int_0^\infty E(t-a)\left(-\frac{\partial \phi_D(a)}{\partial a}\right)da \qquad (2.6)$$

The relationship between a sinusoidal electric field, $E^*(t)=E_0\exp(i\omega t)$, and the resulting charge displacement, $D^*(t)=D_0\exp(i(\omega t-\delta))$, where ω is the angular frequency ($=2\pi\nu$), t is the time of the measurement, E_0 is the electric field amplitude, D_0 is the charge displacement amplitude, δ is the dielectric loss angle and $i = (-1)^{1/2}$, is expressed as;

$$D^*(t) = \varepsilon^* \varepsilon_o E^*(t) \qquad (2.7)$$

ε^* in Equation (2.7) is the complex dielectric permittivity. $E^*(t)$ and $D^*(t)$ are denoted by E^* and D^* from here on. Combining Equation (2.7) with $E^*=E_0\exp(i\omega t)$ and $D^*=D_0\exp(i(\omega t-\delta))$ leads to the equations;

$$\varepsilon^* = \frac{D^*}{E^*\varepsilon_o} = \frac{D_o}{E_o\varepsilon_o}(\cos\delta - i\sin\delta) = \varepsilon' - i\varepsilon'' \qquad (2.8)$$

$$\varepsilon' = |\varepsilon|\cos\delta \qquad (2.9)$$

$$\varepsilon'' = |\varepsilon|\sin\delta \qquad (2.10)$$

$$\tan\delta = \varepsilon''/\varepsilon' \qquad (2.11)$$

Here, ε', ε'', and $\tan\delta$ are referred to as the dielectric permittivity, dielectric loss and loss factor, respectively, and $|\varepsilon| = D_o/E_o\varepsilon_o$.

By treating the superposition principle in the dynamic manner, one obtains,

$$\frac{D^*}{\varepsilon_o} = \varepsilon_\infty E^* + (\varepsilon_s - \varepsilon_\infty)\int_0^\infty E_o \exp(i\omega(t-a))\frac{-\partial\phi_D(a)}{\partial a}da \qquad (2.12)$$

Equation (2.12) is further simplified, and a is replaced by t, to express ε^* in the equation,

$$\varepsilon^* = \varepsilon_\infty + (\varepsilon_s - \varepsilon_\infty)\int_0^\infty \exp(-i\omega t)\left(-\frac{\partial\phi_D(t)}{\partial t}\right)dt \qquad (2.13)$$

The integral term on the right hand side of Equation (2.13) is recognized as a LaPlace transform, therefore this equation can be expressed as,

$$N_\varepsilon^* = \frac{(\varepsilon^* - \varepsilon_\infty)}{(\varepsilon_s - \varepsilon_\infty)} = \mathcal{L}\left(-\frac{\partial\phi_D(t)}{\partial t}\right) \qquad (2.14)$$

where $\mathcal{L}(y)$ is the one-sided LaPlace transform of y, and N_ε^* is the normalized complex dielectric permittivity.

2.1.2 Mechanical Relaxation

When a shearing force is applied over an area of a material, a shear strain results. A mechanical creep experiment allows one to measure the time-dependent strain of a material subjected to a constant shear stress. In a matter analogous to the dielectric case

discussed earlier, the time-dependent shear strain, $\gamma(t)$, is related to the constant shear stress, σ_o, by the equation,

$$\gamma(t) = J(t)\sigma_o \tag{2.15}$$

J(t) is the time-dependent shear compliance of the material at the boundary conditions $J(t\rightarrow 0) = J_U$ (or $\omega\rightarrow\infty$) and $J(t\rightarrow\infty) = J_R$ (or $\omega\rightarrow 0$). J_U and J_R are the unrelaxed and relaxed shear compliance, respectively. J_U and J_R could be expressed in a similar way as with dielectric relaxation theory, i.e. J_∞ and J_s, but it is the convention to use the relaxed and unrelaxed moduli, therefore we use it here. J(t) can be expressed in terms of a (mechanical) relaxation function analogous to Equation (2.3), shown as,

$$J(t) = J_U + (J_R - J_U)(1 - \phi_M(t)) \tag{2.16}$$

Similarly, for a constant shear strain, γ_o, and the time-dependent shear stress, $\sigma(t)$ are related by the equation,

$$\sigma(t) = G(t)\gamma_o \tag{2.17}$$

G(t) is the time-dependent shear modulus of the material at similar boundary conditions as for J(t) and with a similar relation as Equation (2.16).

For incrementally applied stresses, the Boltzmann superposition principle is again used to express the total strain response in terms of a sum of an incrementally applied stress, $d\sigma$, at previous times μ, when $\mu \leq t$. This is shown as,

$$\gamma(t) = \int_{-\infty}^{t} \frac{\partial \sigma(\mu)}{\partial \mu} J(t-\mu) d\mu \qquad (2.18)$$

Integrating Equation (2.18) by parts with the substitution, a = t - μ, one obtains,

$$\gamma(t) = J_U \sigma(t) + \int_0^{\infty} \sigma(t-a) \frac{\partial J(a)}{\partial a} da \qquad (2.19)$$

Substituting Equation (2.16) into Equation (2.19) leads to,

$$\gamma(t) = J_U \sigma(t) + (J_R - J_U) \int_0^{\infty} \sigma(t-a) \left(-\frac{\partial \phi_M(a)}{\partial a} \right) da \qquad (2.20)$$

Mechanical relaxation experiments can also be performed using a sinusoidally applied stress of the form, $\sigma^*(t)=\sigma_o \exp(i\omega t)$, where σ_o is the stress amplitude. The strain response is $\gamma^*(t)=\gamma_o \exp(i\omega(t-\phi))$, where γ_o is the strain amplitude and ϕ is the mechanical loss angle, not to be confused with $\phi_M(t)$, the mechanical relaxation function. The other quantities are described in the previous section. Hereafter, $\sigma^*(t)$ and $\gamma^*(t)$ will be denoted by σ^* and γ^*, respectively. Substituting these expressions into Equation (2.15) leads to the equations;

$$J^* = \frac{\gamma^*}{\sigma^*} = \frac{\gamma_o}{\sigma_o}(\cos\phi - i\sin\phi) = J' - iJ'' \qquad (2.21)$$

$$|J| = \gamma_o / \sigma_o \qquad (2.22)$$

$$J' = |J|\cos\phi \tag{2.23}$$

$$J'' = |J|\sin\phi \tag{2.24}$$

and,

$$\tan\phi = J''/J' \tag{2.25}$$

J' and J", are referred to as the storage and loss compliancies, respectively. The other quantities are described in the previous section.

Because $J^*=1/G^*$, similar relationships for the storage and loss moduli, G' and G", respectively, can be made. In a similar treatment to that of J^*, G^* is related to G' and G" by the equation,

$$G^* = \frac{\sigma^*}{\gamma^*} = \frac{\sigma_o}{\gamma_o}(\cos\phi + i\sin\phi) = G' + iG'' \tag{2.26}$$

Equations (2.16) and (2.21), along with the Boltzmann superposition and the expressions, $\sigma^*(t)=\sigma_o\exp(i\omega t)$ and $\gamma^*(t)=\gamma_o\exp(i\omega(t-\phi))$, allows γ^* to be described by,

$$\gamma^* = J_U\sigma^* + (J_R - J_U)\int_0^\infty \sigma_o \exp(i\omega(t-a))\left(-\frac{\partial\phi_M(a)}{\mu}\right)da \tag{2.27}$$

The substitution, a = t - μ, has been made here as in the dielectric treatment of the previous section. Expanding Equation (2.27) leads to the equation,

$$J^* = J_U + (J_R - J_U)\int_0^\infty \exp(-i\omega t)\left(-\frac{\partial \phi_M(t)}{dt}\right)dt \qquad (2.28)$$

Recognizing the LaPlace transform on the right hand side of Equation (2.28), one simplifies,

$$N_J^* = \frac{(J^* - J_U)}{(J_R - J_U)} = \mathcal{L}\left(-\frac{\partial \phi_M(t)}{\partial t}\right) \qquad (2.29)$$

Here, N_J^* represents the complex mechanical compliance. For the shear modulus, G^*, N_G^* is expressed in a similar form with G^*, G_R and G_U substituted for J^*, J_U and J_R, respectively, in Equation (2.29).

2.1.3 Relaxation Spectra

The Single Relaxation Time

To describe the rate at which a property such as polarization reaches its equilibrium value, one must define a relaxation function $\phi(t)$. In the rare case where the rate is proportional to the property's displacement from its equilibrium value at a constant characteristic relaxation time, τ_o, the relaxation function is exponential decay (Debye 1929, Fröhlich 1949), given by,

$$\phi(t) = \exp\left(-\frac{t}{\tau_o}\right) \tag{2.30}$$

Such behaviour is only observed for dilute solutions of polar molecules in non-polar solvents and for substances at high temperatures. Substitution of Equation (2.30) into either Equation (2.14) or (2.29) leads to,

$$N^* = \frac{1}{1 + i\omega\tau_o} \tag{2.31}$$

Expressions for the normalized storage, N', and loss, N", components are given by;

$$N' = \frac{1}{1 + \omega^2\tau_o^2} \tag{2.32}$$

and

$$N'' = \frac{\omega\tau_o}{1 + \omega^2\tau_o^2} \tag{2.33}$$

where τ_o is the single relaxation time and represents the time required for the total dipolar polarization of a dielectric, or the modulus of a solid, to decrease by a factor of e after the removal of the electric field, or the stress field. This corresponding frequency behaviour is known as the Debye behaviour and is not observed in amorphous solids or highly viscous liquids (Davidson and Cole 1951, Davidson 1961, Johari 1975).

Distribution of Relaxation Times

The relaxation behaviour observed for all amorphous materials is often considered as a superposition of exponential relaxation functions of the form (Fröhlich 1949),

$$\phi(t) = \int_0^\infty \exp\left(\frac{-t}{\tau}\right) g(\tau) d\tau \qquad (2.34)$$

where,

$$\int_0^\infty g(\tau) d\tau = 1 \qquad (2.35)$$

Here, g(t) is the relaxation time distribution function.

Much work has been done on empirical representations of g(t) (Wagner 1913, Whitehead and Banos 1932, Yeager 1936, Fuoss and Kirkwood 1941, Cole and Cole 1941, Davidson and Cole 1950, 1951, Hamon 1952, Havriliak and Negami 1966, Williams and Watts 1970) that best describe the ε' and ε'' data of dielectric materials. The most widely used empirical expression, first used by Kohlrausch (1847) for time-domain creep measurements, then by Douglas (1963, 1966) for stress relaxation measurements, and later adapted by Williams and Watts (1970) for dielectric studies, is expressed as,

$$\phi(t) = \exp\left(-\left(\frac{t}{\tau_o}\right)^{\beta}\right) \qquad (2.36)$$

This is known as the stretched exponential function, where β, sometimes referred to as the KWW parameter, describes the non-exponentiality of the decay for values $0 < \beta < 1$. The stretched exponential becomes the exponential decay function (Debye behaviour) for $\beta = 1$.

The differences between the Debye and stretched exponential behaviours are best illustrated by the complex plane plots of ε'' versus ε', which are known as Cole-Cole plots (Cole and Cole 1941) and are shown in Figure 2.1. The curves in the figure represent β=1 (Debye) and β=0.5 (stretched exponential). The Debye behaviour shown in Figure 2.1 is represented as a semi-circle in the complex plane plot with radius $(\varepsilon_s-\varepsilon_\infty)/2$ and centre at $(\varepsilon_s-\varepsilon_\infty)/2$ on the ε' axis. Since it is a semi-circle, the plots are symmetrical about $\omega\tau_o = 1$, therefore τ_o is the average relaxation time. Most materials however, display a behaviour where the low frequency side of the complex-plane plots remains semi-circular but the high frequency side is drawn out. This is shown in Figure 2.1 for β=0.5. This 'skewed arc' is typical of most dynamic dielectric and mechanical studies. The characteristic relaxation time, τ_o, for the stretched exponential is related to the average relaxation time, $\langle\tau\rangle$, by (Moynihan, Boesch and Laberge 1973),

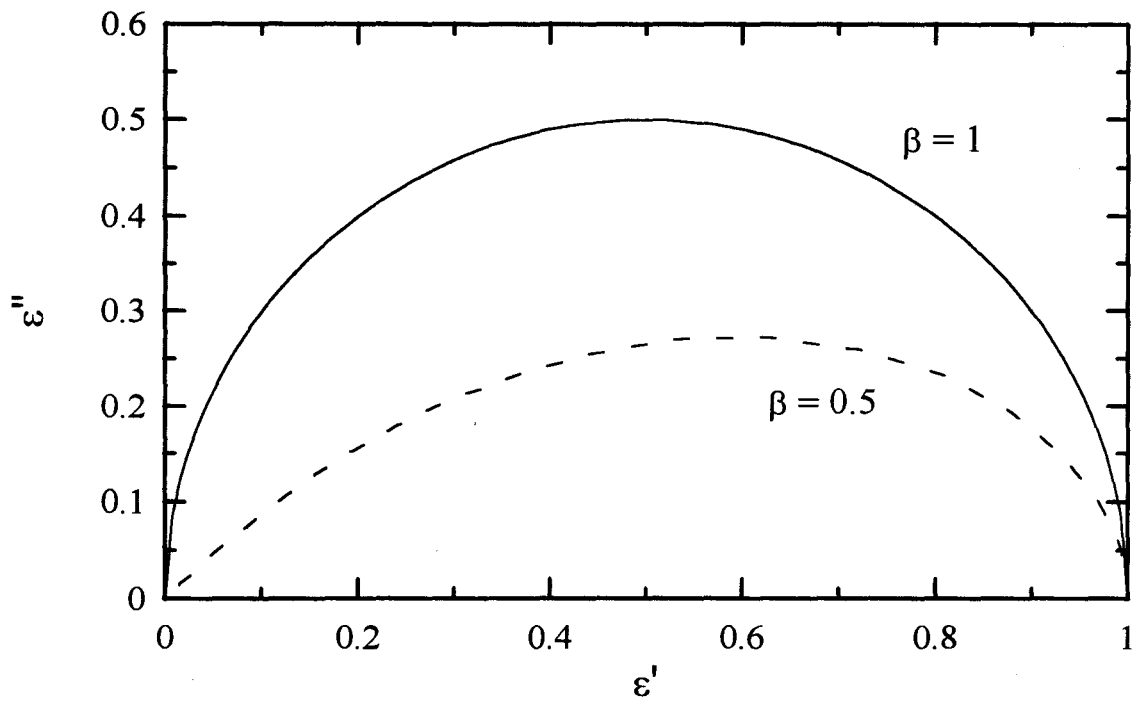

Figure 2.1: A complex-plane plot of ε'' against ε'. The continuous line corresponds to Debye behaviour (β = 1) and the dashed line to the stretched exponential function with β = 0.5.

$$<\tau> = \frac{\tau_o}{\beta}\Gamma\left(\frac{1}{\beta}\right) \tag{2.37}$$

where $\Gamma(y)$ represents the gamma function of y.

The substitution of Equation (2.36) into Equations (2.14) or (2.29) and performing the LaPlace transform, leads to the result (with $z = \omega\tau_o$),

$$N' = \pi z V_\beta(z) - 1 \tag{2.38}$$

and

$$N'' = \pi z Q_\beta(z) \tag{2.39}$$

N' and N" are the real and imaginary components of the normalized complex permittivity (or shear compliance). V_β and Q_β are integrals defined by,

$$V_\beta = \frac{1}{\pi}\int_0^\infty \exp(-u^\beta)\sin(zu)du \tag{2.40}$$

$$Q_\beta = \frac{1}{\pi}\int_0^\infty \exp(-u^\beta)\cos(zu)du \tag{2.41}$$

The evaluation of Equations (2.40) and (2.41) has been done (Moynihan et al. 1973, Lindsey and Patterson 1980, Dishon et al. 1985, Muzeau, Perez and Johari 1991) for $0.1 < \beta < 0.7$ and for $10^{-3} < \omega\tau_o < 10^4$. The values of V_β and Q_β for different values of β

and $\omega\tau_o$ have been organized into tables from which the normalized quantities, N' and N", have been obtained.

2.2 Experimental Procedures

2.2.1 Differential Scanning Calorimetry

Equipment and Measurement Procedure

A Perkin Elmer DSC-4 Differential Scanning Calorimeter (DSC) was used for calorimetric measurements in this study. During normal operation, a sample and reference are maintained at an identical, predetermined temperature, even during a phase transformation or chemical reaction. The measurable quantity, dH/dt, is the amount of power that must be supplied to the sample or the reference to maintain a zero temperature difference as thermodynamic changes occur in the sample.

The sample and reference were contained in identical metal pans within separate compartments consisting of respective heaters and thermometers, as shown in Figure 2.2. During the measurement, the temperature difference between the sample and reference is kept at zero by supplying power to either of the two cells. The mass of the sample and pans was 10-30mg, which is too small to disturb the response of the platinum resistance thermometers embedded in the base of the cells.

dH/dt is proportional to the specific heat, C_p, of the sample, since it is C_p that represents the amount of thermal energy required to change the sample's temperature by one degree. Therefore, any thermal event accompanied by a change in the sample's C_p

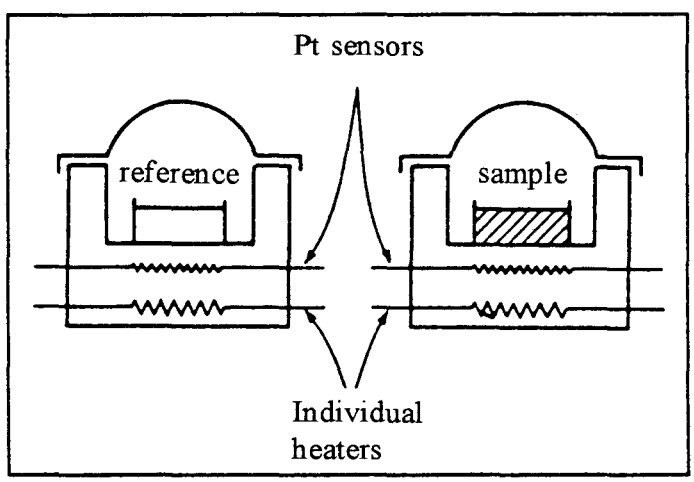

Figure 2.2: A schematic diagram of the DSC assembly.

manifests itself as a power signal to the DSC. Enthalpy changes in the sample can give rise to peaks whose areas are proportional to the total enthalpy change of the transformation. In this mode of operation, the power is measured as a function of temperature for a preprogrammed linear heating (or cooling) rate.

The DSC is also suitable for the measurement of dH/dt as a function of time under isothermal conditions. The operation is similar to that described above, except that the power difference is measured with time at a fixed temperature. The DSC was used for both the temperature and time dependent modes in this study.

The sample pans used to contain the sample and reference were shallow, aluminum pans with a diameter of approximately 5mm, a height of 2mm, a thickness of 0.1mm and a nominal mass of 21mg. The sample and reference pans were placed in separate compartments mounted on identical, isolated bases with separate heaters and thermometers. An empty aluminum pan was placed in the reference compartment to balance the thermal mass with that of the sample compartment. A typical sample mass was 25-30mg with dimensions slightly smaller than that of the aluminum pan. If required, an aluminum lid was sealed onto the sample pan by crimping. This was done when evolution of volatiles or the spilling of the liquids was a concern. The reference pan in such a case was also sealed with a lid to maintain a similar thermal mass. Both open and sealed sample pans were used in this study. The sample and reference pans were closed into their respective compartments by an assembly that allowed a continuous flow of dry nitrogen gas at approximately 25psi to flow through the cells. This was to

maintain an inert environment. By using small sample masses, the thermal lag between the sample and its heater was minimized.

Interfaced with the DSC assembly was a Thermal Analysis Data Station (TADS) computer which allowed one to automate the data acquisition and measurement variables. All data was stored on computer diskettes and analyzed by software supplied by Perkin Elmer. In the early part of the study, a standard IBM personal computer was interfaced to the DSC assembly in place of the Perkin Elmer model computer to increase the flexibility of the data gathering and analysis. The control program was supplied by Dr. Günter Sartor who wrote it in Turbo Pascal. This improved the speed and convenience of the data acquisition. As well, it provided the data in a final format compatible with most standard present day analytical software, unlike the Perkin Elmer software.

The DSC equipment was calibrated periodically using Indium as a sample, such that the measured latent heat and melting temperature deviated by less than 4.0% and 0.05% of literature values. During the DSC measurements over a wide temperature range, the power difference may not remain zero even with empty sample and reference cells. This reproducible deviation was due to the power requirements of the electronics and the thermal properties of the physical construction of the cells and heaters. By measuring this background signal (with empty sample and reference pans) beforehand, the data obtained for the samples could be corrected by subtracting the two measurements later on. All measurements made over a temperature range were corrected in this manner.

In the temperature scanning mode, a linear heating rate of 10K/min was used for

all calorimetry, covering temperature ranges of 228K to 273K and 323K to 563K. dH/dt measurements as a function of reaction time and of temperature were made with a full scale range of 10mcal/s with a reported accuracy of 5%. For isothermal studies, the samples were stabilized at 30K below the desired measurement temperature before heating it at a rate of 50K/min to the predetermined temperature. Since a typical time span for an isothermal experiment in this study was 60000s, any errors due to the time taken to increase the temperature from the initial to the ultimate temperature was insignificant.

2.2.2 Dielectric Spectroscopy

For a parallel plate capacitor, with plate area, A, and separation, l, the capacitance in vacuum is given by,

$$C_o = \frac{A\varepsilon_o}{l} \tag{2.42}$$

where ε_0 = 8.854 pF/m. If a dielectric material is placed between the two plates in full contact with them, the new capacitance is $C = \varepsilon C_0$, where ε is the dielectric permittivity of the material. When a sinusoidal voltage of the form,

$$V^* = V_o \exp(i\omega t) \tag{2.43}$$

is applied across these parallel plates, the capacitance becomes complex such that $C^* = \varepsilon^* C_0$. The resulting current is also a complex quantity and is expressed as,

$$I^* = A\left(\frac{dD^*}{dt}\right) \tag{2.44}$$

Equation (2.44) can be rewritten as,

$$I^* = A\left(\frac{d(C^*V^*)}{dt}\right) \tag{2.45}$$

It can be shown that the expansion of Equation (2.45) leads to the relation,

$$I^* = \omega C_o V^*(\varepsilon'' + i\varepsilon') \tag{2.46}$$

The resulting complex admittance, Y^* ($=I^*/V^*$), can be expressed as

$$Y^* = \omega C_o(\varepsilon'' + i\varepsilon') \tag{2.47}$$

A dielectric material can be represented as a resistance, R_{par}, in parallel with a capacitance, C_{par} whose admittance,

$$Y^* = 1/R_{par} + i\omega C_{par} \tag{2.48}$$

It leads to the current, $I^* = Y^*V^*$. From this, the following relations are found;

$$\varepsilon' = C_{par}/C_o \tag{2.49}$$

$$\varepsilon'' = 1/R_{par}\omega C_o \tag{2.50}$$

$$\tan\delta = 1/R_{par}C_{par}\omega \tag{2.51}$$

The dielectric material can also be represented as a resistance, R_{ser}, in series with

a capacitance, C_{ser}. By the same treatment as above, the impedance, Z^* ($=1/Y^*$) = $R_{ser}+1/i\omega C_{ser}$, results in the following equations;

$$\varepsilon' = C_{ser}/C_o(1+\tan^2\delta) \tag{2.52}$$

$$\varepsilon'' = R_{ser}C_{ser}^2\omega/C_o(1+\tan^2\delta) \tag{2.53}$$

$$\tan\delta = R_{ser}C_{ser}\omega \tag{2.54}$$

For the dielectric studies done here, the parallel circuit representation was used.

The Dielectric Measurement Assembly

All dielectric measurements were made using a microprocessor controlled GenRad, Inc. Digibridge GR 1689 automatic RLC meter. The RLC meter (Digibridge) calculates the desired parameters from a series of 8 voltage measurements which include both quadrature ($\pi/2$) and inverse (π) vector components of the voltages across the material under test, Z_X, and across a standard resistor, R_S, both of which carry the same current. Each set of voltage measurements is made in rapid sequence with the same phase-sensitive detector and analogue-to-digital converter. In this way, properly chosen differences between those measurements cancel out the fixed offset errors, and the ratios between these measurements subtract out the common current and scale factor effects of the detector-converter.

Figure 2.3 shows a schematic block diagram of the Digibridge. I_X is the current

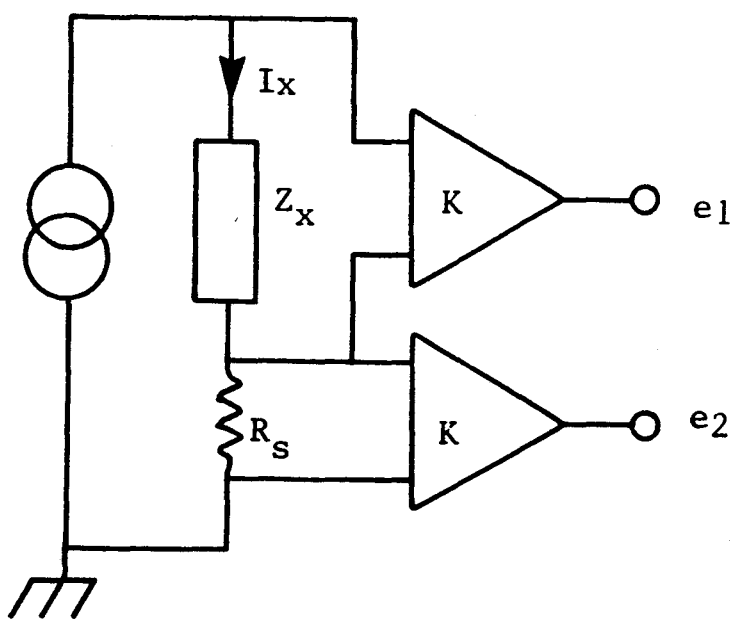

Figure 2.3: A schematic diagram of the GenRad 1689 Digibridge.

provided by the sine-wave generator across the known internal resistance standard, R_s, and the unknown impedance, Z_x, in series. Two voltages, e_1 and e_2 are produced across the impedance sample and resistor standard respectively from individual differential amplifiers with the same gain, K. The voltages produced are,

$$e_1 = KZ_x I_x \tag{2.55}$$

$$e_2 = KR_x I_x \tag{2.56}$$

From Equations (2.55) and (2.56) the unknown quantity, Z^*, can be calculated from

$$Z^* = R_o\left(e_1^* / e_2^*\right) \tag{2.57}$$

Being a complex quantity, Z^* allows determination of capacitance, C_{par} (or C_{ser}), and the loss, tanδ, by the microprocessor. The calculated value of C_{par} and tanδ are accurate to within ≤0.5% and ±0.5% respectively.

The Digibridge was interfaced, via an IEEE card, to an IBM portable computer by J.Y. Cavaille of this group in 1986, allowing increased automation of the Digibridge as well as fully automatic data acquisition on a diskette. The computer programs allowed data to be gathered under both isothermal (variable frequency) and isochronal (fixed frequency, variable temperature) modes.

The Thermostat Assembly and Temperature Control

A metal cylinder (steel or aluminum) typically 6 cm in diameter and 16 cm long

with a concentric 0.5 cm diameter, 5 cm deep bore was used as a thermostat assembly. Woven glass cloth was wrapped around the block and fastened to electrically insulate it. High resistance nichrome wire was wound around the block to provide 600W of heating power. The windings were then coated with plaster of paris to protect them and keep them in position. The unit was placed axially into a slightly larger aluminum can to allow an annular space of approximately 2cm from the wall of the can to the edge of the coated block. While keeping the bore-holed end flush with the top of the can, sand and silica fibres were packed into the airspace around the block for further insulation. Finally, with the leads of the winds insulated with glass cloth and protruding out of the assembly, plaster of paris was used to coat and seal in the exposed sand/silica fibre mix.

For dielectric measurements well above the room temperature, the thermostat assembly was allowed to remain in the ambient air. When colder temperature measurements were required, it was placed in yet another larger aluminum can with a diameter approximately 4cm larger than the thermostat to allow the loose packing of silica fibres in the annular space. This whole set up was then placed in a larger dewar containing liquid nitrogen. The temperature of the furnace was controlled by one of two temperature control units. A Eurotherm 808 temperature control unit made by the Eurotherm Company was used for isothermal temperature control and for a linear heating rate starting above the room temperature. A Valley-Forge Instrument Company PC60105 was used to provide a linear heating rate starting from 100K. Compared with the sample placed within it, the block was massive, and acted as an efficient heat sink such that the

temperature, as limited by the temperature controllers, could be controlled to less than ±0.5K for over a day, and ±0.1K for several hours during the course of isothermal measurements, providing that no extreme exotherms resulted from chemical reactions of the sample under study. The temperature of the sample itself was monitored with the use of a copper-constantan thermocouple that had one end immersed in the sample and the other end in an ice-bath maintained at 273.15K. The EMF produced by the thermocouple was measured with a Hewlett Packard HP 3478A multimeter which was interfaced with the computer for automatic data storage with the respective dielectric measurement at that instant of time.

The Dielectric Cell

A disposable dielectric cell was used for all dielectric measurements. A variable capacitor consisting of 18 rigid steel plates and with an approximate dimensions of a 7mm diameter and 15mm length was used. The capacitance could be varied by rotating 9 of the plates about a common axis relative to the other 9 plates by means of a turn-screw. The model 0109 variable PC mount capacitors used in the study were manufactured by Johnson Trimmer Capacitors. Their nominal air capacitance was approximately 16.5pF, which was measured prior to an experiment.

The capacitor was connected to the Digibridge as follows; The two capacitor leads were soldered to the ends of two shielded RG-174/U coaxial cables, with the other ends of the cables spliced and soldered to respective RG-59/U coaxial cables with

standard BNC plugs on the opposite ends, and connected to the Digibridge assembly. All spliced and exposed wiring was insulated with teflon and electrical tape. The capacitor was then immersed into the liquid sample, contained in a glass vial of dimensions 35mm long by 10mm diameter. A cork stopper was fitted into the open end to secure the coaxial leads and thermocouple. Entrapment of air bubbles between the plates was carefully avoided by rotating the cork and capacitor within the liquid to displace any air. A schematic diagram of the dielectric cell filled with liquid is shown in Figure 2.4. The problem of changing cell geometry during polymerization is eliminated here, since the parallel plates are rigidly and completely surrounded by the liquid. The whole dielectric cell was wrapped with sufficient aluminum foil to provide electrical shielding and adequate thermal contact with the block. Finally, the whole assembly was grounded with a wire from the Digibridge to the furnace block.

2.2.3 The Dynamic Mechanical Spectrometer and the Associated Assembly

The commercially available mechanical spectrometer used in this study is designed to measure the phase lag of a resultant dynamic strain of an imposed sinusoidal stress, as well as their respective amplitudes, σ_o and γ_o. In the case of a sinusoidal applied stress;

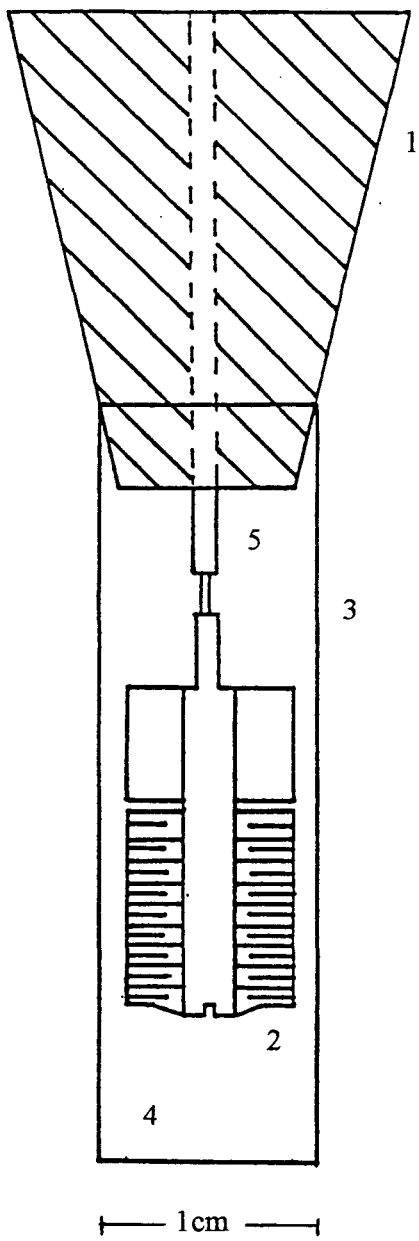

1. Cork
2. Capacitor
3. Vial
4. Thermoset mixture
5. Co-axial cable

Figure 2.4: A schematic diagram of the dielectric cell filled with liquid (Parthun 1991).

$$\sigma(t) = A\sigma_o \cos(\omega t + \phi_1) \tag{2.58}$$

$$\gamma(t) = B[\gamma_o \cos(\omega t + \phi_2)] + \sum_{p=2}^{\infty} \gamma_p \cos(p\omega t + \phi_p) + \gamma_R + d(t) \tag{2.59}$$

where A and B are constants relating to the geometries of the sample being measured and of the mounts, γ_R is the at rest position of the pendulum equipment and d(t) is a non-periodic function representing random noise and drift disturbances (Micromechanalyser user manual, Metravib Instruments, 1988). By evaluating the following integrals,

$$I_1 = \frac{1}{nT} \int_{t_o}^{t_o+nT} \sigma(t)\cos(\omega t)dt \tag{2.60}$$

$$I_2 = \frac{1}{nT} \int_{t_o}^{t_o+nT} \sigma(t)\sin(\omega t)dt \tag{2.61}$$

$$I_3 = \frac{1}{nT} \int_{t_o}^{t_o+nT} \gamma(t)\cos(\omega t)dt \tag{2.62}$$

$$I_4 = \frac{1}{nT} \int_{t_o}^{t_o+nT} \gamma(t)\sin(\omega t)dt \tag{2.63}$$

where $T=2\pi/\omega$ is the period of stress application and n is the number of periods, One obtains σ_o , γ_o and $\tan\phi$ from the relations:

$$\frac{1}{2}A\sigma_o = \sqrt{I_1^2 + I_2^2} \tag{2.64}$$

$$\tan\phi = \tan(\phi_1 - \phi_2) = \frac{I_1 I_4 - I_2 I_3}{I_1 I_3 + I_2 I_4} \tag{2.65}$$

The complex shear modulus can be determined from;

$$G^* = \frac{\sigma_o}{\gamma_o}\exp(i\phi) \tag{2.66}$$

The evaluation of integrals I_1, I_2, I_3 and I_4 eliminates the influence of the harmonics and the zero-sequence component. The influence of disturbances, d(t), on the accuracy of the calculated values (σ_o, γ_o and ϕ) will be as low as the number, n, of integration periods is high.

The Mark IV Dynamic Mechanical Spectrometer, manufactured by Metravib Instruments S.A., France, was used for the measurements of mechanical properties in the torsional oscillation mode. The assembly consists of an inverted torsional pendulum, shown in Figure 2.5 (Pascheto 1991). The sample is affixed at its ends to two clamps(11) made of stainless steel. The upper clamp is secured onto a rotatable rod(12) made of tantalum, while the lower clamp is fixed securely to a rigid mount.

An oscillatory torque is applied to the rotatable rod(12) by the interaction between the magnets(2) and Helmholtz coils(3) carrying a current, I. The suspended counter-weight(1) balances the axial load on the suspension and a tantalum damper(7) reduces parasitical vibrations induced by the surroundings. The strain on the sample is detected

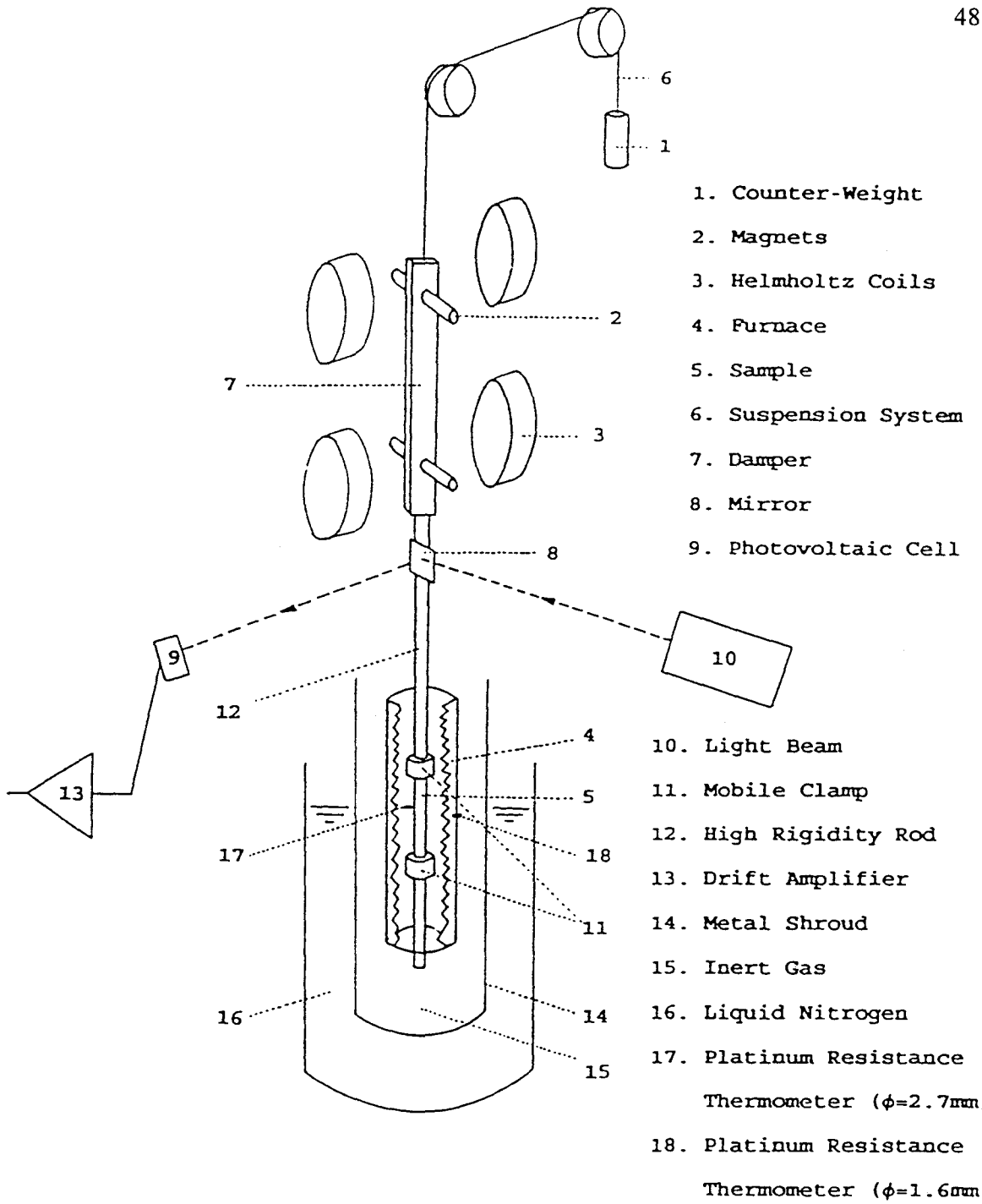

Figure 2.5: A schematic diagram of the dynamic mechanical spectrometer measurement assembly (Pascheto 1991).

by the reflection of a light beam(10) from a mirror(8) attached to the rotatable rod(12). This reflected light falls onto a photovoltaic cell(9) which is connected to a low drift amplifier(13) supplying a voltage proportional to the strain of the sample.

A moveable resistance furnace(4) axially encloses the sample during the measurements. A platinum resistance thermometer(18) monitors the furnace temperature while another(17) measures the temperature at a distance of 1mm from the sample. The furnace is sealed using a steel shroud(14) which allows the study of the sample in a vacuum or in an inert environment of nitrogen, as used here. The steel shroud can be immersed in a coolant to make measurements at lower temperatures. The whole thermal enclosure can be controlled to allow measurements under isothermal conditions or during heating or cooling over a temperature range of 100K to 650K.

The mechanical spectrometer is controlled and the sample is monitored by different modules of the equipment working in conjunction. The interface module consists of a generator that supplies a sinusoidal excitation to the sample via the Helmholtz coils, the frequency of which is set manually or controlled from the computer program. A power amplifier allows the excitation current to be adjusted between 10^{-4} to 1A. A control system enables the selection of operation under either constant strain amplitude or constant stress amplitude. Strain mode is applicable when strain values vary greatly over the course of measurement. In this manner, the control system keeps the strain amplitude constant by varying the stress applied. If this were not the case, large mechanical drift would occur as a sample becomes less rigid, leading to the reflected

beam of light to miss the photovoltaic cell. Because polymers can undergo large variations in rigidity at glass transition temperatures, strain mode was used throughout this study. An LED view meter allows one to view the stress and strain signals' amplitudes to ensure that they are symmetrical about a zero value.

The Microcor II digital temperature controller, made by Coreci, France, was used to regulate the temperature of the furnace(4). It controls the power input to the furnace and continuously measures the temperature by use of the platinum resistance thermometer(18). An oscilloscope, model 1020, manufactured by Leader Electronics Corporation, USA, was added to work in tandem with the LED view meters to ensure that the two waveforms remain sinusoidal and mechanically zeroed about zero deformation.

A Data Train 2801 personal computer made by Data Translation Inc., USA, was interfaced to the measurement assembly. It controls the experiments by using a data acquisition interface, allowing dialogue between the measurement systems and the computer. During the course of an experiment, the computer receives data on the sample's stress, strain and temperature, which it then uses to calculate mechanical loss. A printer and plotter were added to the assembly in order to follow the mechanical properties during the course of the measurements.

The Measurement Procedure

For measurements, the ends of the sample were mounted into clamps and secured by screws through drill-holes in the sample of diameter 2.5mm. The clamps were then

slipped on to the fixed rod (lower clamp) and the rotatable rod (upper clamp) with set screws. Good axial alignment between the sample and the rods was necessary to ensure proper, sinusoidal stress and strain oscillations. By observing the waveforms on the oscilloscope, manual adjustments could be made to correct any incongruities in the signals. Manual adjustments were made possible by a knob which rotated the whole fixture assembly in order to centre the light beam on the photocell. Controlling the strain by varying the input current allowed an oscillation whose amplitude did not cause the reflected light beam to exceed the outer edges of the photocell. A sinusoidal, centred waveform on the oscilloscope ensured proper adjustment. The strain of the sample was held fixed at approximately 10^{-2} rad. The air inside the stainless steel shroud was evacuated of air and replaced by nitrogen maintained at approximately 0.8 atm.

The sample's dimensions are required for the calculation since shear modulus, G, is calculated from G = MCZ, where C is an internal calibration factor, M is a function of sample geometry and Z is the measured quantity related to rigidity of the sample. These were measured to an accuracy of ±0.01mm and entered into the computer program along with the temperature and the measurement frequency.

Measurements of the complex shear modulus, G^*, were performed in two modes. The first was under a fixed oscillation of 1Hz while heating the sample at a constant rate of 1K/min from 350K to 450K, and the second was made at a constant temperature while measuring the properties at various frequencies in the range 10^{-3}Hz to 5Hz. The first mode yields an isochrone and the second the isothermal spectra.

The Sample Preparation For The Dynamic Mechanical Spectrometer

A schematic diagram of the aluminum mould assembly and steel machining guide is given in Figure 2.6(a,b). The monomeric liquid mixture was poured into the mould trough which was lined with an insert constructed of aluminum foil, with the reflective side inwards. The ends of the foil were folded and crimped such that the insert could contain a low viscosity liquid without leaking. The edges of the insert were carefully taped back onto the aluminum block to obtain a taut and smooth surface. The aluminum block was then preheated to a predetermined temperature for which dielectric and calorimetric measurements were also carried out. The monomeric mixture was poured into the foil-lined trough of the block to a level slightly below the bevelled edge as shown in the Figure 2.6(a). Any bubbles that were trapped on the inner surfaces were dislodged by gently tapping the mould. The mould block was then placed in the furnace on a level surface at the predetermined temperature and left for approximately 16 hours.

The resulting vitrified, rigid sample was then left in the block as the temperature of the furnace was raised to 423K and the sample kept for 6 hours to further the polymerization within a rigid support. The sample was then removed from the aluminum block and left to cool in ambient air, still wrapped in foil. Once at room temperature, the foil was peeled off. A transparent sample approximately 16cm x 1cm x 2mm with a slight yellow tint, depending on the curing agent used, was thus obtained. Three samples of roughly equal length were obtained from this initial form.

These samples were then machined to similar sizes as accurately as possible in the

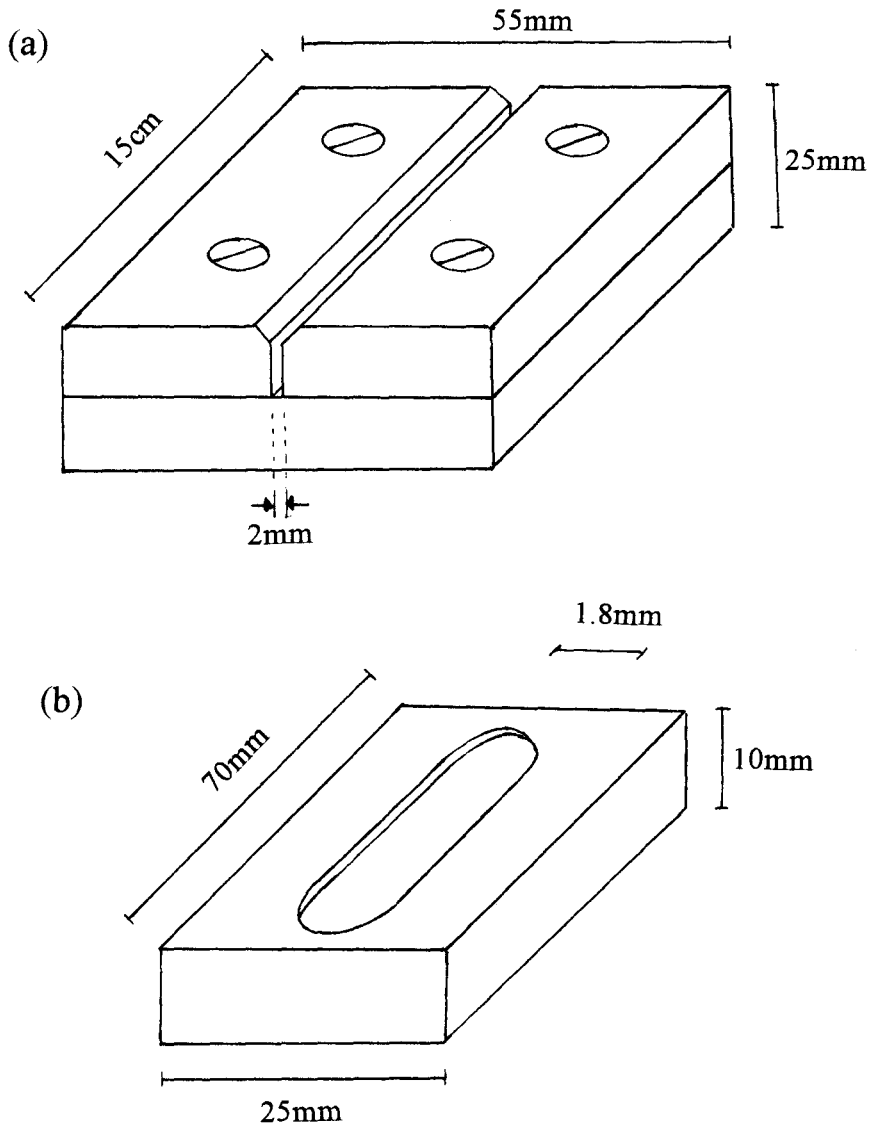

Figure 2.6: (a) The aluminum mould assembly within which the mixtures were polymerized. (b) the steel machining guide used to obtain the final shape of the mechanical samples.

following manner. Firstly, all the edges of a sample were squared by using a rotating flat grinder of 800 grit. Next, the sample was placed as flush as possible in the ground-out form of the steel guide block. The block was held firmly against the grinding wheel with the sample flush as the grinding wheel was started. Once an even, flat surface was obtained, the sample was flipped over in the guide block so that the newly flattened surface was perfectly flush against the inside of the block. The opposite surface was then ground away in the same manner.

The 800 grit sand paper was replaced with 1200 and the whole process repeated using a vernier scale to ensure all dimensions were as accurately uniform as possible. All grinding was done with wet/dry sand paper wheels manufactured by Leco. They were used dry, as it was necessary to keep moisture as far as possible from the samples. Some samples were further polished to obtain a glossy surface finish, but no advantage to this was evident here. All samples were cleaned by wiping them with a methanol-dampened cotton swab and then allowed to dry.

The samples were then prepared for the clamp fixtures. Two 2.5mm diameter holes were drilled in the broad surface at each end of the samples. The holes were centred with the width and spaced 4.5mm from the ends. All the samples of a common composition were placed flat within an envelope of aluminum foil. The wrapped samples were placed between two flat blocks of steel inside a furnace at 443K for 1 hour. The blocks were then removed from the furnace and the whole was allowed to cool to room temperature. This step ensured that all the samples had undergone identical thermal treatment while

maintaining their dimensional trueness.

A typical sample had dimensions of 50mm x 1.5mm x 8mm with deviations between the samples of up to 10mm in length by 1mm in width. Figure 2.7 shows a typical sample in its final form. These dimensions produced the optimum strain intensity detection by the mechanical analyzer because small stresses could still produce detectable strains at low temperatures (high rigidity) and as well, the samples retained enough stiffness at high temperatures (low rigidity) to allow stresses to remain finite, while producing a strain response in the material.

2.2.4 The Preparation of the Thermosetting Polymers

Four reactants were used for preparing the three types of thermosets studied here. These were; aniline, 3-chloroaniline, 4-chloroaniline and a tris(hydroxyphenyl) methane-based epoxy. The three aniline curing agents were of 99.5%, 99% and 98% purity, respectively, and were purchased from Aldrich Chemical Company. The methane-based epoxy resin was obtained from Dow Chemical Company under the trade name Tactix 742, as it will be referred to in this study. All reactants were used in the as-received state, and all but the Tactix 742 were stored in low moisture desiccators. The Tactix 742 was sealed in its container and only a certain amount that was used for the work was stored in a glass jar.

Tactix 742 is described as a trifunctional epoxide resin with a molecular weight of 450-510 by Dow's company literature (Form#296-678-589-A&L p.18). Its glass

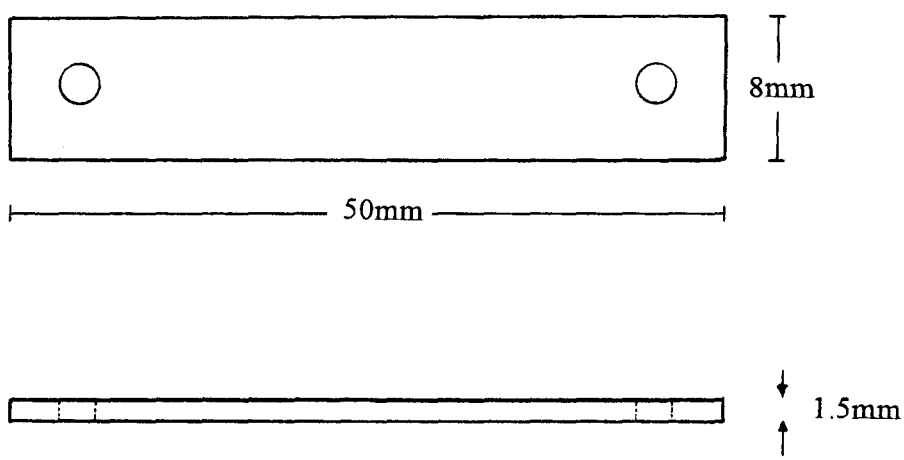

Figure 2.7: A schematic diagram of a typical mechanical sample in its final form.

transition temperature was determined from DSC measurements at a heating rate of 10K/min, and was 286K. The functionalities of the reactants were used to calculate the stoichiometric amounts of Tactix 742, for which the molecular weight used was 480g/mol, and the curing agent required. Aniline and 3-chloroaniline were liquids at room temperatures and the 4-chloroaniline was a crystalline solid with a melting point of 341-344K. Their molecular formula were shown in Figure 1.2.

To ensure consistency among the 3 experimental techniques, it was paramount that the thermosetting mixtures be prepared in an identical manner for all experiments. The curing agents had one amine group, $-NH_2$, located on the phenyl ring and the Tactix 742 had three epoxide rings per molecule. The stoichiometric amounts required for a complete reaction was 2 moles of Tactix 742 for every 3 moles of curing agent. The thermosets were prepared by weighing the viscous Tactix 742 into a glass vial and then adding the stoichiometric amount of curing agent. The vial was then heated to 318K and mixed vigorously with a glass rod. A transparent yellow, homogenous solution was obtained after approximately 10 minutes. The solution was then transferred to a dielectric cell, a DSC pan or the mechanical mould assembly, all described earlier. The time elapsed between obtaining a solution and commencing the measurements was approximately three minutes for both the DSC and dielectric studies for isothermal polymerization. The Tactix 742:aniline mixture is referred to as Tactix-AN in this study, similarly, Tactix 742:3-chloroaniline and Tactix 742:4-chloroaniline are referred to as Tactix-3CA and Tactix-4CA, respectively.

CHAPTER III

RESULTS AND DATA ANALYSIS

3.1 Calorimetric Studies

3.1.1 Polymerization During Heating at a Constant Rate

Plots of $(dH/dt)_q$ against temperature, with a constant heating rate, q, of 10K/min, are shown in Figure 3.1 for Tactix-AN, Tactix-3CA and Tactix-4CA. Initially, $(dH/dt)_q$ is nearly constant with temperature, then decreases rapidly with increasing temperature toward a minimum value, and finally increases rapidly to a plateau value similar to the low temperature plateau value. This indicates that no more heat of reaction is evolved; therefore the chemical reaction is complete. For Tactix-4CA in Figure 3.1, a small peak is observed in $(dH/dt)_q$ before the exotherm. This peak is due to the dissolution of the remaining crystalline 4-chloroaniline in Tactix 742. The $(dH/dt)_q$ plots for Tactix-AN and Tactix-3CA do not show this peak because the curing agents, aniline and 3-chloroaniline, respectively, were liquids at room temperature and were more thoroughly mixed.

For both Tactix-3CA and Tactix-4CA a small shoulder in $(dH/dt)_q$ with temperature is observed in Figure 3.1. The shoulder appears as a small, depressed region at approximately 410K for Tactix-3CA and at approximately 395K for Tactix-4CA. This is due to the evaporation of low-boiling, or the reaction of, any impurities in the less pure

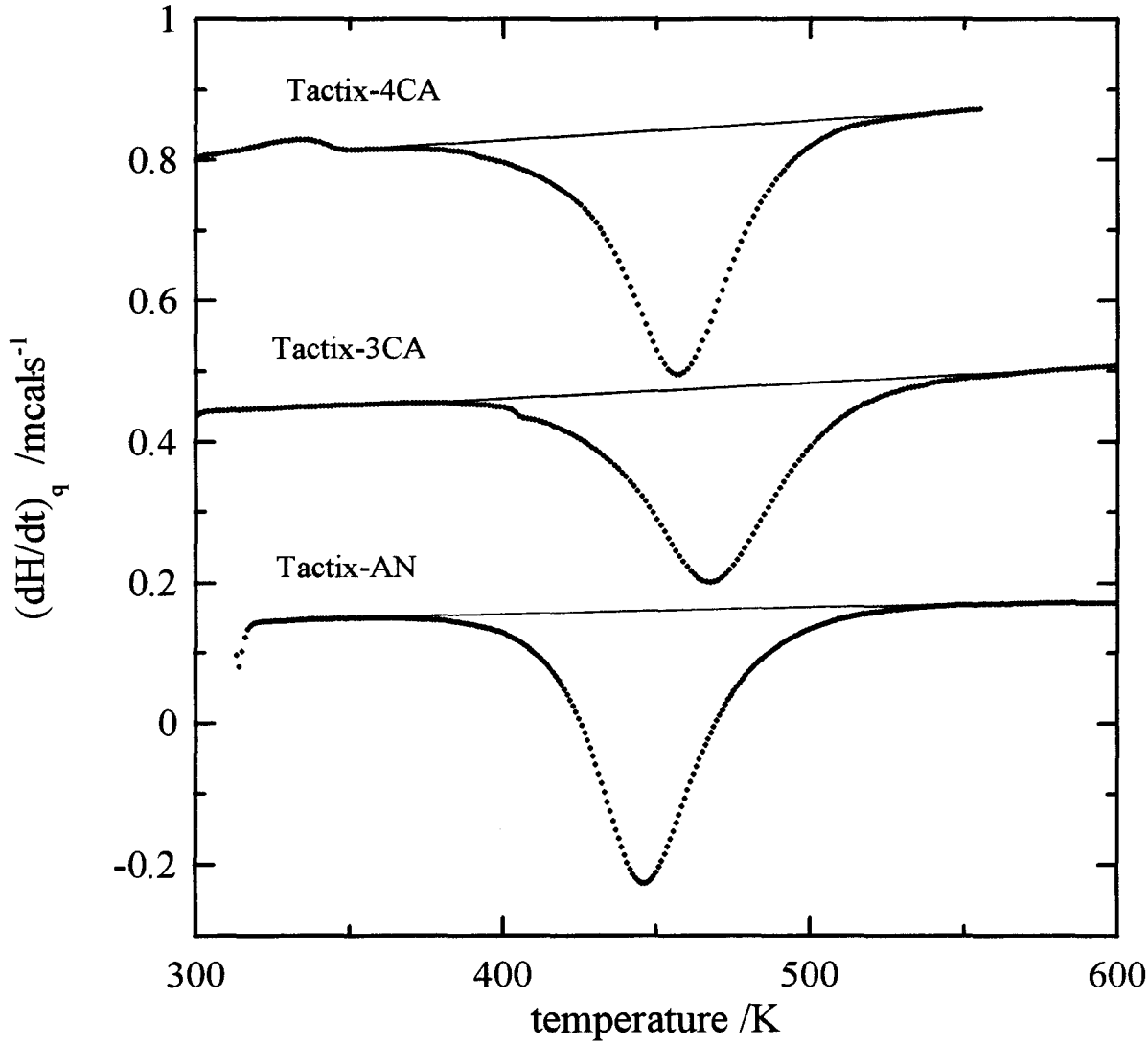

Figure 3.1: $(dH/dt)_q$ plotted against temperature at a heating rate of 10K/min for the three mixtures.

two chloroaniline. Its presence has a negligible effect on our calculated values.

3.1.2 Polymerization Under Isothermal Conditions

The isothermal polymerization of Tactix-AN, Tactix-3CA and Tactix-4CA was done at temperatures of 332.0K, 360.6K and 349.5K, respectively. The curves of $(dH/dt)_T$ against the reaction time, t, are shown in Figures 3.2, 3.3 and 3.4 for Tactix-AN, Tactix-3CA and Tactix-4CA, respectively. $(dH/dt)_T$ initially decreases steadily to a minimum value, then increases to a plateau value with t. At this time the sample has vitrified and reactions then occur only when an exceptionally long period is allowed at that temperature. The duration over which $(dH/dt)_T$ was measured was at most 60000s. Figures 3.3 and 3.4 show curves of $(dH/dt)_T$ against t with a final plateau value that is less than the initial value of $(dH/dt)_T$. This behaviour is not observed with Tactix-AN in Figure 3.2. Reasons for this are discussed in Section 4.1.

To determine the total heat of reaction, each sample, after the isothermal polymerization, was heated at a constant rate of 10K/min from 320K to 570K. $(dH/dt)_q$ measurements with temperature are shown in Figure 3.5 for Tactix-AN, Figure 3.6 for Tactix-3CA and Figure 3.7 for Tactix-4CA. The shape of the curves is qualitatively similar to that of Figure 3.1, except that the exotherm is preceded by a sharp endothermic peak. This peak is due to the glass → liquid or gel transition of the partially polymerized mixture which had physically aged, as observed by Plazek and Frund(1990), Wisanrakkit and Gillham (1990), and Wasserman and Johari (1993,1994). The heats of reaction for

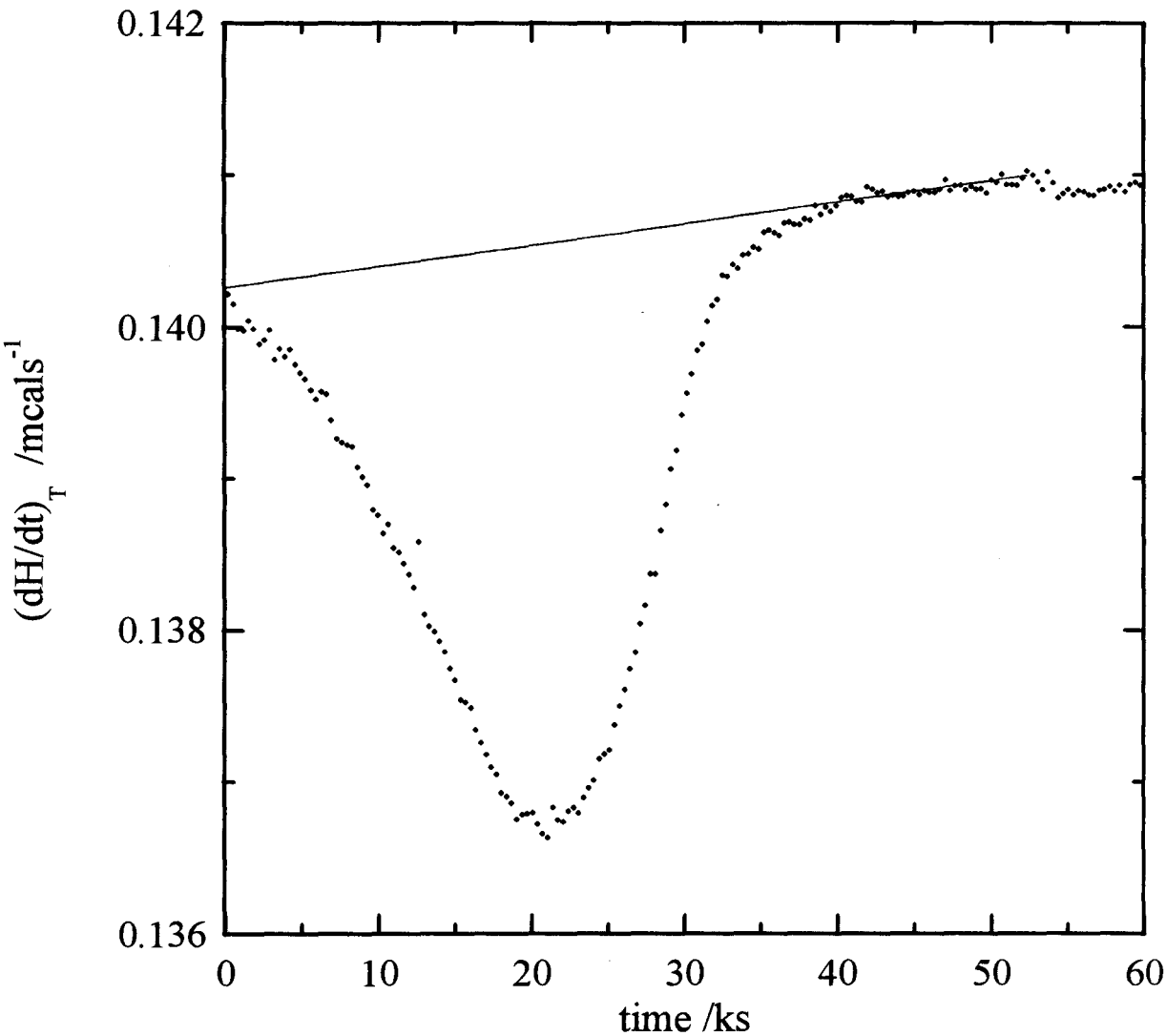

Figure 3.2: $(dH/dt)_T$ plotted against the reaction time for the isothermal polymerization of Tactix-AN at 332.0K.

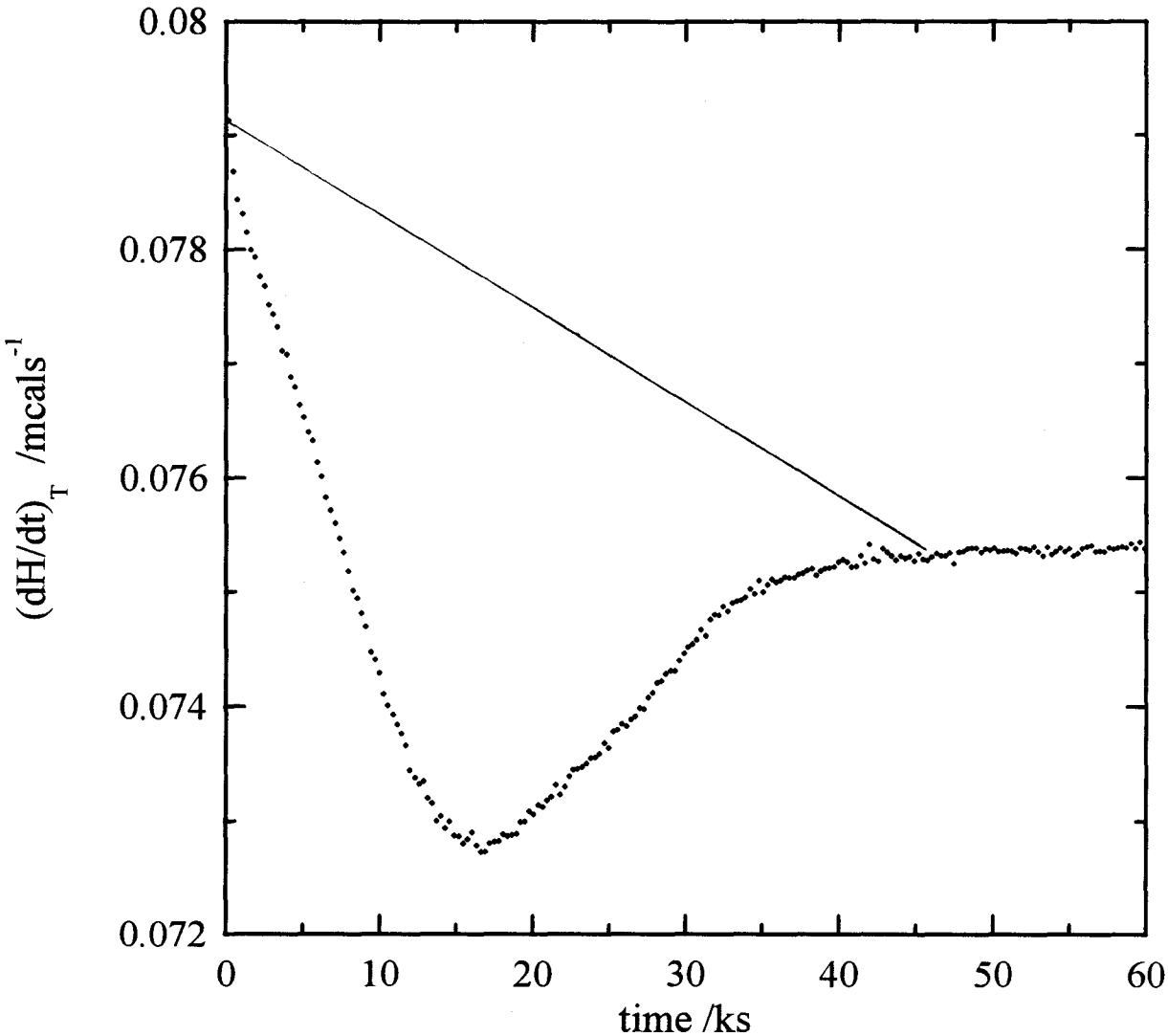

Figure 3.3: $(dH/dt)_T$ plotted against reaction time for the isothermal polymerization of Tactix-3CA at 360.6K.

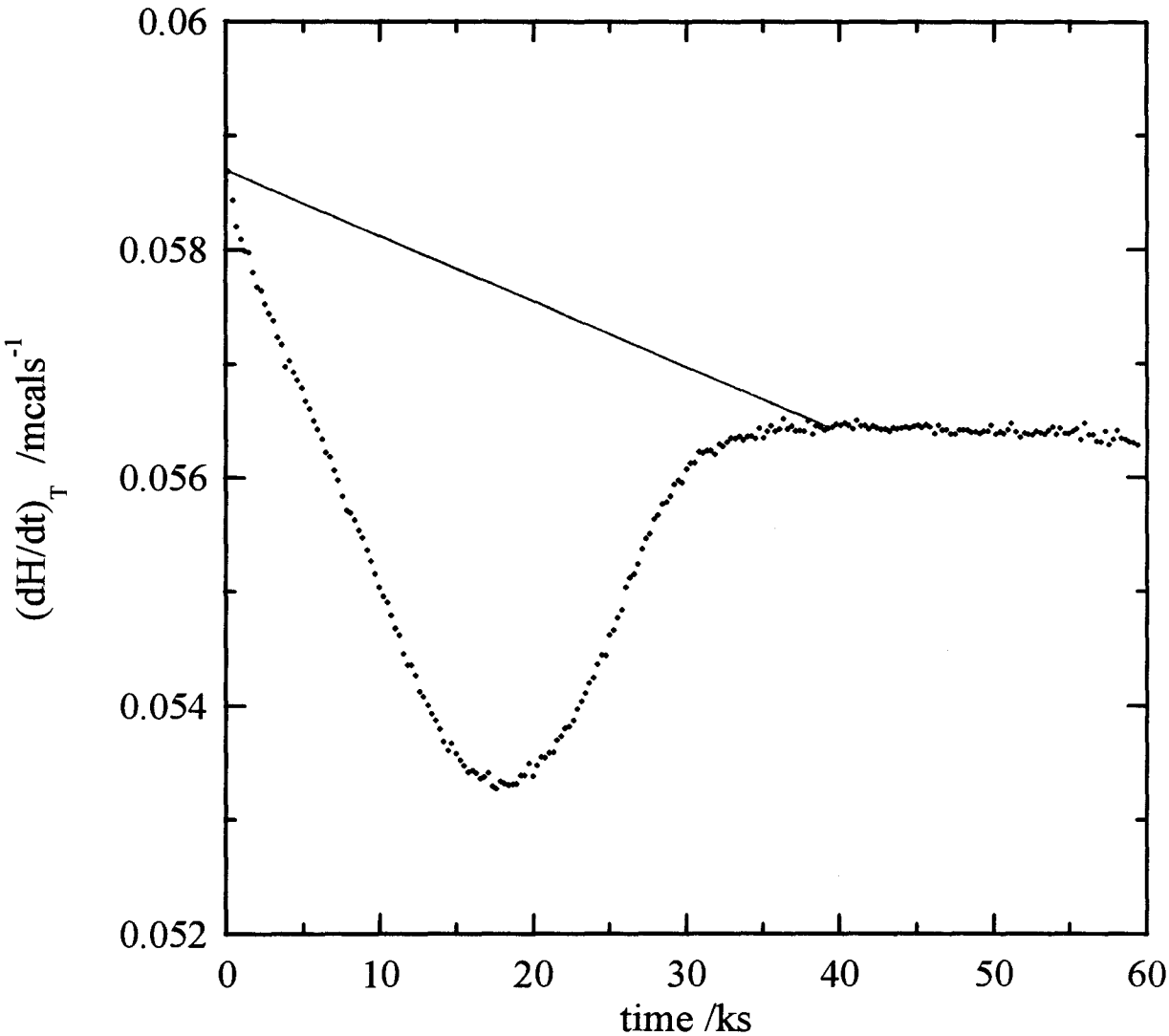

Figure 3.4: $(dH/dt)_T$ plotted against reaction time for the isothermal polymerization of Tactix-4CA at 349.5K.

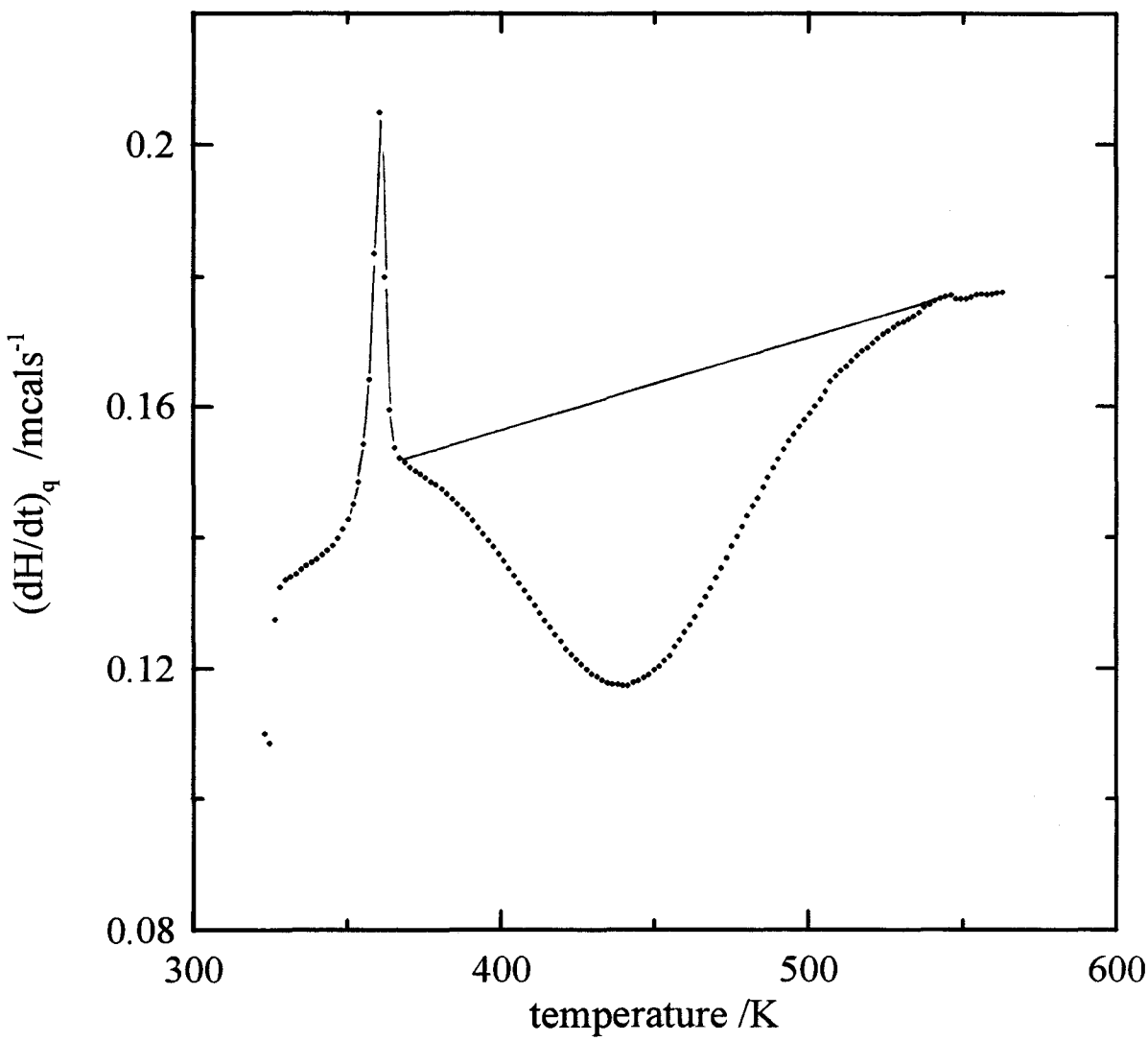

Figure 3.5: $(dH/dt)_q$ plotted against temperature at a heating rate of 10K/min for Tactix-AN following an isothermal polymerization at 332.0K.

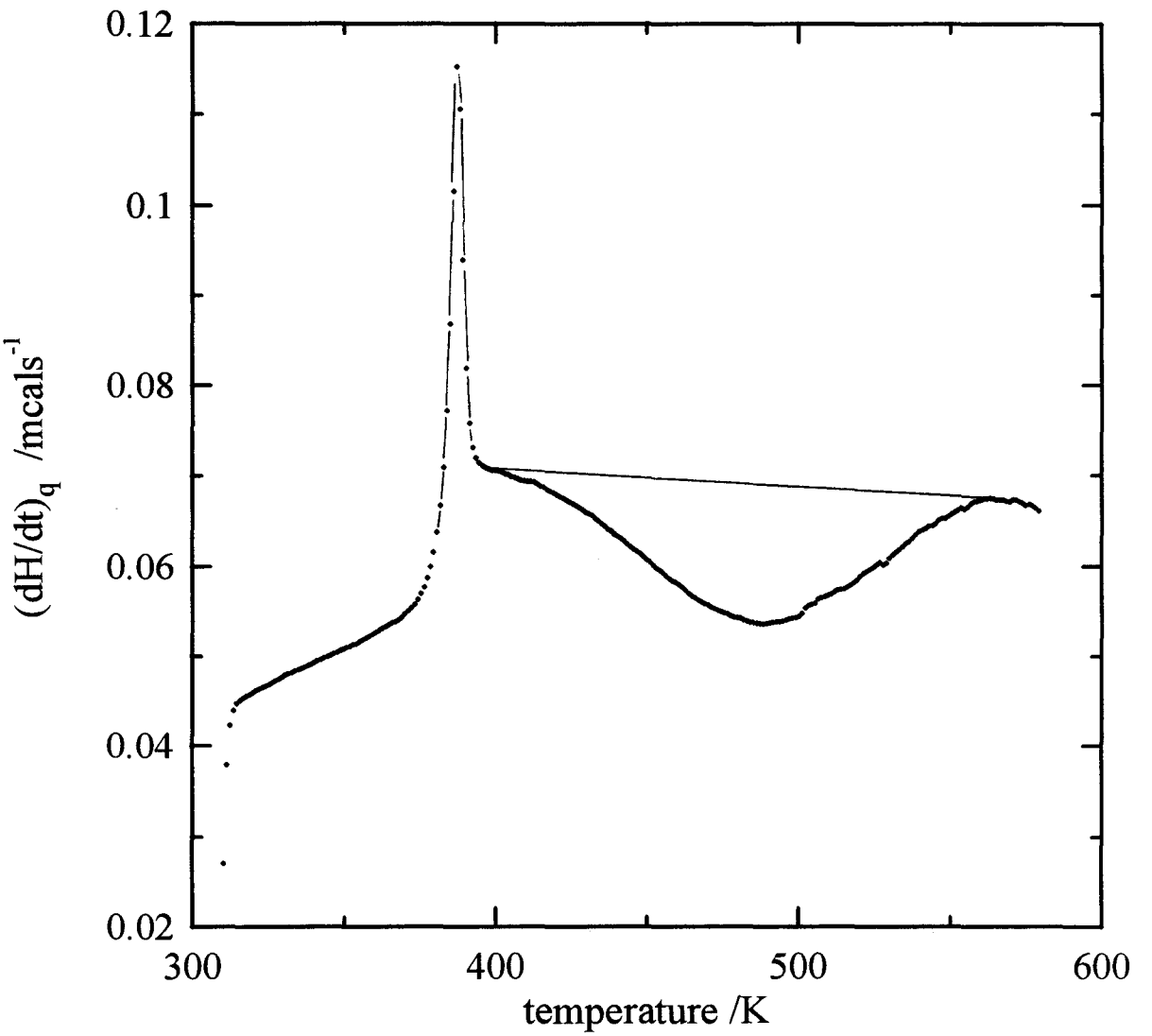

Figure 3.6: $(dH/dt)_q$ plotted against temperature at a heating rate of 10K/min for Tactix-3CA following an isothermal polymerization at 360.6K.

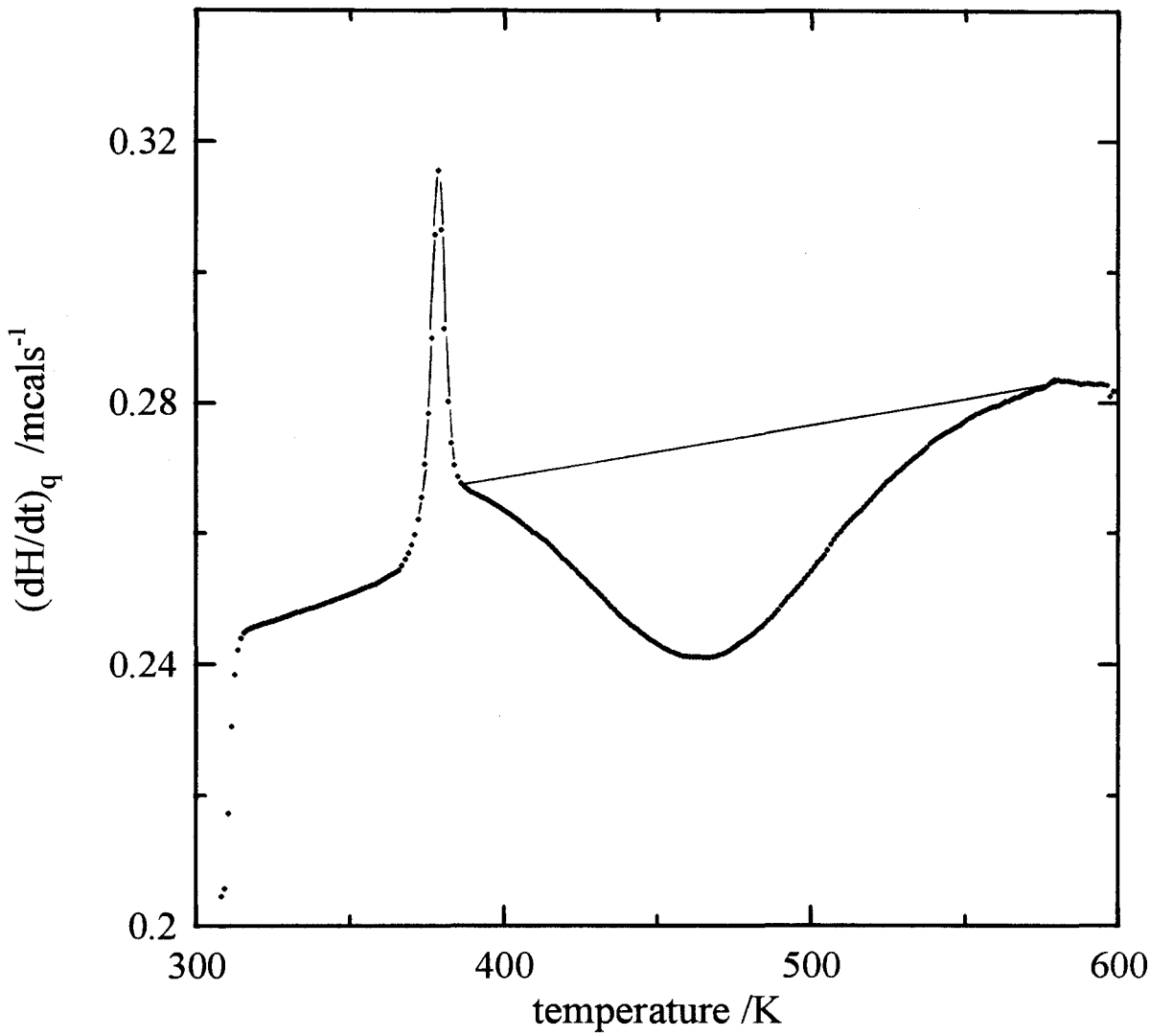

Figure 3.7: $(dH/dt)_q$ plotted against temperature at a heating rate of 10K/min for Tactix-4CA following an isothermal polymerization at 349.5K.

each of the three mixtures were less than those determined from the area of the $(dH/dt)_T$ curves in Figure 3.2, 3.3 and 3.4, indicating that most of the polymerization had already occurred.

The total heat of reaction for the polymerization of each of the three mixtures was obtained by integrating the sample's isothermal plot from t = 0 to a time for which the evolution of reaction heat was unobservable, typically 40ks, and adding to this value the integration of the area under the plot obtained upon further heating of the sample from temperature, T_1, below T_g, to a final temperature, T_2, at a heating rate of 10K/min. Thus the total heat of reaction is expressed as,

$$\Delta H^{o}_{total} = \int_0^t \left(\frac{\partial H}{\partial t}\right)_T dt + \frac{1}{q}\int_{T_1}^{T_2} \left(\frac{\partial H}{\partial t}\right)_q dT \qquad (3.1)$$

ΔH^0_{total} was found to be 155.6 kJ/mol of aniline for Tactix-AN, 136.9kJ/mol of 3-chloroaniline for Tactix-3CA and 139.2kJ/mol of 4-chloroaniline for Tactix-4CA..

The partial heat of reaction at any instant of time, t, is then calculated from the expression,

$$\alpha(t) = \frac{\Delta H^0(t)}{\Delta H^0_{total}} \qquad (3.2)$$

where $\alpha(t)$ is the extent of reaction, and $\Delta H^0(t)$ is the amount of heat evolved up to the time, t. Since the heat is evolved when covalent bonds form during polymerization, the number of bonds, N(t) can be determined from the equation,

$$N(t) = N_A B \alpha(t) \qquad (3.3)$$

where N_A is the Avogadro number and B the number of bonds formed per molecule of both reactants. In the case of triepoxide molecules and aniline molecules present in a stoichiometric ratio of 2:3, B = 6/5 (This is also the case for 3-chloroaniline and 4-chloroaniline). Thus, it is possible to re-express $\Delta H(t)$ or $\alpha(t)$ as N(t). Plots of $\alpha(t)$ and N(t) against t are given in Figures 3.8, 3.9 and 3.10 for Tactix-AN, Tactix-3CA and Tactix-4CA, respectively. Note that the left side of each figure displays the scale for $\alpha(t)$, while the right displays N(t).

The integration of the isothermal plots of Figures 3.2 to 3.4 required a baseline to define the limits of the enclosed area. In Figure 3.2, this baseline is a straight line connecting the first data measurement to the time at which $(dH/dt)_T$ reaches a plateau value. Figures 3.3 and 3.4 show that the magnitude of the plateau in $(dH/dt)_T$ is significantly less than the initial measurement, which leads to errors when a straight line is used to enclose the area. Barton (1985) described a reiterative calculation to obtain a non-linear baseline based on the extent of reaction, $\alpha(t)$. However, this method is still dependent on one's choice of the long-time end of the baseline. Since errors are introduced by either the straight-line or non-linear baseline methods, the former was chosen for the calculation.

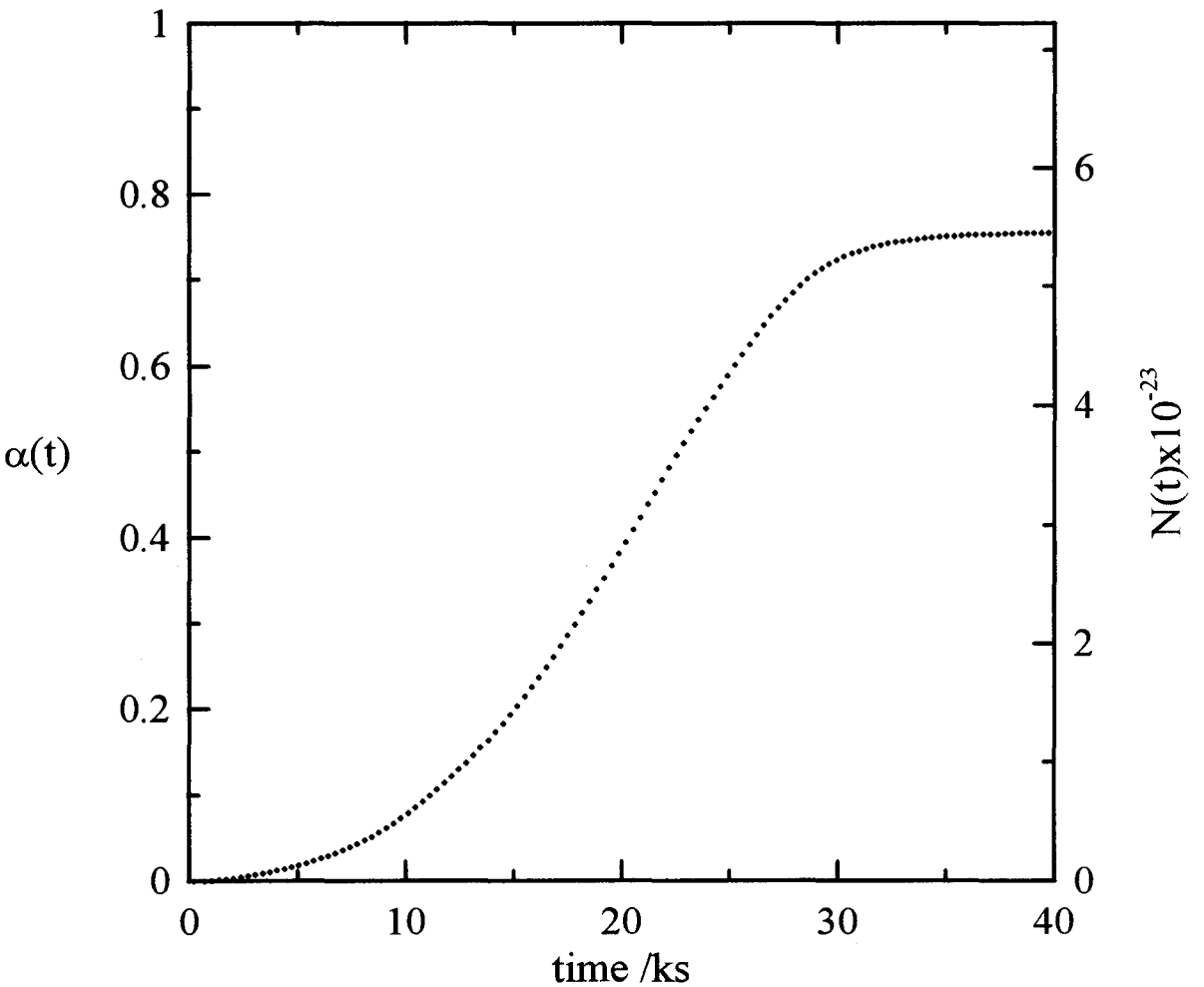

Figure 3.8: α(t) (left most axis) and N(t) (right most axis) plotted against reaction time for the isothermal polymerization of Tactix-AN at 332.0K.

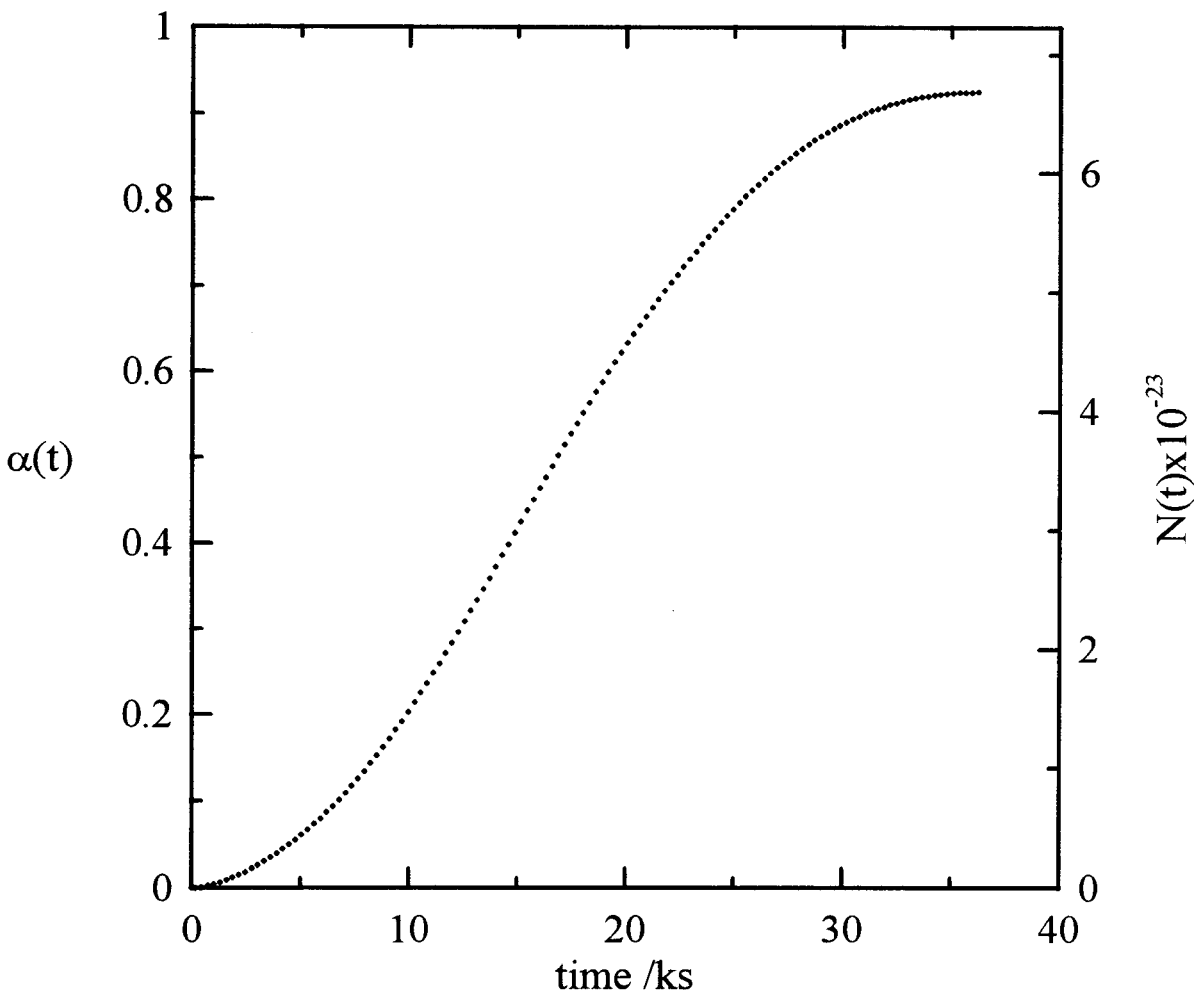

Figure 3.9: α(t) (left most axis) and N(t) (right most axis) plotted against reaction time for the isothermal polymerization of Tactix-3CA at 360.6K.

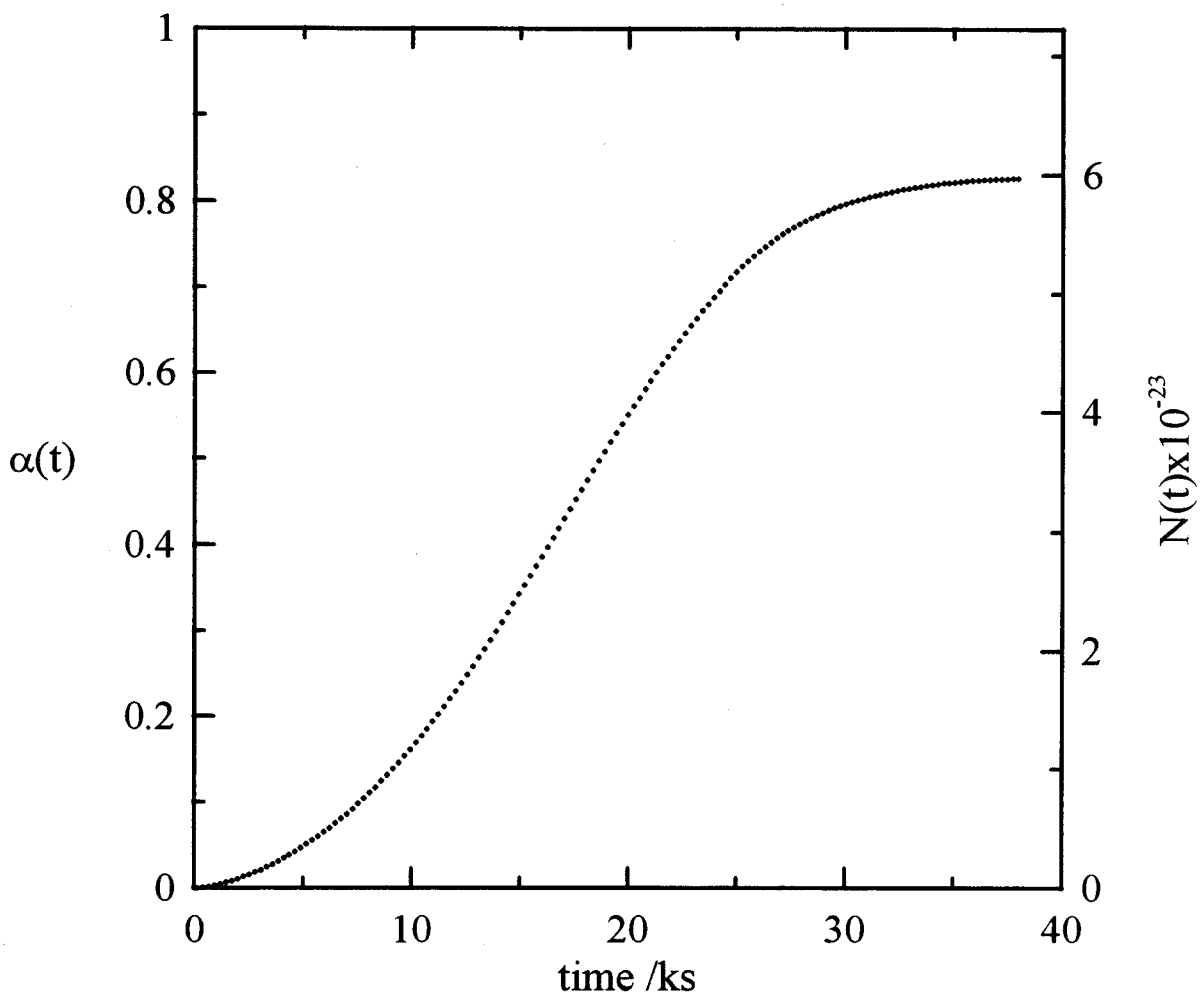

Figure 3.10: α(t) (left most axis) and N(t) (right most axis) plotted against reaction time for the isothermal polymerization of Tactix-4CA at 349.5K.

3.1.3 The Glass Transition Temperature

$(dH/dt)_q$ was measured for the completely polymerized Tactix-AN, Tactix-3CA and Tactix-4CA for q = 10K/min against the temperature, and is shown in Figure 3.11. In this figure, $(dH/dt)_q$ initially increases slowly, goes through a stretched S shaped increase, and then becomes constant with increasing temperature. The tangent to the initial plateau of $(dH/dt)_q$ and to the point of inflection of the stretched S shaped increase intersect at the glass transition temperature, T_g. The T_g's of Tactix-AN, Tactix-3CA and Tactix-4CA are 406.8K, 413.2K and 419.2K respectively.

3.2 Dielectric Relaxation Studies

3.2.1 Polymerization Under Isothermal Conditions

To further the understanding of the polymerization process of the three mixtures of Tactix 742 and the monoamines, it was necessary to study the dielectric properties as the reaction occurred. The real and imaginary components, ε' and ε'', respectively, of the complex permittivity, $\varepsilon^*(t,\omega,T)$, are plotted as a function of the reaction time, t, at 25 frequencies in Figures 3.12, 3.13 and 3.14 for Tactix-AN, Tactix-3CA and Tactix-4CA, respectively. The curves in the figures are for measurements made at 25 fixed frequencies of; 0.012, 0.015, 0.02, 0.03, 0.05, 0.07, 0.1, 0.15, 0.2, 0.3, 0.5, 0.7, 1, 1.5, 2, 3, 5, 7, 10, 15, 20, 30, 50, 70 and 100kHz.

As seen in Figures 3.12 to 3.14, ε' for the lowest measurement frequencies initially decreases from a large value to a plateau value as t increases.. From this plateau, ε'

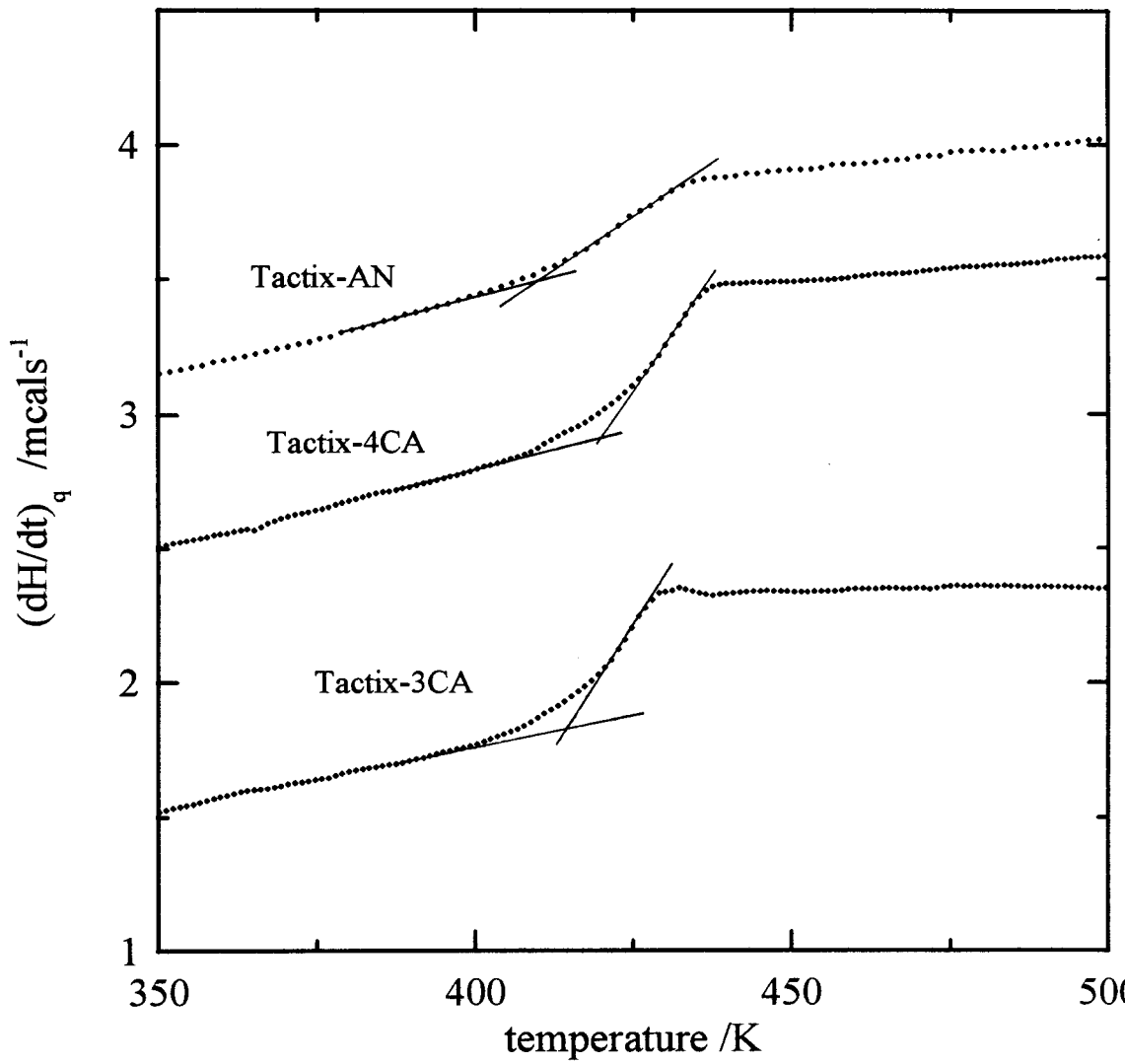

Figure 3.11: $(dH/dt)_q$ plotted against temperature at a heating rate of 10K/min for the three fully reacted polymeric materials.

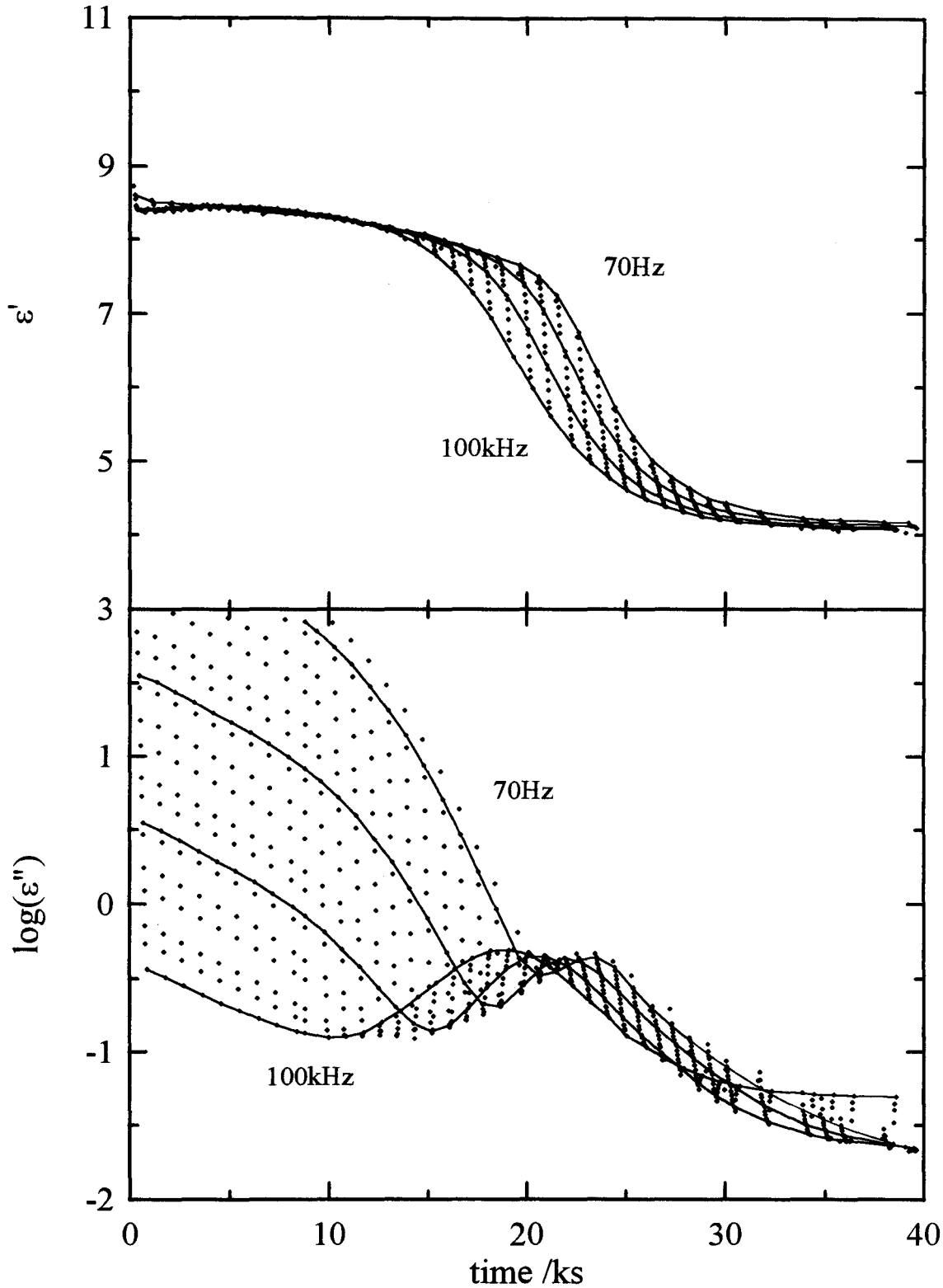

Figure 3.12: The permittivity, ε', and loss, ε" plotted as a function of reaction time for the isothermal polymerization of Tactix-AN at 332.0K at measurement frequencies listed in the text. Frequencies less than 70Hz are excluded for clarity.

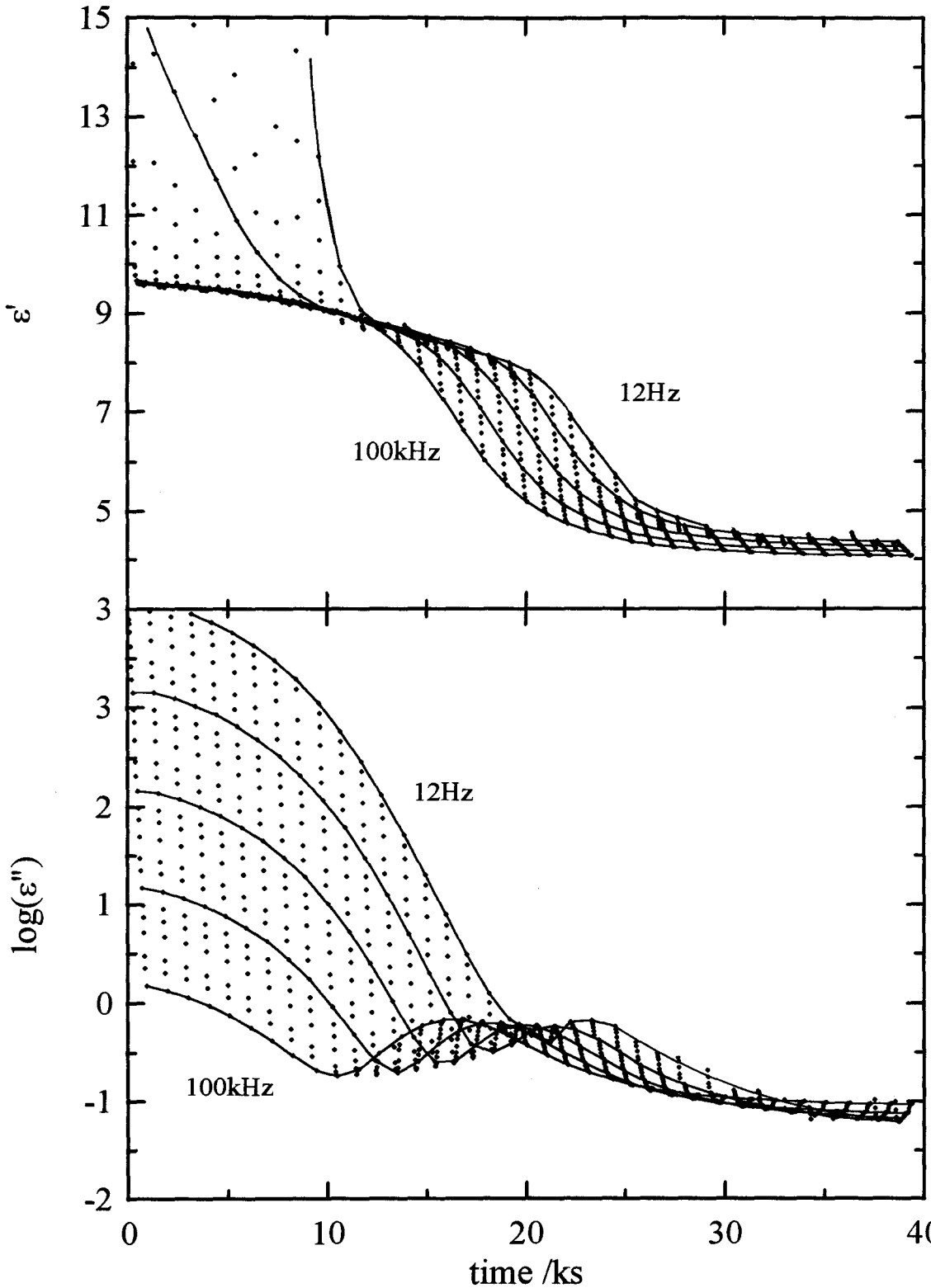

Figure 3.13: The permittivity, ε', and loss, ε" plotted as a function of reaction time for the isothermal polymerization of Tactix-3CA at 360.6K at measurement frequencies listed in the text.

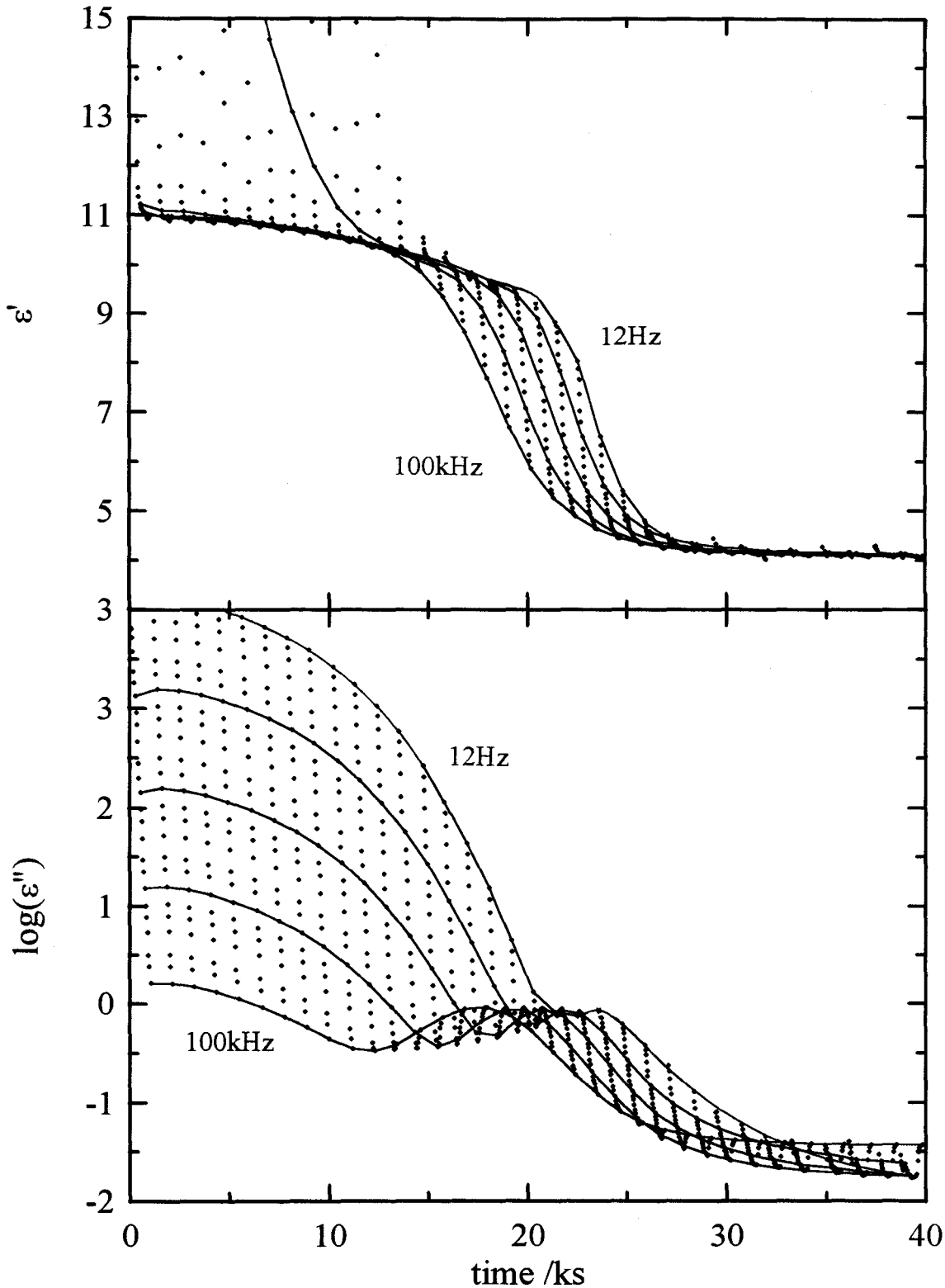

Figure 3.14: The permittivity, ε', and loss, ε'' plotted as a function of reaction time for the isothermal polymerization of Tactix-4CA at 349.5K at measurement frequencies listed in the text.

decreases slowly with increasing t, goes through an inflection point, then decreases gradually toward a limiting value as $t \rightarrow \infty$. For increasing values of the measurement frequencies, the point of inflection shifts to earlier times. The initial value of ε' at $t \rightarrow 0$ decreases toward a limiting value with an increase in the measurement frequency. All the curves for the various measurement frequencies approach a single limiting value, $\varepsilon'(t \rightarrow \infty)$, as t approaches infinity. $\varepsilon'(t \rightarrow \infty)$ for Tactix-AN is 4.1, for Tactix-3CA is 4.1 and for Tactix-4CA is 4.8. The limiting value as t approaches zero, denoted by $\varepsilon'(t \rightarrow 0)$, for Tactix-AN is 8.5, for Tactix-3CA is 9.6 and for Tactix-4CA is 11.2.

The dielectric loss, ε'', as seen in Figures 3.12 to 3.14, decreases to a local minimum, increases to a maximum, then ultimately decreases toward a limiting value with increasing t. The height of the initial plateau is observed to decrease, and the positions of the minimum and maximum in ε'' shift to earlier times, with an increase in the measurement frequency. The limiting value of ε'' with $t \rightarrow \infty$ increases with a decrease in the measurement frequency except in certain circumstances. Reasons for which will be given in Section 4.2.4.

From the plots in Figures 3.12 to 3.14, ε' and ε'' were determined for several fixed instants of time as a function of frequency. This was done by using ε' and ε'' data at adjacent times to linearly interpolate for values at specific values of constant time, t. This gave ε' and ε'' spectra at different instants of time during the reaction. Since the number of measured ε' and ε'' was large and interpolation done from close intervals of data points, the errors associated with the interpolation were negligible in comparison with the

measurement uncertainties. The reaction time at which the spectrum was thus obtained was converted to the number of bonds formed, N(t), using the data plotted in Figures 3.8 to 3.10. Figure 3.15 shows this ε' and ε'' spectra at different N(t) during the polymerization of Tactix-AN. The N(t) values for each of the curves in Figure 3.15 are, from right to left , N(t) = 2.92, 3.16, 3.46, 3.71, 3.89, 4.06 and 4.25 $x10^{23}$. The time-invariant spectra against frequency for Tactix-3CA are shown in Figure 3.16, with N(t) = 3.46, 3.71, 3.89, 4.06, 4.25, 4.41, 4.58 and 4.74 $x10^{23}$, and for Tactix-4CA, in Figure 3.17 for N(t) = 3.46, 3.71, 3.89, 4.06, 4.25, 4.41, 4.58 and 4.74 $x10^{23}$.

3.2.2 The Temperature Dependence of the Dielectric Properties During Polymerization

The complex dielectric permittivity, $\varepsilon^*(t,\omega,T)$, was measured as a function of temperature for a heating rate of 1K/min for the unreacted mixtures, Tactix-AN, Tactix-3CA and Tactix-4CA, as the temperature of the mixtures were increased from 100K to 450K. For this purpose, the mixtures were cooled to the starting temperature immediately after thorough mixing, ensuring that no or negligible chemical reactions between the epoxy and curing agent molecules occurred. Figures 3.18, 3.19 and 3.20 show ε' and ε'' for Tactix-AN, Tactix-3CA and Tactix-4CA, respectively.

ε' in the above-mentioned figures initially increases slowly, then increases sharply to a maximum with an increase in the temperature. From there, ε' decreases steadily towards a point of inflection followed by a sharp decrease with an increase in the

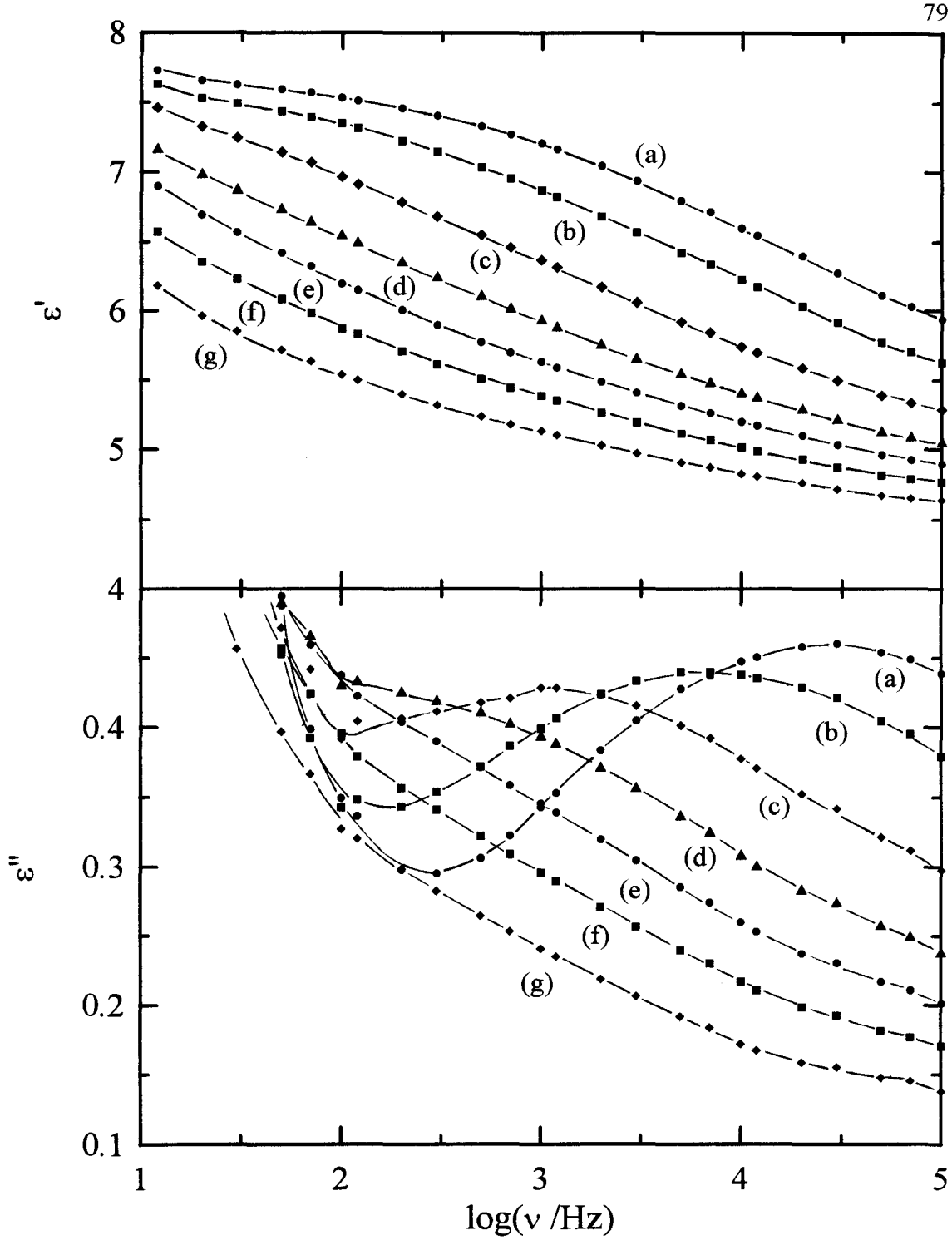

Figure 3.15: ε' and ε" plotted against the log of frequency for fixed reaction times, or equivalently, fixed number of bonds, for the isothermal polymerization of Tactix-AN at 332.0K. The curves correspond to N(t) = (a) 2.92, (b) 3.16, (c) 3.46, (d) 3.71, (e) 3.89, (f) 4.06 and (g) 4.25 $x10^{23}$.

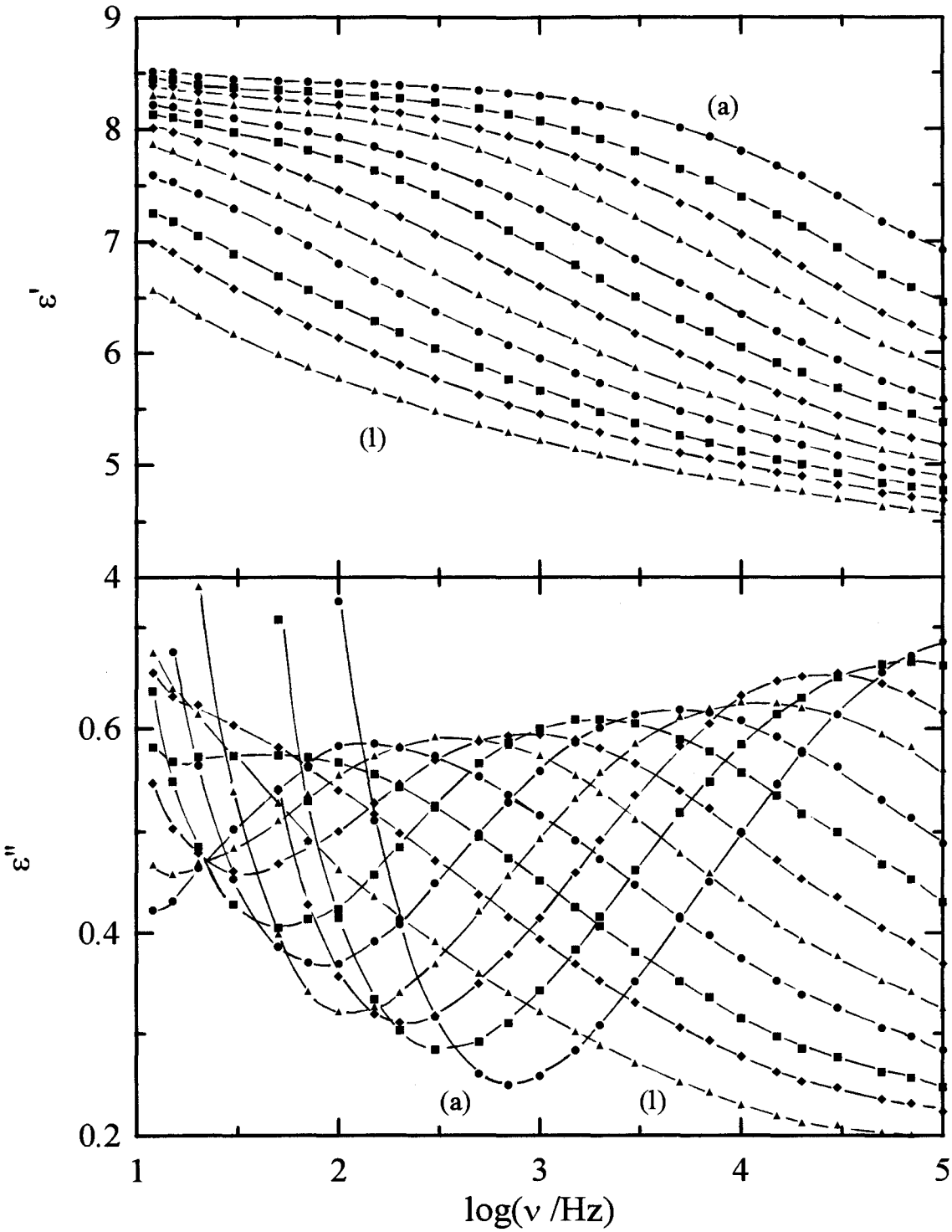

Figure 3.16: ε' and ε" plotted against the log of frequency for fixed reaction times, or equivalently, fixed number of bonds, for the isothermal polymerization of Tactix-3CA at 360.6K. The curves correspond to N(t) = (a) 3.46, (b) 3.71, (c) 3.89, (d) 4.06, (e) 4.25, (f) 4.41, (g) 4.58, (h) 4.74, (i) 4.90, (j) 5.06, (k) 5.19 and (l) 5.38 $x10^{23}$.

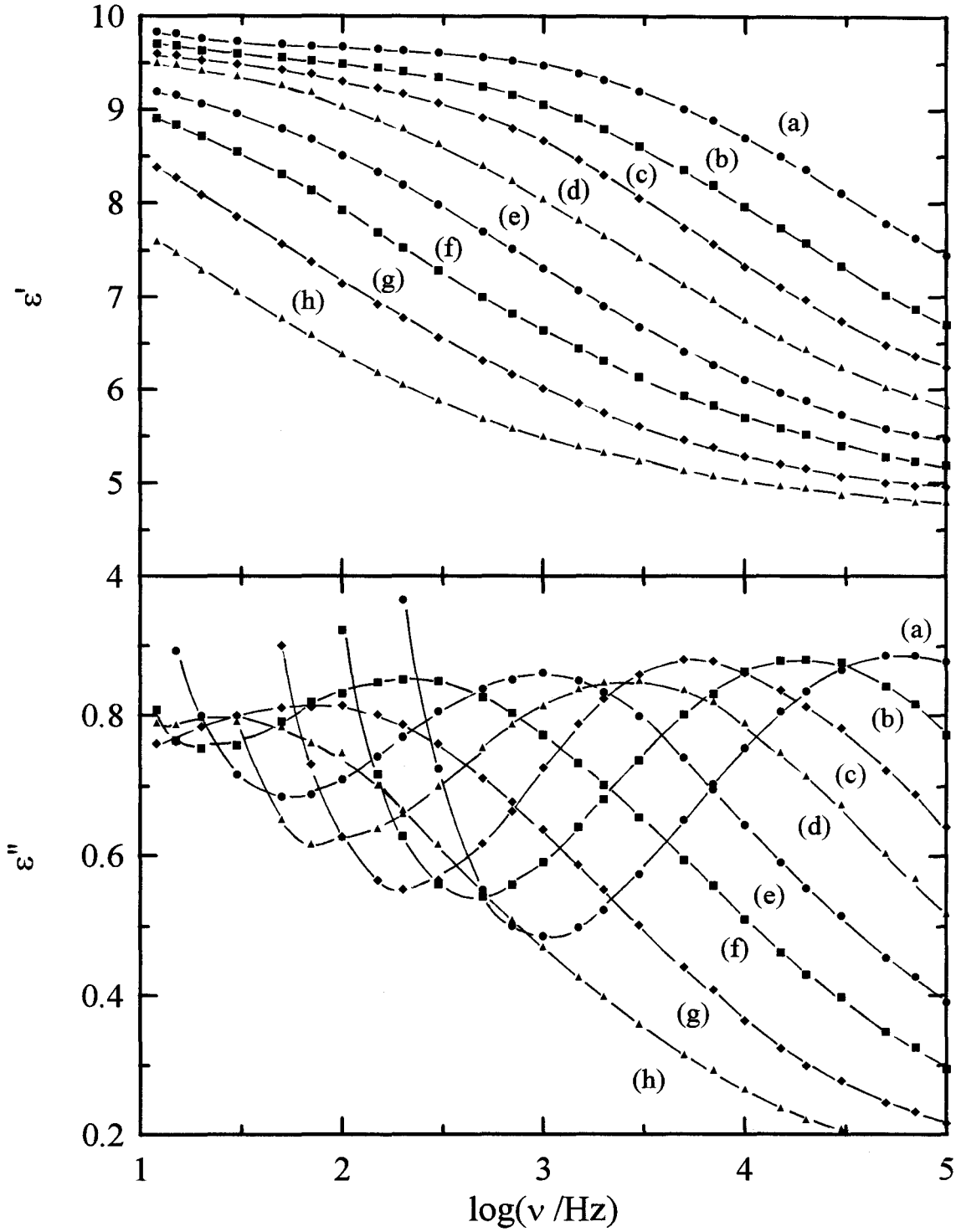

Figure 3.17: ε' and ε" plotted against the log of frequency for fixed reaction times, or equivalently, fixed number of bonds, for the isothermal polymerization of Tactix-4CA at 349.5K. The curves correspond to N(t) = (a) 3.46, (b) 3.71, (c) 3.89, (d) 4.06, (e) 4.25, (f) 4.41, (g) 4.58 and (h) 4.74 $x10^{23}$.

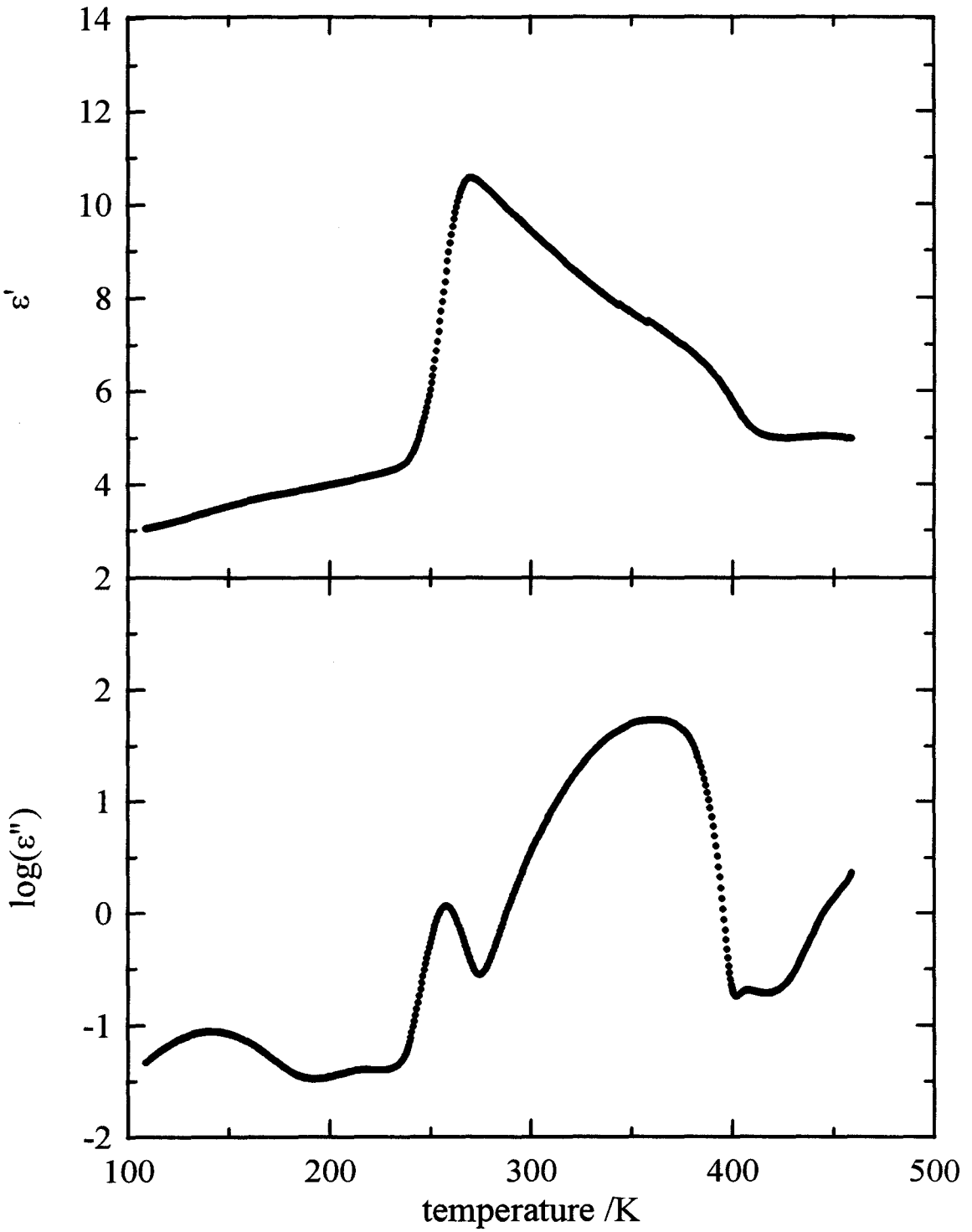

Figure 3.18: ε' and ε" plotted against temperature at a heating rate of 1K/min for the initially unreacted Tactix-AN at a measurement frequency of 1kHz.

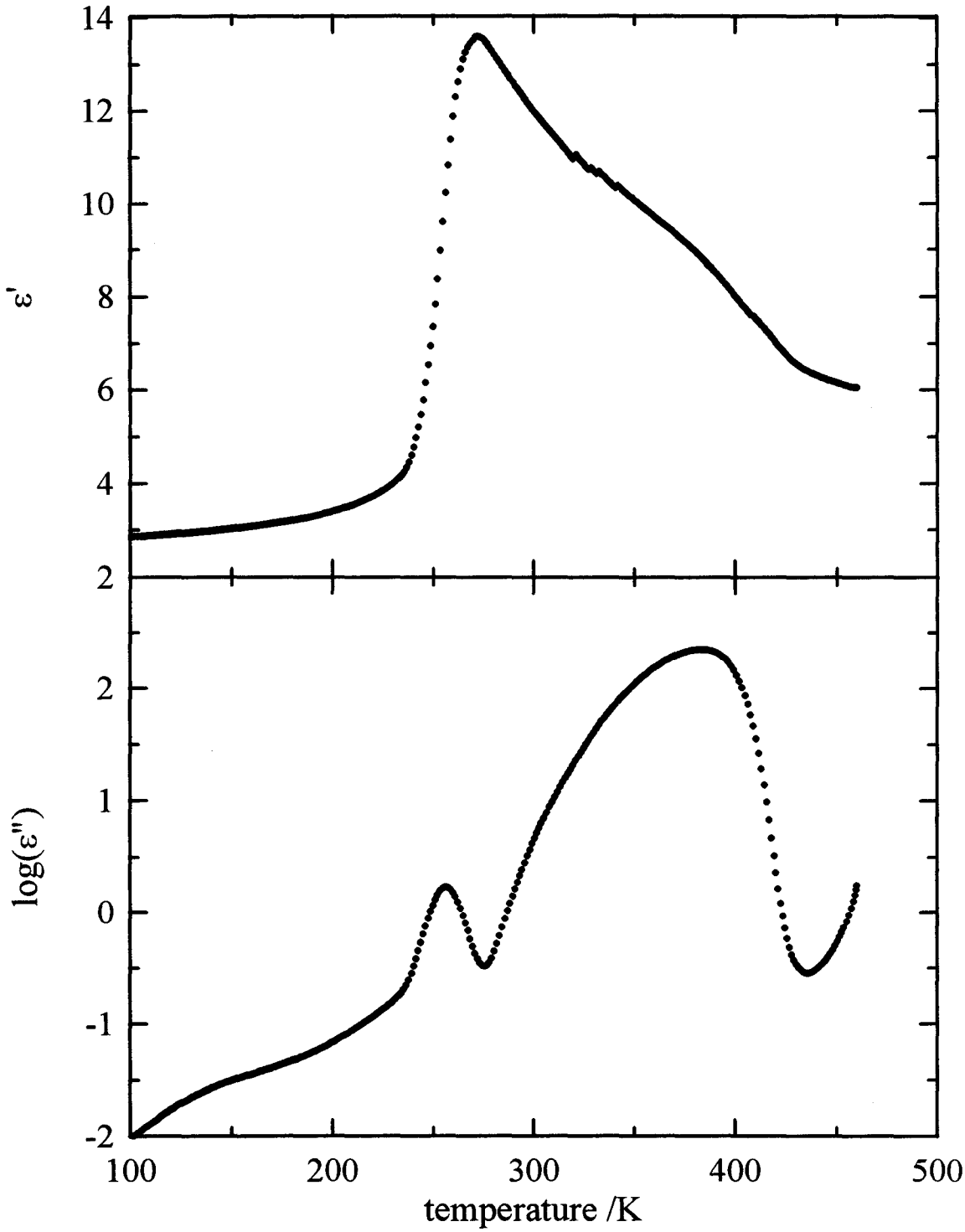

Figure 3.19: ε' and ε" plotted against temperature at a heating rate of 1K/min and a measurement frequency of 1kHz for the initially unreacted Tactix-3CA.

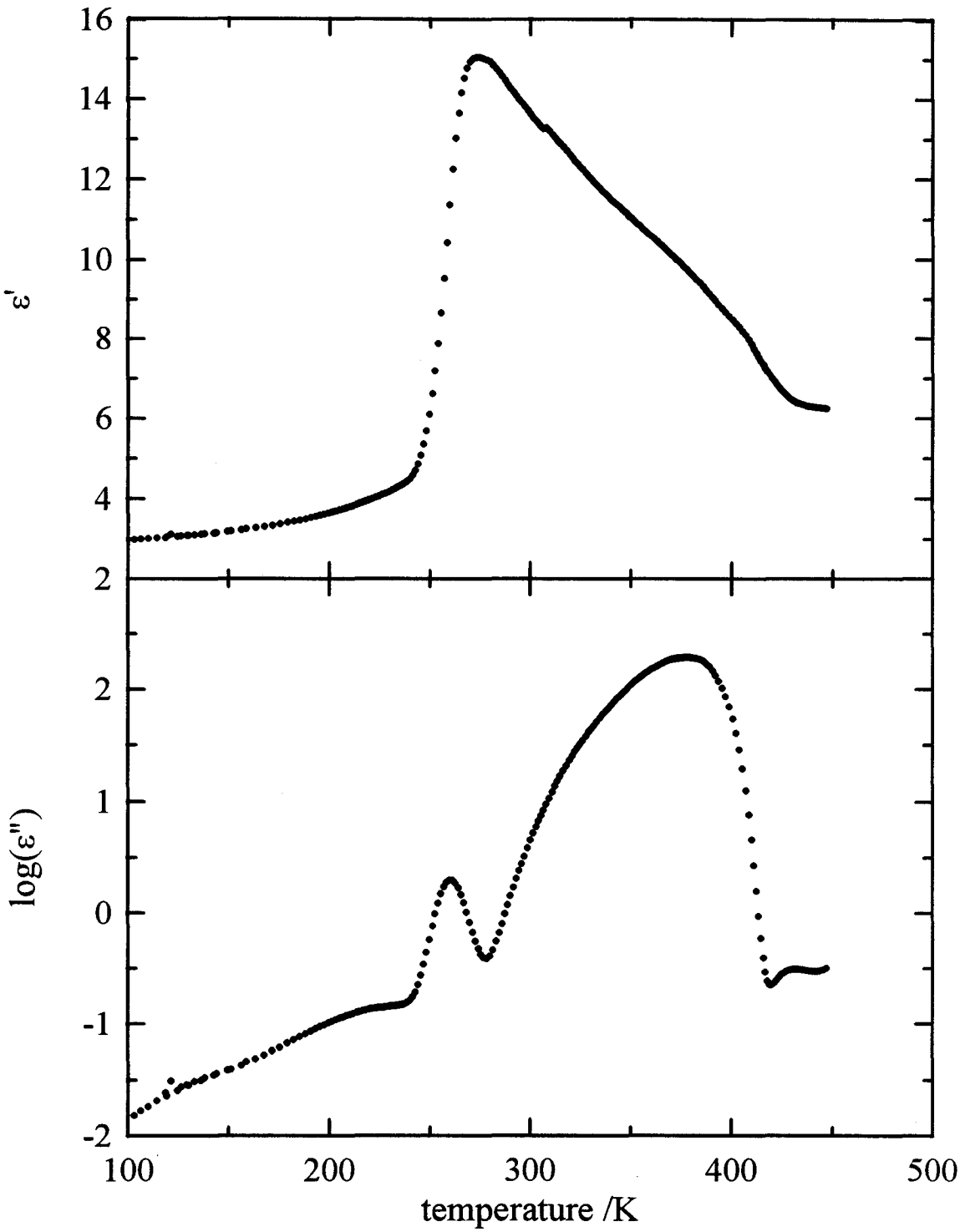

Figure 3.20: ε' and ε" plotted against temperature at a heating rate of 1K/min and a measurement frequency of 1kHz for the initially unreacted Tactix-4CA.

temperature, then approaches a constant value. The rapid increase in ε' with the temperature is due to the dipolar relaxation of the unreacted monomer mixture. The high temperature, limiting value of ε' for Tactix-AN is about 5.1, for Tactix-3CA is 5.7 and for Tactix-4CA is 6.1.

ε" in Figures 3.18 to 3.20 initially increases slowly, then rapidly, to a local maximum with the temperature. It then decreases rapidly to a local minimum, increases towards a larger maximum than the last, and finally decreases to a minimum with an increase in the temperature. The first peak in ε" is due to the dipolar relaxation of the unreacted monomeric mixture. The temperature at which this peak appears for Tactix-AN is approximately 258K. The corresponding peak for Tactix-3CA and Tactix-4CA occurs at 256K and 260K, respectively. ε" in Figure 3.18 shows two more peaks occurring at temperatures lower than the aforementioned relaxation peaks for Tactix-AN. These peaks are due to sub-T_g relaxation processes of the monomeric mixture and are not investigated further here, although their origins will be discussed in Chapter 5. ε" from Figures 3.18 and 3.20 show one further small peak on increasing the temperature above 380K. This is due to the dipolar relaxation in the mixtures after they became partially polymerized.

3.3 Mechanical Relaxation Studies

3.3.1 The Temperature Dependence of The Shear Modulus

The real and imaginary components, G' and G", respectively, of the complex shear modulus, $G^*(\omega,T)$, at a measurement frequency of 1Hz, are plotted as functions of

temperature in Figure 3.21, 3.22 and 3.23 for Tactix-AN, Tactix-3CA and Tactix-4CA, respectively. For the three polymers, the storage modulus, G', decreases gradually with an increase in the temperature. Thereafter it decreases rapidly, passes through an inflection point, then ultimately levels off to a slowly increasing value with an increase in the temperature. At the low and high temperature limits, G' approaches a constant value. G_U, the low temperature limit of G', shown in Figures 3.21, 3.22 and 3.23 is approximately 1.55GPa, 1.43GPa and 1.42GPa for Tactix-AN, Tactix-3CA and Tactix-4CA, respectively. Similarly, G_R, the high temperature limit of G', is approximately 8.8MPa for Tactix-AN, 6.6MPa for Tactix-3CA and 11.1MPa for Tactix-4CA. G_U is more than 100 times G_R for the three thermosets of this work.

The loss modulus, G", as seen in Figures 3.21 to 3.23, increases slowly with temperature initially before rapidly increasing to a peak value, $G"_{max}$, at a temperature T_{max}. G" then decreases rapidly before slowly decaying toward a limiting value with an increase in the temperature. This peak in G" is associated with the mechanical α-relaxation process of the polymer. The height of the G" peak is approximately 120MPa for Tactix-AN, 120MPa for Tactix-3CA and 110MPa for Tactix-4CA.

3.3.2 The Frequency Dependence of The Shear Modulus

The mechanical shear modulus was monitored at varying oscillation frequencies for fixed temperatures of measurement to obtain mechanical spectra. The G' and G" spectra of the complex shear modulus, $G^*(\omega,T)$, are shown in Figures 3.24, 3.25 and 3.26

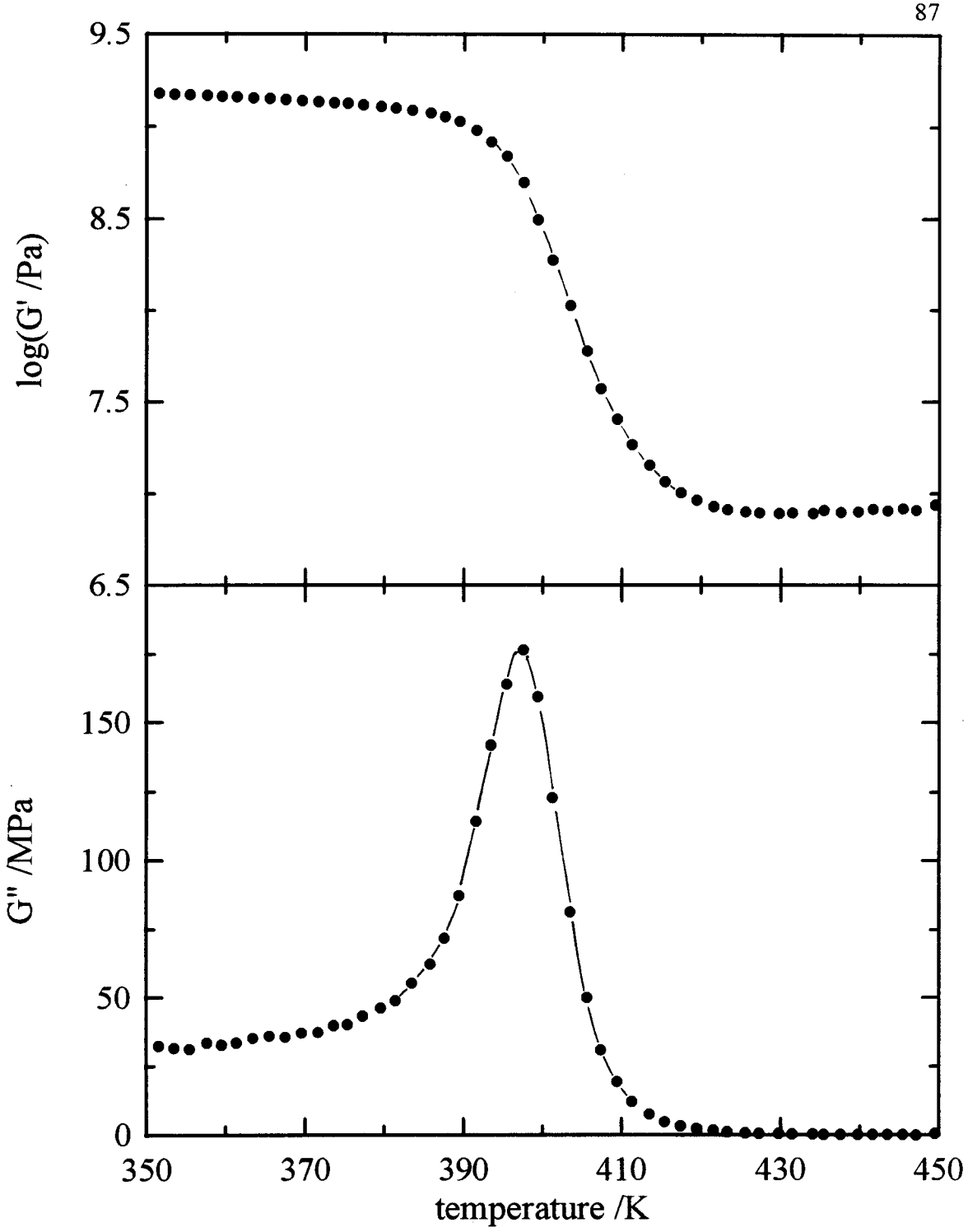

Figure 3.21: The storage modulus, G', and loss modulus, G", plotted against temperature at a heating rate of 1K/min and a measurement frequency of 1Hz for the fully reacted Tactix-AN.

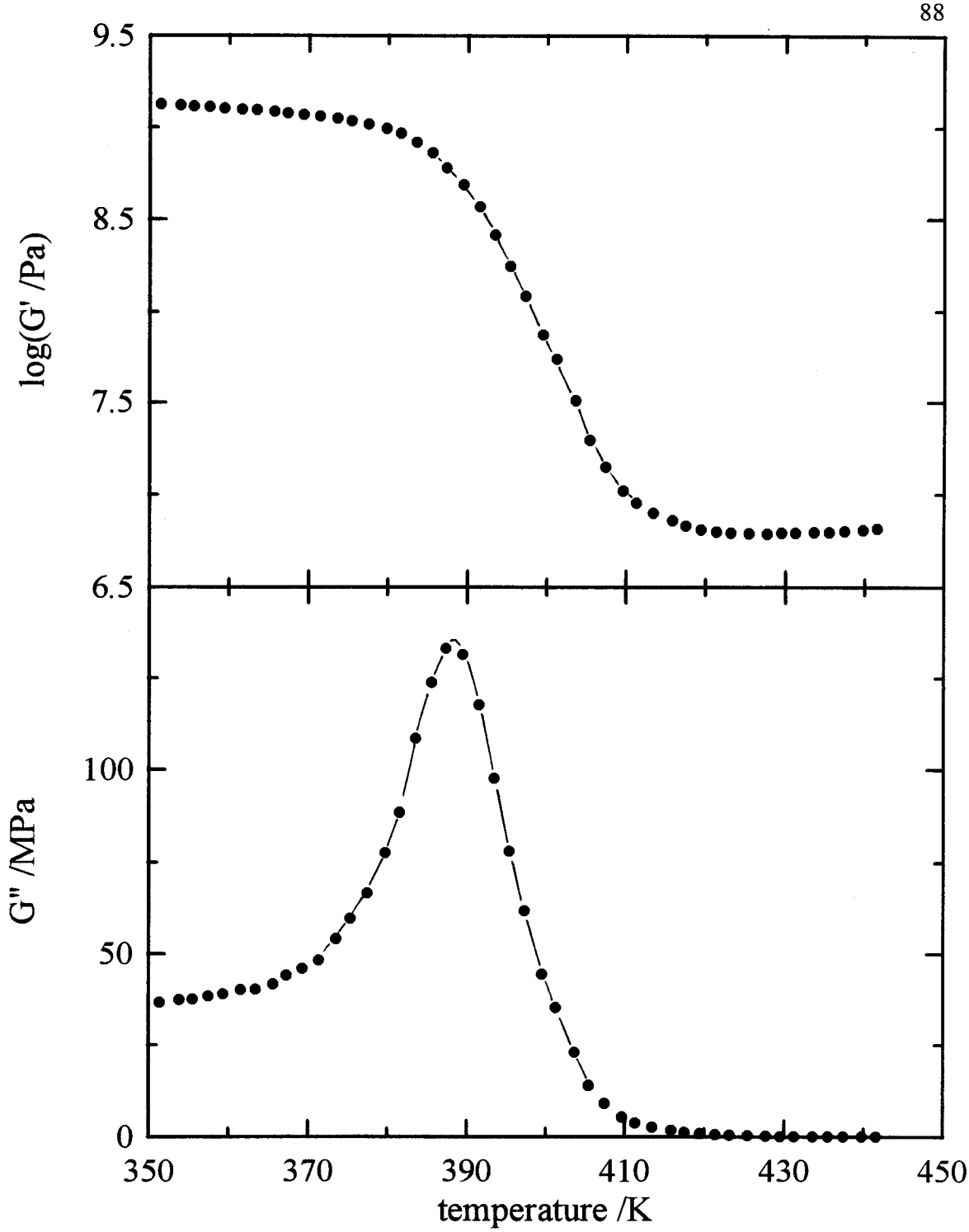

Figure 3.22: The storage modulus, G', and loss modulus, G", plotted against temperature at a heating rate of 1K/min and a measurement frequency of 1Hz for the fully reacted Tactix-3CA.

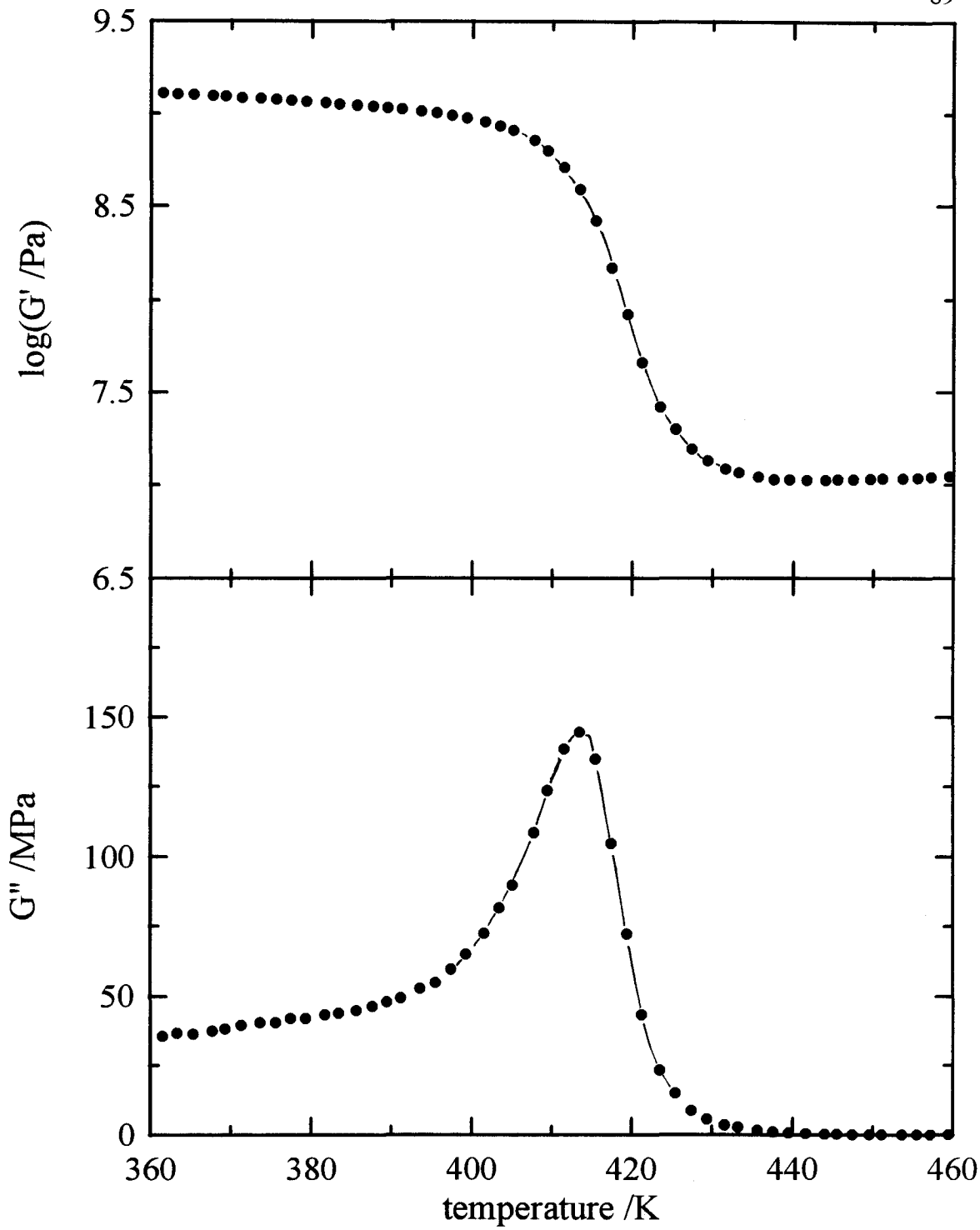

Figure 3.23: The storage modulus, G', and loss modulus, G", plotted against temperature at a heating rate of 1K/min and a measurement frequency of 1Hz for the fully reacted Tactix-4CA.

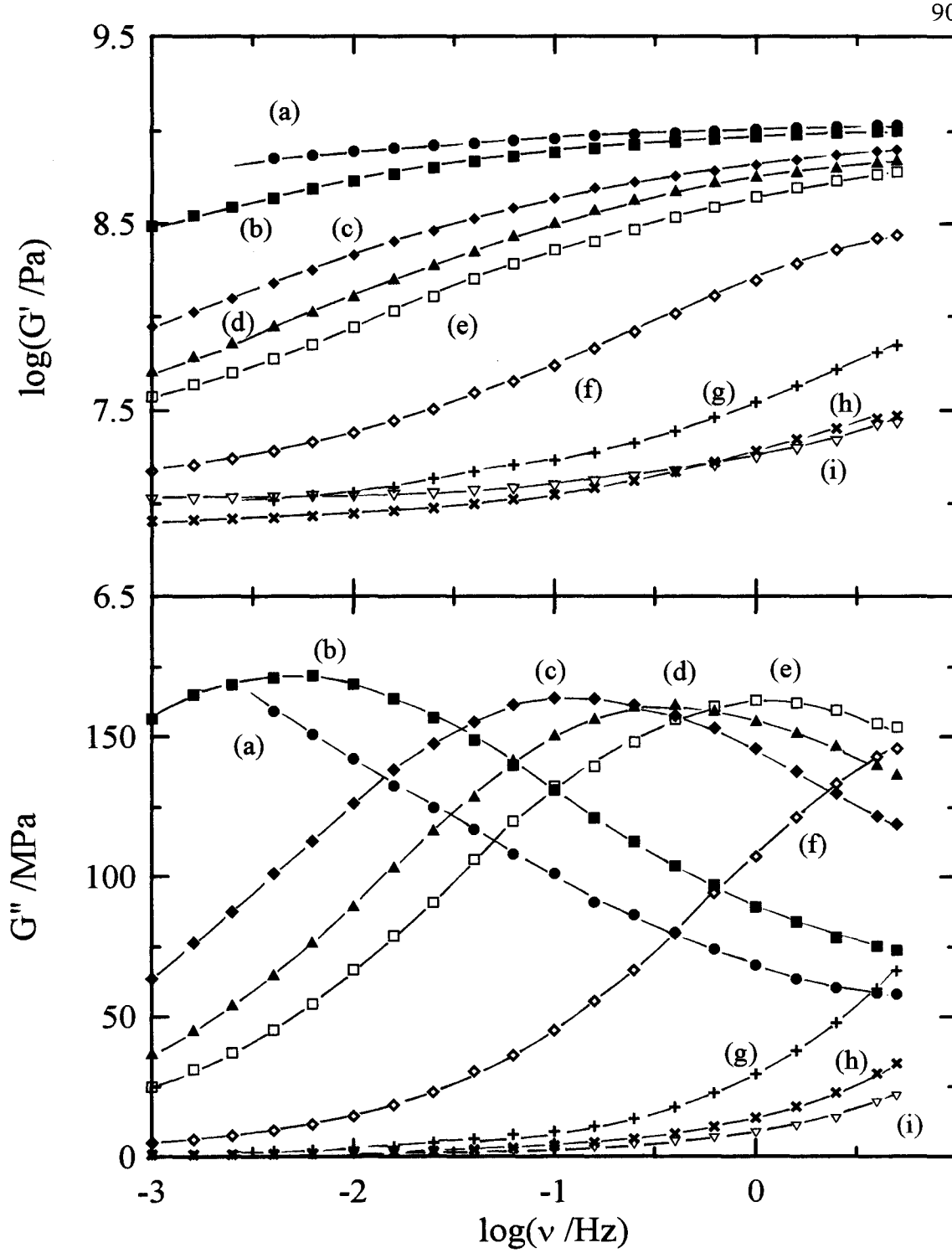

Figure 3.24: G' and G" plotted against the log of frequency for Tactix-AN at the following measurement temperatures; (a) 386.1, (b) 389.8, (c) 393.4, (d) 395.2, (e) 396.2, (f) 401.2, (g) 406.4, (h) 412.0 and (i) 423.0K.

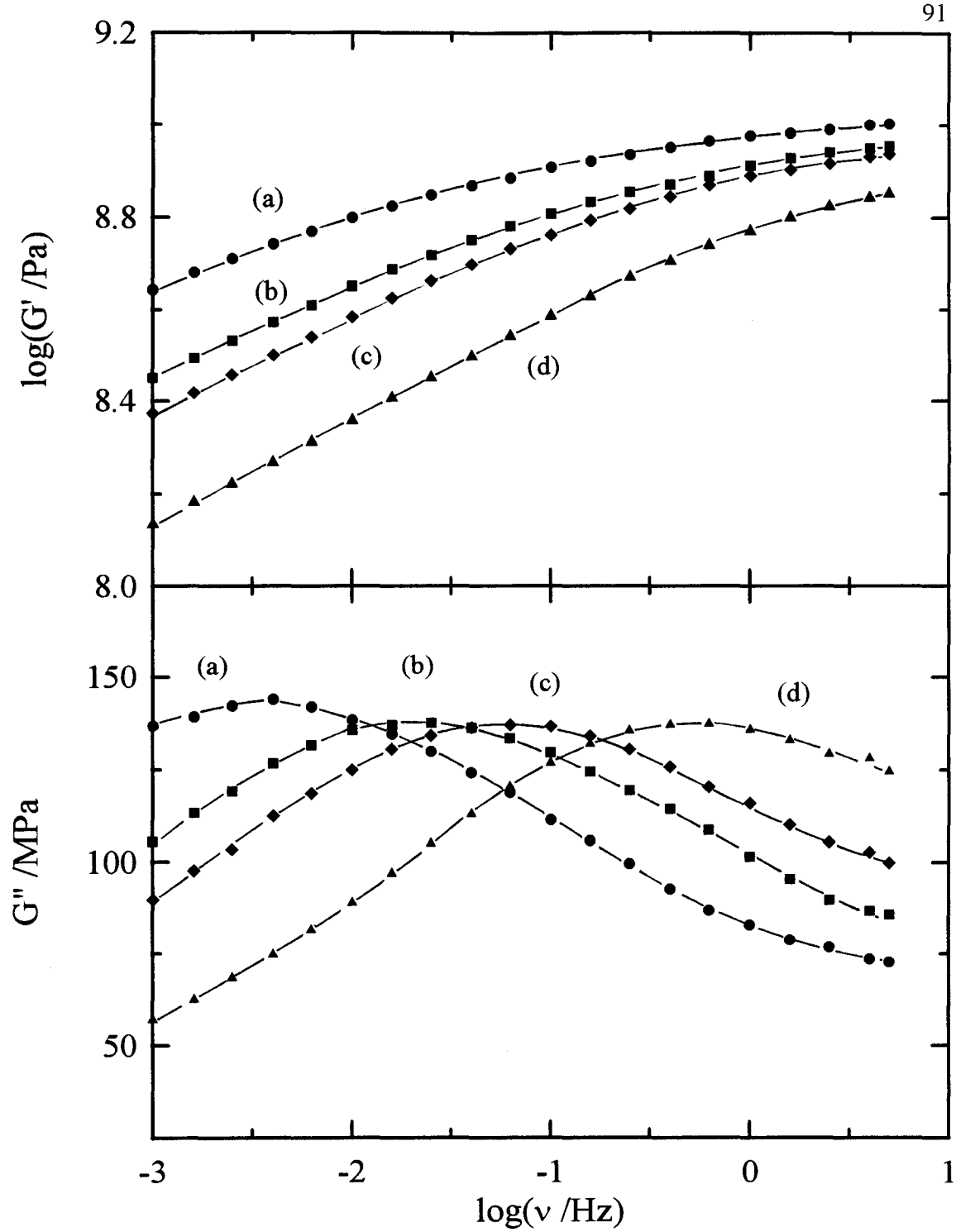

Figure 3.25: G' and G" plotted against the log of frequency for Tactix-3CA at the following measurement temperatures; (a) 380.1, (b) 382.3, (c) 383.5 and (d) 386.2K.

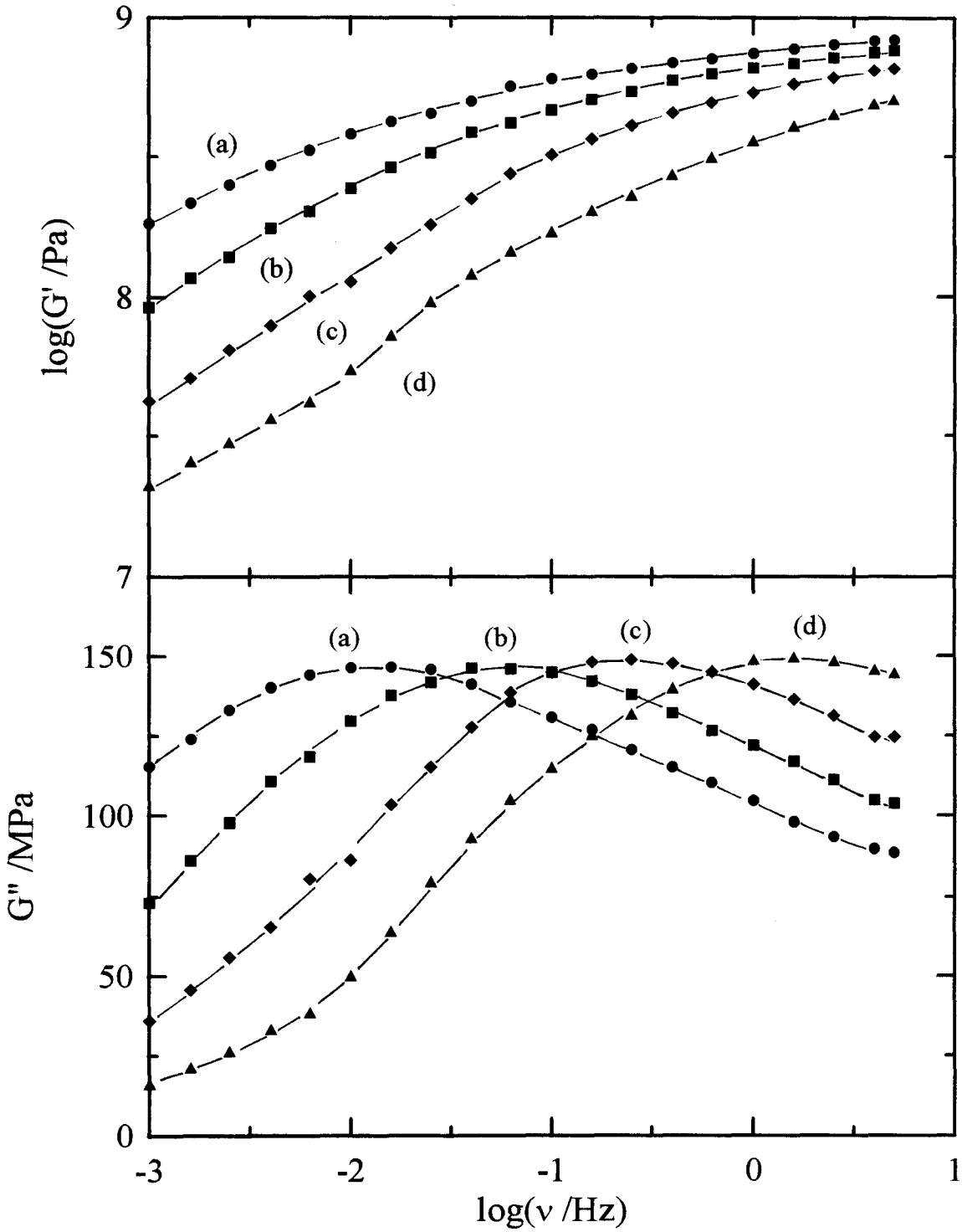

Figure 3.26: G' and G" plotted against the log of frequency for Tactix-4CA at the following measurement temperatures; (a) 407.5, (b) 409.3, (c) 410.7 and (d) 412.6K..

for Tactix-AN, Tactix-3CA and Tactix-4CA, respectively. The spectra shown in Figure 3.24 correspond to measurements made at 386.1K, 389.8K, 393.4K, 395.2K, 396.2, 401.2K, 406.5, 412.0 and 423.1K. Similarly, in Figure 3.25, they are for measurements at 380.1K, 382.3K, 383.5K, and 386.2K, and in Figure 3.26, they are for measurements at 407.5K, 409.3K, 410.7K and 412.6K. Mechanical frequencies for obtaining the spectrum were chosen between 0.001Hz and 5Hz such that they were evenly spaced on a logarithmic scale.

G' for all the polymers initially increases gradually, reaches a point of inflection, then ultimately increases towards a constant value with an increase in the frequency. G' approaches a low-frequency or relaxed modulus, G_R, with decreasing frequency, and a high-frequency or unrelaxed modulus, G_U, with increasing frequency. The points of inflection of each curve shift to higher frequencies with an increase in the measurement temperature. G" initially increases at a steady rate, reaches a peak value, then decreases steadily with increasing frequency, for the three polymers. The positions of the peaks shift to higher frequencies, with an increase in the temperature. The heights of the peaks decrease for Tactix-AN and Tactix-3CA but remained constant for Tactix-4CA, with an increase in the measurement temperature.

CHAPTER IV

DISCUSSION OF THE POLYMERIZATION

4.1 Calorimetric Studies of the Polymerization

The polymerization of the epoxy-monoamines will now be discussed in relation to the extent of reaction measured by the heat evolved, i.e. by calorimetry, and then in relation to changes that occurred in the dielectric properties.

A review of the use of differential scanning calorimetry, DSC, for determining the polymerization kinetics of thermosets was recently provided by Barton (1985). He compared the various equations used with both the isothermal and ramp polymerization measurements, and Wasserman and Johari (1993, 1994) reexamined the applicability of the formalisms. It was shown that, when the primary and secondary amines are of approximately equal reactivity,

$$\frac{\partial \alpha}{\partial t} = (K_1 + K_2 \alpha^{\overline{m}})(1 - \alpha)^{\overline{n}} \qquad (4.1)$$

can be used to fit the data measured during the isothermal polymerization by addition reactions. Here, α is the extent of reaction, K_1, and K_2, are constants related to the rate constants of the two reactions, which were discussed by Horie et al. (1970), and $\overline{m}$ and $\overline{n}$ are empirical parameters. In several other studies of the curing kinetics of diglycidyl

ether of biphenyl-A (DGEBA) diamine thermosets, Barton found that $\overline{m}$ was equal to 1 and $\overline{n}$ = 2. With these values of $\overline{m}$, $\overline{n}$ and Equation (4.1), the reduced rate, r, is then given by,

$$r = \frac{\partial \alpha}{\partial t}(1-\alpha)^{-2} = K_1 + K_2\alpha \qquad \textbf{(4.2)}$$

Equation (4.2) means that a plot of r against α(t) should be a straight line with slope K_2 and intercept K_1.

The total heat of reaction, ΔH_{total}, was calculated in two ways in this study, specifically, first by measuring $(dH/dt)_T$ during isothermal polymerization, followed by measuring $(dH/dt)_q$ during heating at a constant rate and second, by measuring $(dH/dt)_q$ during heating of the unreacted mixture at a constant heating rate during ramp-polymerization. In this study, the ΔH_{total} obtained by the two methods differed by less than 6%, so the deviations between the plots of α against time obtained by either of the two values of ΔH_{total} were at most 6%, which is neglected here. The ΔH_{total} used in the calculation of α here was obtained by the first of the two methods mentioned above.

As mentioned in Section 3.1.2, the final plateau value of $(dH/dt)_T$ in Figures 3.3 and 3.4 is less than the initial value at the start of the reaction. This can be attributed to the lower heat capacity, C_p, of the final, partially polymerized mixture, as compared to the C_p of the initial, monomeric liquid. The lower heat capacity means that less power is required by the DSC to maintain the sample at the isothermal temperature of the measurement. This is seen as a lower $(dH/dt)_T$ value at long reaction times after a

significant amount of heat has been evolved from the chemical reactions.

The kinetics of temperature ramp polymerization by DSC can be obtained by a method given by Barrett (1967). In this case, the fractional conversion up to a certain temperature, T, is given by,

$$\alpha(T) = \frac{1}{\Delta H_{ramp}} \int_{T_1}^{T} \frac{\partial \Delta H}{\partial T} dT \qquad (4.3)$$

Here, ΔH_{ramp}, the total heat of reaction, is calculated by integrating the area of the $(dH/dt)_q$ plot for the unreacted liquid to a polymeric material from an initial temperature, T_1, to a temperature, T_2, where no more heat is evolved. The plots of $\alpha(T)$ against T are given in Figure 4.1 for Tactix-AN, Tactix-3CA and Tactix-4CA. Using Equation (4.3), Barrett (1967) showed that the rate of conversion , $\partial\alpha/\partial t$, can be expressed as,

$$\frac{\partial \alpha(T)}{\partial t} = A f(\alpha) \exp\left(\frac{-E_\alpha}{RT}\right) \qquad (4.4)$$

where E_α is the activation energy for the chemical reactions assumed to be the same for reactions of the primary or secondary amines, and $f(\alpha)$ is a function of α, which has been found by several other studies (Souror and Kamal 1976, Horie et al. 1970, Barrett 1967, Charlesworth 1980, Grenier-Loustalot and co-workers 1987, 1988) to be of the form $f(\alpha) = (1 - \alpha)^2$. Substitution of $f(\alpha)$ into Equation (4.4) and solving for the reduced rate, r, gives,

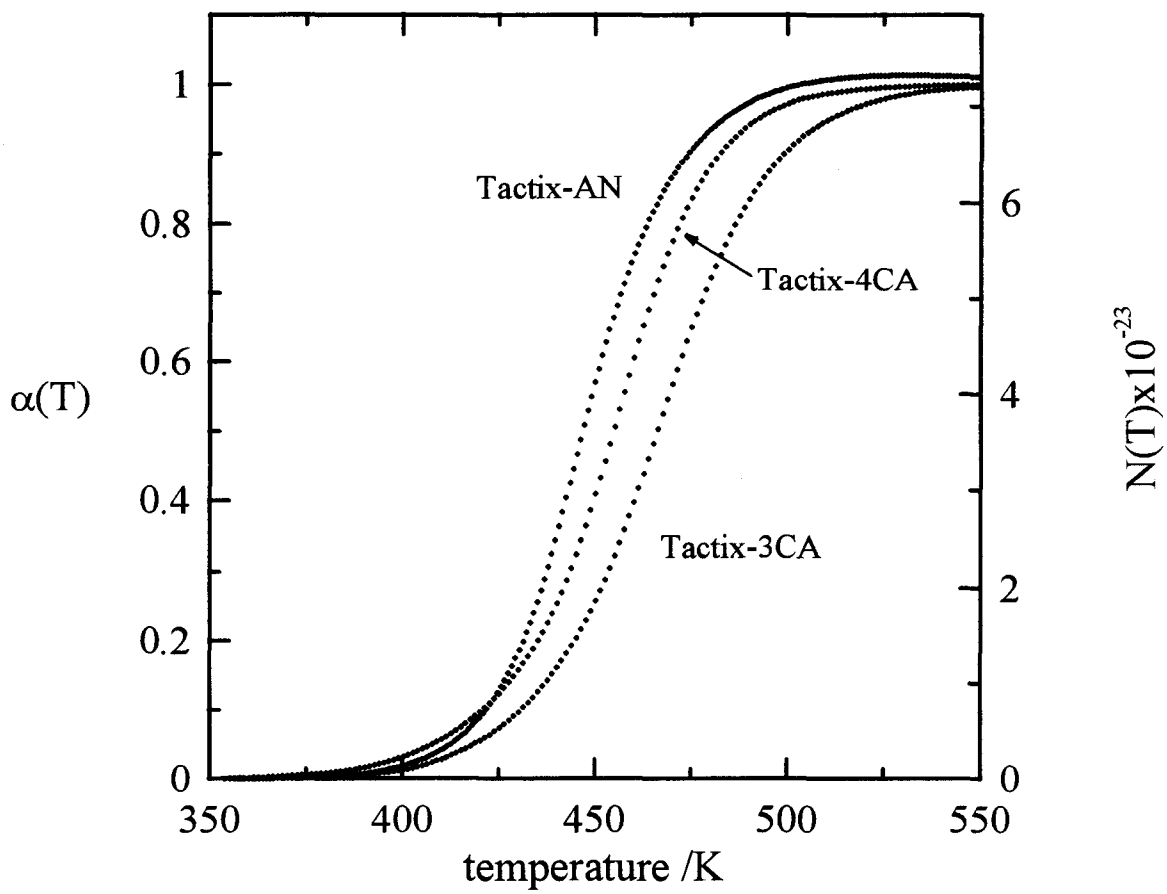

Figure 4.1: The fractional conversion, $\alpha(T)$, and the number of bonds formed, N(T), plotted against temperature for the initially unreacted Tactix-AN, Tactix-3CA and Tactix-4CA heated at a rate of 10K/min. Note that the left most axis measures $\alpha(T)$ and the right most measures N(T).

$$\ln(r) = \ln\left((\partial\alpha(T)/\partial t)(1-\alpha(T))^2\right) = \ln A - E_A/RT \qquad \textbf{(4.5)}$$

Equation (4.5) defines a straight line for a plot of ln(r) against 1/T with a slope, $-E_A$ and intercept, lnA.

4.1.1 The Kinetics During Isothermal Polymerization

We first discuss the polymerization of Tactix-742 with each of the three amines in terms of the previously given formalisms. The usefulness of Equations (4.1) and (4.2) as a description of the calorimetric data obtained during isothermal polymerization has been the subject of recent reviews. These reviews have been based on the fitting of data to Equation (4.1) with $\overline{m}$ and $\overline{n}$ as adjustable parameters. Horie et al. (1970) found $\overline{m}$ = 1 and $\overline{n}$ = 2. The results have been confirmed by the recent analysis by Riccardi and co-workers (1984 and 1986) for the DGEBA-ethylenediamine (EDA) thermoset and by several other workers (Charlesworth 1980, Grenier-Loustalot and co-workers 1987, 1988) who used chemically different thermosets. Barton (1985) showed that $\overline{m} = \overline{n} = 1$ with the assumption that the rate-determining step is the autocatalyzed reaction of a rapidly formed complex of the epoxy and diamine. However, other studies (Ryan and Dutta 1979, Foun et al. 1984, Mijovic, Kim and Slaby 1984, Mijovic 1986, Moroni et al. 1986) observed that, although $\overline{m} + \overline{n} = 2$, $\overline{m}$ varies with temperature, and in particular, Ryan and Dutta (1979) showed that $\overline{m}$ increases from 0.6 to 1.2 with increasing temperature. Thus, both

$\overline{m}$ and $\overline{n}$ can have fractional values, and that an increase in the magnitude of one causes a decrease in that of the other. More recently, Carrozzino et al (1990) observed that $\overline{n}$ for DGEBA-EDA thermosets may be within 1 and 1.5 while $\overline{m} = 1$.

In an alternative approach, Mijovic and co-workers (1984, 1986), found that $\overline{m}$ varies with α, and increases from 0.5 to 0.7, reaches a maximum, and thereafter decreases with an increase in the polymerization temperature. Its value was interpreted as a measure of the kinetics of the subsequent step addition reactions that followed the autocatalytic nature of the chemical reactions that occurred initially. They found that the exponent $\overline{n}$ also varied from 1.1 to 1.3.

Although Equations (4.1) and (4.2) and the parameters $\overline{m}$ and $\overline{n}$ are based on the assumption that the reactions follow first- or second-order autocatalytic reaction kinetics, several authors (Enns and Gillham 1983, Wisanrakkit, Gillham and Enns 1987, Kim and Kim 1987, Glover, Duffy, Hartmann 1988, Spacek, Poucly and Biros 1987, Flammersheim et al. 1983) proposed that the average order of reaction may be fractional, with a single rate constant. This average fractional order of reactions has been suggested as 1.64 for the DGEBA polymerized with triethylenetetramine (Kim and Kim 1987) and 1.7 for DGEBA cured with bis(p-aminocyclo-hexyl) methane (Enns et al. 1983, Wisanrakkit et al. 1987).

Despite the aforementioned ambiguities in the validity of Equations (4.1) and (4.2), Wasserman and Johari (1994) concluded that α_{vit}, the extent of reaction at vitrification, can be obtained from the plots of r against $\alpha(t)$. This is possible since the rate of

reaction, or $\partial\alpha/\partial t$, approaches zero as the time of vitrification is approached. Thus, in the plots of r against $\alpha(t)$, the value of α_{vit} at r = 0 is formally independent of the numerical value of $\bar{n}$, but not of $\bar{m}$. Figures 4.2, 4.3 and 4.4 show the plots of r against $\alpha(t)$ for Tactix-AN, Tactix-3CA and Tactix-4CA, respectively. The values of α_{vit} thus calculated are 0.754, 0.926 and 0.826, which correspond to the number of bonds formed, 5.45×10^{23}, 6.69×10^{23} and 5.97×10^{23}, for Tactix-AN, Tactix-3CA and Tactix-4CA, respectively. It is appropriate to show that in Figures 4.2, 4.3 and 4.4 for Tactix-AN, Tactix-3CA and Tactix-4CA, the reduced rate does not increase linearly with α over as wide a range as other workers have observed (Souror and Kamal 1976, Horie et al. 1970, Riccardi et al. 1984, 1986) although the initial increase is linear. Clearly, the values of $\bar{m}$ and $\bar{n}$ are not likely to be the same, which means that the primary and secondary amines are not equally reactive. As mentioned above, $\bar{m}$ and $\bar{n}$ are found to be in the range of less than one to two, and have been interpreted as an indication for the forming of H-bonded complexes, and hetero- and auto-complexes of the reactants with the reaction products. One expects that for all cases of this type, the rate constants, K_1 and K_2, would depend on the thermodynamics of complex formation, the rate of diffusion of reactants, and the steric hindrances of the reacting groups. It is possible that a distribution of reaction rates, rather than a single reaction rate process, becomes dominant as α increases, and this dominance causes the experimental data to deviate from the generalized Equation (4.1) (Wasserman and Johari 1993). It is also possible that the variation of $\bar{m}$ and $\bar{n}$ with α itself is one of the sources of discrepancies, as pointed out by Mijovic (1986). These implications need

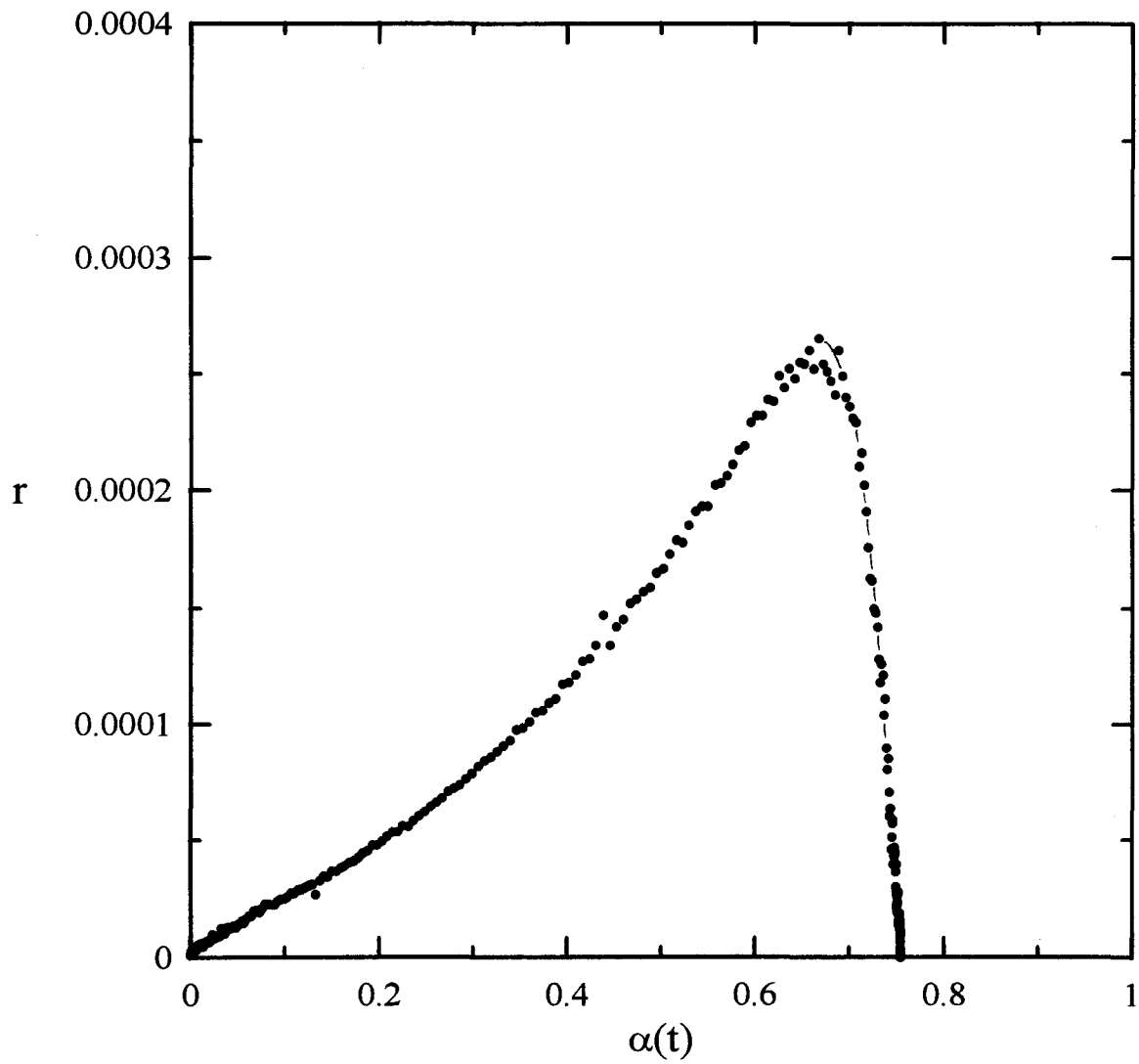

Figure 4.2: The reduced rate, r, plotted against $\alpha(t)$ for the isothermal polymerization of Tactix-AN at 332.0K.

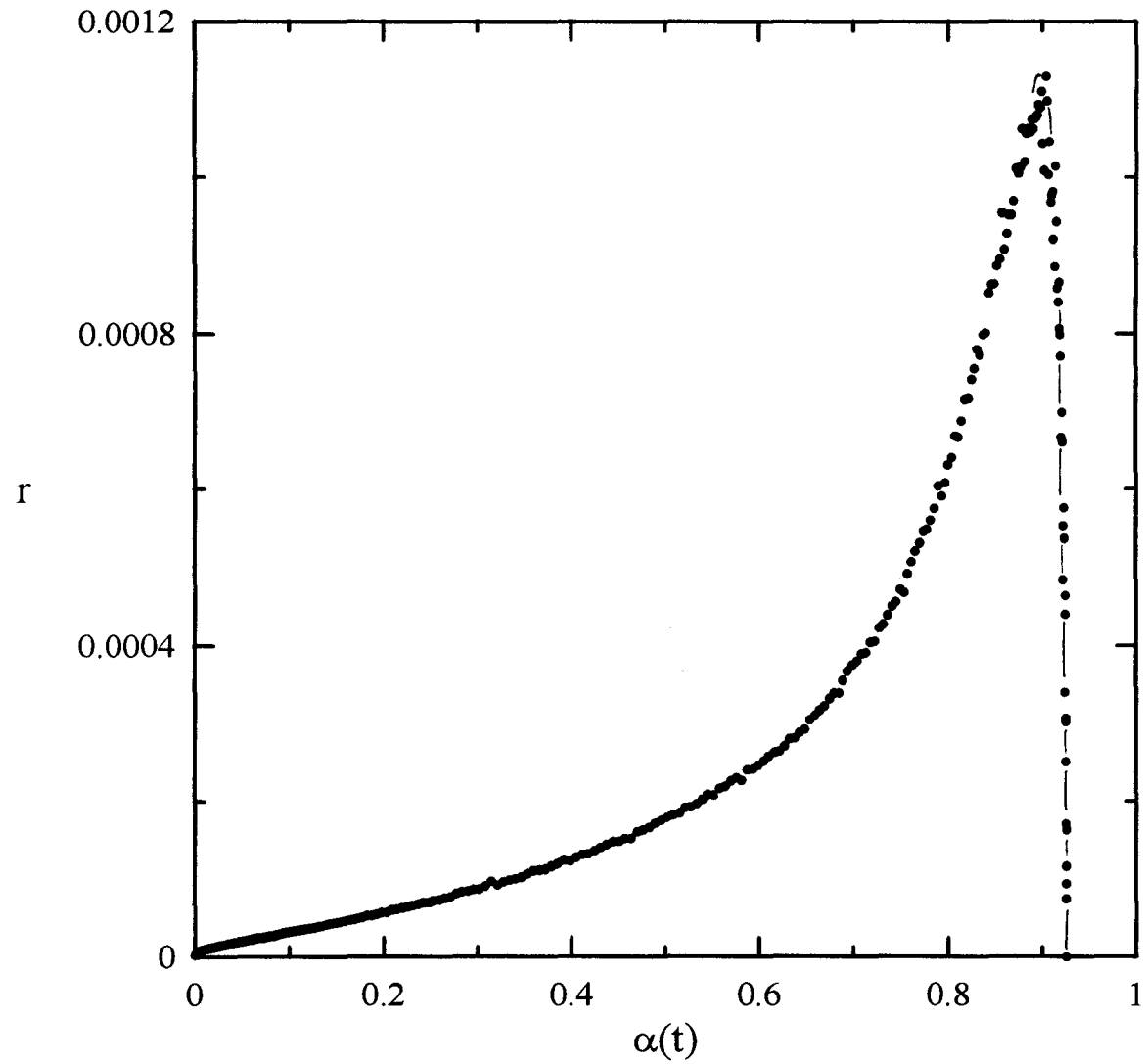

Figure 4.3: The reduced rate, r, plotted against $\alpha(t)$ for the isothermal polymerization of Tactix-3CA at 360.6K.

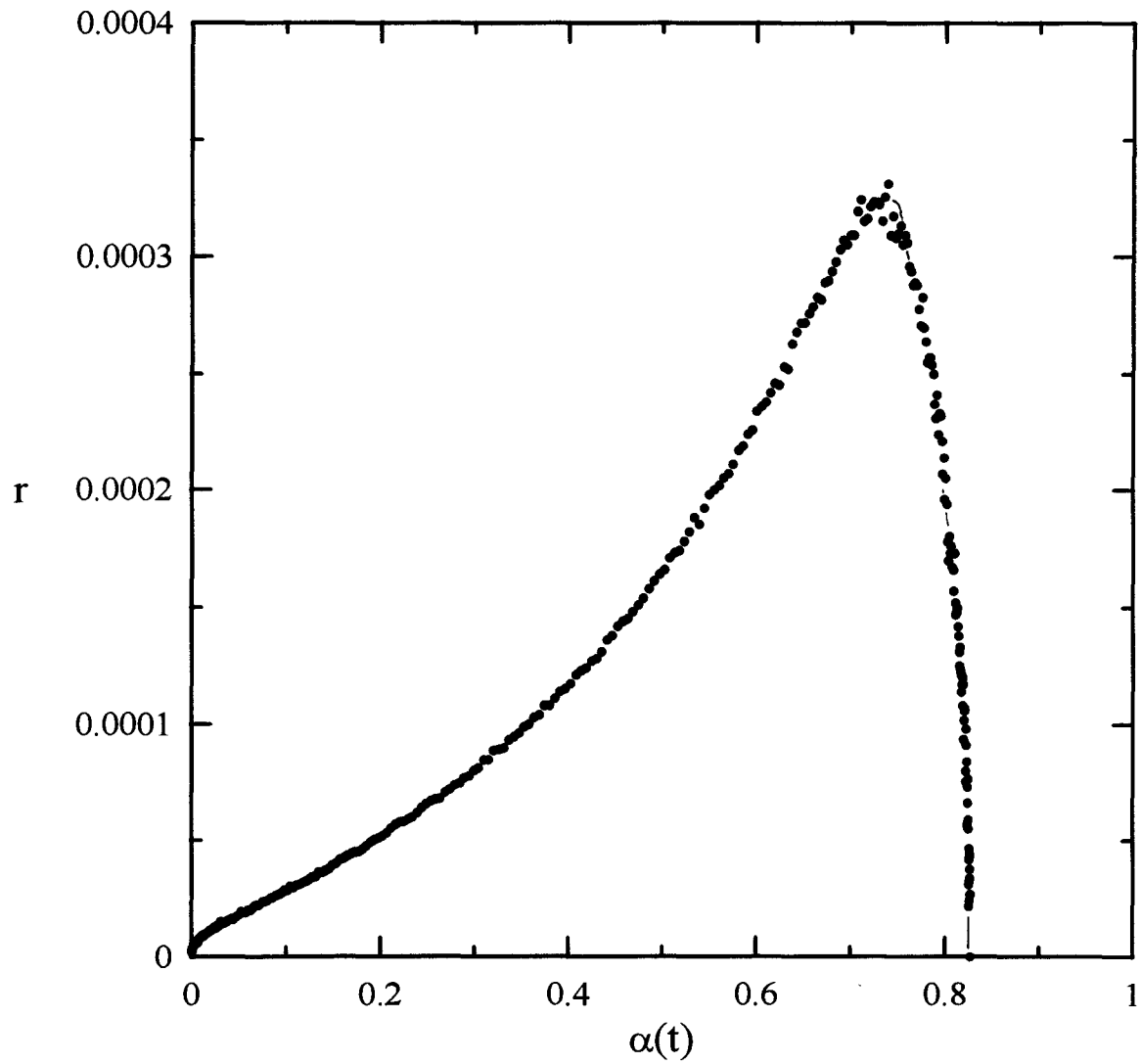

Figure 4.4: The reduced rate, r, plotted against $\alpha(t)$ for the isothermal polymerization of Tactix-4CA at 349.5K.

to be investigated further.

4.1.2 The Kinetics During Temperature-Ramp Polymerization

It is known that the kinetic parameters obtained from ramp-heating in the DSC experiments generally differ from, and are often higher than, the corresponding parameters obtained from isothermal experiments (Souror and Kamal 1976, Horie et al. 1970, Riccardi et al. 1984, 1986). This difference is a reflection of two possible reaction paths, with different kinetic parameters whose relative importance varies with the temperature. These reactions are; (i) non-catalytic, with a higher activation energy, and (ii) autocatalytic, with a lower activation energy. The conclusion is based on the finding that the activation energy, E_A, obtained from the polymerization done at a constant heating rate and Equation (4.5) differs from E_A obtained from the isothermal polymerization at several temperatures (Prime 1973) and using Equation (4.2).

Figures 4.5, 4.6 and 4.7 show the plots of ln(r) against 1/T for tactix-AN, Tactix-3CA and Tactix-4CA, respectively. The activation energies for each of the overall reactions, calculated from the linear portion of the plots and Equation (4.5), is 116.7kJ/mol, 90.1kJ/mol and 88.8kJ/mol for Tactix-AN, Tactix-3CA and Tactix-4CA, respectively. The other parameters calculated from Equation (4.5), $\bar{n}$ and lnA, are as follows; 1.7 and 26.8 for Tactix-AN, 1.5 and 18.34 for Tactix-3CA and 1.4 and 18.61 for Tactix-4CA.

As previously mentioned, for the isothermal polymerization of the three mixtures,

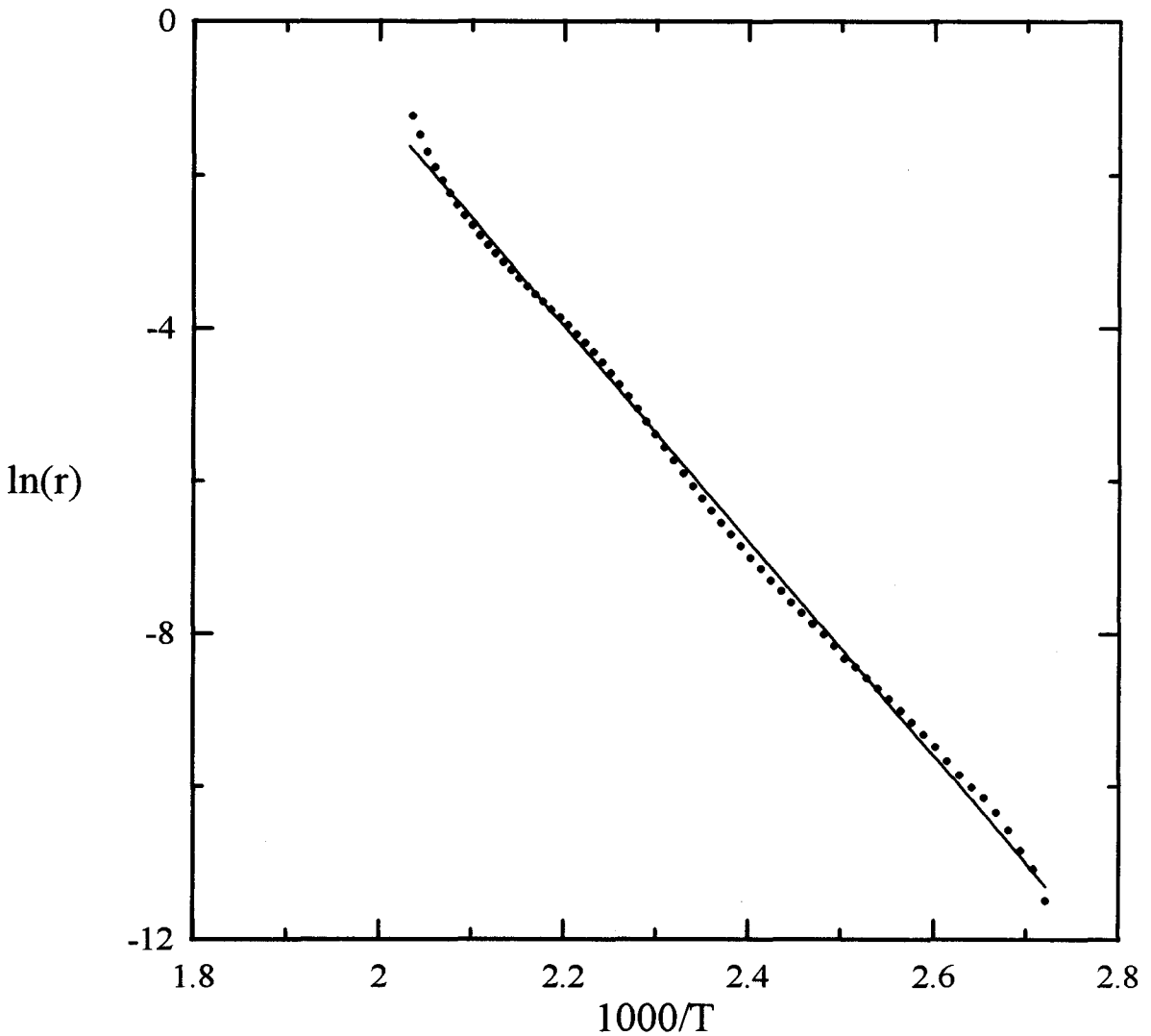

Figure 4.5: ln(r) plotted against the reciprocal temperature for Tactix-AN at a heating rate of 10K/min. The straight line is the best fit to Equation (4.5).

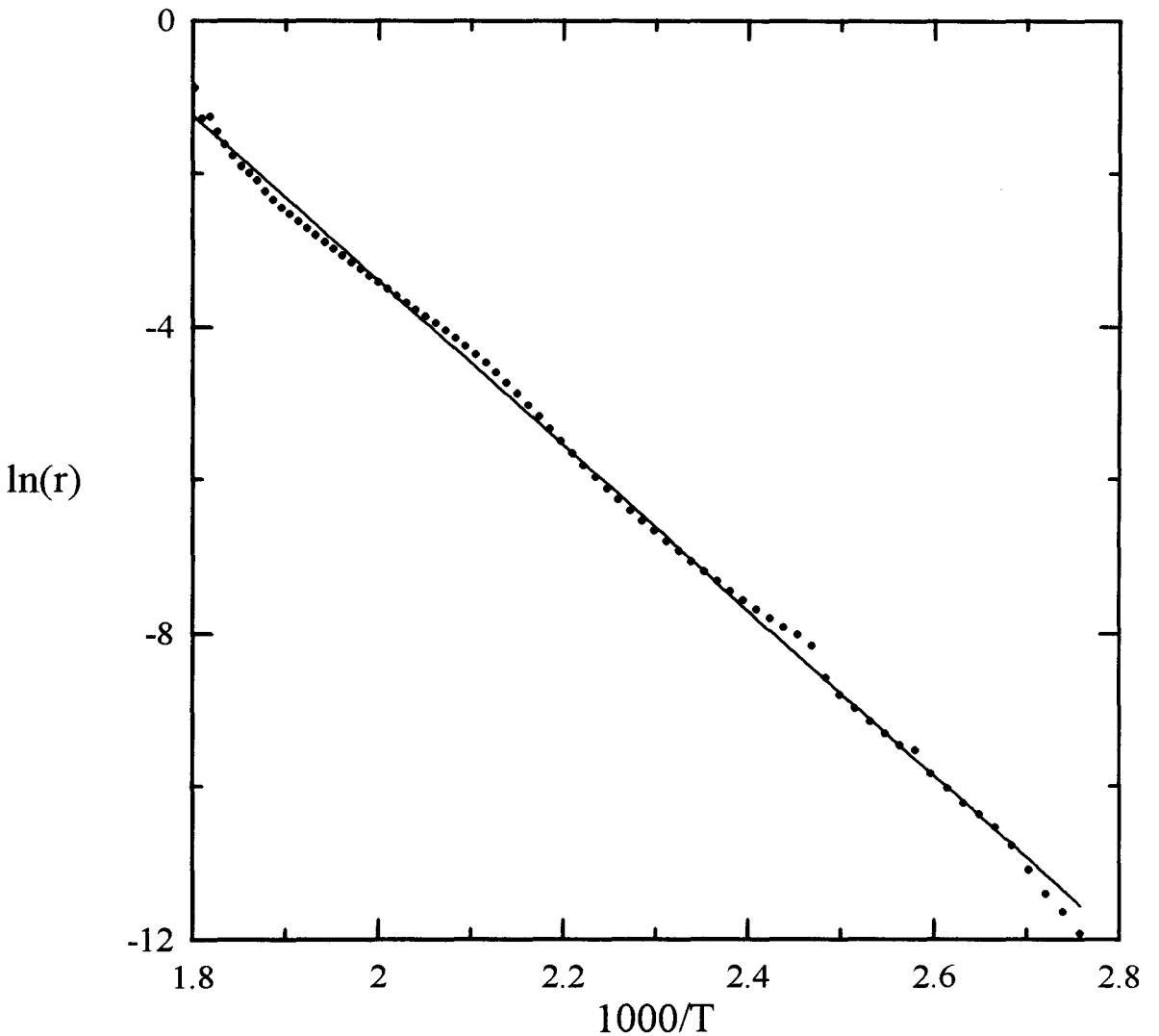

Figure 4.6: ln(r) plotted against the reciprocal temperature at a heating rate of 10K/min for Tactix-3CA. The straight line is the best fit to Equation (4.5).

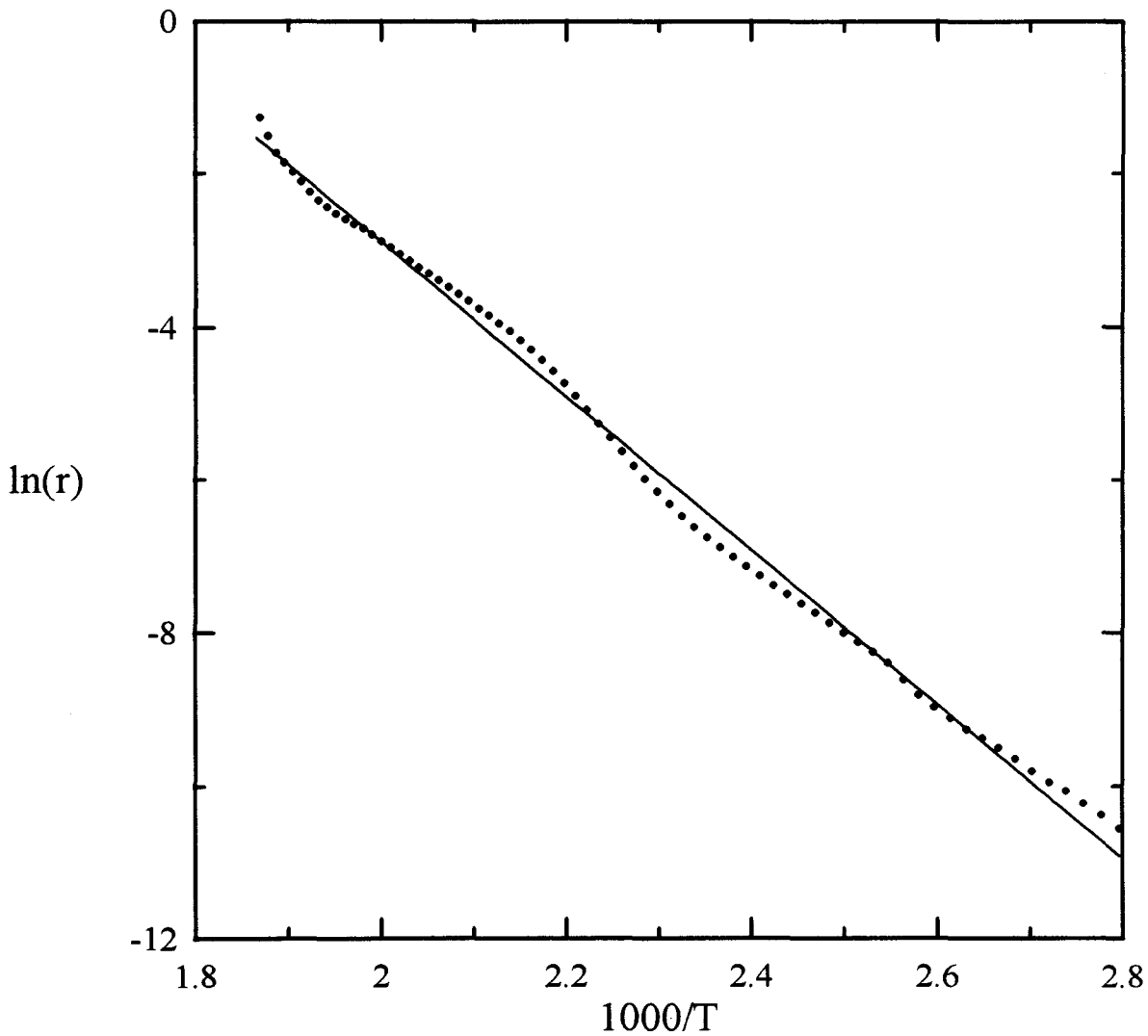

Figure 4.7: ln(r) plotted against the reciprocal temperature at a heating rate of 10K/min for Tactix-4CA. The straight line is the best fit to Equation (4.5).

Figures 4.2, 4.3 and 4.4 do not show a linear increase of r with α over a sufficient range to allow the evaluation of the K_1 and K_2. As is already shown (Wasserman and Johari 1993, 1994), there is no anticipated overlap of linear regions for polymerization at several different fixed temperatures. The results obtained from this study thus agree with the results of the diepoxide-diamine reaction.

4.2 The Dielectric Properties During the Polymerization

4.2.1 Examining the Analytical Procedure with Simulated Data

We first investigate whether the parameters determined from an analysis of the time-variant, i.e. fixed frequency, dielectric data yield the same conclusions as the time-invariant dielectric data, i.e. dielectric spectrum measured at different reaction times. For this purpose we begin by simulating the dielectric data for time-invariant conditions and then analyze the data for fixed frequencies under the time-variant conditions. This is necessary for determining whether the less time-consuming measurements at a single ac frequency can be used for monitoring the polymerization.

4.2.1a The Simulation of Time-Variant Dielectric Data From Time-invariant Spectra

For simulating the dielectric spectrum at various stages of polymerization, we take into account all the phenomena that contribute to the dielectric properties as follows: The measured dielectric data of a material generally contains contributions from three processes: (1) the rotational diffusion of a molecule as a whole, of its segments, or of ion

pairs, when such reorientation leads to a change in the dipole vector, (2) the translational diffusion of ionic charges via the migration of ions, and (3) the impedance behaviour of the capacitor formed at the electrode/material interface when ions are blocked at the interface (Johari, Wasylyshyn and Jain 1994, Parthun and Johari 1995). The first contribution leads to an understanding of the mechanisms of molecular relaxation, and the second to that of dc conductivity. The third, often an extraneous effect known as interfacial polarization, is dependent on the sample's geometry, its dc conductivity and upon the electrode's material. Although it is dependent on the dc conductivity of the sample, it is not treated as an intrinsic property of the material.

The magnitude of the contributions from the three processes are found to vary from one material to another. For a particular material, these contributions are dependent on the metal used as an electrode, the geometry of the sample, the ac frequency at which the measurements are made, and the sample's temperature. For materials which are relatively free from mobile ions, the last two effects contribute negligibly and the measured data are treated conveniently in terms of dipolar relaxation alone. However, when the concentration of mobile ions is significant, the dc conductivity and the interfacial polarization also become significant, requiring an analysis which separates the individual contributions from the three processes (Parthun and Johari 1995b).

ε' measured for a frequency ω and after a time of chemical reaction, t, at a temperature T may be written as (Johnson and Cole 1951, Cole and Tombari 1991),

$$\varepsilon'(\omega,t,T) = \varepsilon'_{dip}(\omega,t,T) + \left[Z_o(T)\sin\left(\frac{n(T)\pi}{2}\right)\right]\frac{[\sigma_{dc} + \sigma_{dip}(\omega,t,T)]^2 C_o}{\varepsilon_o^2}\omega^{-(n(T)+1)} \quad (4.6)$$

where $\varepsilon'_{dip}(\omega,t,T)$ and $\varepsilon'_{dc}(\omega,t,T)$ are the dipolar and dc contributions to the dielectric permittivity, respectively, ε_o is the permittivity of vacuum (=8.854pF/m), n(T) is an empirical parameter, and $Z_o(T)$, the electrode impedance, is defined by the complex function $Z^*_{el} = Z_o(T)[i\omega]^{-n}$. Z_o and n are characteristic of the electrode/material interface. This terminology refers to a "constant phase element" in series with the bulk dielectric properties of the material, as discussed by (MacDonald 1987). Equation (4.6) is obtained by writing the measured conductance, G (in Siemens) as;

$$\frac{G_{meas}(\omega,t,T)}{C_o} + i\omega\varepsilon'_{meas}(\omega,t,T) = \frac{G(\omega,t,T)/C_o + i\omega\varepsilon'(\omega,t,T)}{1 + Z^*_{el}(T)\left[G(\omega,t,T)/C_o + i\omega\varepsilon'(\omega,t,T)\right]C_o} \quad (4.7)$$

leading to the equation,

$$\frac{G(\omega,t,T)}{C_o} = \frac{[\sigma_{dc}(t,T) + \sigma_{dip}(\omega,t,T)]}{\varepsilon_o} \quad (4.8)$$

where C_o is the capacitance of the dielectric cell in air, σ_{dc} is the dc conductivity and σ_{dip} the ac conductivity resulting from dipolar reorientation.

Using the constant phase element considerations, the dielectric loss, $\varepsilon''(\omega,t,T)$, can be described by the following equation;

$$\varepsilon''(\omega,t,T) = \varepsilon''_{dc}(t,T) + \varepsilon''_{dip}(\omega,t,T) - \left[Z_o(T)\cos\left(\frac{n(T)\pi}{2}\right)\right]C_o\left[\varepsilon''_{dc}(t,T) + \varepsilon''_{dip}(\omega,t,T)\right]^2\omega^{1-n(T)} \quad (4.9)$$

The last term on the right hand side of Equations (4.6) and (4.9) represent the contribution from the interfacial polarization. This was obtained by expanding Equation (4.7) as a Taylor series, and truncating after the first order terms under the conditions $G(\omega,t,T) >> \omega\varepsilon'_{dip}(\omega,t,T)$ and $Z_o(T)G(t,T)\omega^{-n(T)} << 1$. To calculate the interfacial polarization contribution to the dielectric properties, the interfacial terms on the right hand side of Equations (4.6) and (4.7) were used with parameters of $Z_o=1x10^5S^{-1}s^{-n}$, n=0.5 and C_o=16pF.

In earlier studies (Johari 1991, 1993a, Parthun and Johari 1992c, Mangion and Johari 1991a,b,c) it was found that up to the time of reaction where σ_{dc} is equal to σ_{meas}, within the experimental and analytical uncertainties, σ_{dc}'s variation with time can be described by the equation,

$$\sigma_{dc}(t) = \sigma_{dc}(t\rightarrow 0)\left((t_{gel}-t)/t_{gel}\right)^{x} \qquad (4.10)$$

where $\sigma(t\rightarrow 0)$ is the dc conductivity at the beginning of the reaction, t_{gel} is the time to reach the gelation point if the macromolecule formed had a network structure, and x is the critical exponent of the scaling equation used as a generalized property function (Stauffer et al. 1982, Djabourov 1988). (Note that σ_{dc} does not become zero when $t = t_{gel}$, because the ionic impurities continue to contribute to σ_{dc}. The concept implicit here is that the dc conductivity is predominantly associated with proton transfer in an H-bonded network in the unreacted liquid.). It was found also that an equation that described an approach of the dc conductivity towards a singularity could be used to fit the data (Johari

1991,1993a, Parthun and Johari 1992c, Mangion and Johari 1991a,b,c);

$$\sigma_{dc}(t) = A_\sigma \exp\left(B_\sigma/(t_o - t)\right) \tag{4.11}$$

Here, t_o (as in the Vogel-Fulcher-Tamman equation described by McCrum et al. 1967, pp.169-174), is the point of singularity (σ_{dc} approaches zero as t approaches t_o), and A_σ and B_σ are temperature-dependent empirical constants, which determine σ_{dc} at $t \rightarrow 0$ and the rate at which σ_{dc} approaches zero as $t \rightarrow t_o$. Either expression has been found to satisfactorily describe the time-dependent dc conductivity of a forming polymer network, but in this simulation, Equation (4.10) was used with $\sigma_{dc}(t\rightarrow 0) = 10\mu S/m$, $t_{gel} = 18ks$ and $x = 3$.

The calculation of ε'_{dip} and ε''_{dip} required the use of a relaxation function which adequately described the relaxation behaviour. This function may represent a single relaxation time or a sum of distribution of relaxation each representing a single

According to the theory of dielectrics, the dipolar contribution to the complex permittivity is shown to be (Manning and Bell 1940),

$$\frac{\varepsilon^*(\omega,t,T) - \varepsilon_\infty(t,T)}{\varepsilon_s(t,T) - \varepsilon_\infty(t,T)} = \mathcal{L}\left(-\frac{\partial\phi}{\partial t}\right) \tag{4.12}$$

where $\phi(t)$ represents a relaxation function. To simulate the time-variant relaxation properties, from the time-invariant spectrum, the empirical stretched exponential relaxation function, $\phi(t) = \exp(-(t/\tau_o)^\gamma)$ was used. Tables of normalized $\varepsilon'_{dip}(\omega,\tau)$ and $\varepsilon''_{dip}(\omega,\tau)$ have been calculated from Equation (4.12) by Moynihan et al. (1973) and Dishon et al.

(1985). For the simulation, we chose $\beta = 0.35$ and determined the normalized quantities from Moynihan et al.'s (1973) tabulated values.

The characteristic relaxation time, τ_o, during the growth of a macromolecule has been found to increase with reaction time under isothermal conditions according to the empirical expression (Parthun and Johari 1992a,b),

$$\tau_o = \tau_o(t \to 0)\exp(S\alpha^P) \tag{4.13}$$

where α is the extent of chemical reaction, $S = \ln[(\tau_0(\tau \to \infty))/(\tau_0(\tau \to 0))]$, P is an empirical parameter, and $\tau_0(\tau \to \infty)$ and $\tau_0(\tau \to 0)$ are constants. Their values may lie over a wide range, depending upon the material and the isothermal temperature at which the polymerization occurred. Typically, $\tau_0(\tau \to 0)$ is the ns range, and $\tau_0(\tau \to \infty)$ can vary from one nanosecond to infinity, depending on the relaxation time of the product ultimately formed and the temperature (Johari 1993a).

The extent of chemical reaction during a macromolecule's growth is generally found to increase with the logarithm of reaction time in a sigmoid manner. The simplest equation which produces this shape is of the form,

$$\alpha = 1 - \exp(-kt^m) \tag{4.14}$$

where k is an empirical constant with units of s^{-m} and m is an empirical parameter. To simulate $\tau_0(t)$ data, Equation (4.14) was used with m = 1 and $k = 5 \times 10^{-5} s^{-1}$. Using the $\alpha(t)$ thus generated, τ_0 was calculated from Equation (4.13). The average relaxation time, $\langle\tau\rangle$, for the stretched exponential function has been found by Moynihan et al. (1973) to

be of the form,

$$<\tau> = \frac{\tau_o}{\beta}\Gamma\left(\frac{1}{\beta}\right) \qquad (4.15)$$

where $\Gamma(1/\beta)$ is the gamma function of $1/\beta$.

The low and high frequency limiting permittivities, ε_s and ε_∞, as a function of the reaction time were also required for the simulation of the spectrum. Typically, ε_s is found to decrease by less than 20% during the growth of the macromolecule, and ε_∞ by about 5% (Tombari and Johari 1992, Parthun and Johari 1995a). The following equations were used to simulate the permittivities as a function of reaction time;

$$\varepsilon_s(t) = \varepsilon_s(t\to\infty) + (\varepsilon_s(t\to 0) - \varepsilon_s(t\to\infty))\exp(-A_1 t) \qquad (4.16)$$

and,

$$\varepsilon_\infty(t) = \varepsilon_\infty(t\to\infty) + (\varepsilon_\infty(t\to 0) - \varepsilon_\infty(t\to\infty))\exp(-A_2 t) \qquad (4.17)$$

Equations (4.16) and (4.17) give a sigmoidal decrease of ε_s and ε_∞ with an increase in the reaction time. The values of A_1 and A_2 are set equal to k from Equation (4.14), so that the inflection point would occur at the same time for $\alpha(t)$, $\varepsilon_s(t)$ and $\varepsilon_\infty(t)$. The other parameters used in Equations (4.16) and (4.17) are $\varepsilon_s(t\to 0) = 10$, $\varepsilon_s(t\to\infty) = 8$, $\varepsilon_\infty(t\to 0) = 3.15$ and $\varepsilon_\infty(t\to\infty) = 3.00$. Thus, ε'_{dip} and ε''_{dip} was calculated from the quantities derived from Equations (4.12), (4.13), (4.16) and (4.17).

In summary, 17 parameters were required to produce one plot of ε' and ε'' for a time-variant system at a fixed frequency. The parameters used were: $Z_o = 1\text{x}10^5 S^{-1}s^{-n}$,

$n = 0.5$, $C_o = 16pF$, $\sigma_{dc}(t \rightarrow 0) = 10\mu S/m$, $t_{gel} = 18ks$, $x = 3$, $\beta = 0.35$, $\tau_o(t \rightarrow 0) = 0.1ns$, $\tau_o(t \rightarrow \infty) = 1Ms$, $A_1 = A_2 = k = 5x10^{-5}s^{-1}$, $\varepsilon_s(t \rightarrow 0) = 10$, $\varepsilon_s(t \rightarrow \infty) = 8$, $\varepsilon_\infty(t \rightarrow 0) = 3.15$, $\varepsilon_\infty(t \rightarrow \infty) = 3.00$ and ω. ε' and ε'' data were simulated using the above-mentioned equations and the parameters for six values of ω, specifically, 10Hz, 100Hz, 1kHz, 10kHz, 100kHz and 1MHz. Each set of ε' and ε'' data at a certain ω and reaction time corresponds to a relaxation spectrum at that time, or for a time-invariant state. Thus, the ε' and ε'' data at a single frequency when plotted against the time yield a curve for time-variant dielectric behaviour during the polymerization. These curves of ε' and ε'' are shown as a function of time in Figure 4.8, and shown as complex-plane plots in Figure 4.9. As mentioned before, the objective here was to treat this data as if it were experimentally obtained, then to see whether the analysis yielded the original parameters. The ε' and ε'' data sets were simulated by M.G. Parthun and were given to me for analysis. I had no information on the numerical values of the above-given parameters that M.G. Parthun used in the simulation.

4.2.1b The Analysis of the Simulated Time-Variant Dielectric Properties

We now analyze the simulated ε' and ε'' data in the same manner as earlier studies (Parthun and Johari 1992a,b) to obtain dielectric parameters. When no approximations are made, correct analysis of the data in Figures 4.8 and 4.9 must yield the original values of the parameters Z_o, n, ε_s, ε_∞, σ_{dc}, τ_o, and β. However, to analyze the data corresponding to a time-variant system, it was necessary to assume that ε_s and

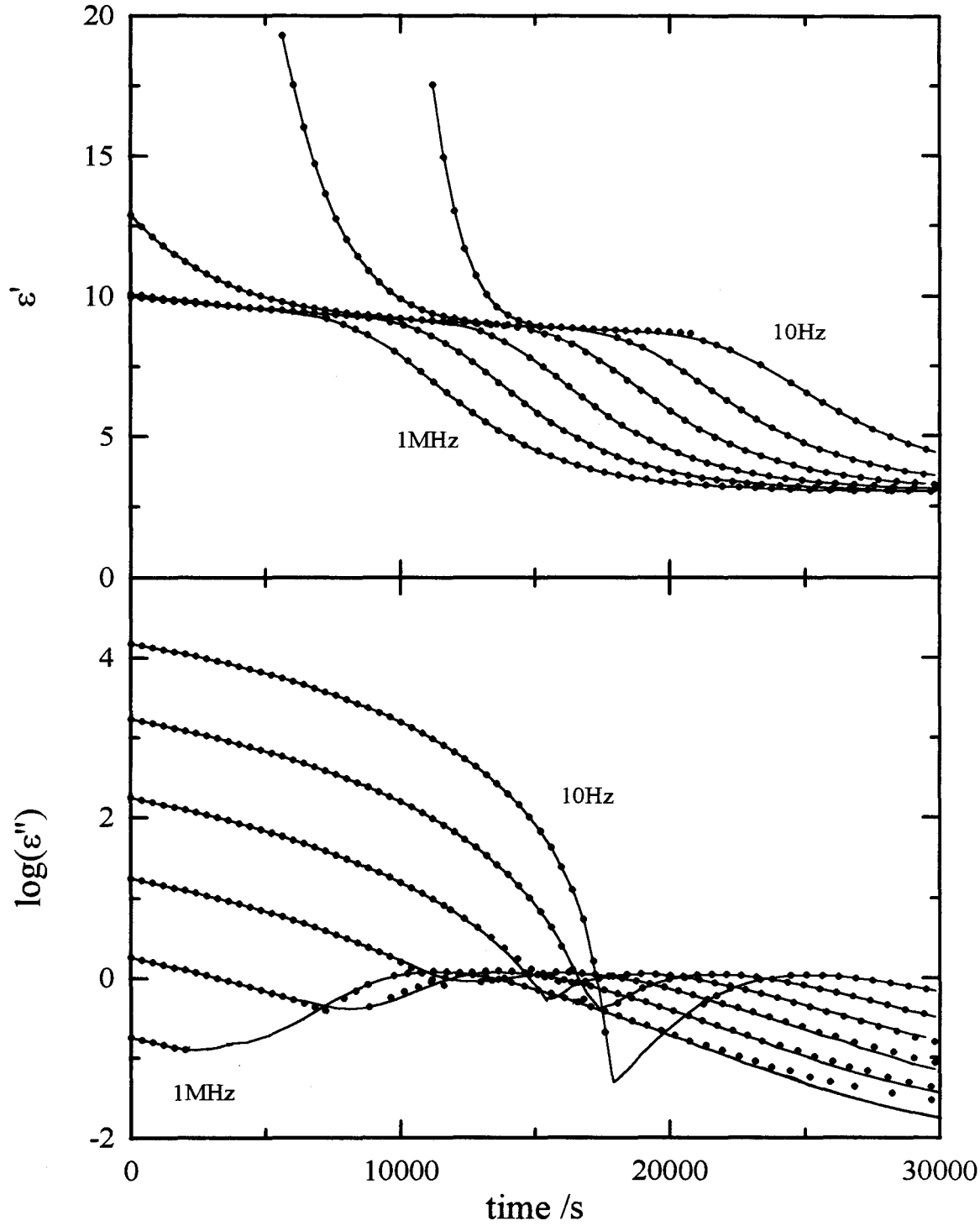

Figure 4.8: The simulated ε' and ε'' values (continuous lines) plotted against reaction time for six frequencies; 10Hz, 100Hz, 1kHz, 10kHz, 100kHz and 1MHz. The symbols are the values calculated from the analysis procedure.

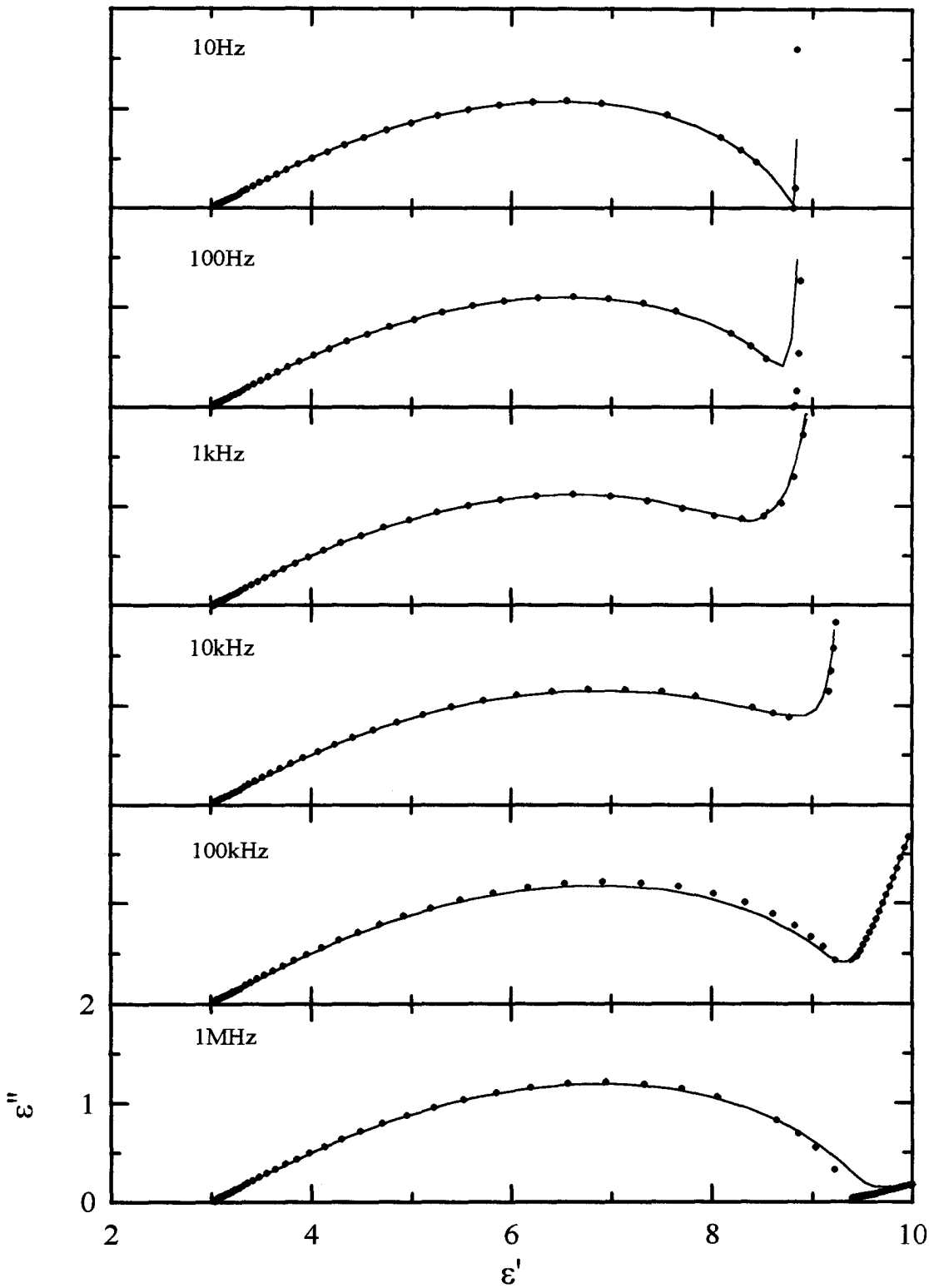

Figure 4.9: The complex plane plot of the data from Figure 4.1. The continuous lines are the simulated data and the symbols are those calculated from the analysis procedure.

ε_∞ vary only negligibly with time. Otherwise the procedure becomes too complex and time-consuming to outweigh the advantages from the accuracy with which the ultimate parameters can be obtained.

In order to calculate the dc conductivity, it was necessary to ascertain the accuracy with which its value could be computed. This was done by constructing complex-plane plots of the dielectric modulus, $M^* = 1/\varepsilon^*$, such that,

$$M' = \frac{\varepsilon'}{\varepsilon'^2 + \varepsilon''^2} \tag{4.18}$$

$$M'' = \frac{\varepsilon''}{\varepsilon'^2 + \varepsilon''^2} \tag{4.19}$$

and,

$$M^*(t) = \frac{M_s(t) i\omega\tau_\sigma(t)}{1 + i\omega\tau_\sigma(t)} \; ; \qquad M_s = \frac{1}{\varepsilon_s} \tag{4.20}$$

In doing so, we assume ε_s to remain constant with increasing reaction time, and that the interfacial polarization effects are initially negligible, so that (Mangion and Johari 1991a),

$$\sigma_{dc}(t) = \frac{\varepsilon_o \varepsilon_s(t)}{\tau_\sigma(t)} \approx \frac{\varepsilon_o \varepsilon_s}{\tau_\sigma(t)} \tag{4.21}$$

where $\tau_\sigma(t)$ is the Maxwellian conductivity relaxation time and ε_0 is the permittivity of vacuum (=8.854pF/m). Figure 4.10 shows the complex-plane plots of M' and M" calculated from the simulated data at six frequencies. Since Equation (4.20) is

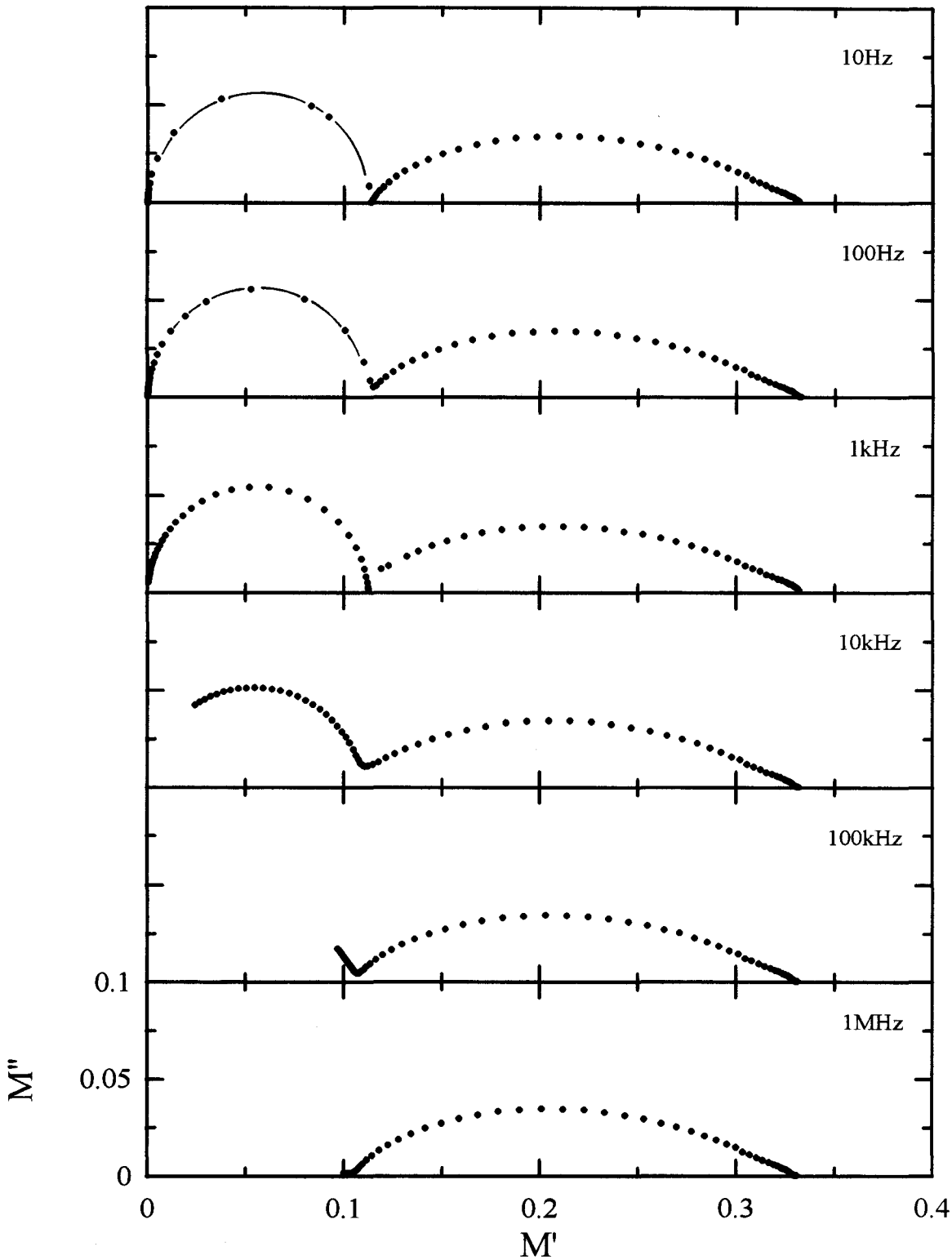

Figure 4.10: The complex plane plots of M'' against M' with data from all six measurement frequencies as shown in Figure 4.8.

mathematically independent of one's choice of ω or $\tau_\sigma(t)$ as a variable, each data point in the M" against M' plot, or M" and M' against t plot, corresponds to a certain value of $\omega\tau_\sigma(t)$, and when ω is known, τ_σ or σ_{dc} may be computed. From the complex plots, the latest time for which the contributions to $\sigma(t)$ were predominated by $\sigma_{dc}(t)$ can be determined, and thus the range of conductivity to be fitted to Equation (4.10) to obtain the parameters, $\sigma_{dc}(t \rightarrow 0)$, x and t_{gel} could be determined. However, the conductivity computed from these parameters differed significantly from the original (simulated) values as $t \rightarrow 0$. This was a reflection of our neglect of the contributions to σ from interfacial polarization. These contributions were then calculated as follows:

The total conductivity is given by,

$$\sigma(\omega,t) = \sigma_{dc}(t) + \sigma_{dip}(\omega,t) - \left(\left[Z_o \cos\left(\frac{n\pi}{2}\right)\right]\frac{[\sigma_{dc}(t) + \sigma_{dip}(\omega,t)]^2}{\varepsilon_o}C_o\right)\omega^{-n} \qquad (4.22)$$

where T has been dropped from the functions since it is for the isothermal case. The last term on the right hand side of Equation (4.22) is the contribution from interfacial polarization, which varies with σ_{dc}, σ_{dip} and ω when Z_o and n are constant. At $t \rightarrow 0$, $\varepsilon' \approx \varepsilon_s$, $\sigma_{dip} \approx 0$ and ω is known, one still requires knowledge of σ_{dc}, Z_o and n. To deduce this, Equation (4.6) was rewritten for the difference between the values of different ω's, ie. ω_i and ω_j, such that,

$$\varepsilon'(\omega_i,t) - \varepsilon'(\omega_j,t) = Z_o \sin\left(\frac{n\pi}{2}\right)\left(\omega_i^{-(n+1)} - \omega_j^{-(n+1)}\right)\frac{\sigma_{dc}(t)^2 C_o}{\varepsilon_o^2} \qquad (4.23)$$

for the range of t where σ_{dip} is insignificant in comparison with σ_{dc}.

The ratio of two equations of the form of Equation (4.23) for differences between ω_i and ω_j in one instance, and ω_i and ω_k in the other, is,

$$r = \frac{\varepsilon'(\omega_i) - \varepsilon'(\omega_j)}{\varepsilon'(\omega_i) - \varepsilon'(\omega_k)} = \frac{\omega_i^{-(n+1)} - \omega_j^{-(n+1)}}{\omega_i^{-(n+1)} - \omega_k^{-(n+1)}} \qquad \textbf{(4.24)}$$

Thus n being the only unknown is calculated by evaluating the equation for different pairs of frequencies, as described by Wasylyshyn, Parthun and Johari (1995). The frequencies, 10Hz, 100Hz and 1kHz, which were used, gave n = 0.5.

To calculate Z_o and $\sigma_{dc}(t)$, a reiterative procedure which required both Equations (4.22) and (4.23) was used. In this procedure, the left hand side of Equation (4.23) was plotted as a function of σ_{dc}^2, assuming that the measured conductivity was only from dc contributions during the appropriate time range. Equation (4.23) would then describe a straight line with a slope that yielded an initial value of Z_o, with all the other quantities known. Equation (4.22) was then re-expressed as,

$$\sigma(\omega,t) = \sigma_{dc}(t) - \left[Z_o \cos\left(\frac{n\pi}{2}\right) \frac{C_o \omega^{-n}}{\varepsilon_o} \right] \sigma_{dc}(t)^2 \qquad \textbf{(4.25)}$$

and the initial value of Z_o substituted into this quadratic equation, from which $\sigma_{dc}(t)$ was calculated over the time range of the available data. This new $\sigma_{dc}(t)$ was then used to re-evaluate Z_o from Equation (4.23). The procedure continued for 7 steps, until values of Z_o changed by less than 0.1%. This gave final values of $Z_o = 9.999 \times 10^4 S^{-1} s^{-n}$, and

$\sigma_{dc}(t)$, when C_o = 16pF and ε_o = 8.854pF/m.

With $\sigma_{dc}(t)$ now containing contributions from the dc conductivity alone, the analysis was continued with the time-dependence of σ_{dc}, by curve fitting $\log(\sigma_{dc}(t))$ against $\log((t_{gel} - t) / t_{gel})$ and adjusting for t_{gel} until a straight line is obtained with slope x and intercept $\log(\sigma_{dc}(t \rightarrow 0))$ as required by Equation (4.10). Figure 4.11 shows the results of the dc conductivity analysis and the dipolar analysis as $\log(\sigma)$ against t. The continuous lines are the original (simulated) data for the six fixed frequencies, and the symbols are the calculated values. The procedure gave x = 3.006, t_{gel} = 18.01ks and $\sigma_{dc}(t \rightarrow 0)$ = 1.005μS/m. When $\sigma_{dc}(t)$ was compared to the original (simulated) data, their ratio was close to unity for $t \rightarrow 0$ but deviated as t increased towards infinity. These deviations were caused by the onset of the dipolar relaxation process, which was analyzed as follows.

For this analysis, knowledge of both the relaxation time and its distribution is needed as a function of time. Rewriting Equation (4.12) to account for time-variance leads to (Manning and Bell 1940),

$$\frac{\varepsilon^*(\omega,t) - \varepsilon_\infty(t)}{\varepsilon_s(t) - \varepsilon_\infty(t)} = \int_0^\infty \exp(-i\omega t') \left(-\frac{\partial \phi(t')}{\partial t} \right) dt' \qquad (4.26)$$

with the quantities defined earlier in this section. Here, t' refers to the time for the decay of the polarization for a chemical structure that remains unchanged during the measurement time, or when the chemical reaction occurs too slowly in comparison with

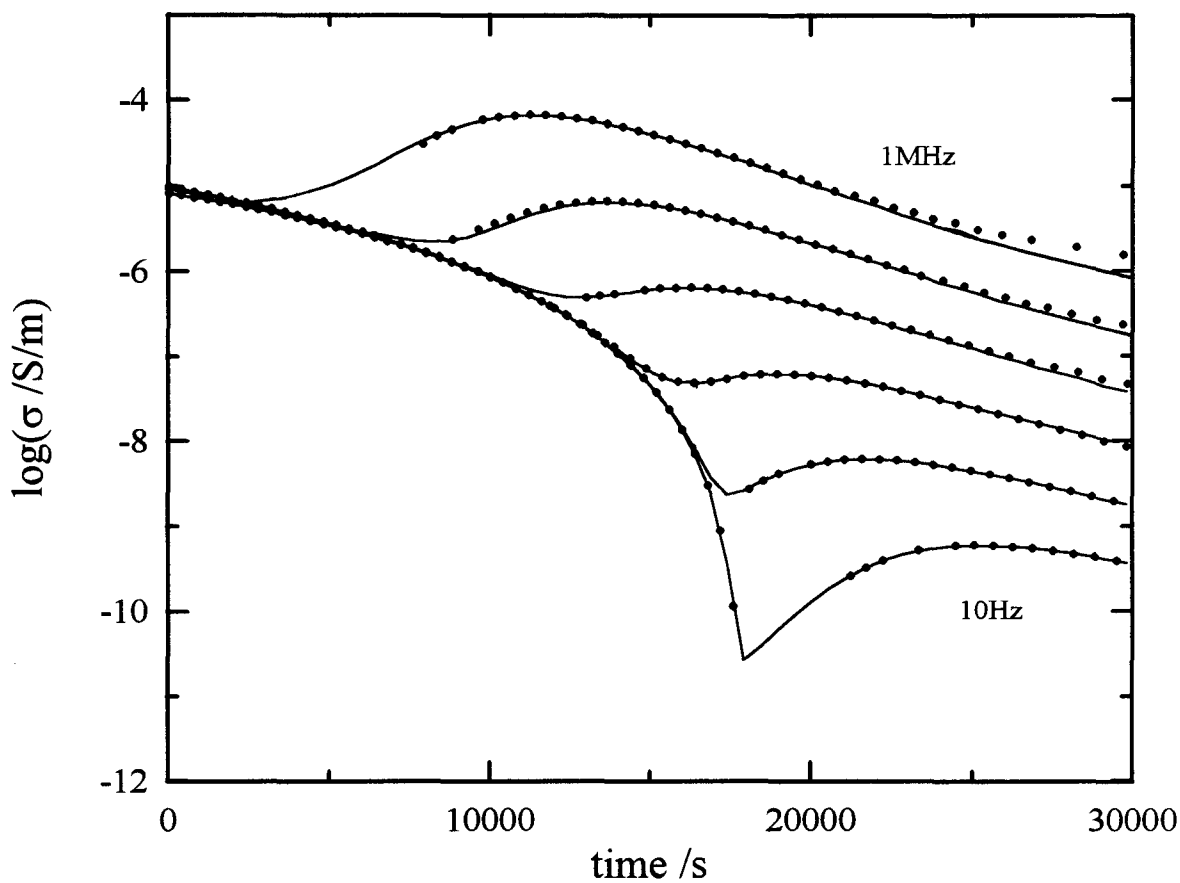

Figure 4.11: The conductivity, σ, plotted against the reaction time for the simulated (continuous line) and calculated (symbols) values.

the time for the measurement. In Equation (4.26), $\phi(t')$ represents a relaxation function whose normalized form at a given instant t, for a time-invariant system, is given by,

$$[\phi(t')]_t = \exp\left[-\left(\frac{t'}{\tau_o}\right)^{\beta}\right]_t \qquad \textbf{(4.27)}$$

where β is the stretched exponential parameter and τ_0 is the characteristic relaxation time. For the majority of viscous liquids, β is found to be in the range 0.2 to 1.0.

For a time-variant system, t' and τ_0 in Equations (4.26) and (4.27) have a strict meaning. If relaxation processes are considered to be acting in parallel rather than in series, then it is the time for the decay in the polarization, during which τ_0 remains invariant with time. Since τ_0 is time-variant here, we must make the approximation that for measurement frequencies greater than 1kHz, t' in Equation (4.27) is less than 1 ms and the effects from irreversible changes of the system during this period can be justifiably assumed to be negligible, particularly when the total time approaches 1Ms. This allows us to re-express Equation (4.26) in a form that is also useful for a time-variant system as follows,

$$N^*(\omega\tau_o) = \int_0^{\infty} \exp(-i\omega t')\left(-\frac{\partial\phi}{\partial t'}\right)dt' \qquad \textbf{(4.28)}$$

and,

$$N'(\omega\tau_o) - iN''(\omega\tau_o) = \mathcal{L}\left(-\frac{\partial\phi}{\partial t'}\right) \tag{4.29}$$

The normalized quantity is a function of $\omega\tau_o$, or the product of ω and τ_o at a given time, and $\mathcal{L}$ represents the one-sided LaPlace transform. Thus, ε' and ε'' are written in terms of N' and N'' as,

$$\varepsilon'(\omega,t) = \varepsilon_\infty(t) + [\varepsilon_s(t) - \varepsilon_\infty(t)]N'(\omega\tau_o(t)) \tag{4.30}$$

and,

$$\varepsilon''(\omega,t) = [\varepsilon_s(t) - \varepsilon_\infty(t)]N''(\omega\tau_o(t)) \tag{4.31}$$

We further assume that ε_s and ε_∞, as well as $(\partial\phi/\partial t')$ remain constant with t and combine Equations (4.30) and (4.31) to obtain,

$$\varepsilon^*(\omega,t) = \varepsilon_\infty + [\varepsilon_s - \varepsilon_\infty]N^*(\omega\tau_o(t)) \tag{4.32}$$

Equation (4.32) is phenomenologically invariant of ω and of τ_o because the two quantities appear as a product, and it is the product that is important, not the separate terms. This means that several shapes of the relaxation spectrum can be obtained by varying ω or τ_o. Thus the shape of the plots of ε' and ε'' against time resembles the dielectric dispersion and loss spectrum. This shape can be approximated by a relaxation function when the measurements are made for a fixed frequency. The form of the relaxation function can then be written as,

$$\phi(t') = \exp\left[-\left(\frac{t'}{\tau_o(t)}\right)^{\gamma}\right] \tag{4.33}$$

where $\tau_0(t)$ is now a pseudo-equilibrium value of τ_0 at instant t, which is determined by using the limiting short- and long-time values of $\varepsilon'(\omega,t)$, namely, $\varepsilon'(t \rightarrow 0)$ and $\varepsilon'(t \rightarrow \infty)$ with τ_0 as a variable of t. The parameter γ, which is called the reaction parameter, differs from β of Equation (4.27) because the former ignores the time-dependence of ε_s and ε_∞. It should be noted also that Equation (4.33) cannot be transformed readily into the frequency domain, while Equation (4.27) can.

The simulated data was then analyzed using the relaxation function of Equation (4.33), which mathematically produces the same results as the time-invariant relaxation function used in Equation (4.12). For these calculations, one requires a spectrum of $N^*(\omega\tau_0)$ for various values of γ. These have been provided by Moynihan et al. (1973) and Dishon et al. (1985) for values of $\log(\omega\tau_0)$ from -3 to 8, which we used in this study. With the parameters $\varepsilon'(t \rightarrow 0)$, $\varepsilon'(t \rightarrow \infty)$ and γ, the original data was normalized by the equations,

$$N'(\omega\tau_o(t)) = \frac{\varepsilon'(\omega\tau_o(t)) - \varepsilon'(t \rightarrow \infty)}{\varepsilon'(t \rightarrow 0) - \varepsilon'(t \rightarrow \infty)} \tag{4.34}$$

and,

$$N''(\omega\tau_o(t)) = \frac{\varepsilon''(\omega\tau_o(t))}{\varepsilon'(t\to 0) - \varepsilon'(t\to\infty)} \qquad (4.35)$$

Figure 4.8 shows the plots of the simulated ε'(t) and ε"(t) versus t data as continuous lines and the data obtained from the analysis by crosses. The shape of the curves in Figures 4.8 and 4.9 are a result of an increase in τ_0 with t only. The values obtained for $\varepsilon'(t \to 0)$, $\varepsilon'(t\to \infty)$ and γ for each of the six frequencies are shown in Table 4.1.

We now calculate the relaxation time, τ_0, as a function of reaction time, t. Each calculated data point (not simulated) in Figures 4.8 and 4.9 corresponds to a unique value of normalized complex permittivity, $N^*(\omega\tau_0)$, which in turn corresponds to a unique set of ε' and ε" values from Equations (4.34) and (4.35). Thus, N^* becomes a unique function of τ_0 alone, since ω is fixed. Hence, each calculated set of ε' and ε" data corresponds to a particular value of τ_0. By matching each calculated pair of ε' and ε" with the simulated one, a τ_0 value could be associated with each instance of the reaction time of the measurement. For the case where a calculated point did not fall precisely on a simulated one, a value for the relaxation time was linearly interpolated from the two adjacent simulated values. Thus the ε' and ε" data for the six frequencies was fitted to Equations (4.34) and (4.35) to obtain about 60 $\tau_0(t)$ values at different times. The τ_0 values were converted to the average relaxation time, $\langle\tau\rangle$ with Equation (4.15) written as, $\langle\tau\rangle = (\tau_0/\gamma)\Gamma(1/\gamma)$. Figure 4.12 shows plots of both the simulated and the calculated $\log(\langle\tau\rangle)$ against time, by a continuous line and by symbols, respectively. The calculated

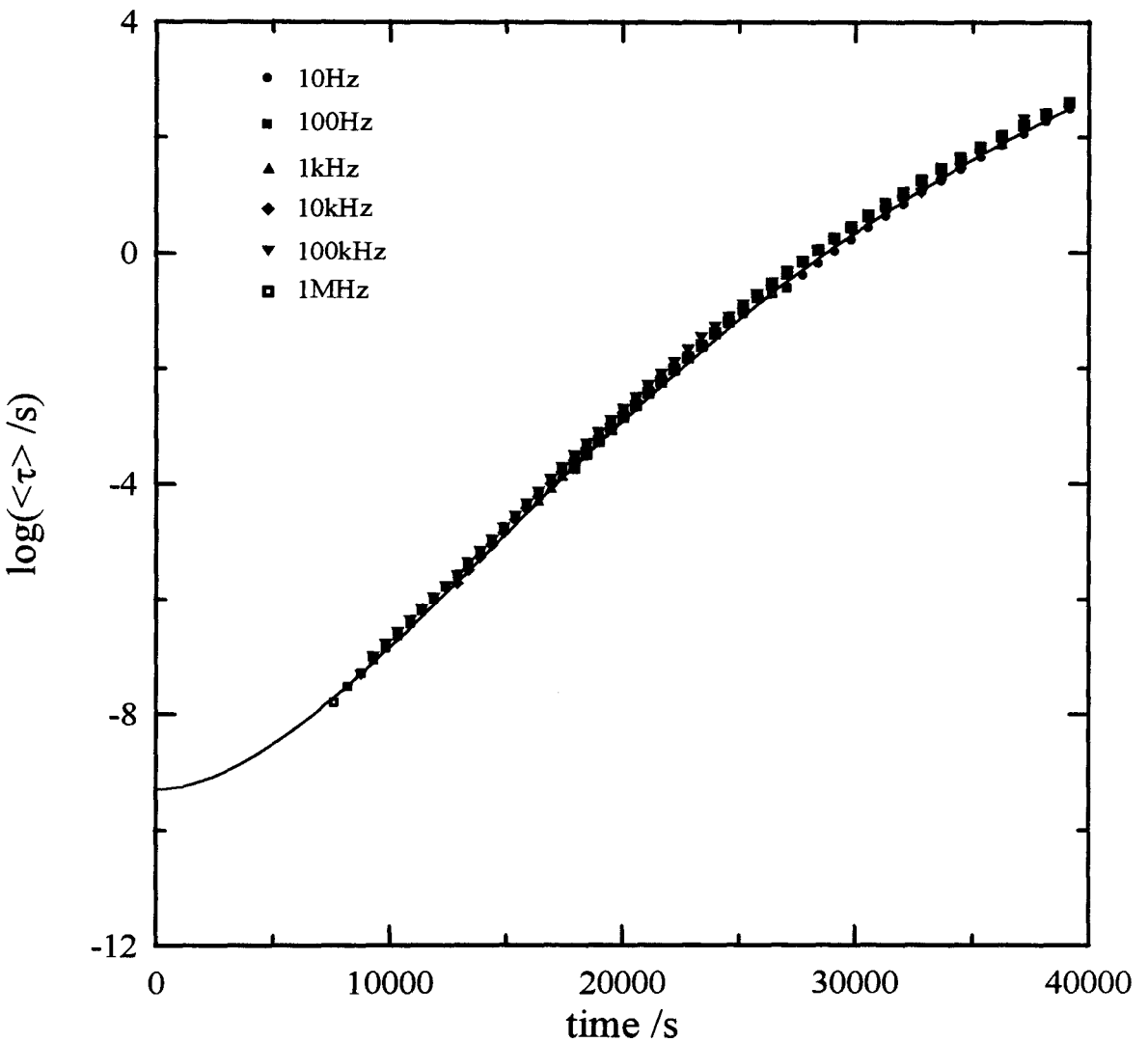

Figure 4.12: The average relaxation time is plotted against reaction time for the simulated (continuous line) and calculated (symbols) values.

Table 4.1: The parameters used in the analysis of the time-variant data at different frequencies obtained by the simulation of the spectra.

Freq /kHz	γ	$\varepsilon'(t \rightarrow 0)$	$\varepsilon'(t \rightarrow \infty)$
0.01	0.34	8.70	3.00
0.1	0.34	8.81	3.00
1.0	0.34	8.90	3.00
10	0.34	9.05	3.00
100	0.34	9.30	3.02
1000	0.34	9.32	3.02

and the original $<\tau>$ agree within 20%.

We conclude that the agreement between the parameters, Z_0, n, ε_s ε_∞ and $<\tau>$ obtained from the fixed frequency data analysis and those used in the simulation of the data from isothermal spectra demonstrates that the procedure of using a few measurement frequencies to monitor the growth of a macromolecule is satisfactory from a technological standpoint, and largely accurate. The deviations of the calculated values from the original values are no more than the deviations found when the experimental data is analyzed.

4.2.2 The Conductivity Change During Polymerization

The total current observed after applying a static electric field to a dielectric material consists of contributions from two sources; (1) diffusion of ionic charge carriers and (2) reorientation of dipoles. The relative magnitude of the two contributions varies

with one material to another, the time of observation after the application of the field and the temperature of the material. When polarization of the electrode-material interface also occurs, the measured dielectric properties are written as (Johnson and Cole 1951):

$$\varepsilon'_{meas}(\omega,t,T) = \varepsilon'_{dip}(\omega,t,T) + \varepsilon'_{inter}(\omega,t,T) \tag{4.36}$$

$$\varepsilon''_{meas} = \varepsilon''_{dip}(\omega,t,T) - \varepsilon''_{inter}(\omega,t,T) + \varepsilon''_{dc}(\omega,t,T) \tag{4.37}$$

$$\sigma(\omega,t,T) = \sigma_{dip}(\omega,t,T) - \sigma_{inter}(\omega,t,T) + \sigma_{dc}(\omega,t,T) \tag{4.38}$$

where,

$$\sigma_{inter} = \frac{Z_o C_o (\sigma_{dc} + \sigma_{dip})^2 \cos(n\pi/2)}{\varepsilon_o \sqrt{\omega}} \tag{4.39}$$

The subscripts refer to the measured, dipolar, interfacial and direct current contributions to the measured conductivity, τ_0 the dielectric relaxation time and ε_0 to the permittivity of vacuum (=8.854pF/m). Z_0 is a characteristic of the electrode/material interface in the equation for complex impedance, specifically, $Z_{el}^* = Z_0(i\omega)^{-n}$, as is the parameter n (this n is n(T) in the Section 4.2.1). C_0 is the geometric capacitance of the empty dielectric cell and ω is the angular frequency.

σ_{dip} can be written in terms of a sum of m number of a single relaxation or Debye-type process such that,

ε_s is the static permittivity and ε_∞ is the high-frequency permittivity of orientational

$$\sigma_{dip}(\omega,t,T) = \frac{\sum_{0}^{m} \omega^2 \tau_o(t,T)\varepsilon_o(\varepsilon_s(t,T) - \varepsilon_\infty(t,T))}{(1+\omega^2\tau_o^2(t,T))} \qquad (4.40)$$

polarization. This representation of σ_{dip} eliminates any bias towards a particular one amongst the many empirical equations currently used for fitting to the data (Parthun and Johari 1995a).

According to Equation (4.39), the interfacial contributions to σ_{meas} is highest at the lowest frequencies and decreases rapidly as the frequency is increased. It is also large when σ_{dc} is large. Figures 4.13, 4.14 and 4.15, show the change in σ_{meas} for various fixed frequencies with reaction time, t, for Tactix-AN, Tactix-3CA and Tactix-4CA, respectively. These figures show that σ_{meas} at high frequencies is higher than at low frequencies over a range of t far from the beginning, particularly when σ_{dip} becomes significant. If neither σ_{dip} nor σ_{inter} is significant, then σ_{meas} would be equal to σ_{dc}, and would for all frequencies lie on a single curve within the measurement accuracy. This curve would be a horizontal line if σ_{dc} did not vary with t, or N(t), and curved if it varied, as observed in Figures 4.13, 4.14 and 4.15 for the three polymerizing mixtures. These observations can be used as criterion to determine the range of t, or N(t), where the measured conductivity is predominantly dc conductivity.

An alternative procedure for determining the range of times over which σ_{meas} is dominated by contributions from σ_{dc} is to analyze the ε^* data in terms of M^* ($M^* = 1/\varepsilon^*$), as has been described elsewhere (Parthun and Johari 1992c, Johari 1993a, Parthun,

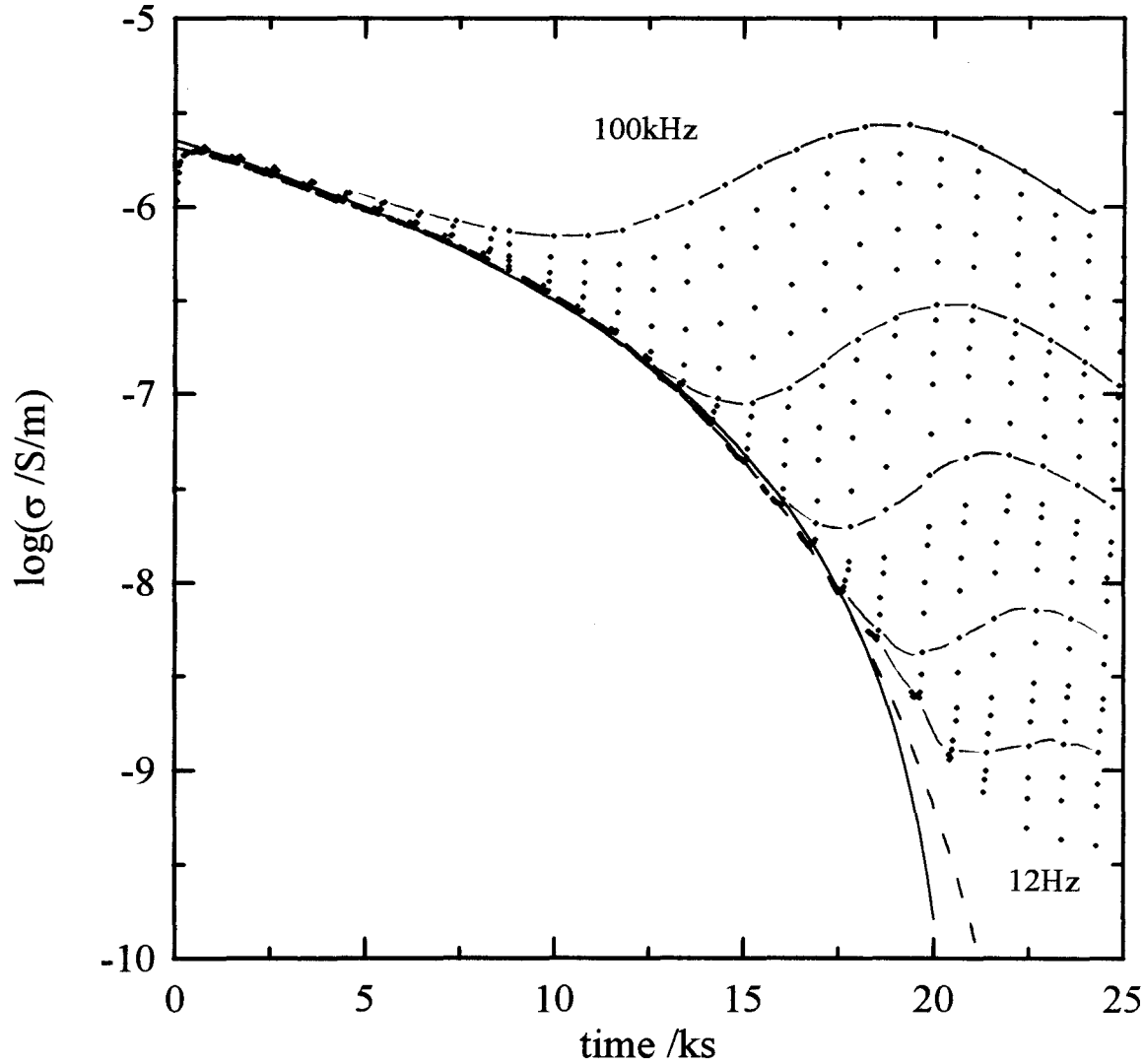

Figure 4.13: The log of conductivity plotted as a function of reaction time with the filled circles representing the measured data for the initially uncured Tactix-AN. The continuous line was generated from Equation (4.10) and the dashed line from Equation (4.11), with parameters for each listed in Table 4.3.

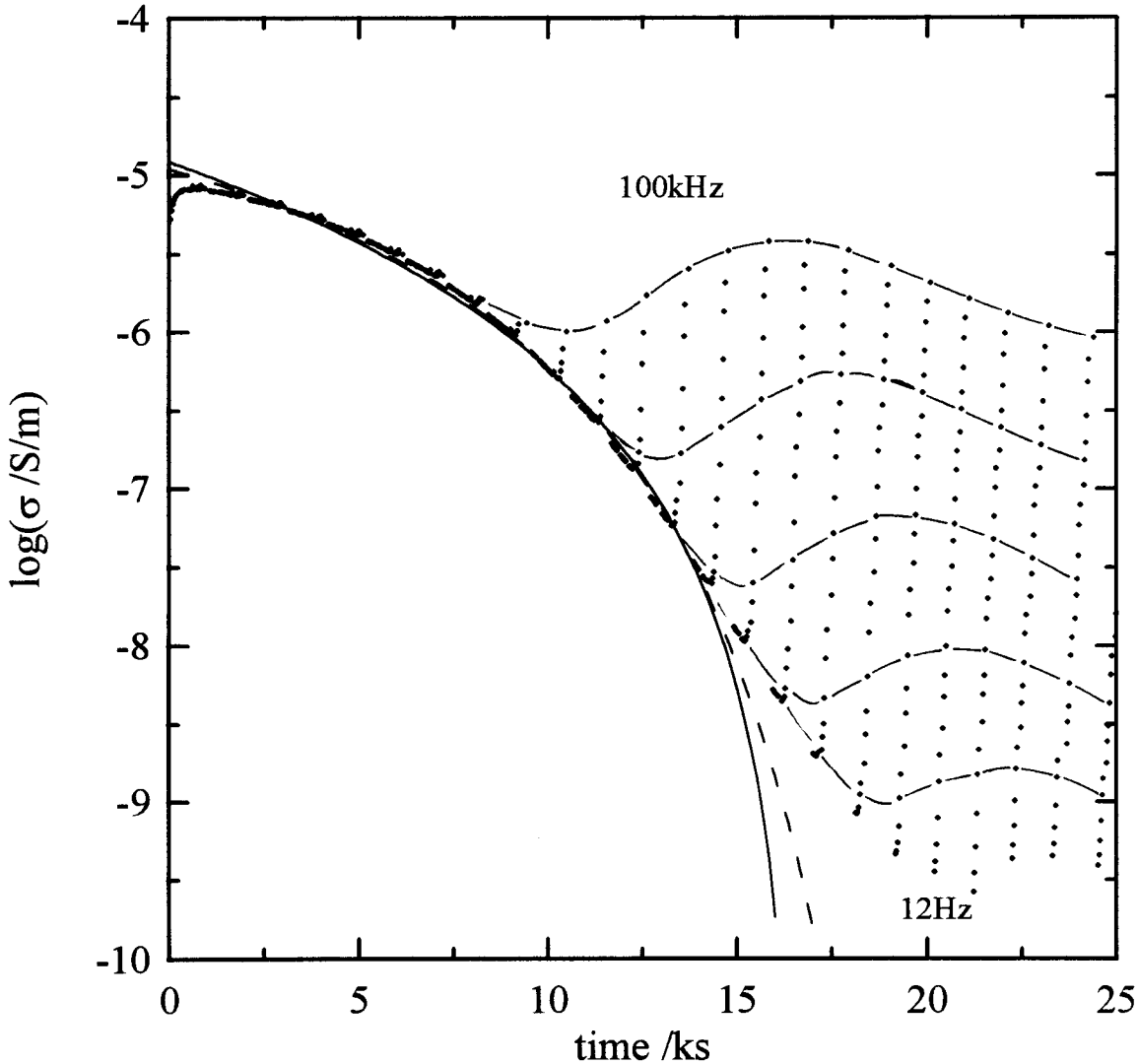

Figure 4.14: The log of conductivity plotted as a function of reaction time with the filled circles representing the measured data for the initially uncured Tactix-3CA. The continuous line was generated from Equation (4.10) and the dashed line from Equation (4.11), with parameters for each listed in Table 4.3.

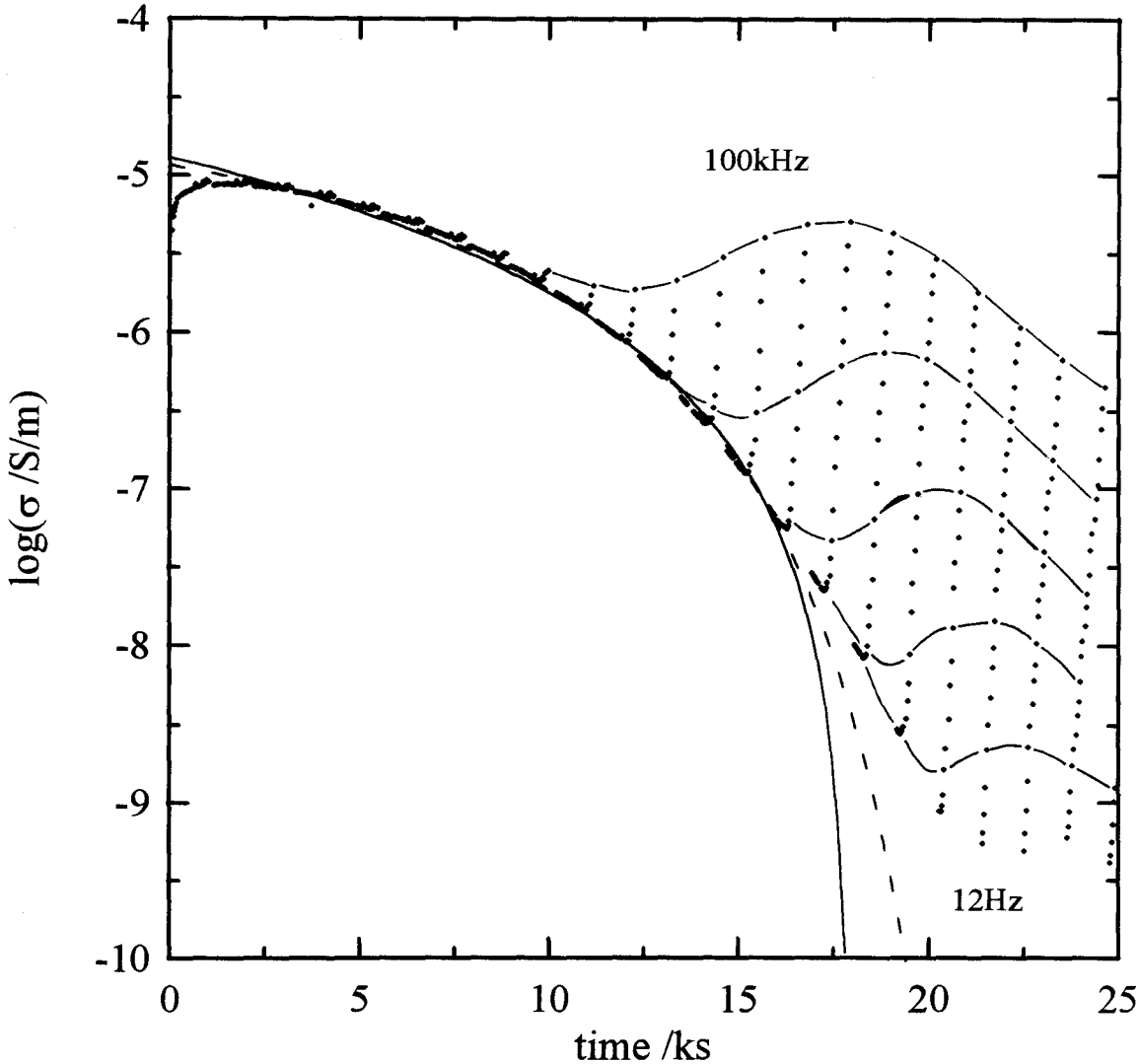

Figure 4.15: The log of conductivity plotted as a function of reaction time with the filled circles representing the measured data for the initially uncured Tactix-4CA. The continuous line was generated from Equation (4.10) and the dashed line from Equation (4.11), with parameters for each listed in Table 4.3.

Wasylyshyn and Johari 1995) as well as in Section 4.2.1. This procedure is mathematically valid only when ε_s and ε_∞ are invariant of time, and approximate but satisfactory when it is not. It does require knowledge of ε' and is therefore not as direct as an analysis of σ_{meas} alone. Complex plane plots of M" against M' are given in Figure 4.16 for Tactix-AN, Tactix-3CA and Tactix-4CA. The curves are initially semicircular near the origin but deviate from this further away from it. Each data point in the plots corresponds to a measurement of ε' and ε'' at a certain time, t. The data points that lie on the semicircle indicate the time, t, or N(t), when the measured conductivity is dominated by σ_{dc}, and the deviations from the semicircle indicate the contributions from the dipolar relaxations to σ_{meas}. The last data lying on the semicircle corresponds to the maximum time up to which σ_{meas} is dominated by σ_{dc}.

Figures 4.13, 4.14 and 4.15 show that the contributions of the frequency-dependent σ_{inter} is relatively insignificant near the origin of the curves where it is expected to be large because σ_{dc} is largest here. The increase in σ seen at the beginning of the polymerization is predominantly an effect of the changing temperature of the sample as it warmed from the ambient to the isothermal temperature at which the polymerization was done. In these figures, data for all frequencies lie on the same curve in the early stages of the experiment but the data deviates from a single curve when t has increased to a certain extent. This extent is high when the frequency is low and low when the frequency is high, as shown by the data points for 30Hz and 10^5Hz frequencies. If ω were decreased towards zero, σ_{meas} would follow a curved path of increasing negative

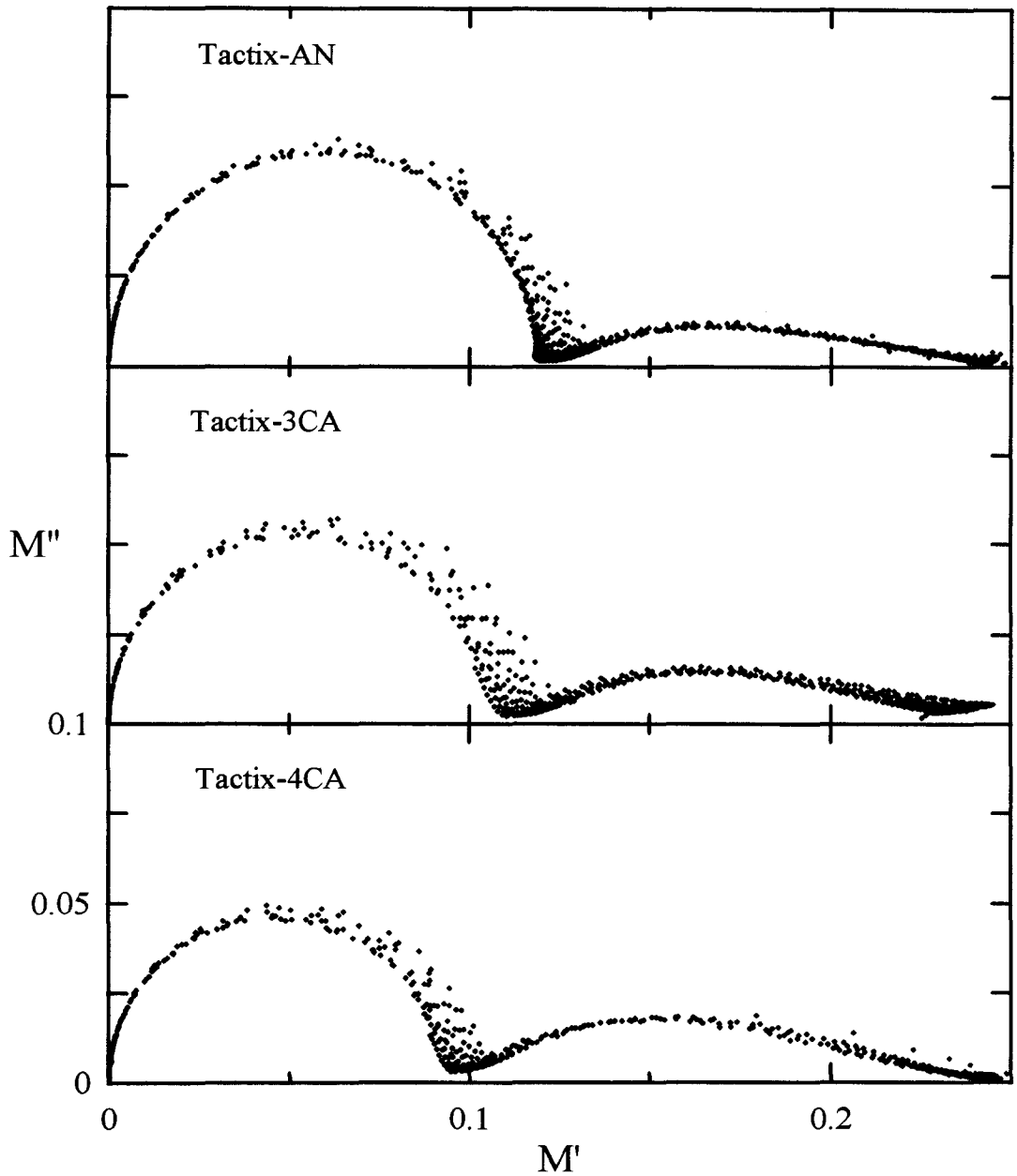

Figure 4.16: The complex plane plots of M" against M' measured during the isothermal polymerization of each of the three mixtures.

slope as t approached infinity, but if ω was increased to a large value, say 10^{11}Hz, σ_{meas} would remain near its σ_{dc} plateau value as t approached infinity.

σ_{dc} decreases with t for at least three reasons: (1) a decrease in the diffusion coefficient of both the impurities and ions present in the pure substance and zwitter ions (Johari 1993a, 1994, Alig and Johari 1993) formed in the reacting mixture as the viscosity of the mixture irreversibly increases, (2) a disruption of the H-bonded network, and hence a disruption of the proton transfer mechanism for dc conduction, as the H-bonding protons of the amine groups are replaced by the covalent bond between the carbon atom of the epoxide and the nitrogen atom of the amine and (3) a decrease in the population of impurity ions as they form ion-pairs in increasingly large numbers when ε_s of the mixture decreases on polymerization. This last effect can be expressed in terms of an association constant (Fuoss 1958, Davies 1962),

$$K_A = \frac{C_{ion\text{-}pair}}{C_{cation}C_{anion}} = \frac{4\pi N_A^3}{3000}\exp\left(\frac{z_1 z_2 e^2}{a\epsilon_s k_B T}\right) \qquad (4.41)$$

where C refers to the concentration of the entity written in subscripts, z_1 and z_2 are the ionic charges, e is the electronic charge, **a** is the ion-size parameter and k_BT is the thermal energy. During the isothermal growth of a macromolecule, the only variable in Equation (4.41) is ε_s, which decreases and thus K_A increases, or $C_{ion\text{-}pairs}$ increases at the expense of free ions.

The dc conductivity during the isothermal polymerization of the three mixtures

was analyzed in a similar manner as described in Section 4.2.1b, namely, the dielectric conductivity data, σ_{dc} was fitted to Equations (4.10) and (4.11), both of which have been found to adequately describe the decrease in dc conductivity during the polymerization of monomeric liquids to ultimately cross-linked network polymers (Johari 1991,1993a, Parthun and Johari 1992c, Mangion and Johari 1991a,b,c). The continuous line in Figures 4.13, 4.14 and 4.15 are the best fits to the σ_{dc} data for Tactix-AN, Tactix-3CA and Tactix-4CA from Equation (4.10), and the dashed line in the same figures represents the fit using Equation (4.11). The parameters used in the fittings for each of the mixtures are listed in Table 4.2.

The plots and associated analysis confirms that Equations (4.10) and (4.11) describe the conductivity data quite reasonably. This is also observed with the formation of other network structures, such as those formed from the reaction of diepoxides with diamines. However, in the instance of linear chains formed by the reaction of diepoxides with monoamines, Equations (4.10) and (4.11) do not adequately describe the conductivity data (Parthun and Johari 1992c, Mangion and Johari 1991c). This is because the reaction of diepoxides with monoamines forms linear chains, and not continuous, cross-linked network structures, and the linear chains formed are too short to become an entangled structure required for gelation.

Table 4.2: The parameters used to calculate $\sigma_{dc}(t)$ for Tactix-AN, Tactix-3CA and Tactix-4CA, using Equations (4.10) and (4.11).

	Tactix-AN	Tactix-3CA	Tactix-4CA
$\log(\sigma\ /Sm^{-1})$	-5.64	-4.91	-4.88
x	3.03	3.28	2.44
t_{gel} /ks	20.90	16.57	17.95
$\alpha(t_{gel})$	0.42	0.49	0.47
$N(t_{gel})x10^{-23}$	3.07	3.52	3.39
$\ln A_{\sigma}$	-9.56	-7.75	-8.90
B_{σ}	100843.0	82798.3	57861.9
t_o /ks	28.70	22.57	23.50
$\alpha(t_o)$	0.70	0.72	0.68
$N(t_o)x10^{-23}$	5.07	5.21	4.88
α_{gel}	0.714	0.714	0.714
$N_{gel}x10^{-23}$	5.16	5.16	5.16

4.2.3 Critical Conditions for the Gel for Infinite Network Formation

There are two critical conditions that characterize gelation: (i) The extent of reaction or the number of bonds formed at gelation, and (ii), which is less certain, is the magnitude of the critical exponent of Equation (4.10). The requirement for the number of bonds formed when the gel forms is statistically determined by Flory (1942) for polymer networks. He deduced the conditions underwhich an infinitely connected

network or gel will form as follows. Consider the polymerization of two chemicals; one contains a difunctional unit A-A or a trifunctional unit $A_{\overset{|}{A}}A$, and the other contains a difunctional unit B-B, where the chemical reaction occurs exclusively between A and B functions or groups to produce -A-B- as a condensation product. Assuming that the reactions between the A and B groups of the product are forbidden and cyclic structures do not form, Flory (1942) further considered that a cross-linked, infinitely connected network or macromolecule is an assemblage of chains connected at cross-linking points. He then determined the conditions for a finite probability for a selected chain being a part of an infinitely connected network. He calculated the probabilities of reaction between A and B groups in terms of the ratio of A belonging to a reacting branch or segment units to the total number of A's in the mixture, and generalized the statistical treatment to show the conditions for the formation of an infinite network or gelled structure are such that the extent of reaction, α, (Flory 1942),

$$\alpha = \frac{1}{(f-1)} \qquad \textbf{(4.42)}$$

where f is the functionality of the Branching unit. For systems with more than one type of branching units, (f-1) is replaced by a weighted average, which is calculated from the number of functional groups present and the stoichiometric molar amounts, M. Thus, for the weighted average, (f-1) of Equation (4.42) is,

$$(f-1)=\sum_{0}^{i}\frac{(f_i-1)}{M_i} \tag{4.43}$$

For the polymerization of trifunctional Tactix-742 with a difunctional amine as in our studies, the stoichiometric amounts used were 2 moles of Tactix-742 with 3 moles of the amines. Hence,

$$(f-1)=\frac{(2(3-1)+3(2-1))}{5}=\frac{7}{5} \tag{4.44}$$

So, substituting this value into Equation (4.42) gives the extent of the reaction at gelation, or α_{gel}, as 0.714. This value is the same for all three polymers. The parameters calculated from Equation (4.10) are listed in Table 4.2, where the extent of reaction determined from the DSC measurements at the gelation time, $\alpha(t_{gel})$, and the number of bonds formed $N(t_{gel})$ are also given. The corresponding values for the time, t_o, calculated from Equation (4.11), namely $\alpha(t_o)$ and $N(t_o)$, are given and the values of α_{gel} and N_{gel} calculated from Flory's theory are also given. The experimental value of $\alpha(t_{gel})$, which is 0.42 for Tactix-AN, 0.49 for Tactix-3CA and 0.47 for Tactix-4CA, determined from the dc conductivity and the DSC data are about 50% less than the values calculated from Flory's theory.

The discrepancies may occur for a number of reasons which are worth considering. Such discrepancies have been found by Parthun and Johari (1992) for polymerization of a diepoxide with diamines and the differences attributed to the unrealistic assumptions

made by Flory to simplify the statistical probabilities of bonding between A and B groups. Its also possible that the unreacted functional groups do not have the same probability of reaction as the unreacted functional groups of reacted molecules or the functional groups at the free ends of a chain which have not reacted. The probability of reaction of these groups when the reaction becomes diffusion controlled depends upon the steric hindrance for the rotational diffusion of the functional groups in the liquid, which is different from that of a reacted group within the segment of a partially connected network or a short chain. Stockmayer (1943) also pointed out that if the cyclic structures, which are not part of the network, like loops, did occur, the α_{gel} calculated from Flory's method will be uncertain by as much as 5%. This effect of the formation of intramolecular rings would thus be to increase the chemical reactions without contributing to the formation of the network. In the present studies the nitrogen atom of the anilines joins the terminal carbon atoms of the Tactix-742 molecules and the benzene ring of the aniline is not a part of the cross-link. Furthermore, the length of the cross-links thus formed is much greater than with diepoxides cured with diamines, thereby causing a greater flexibility of the network structure. It seems that the above-mentioned effect can cause deviations in the value of $\alpha(t_{gel})$ from that predicted by Flory's theory for gelation. This is so because both the length of the chains forming the cross-links and the unequal probabilities of the partially reacted and unreacted functional groups influence the rate of chemical reactions in a manner which is inconsistent with the assumptions made in the theory. It is also significant to note that α_{gel} for Flory's theory agrees with the $\alpha(t_o)$ as

seen in Table 4.2. This implies that Equation (4.11) is a better representation for gelation than Equation (4.10), which is based on percolation theory. This observation needs to be confirmed from studies in which diepoxies are reacted with trifunctional amines.

We now discuss the magnitude of the critical exponent, x, obtained from Equation (4.10) and listed in Table 4.2. For the polymerization of Tactix-AN x = 3.03, for Tactix-3CA x = 3.28 and for Tactix-4CA x = 2.44. Adolf et al. (1990) have critically reviewed the magnitude of the critical exponents obtained from the various equilibrium and dynamic properties measured during the course of gelation. For equilibrium properties such as the unrelaxed shear modulus and dc conductivity, where the functional form is $(P_{gel}/(P_{gel} - P))^x$, x is 2.0 to 2.7. The values of x observed here were in the range 3.03 to 2.44. These are comparable with those deduced by Adolf et al. (1990). We also note that for the polymerization of diepoxies and diamines x was found to be 2.63 to 4.38 (Parthun and Johari 1992) for polymerization at different temperatures. Evidently the critical exponent for the percolation determined here is consistent with that observed for the equilibrium property, G_U. Thus, the validity of Equation (4.10) seems to be justified.

4.2.4 The Evolution of Molecular Dynamics

The irreversible changes in the dielectric properties that occurs during polymerization are dominated by (Johari 1993a):

(1) A general decrease of the dc conductivity as the diffusion coefficient of the impurity ions initially present and zwitter ions (Alig and Johari 1993) formed in

the reacting mixture decreases with an increase in the liquid's viscosity, and the decrease of proton transfer along the H-bonded network due to the consumption of inter-monomer hydrogen bonds between the reactants.

(2) An increase in the relaxation times as a result of which the measured dielectric permittivity measured at a fixed frequency decreases monotonically towards a value corresponding to the infrared region.

(3) A change in the number of dipoles per unit volume and therefore in the contribution to permittivity from orientation polarization, $\Delta\varepsilon$, as a result of chemical reactions which alter the dipole moment and the volume contraction which raises the number density of dipoles.

(4) A change in the dielectric relaxation function as the chemical structure of the liquid changes and its viscosity and density increase.

(5) A change in the contribution to permittivity due to infrared polarization, $\Delta\varepsilon_{ir}$, as the vibrational frequencies of the various modes in the structure change on cross-linking and densification.

(6) A change in the optical refractive index or optical polarization as the network structure forms and densifies.

(7) A splitting of the unimodal relaxation function into a bimodal relaxation function (Tombari and Johari 1992).

As described in Section 4.2.1b, the dielectric relaxation spectrum during

polymerization is similar to that of a chemically and physically stable system, since the shape of the spectrum is dominated by changes in either ω or τ_o. For time-variant systems, the parameter γ is used to describe the shape of the relaxation spectra instead of the time-invariant β parameter, and $\tau_o(t)$ represents the time-dependent characteristic relaxation time (Mangion and Johari, 1990b). In a study of the time-invariant state of a substance, ω is varied so that a change in $\omega\tau$ could be used to obtain the relaxation spectrum. In a study of time-variant states, such as in polymerization, τ itself increases irreversibly as the macromolecule grows. Thus, for fixed frequency measurements, a spontaneous increase in $\omega\tau$ produces a plot of ε'' against ε' whose shape is determined by γ as well as the magnitude of the seven effects described above (Johari 1993a).

γ was determined from the fixed frequency Cole-Cole plots by fitting the measured data to tables of normalized dielectric loss and permittivity (Moynihan et al. 1973, Dishon et al. 1985) with parameters of $\varepsilon(t\rightarrow\infty)$ and $\varepsilon(t\rightarrow 0)$ (these are analogous to ε_∞ and ε_s in time-invariant states) and γ, as described in Section 4.2.1b. Figures 4.17, 4.18 and 4.19 show the complex-plane plots of the dielectric loss, ε'', against the dielectric permittivity, ε', during the polymerization of Tactix-AN, Tactix-3CA and Tactix-4CA, respectively. The closed circles in each plot corresponds to the measured data at fixed frequencies, namely, 0.030, 0.1, 0.3, 1, 3, 10, 30 and 100kHz, made during the course of the polymerization. The reaction time, t, or equivalently the number of covalent bonds, N(t), increases from right to left. The fits to each fixed frequency measurement are shown as a continuous lines in these figures, with the parameters

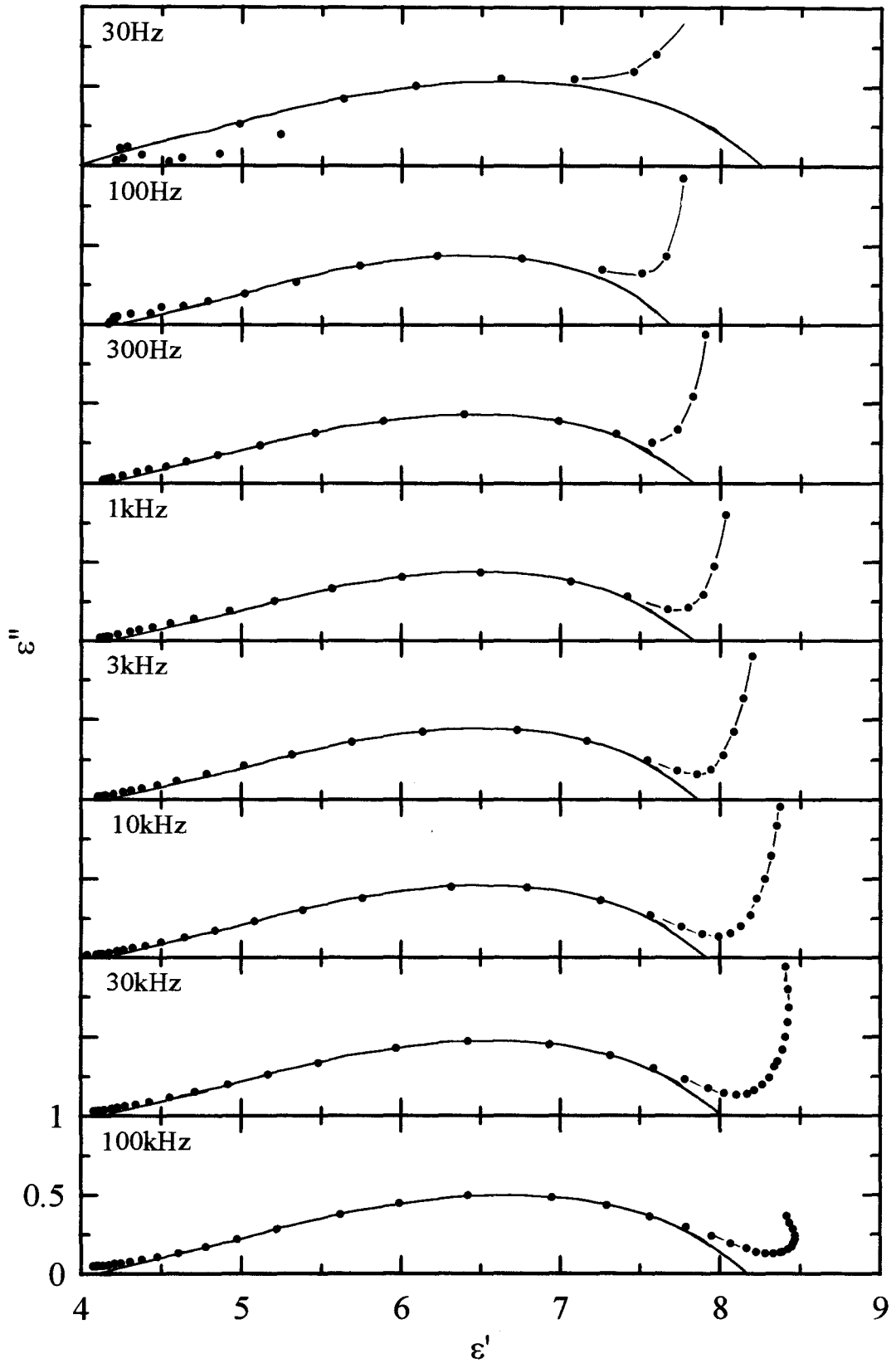

Figure 4.17: Complex plane plots of ε" against ε' at selected fixed frequencies of 30Hz, 100Hz, 300Hz, 1kHz, 3kHz, 10kHz, 30kHz and 100kHz for the isothermal polymerization of Tactix-AN at 332.0K.

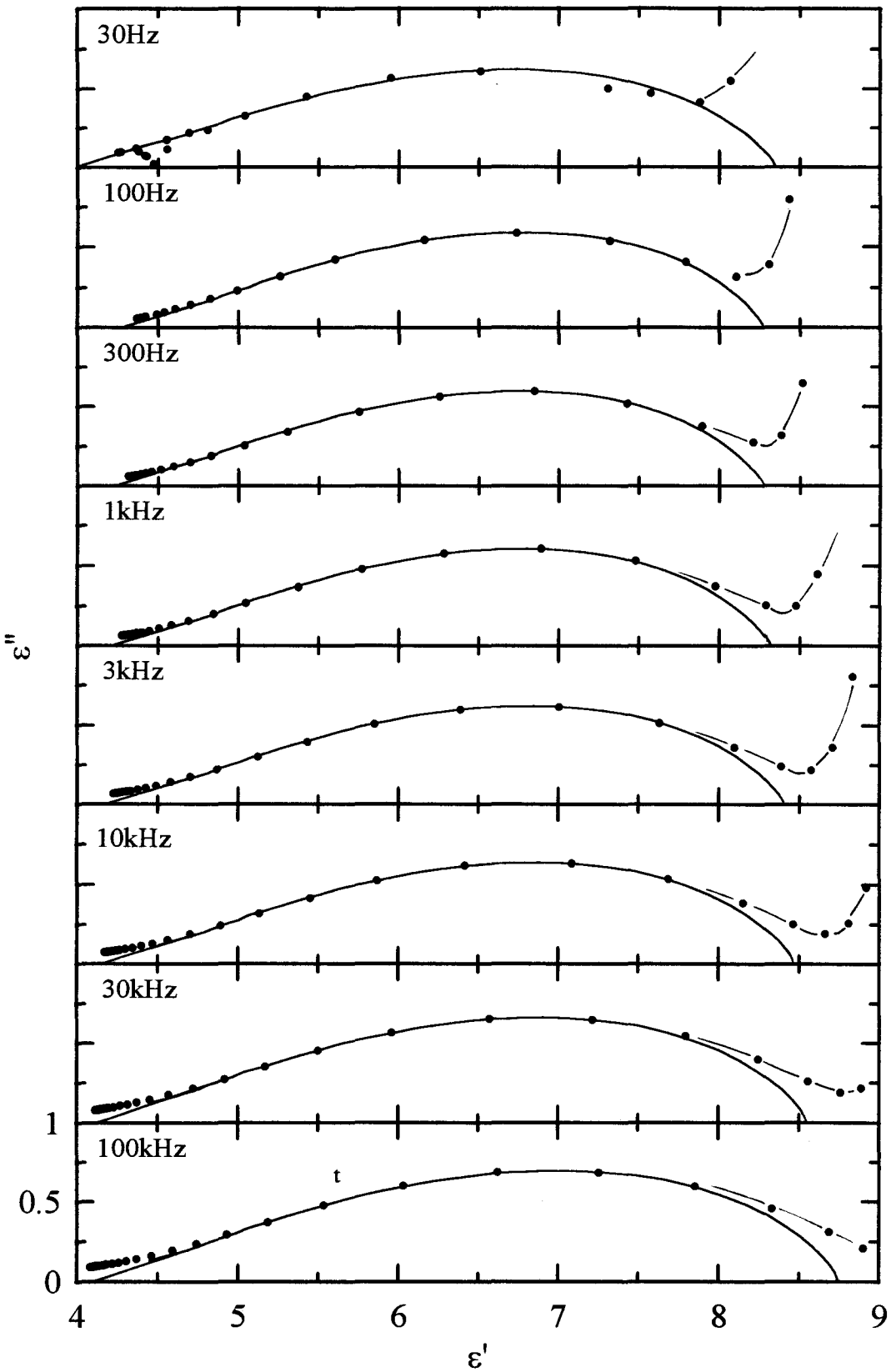

Figure 4.18: Complex plane plots of ε" against ε' at selected fixed frequencies of 30Hz, 100Hz, 300Hz, 1kHz, 3kHz, 10kHz, 30kHz and 100kHz for the isothermal polymerization of Tactix-3CA at 360.6K.

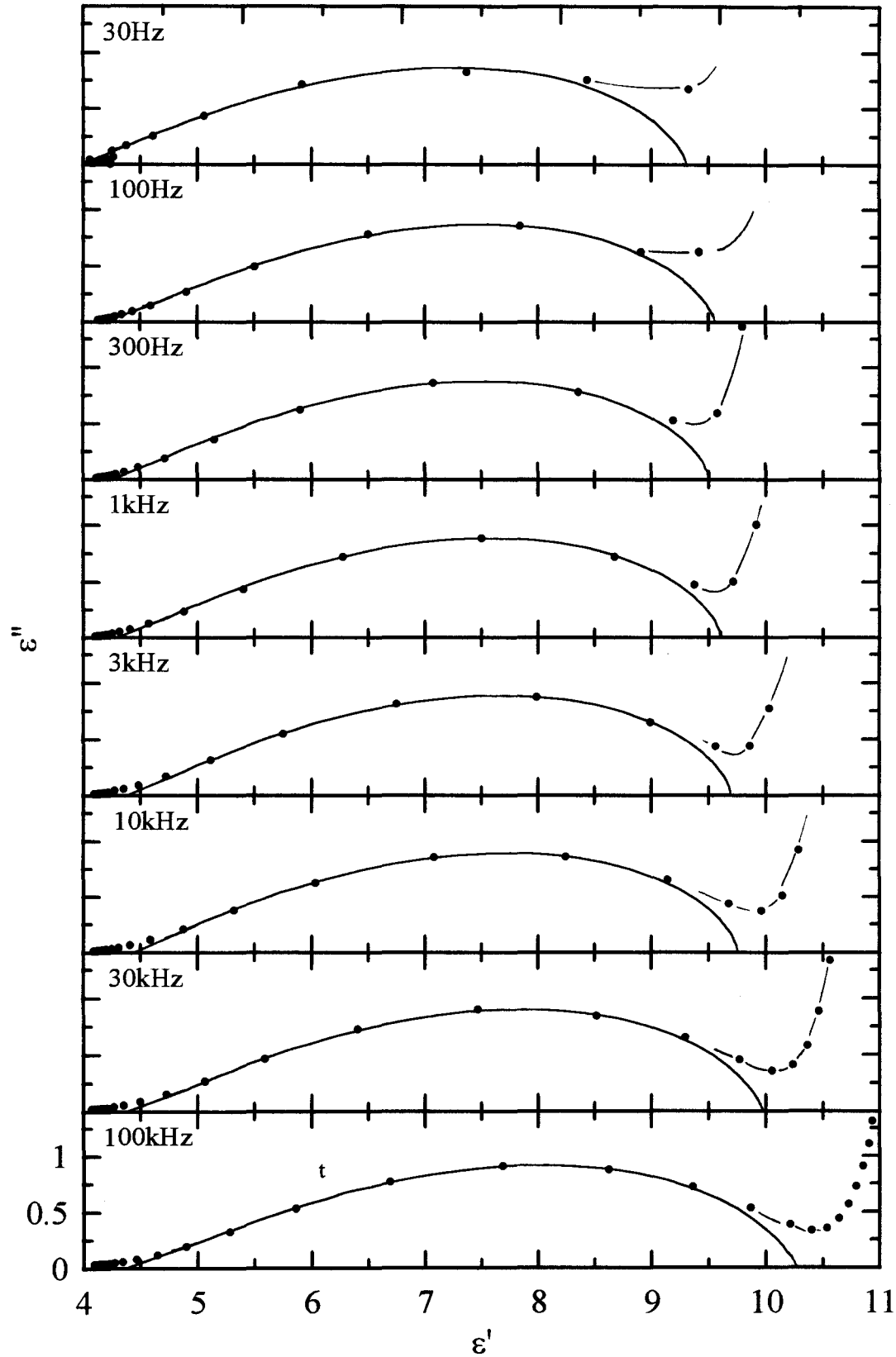

Figure 4.19: Complex plane plots of ε" against ε' at selected fixed frequencies of 30Hz, 100Hz, 300Hz, 1kHz, 3kHz, 10kHz, 30kHz and 100kHz for the isothermal polymerization of Tactix-4CA at 349.5K.

deduced given in Table 4.3. The deviations from the fitted curves at high values of ε' (low values of N(t) and t) is due to the dc conductivity, σ_{dc}, which predominates σ_{dip}. Each calculated point on the fitted curve corresponds to a particular value of $\tau_o(t)$.

The relaxation time, $\tau_o(t)$, was then calculated in the following manner from the fixed frequency measurements and the analyzed data in the same manner as described in Section 4.2.1b. Eight sets of five to eight τ_o and t (hence N(t)) were obtained for the Tactix-AN, Tactix-3CA and Tactix-4CA mixtures. The average relaxation time was then calculated from the equation $<\tau> = (\tau_o/\gamma)\Gamma(1/\gamma)$, where $\Gamma(y)$ represents the gamma function of y (Moynihan et al. 1973). Plots of $\log(<\tau>)$ against N(t) are given in the plots of Figures 4.20, 4.21, and 4.22 for Tactix-AN, Tactix-3CA and Tactix-4CA, respectively. The regions of overlapping data for the different sets calculated from different frequencies confirm that the relaxation time at a given instant of reaction, but obtained from measurements at different frequencies is the same within the experimental and analytical uncertainties. This also confirms the phenomenology of the dielectric behaviour of the chemically reacting systems described by Tombari and Johari (1993).

The dielectric spectra of the partially polymerized mixture were also obtained at predetermined number of bonds, N(t) during the polymerization, as described in Section 3.2.1. The complex plane plots of ε" against ε' for values of N(t) are shown in Figures 4.23, 4.24 and 4.25, for Tactix-AN, Tactix-3CA and Tactix-4CA, respectively. These spectra were fitted to the tabulated values (Moynihan et al. 1973, Dishon et al. 1985) in the following manner (The tables provided by Moynihan et al. 1973 and Dishon et

Table 4.3: The parameters obtained from the analysis of the time-variant dielectric properties at eight frequencies for Tactix-AN, Tactix-3CA and Tactix-4CA.

Freq /Hz	$\Delta\varepsilon$	$\varepsilon'(t \to 0)$	$\varepsilon'(t \to \infty)$	γ
Tactix-AN				
30	4.1	8.2	4.1	0.23
100	3.24	7.65	4.41	0.24
300	3.46	7.78	4.32	0.22
1000	3.38	7.77	4.39	0.23
3000	3.43	7.81	4.38	0.23
10000	3.52	7.86	4.34	0.23
30000	3.64	7.95	4.31	0.23
100000	3.81	8.11	4.30	0.23
Tactix-3CA				
30	4.23	8.33	4.1	0.26
100	3.88	8.26	4.38	0.27
300	3.93	8.26	4.33	0.27
1000	3.98	8.30	4.32	0.27
3000	4.1	8.39	4.29	0.27
10000	4.2	8.46	4.26	0.27
30000	4.34	8.54	4.20	0.27
100000	4.56	8.74	4.18	0.27
Tactix-4CA				
30	5.3	9.3	4.0	0.29
100	5.3	9.55	4.25	0.29
300	5.2	9.5	4.3	0.3
1000	5.25	9.6	4.35	0.3
3000	5.27	9.69	4.42	0.3
10000	5.29	9.75	4.46	0.3
30000	5.51	9.96	4.45	0.29
100000	5.8	10.25	4.45	0.28

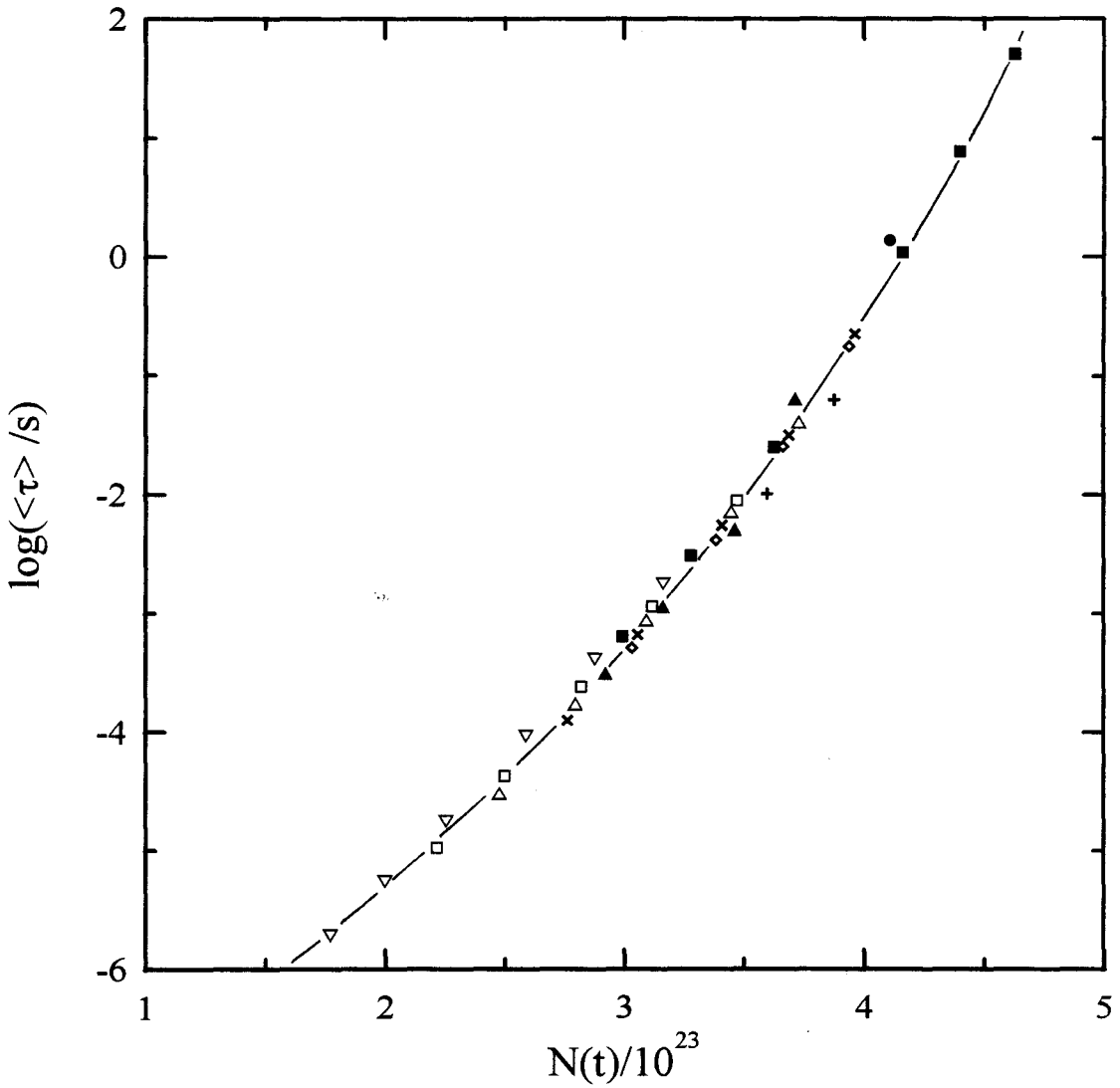

Figure 4.20: The log of the average relaxation time, $<\tau>$, plotted as a function of the number of bonds formed during the isothermal polarization of Tactix-AN at 332.0K. Filled triangles are the values calculated from the time-invariant spectra.

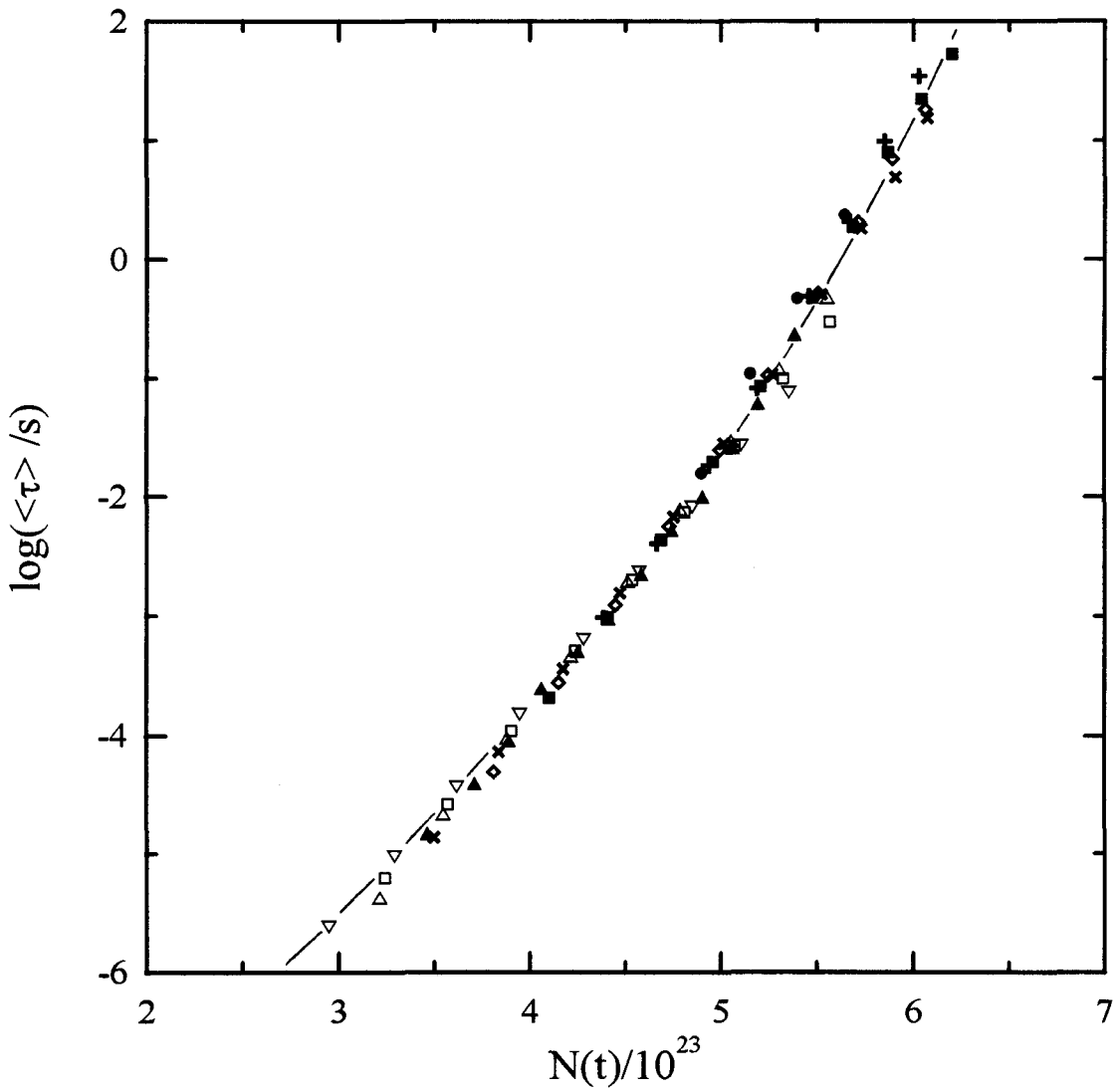

Figure 4.21: The log of the average relaxation time, $<\tau>$, plotted as a function of the number of bonds formed during the isothermal polarization of Tactix-3CA at 360.6K. Filled triangles are the values calculated from the time-invariant spectra.

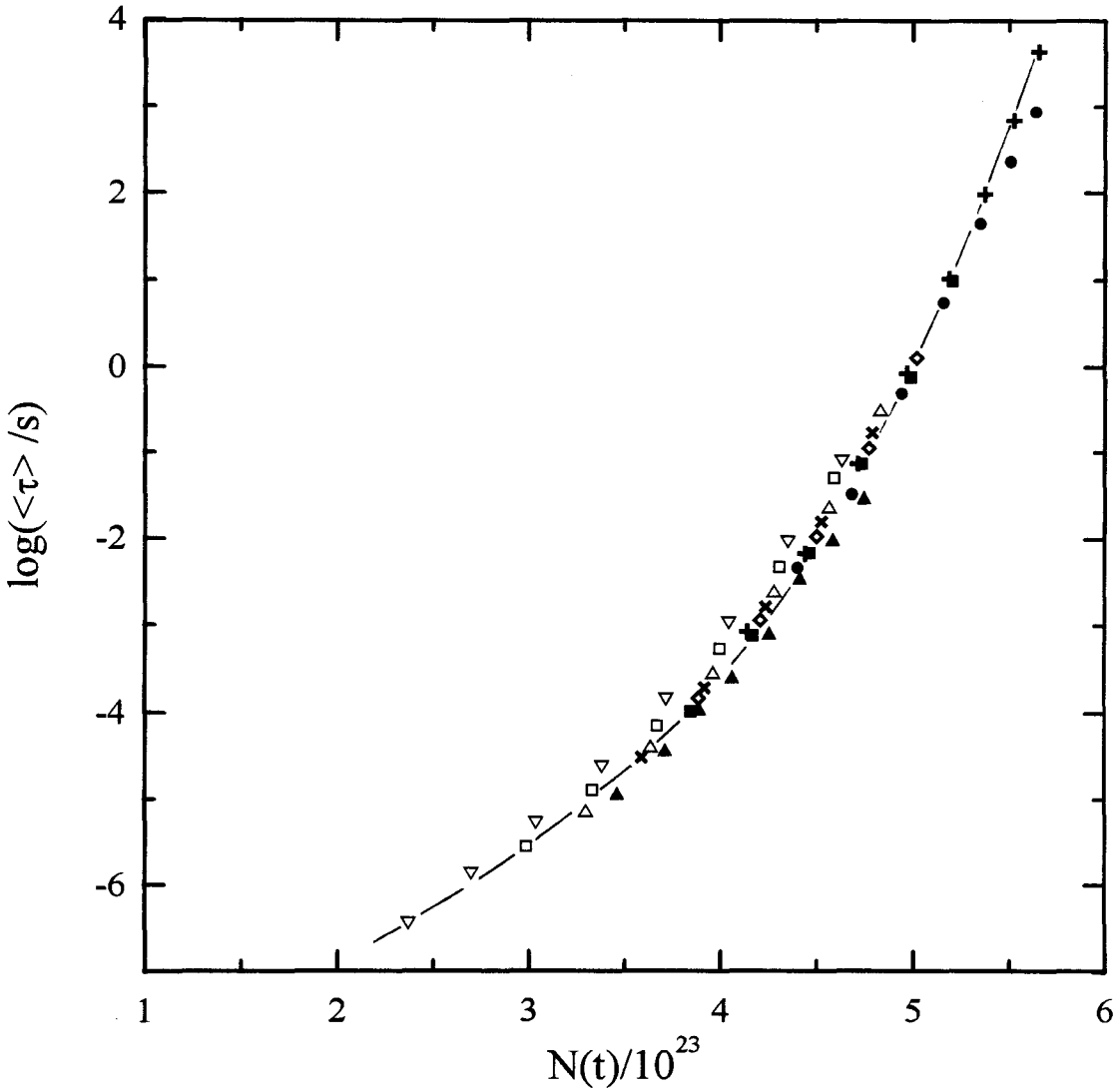

Figure 4.22: The log of the average relaxation time, <τ>, plotted as a function of the number of bonds formed during the isothermal polarization of Tactix-4CA at 349.5K. Filled triangles are the values calculated from the time-invariant spectra.

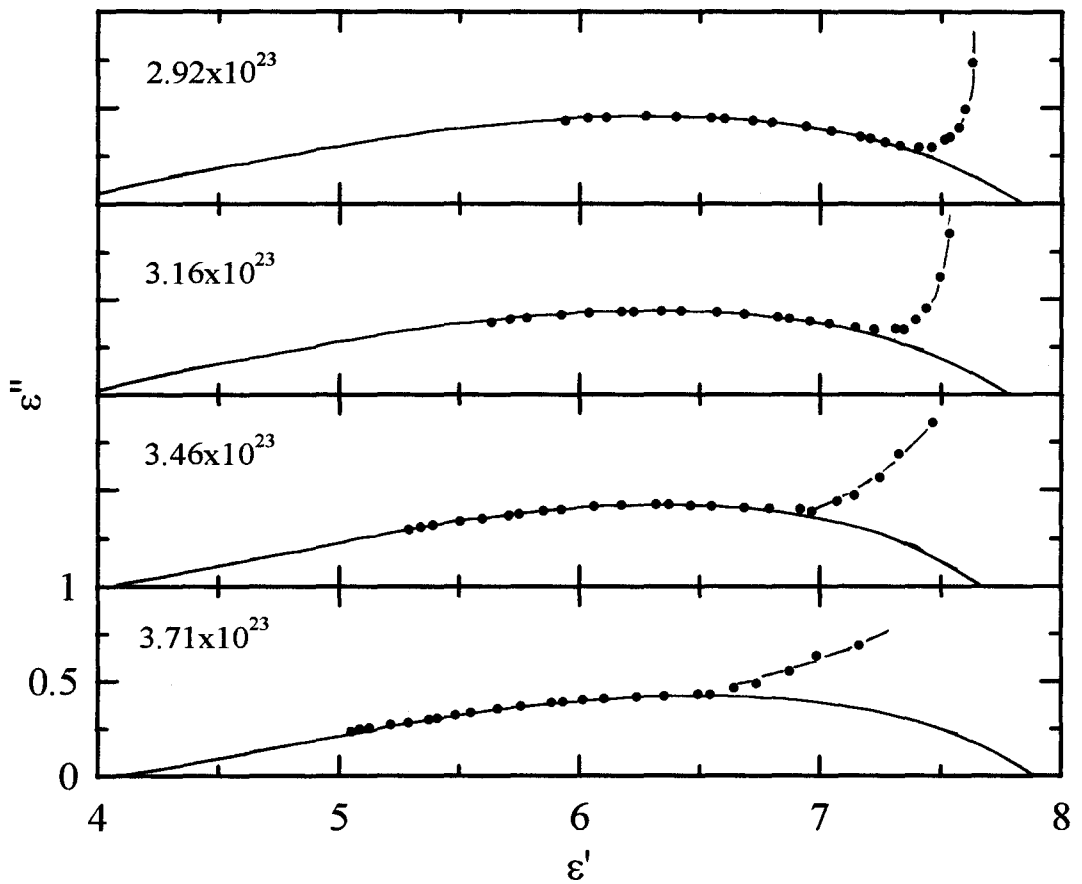

Figure 4.23: Complex plane plots of ε'' against ε' for constant values of N(t), during the isothermal polymerization of Tactix-AN at 332.0K. The continuous lines are calculated from parameters in Table 4.4.

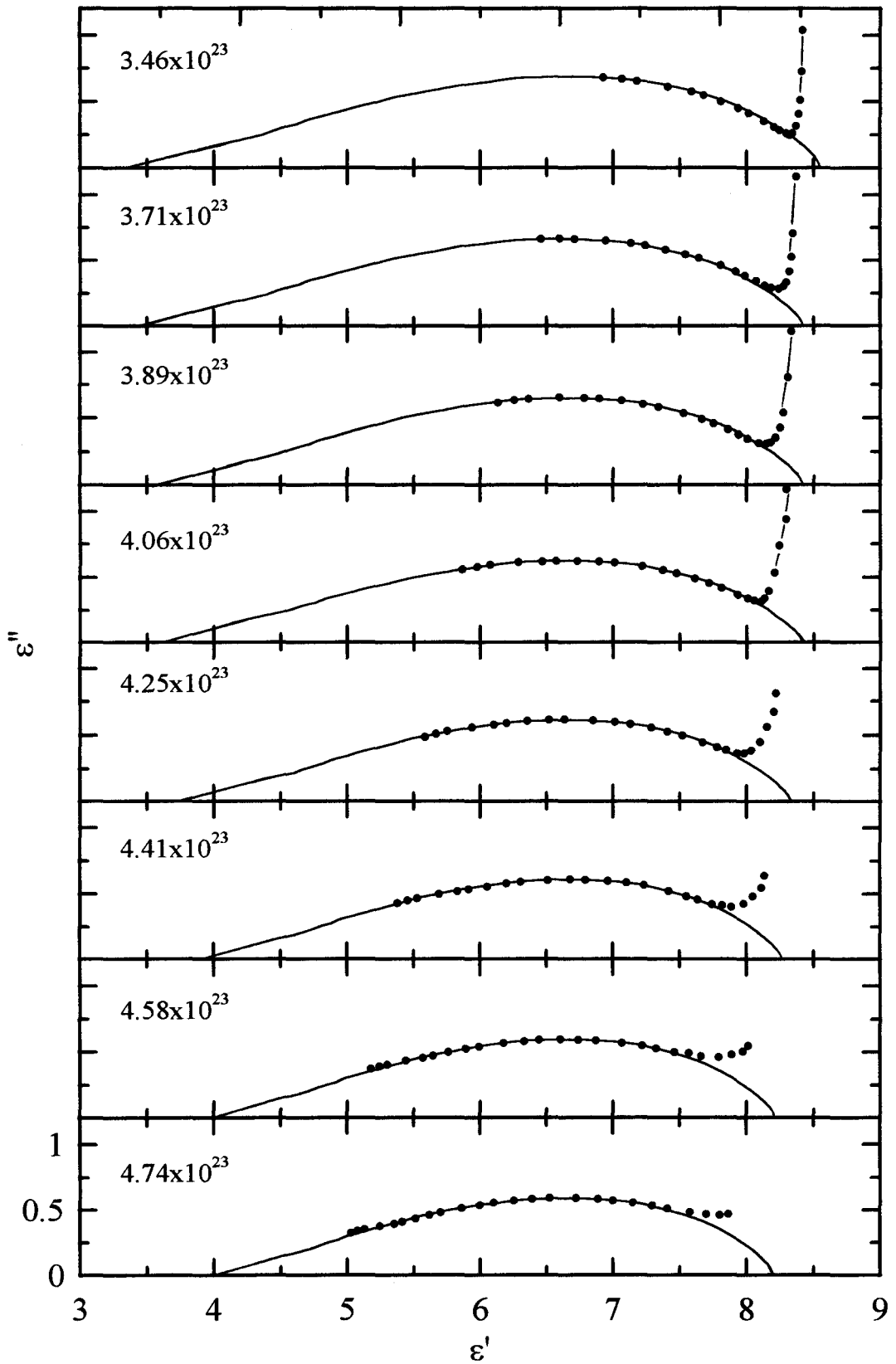

Figure 4.24: Complex plane plots of ε" against ε' for constant values of N(t), during the isothermal polymerization of Tactix-3CA at 360.6K. The continuous lines are calculated from parameters in Table 4.5.

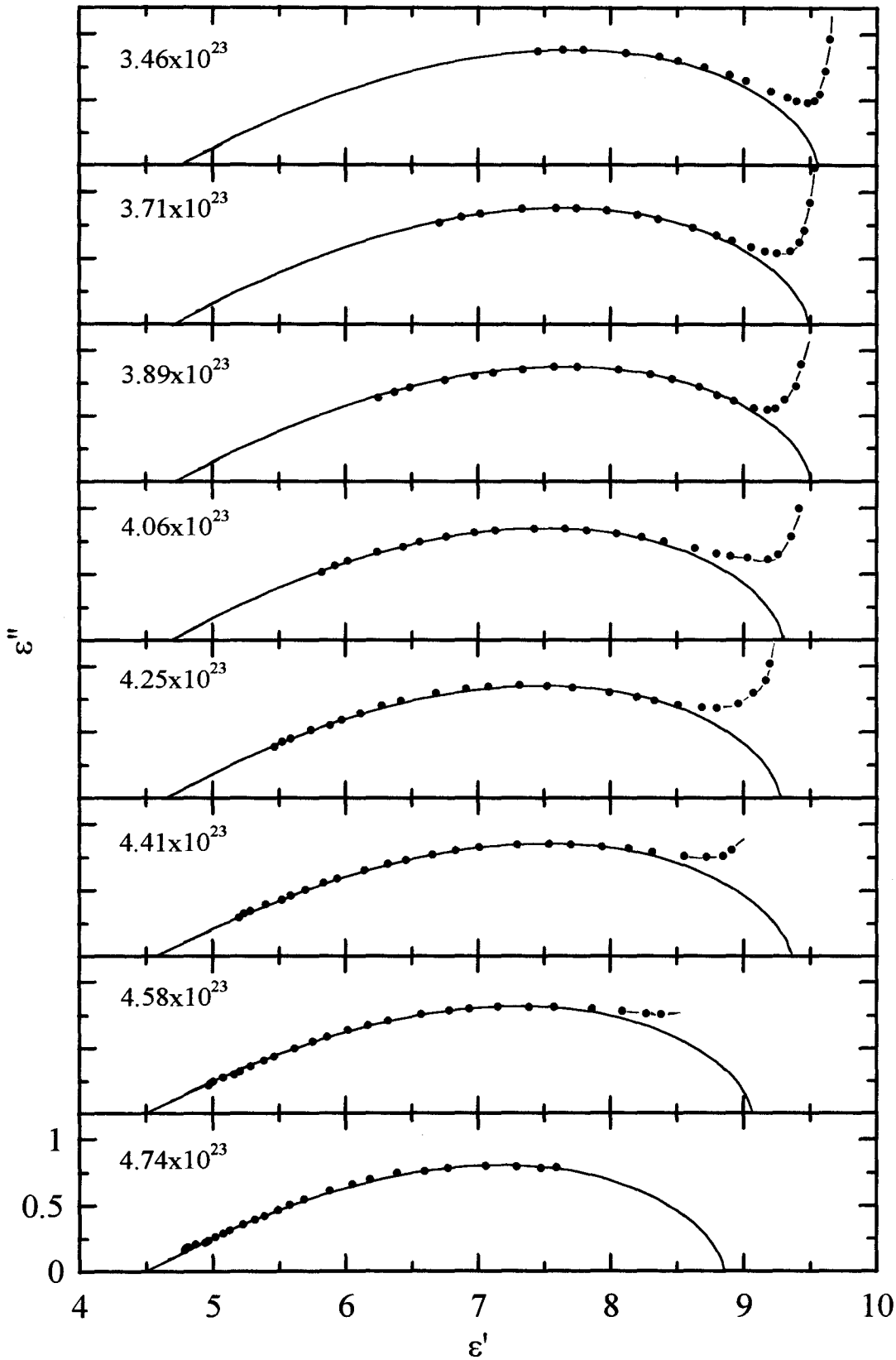

Figure 4.25: Complex plane plots of ε'' against ε' for constant values of N(t), during the isothermal polymerization of Tactix-4CA at 349.5K. The continuous lines are calculated from parameters in Table 4.6.

al.1985 are referred to here as the tabulated values). Firstly, the dielectric relaxation data were normalized along the frequency axis by the factor $\omega\tau_0$, such that the ε'' peak in the normalized data corresponded with the peak of the tabulated values. Secondly, the height of the ε'' peak was normalized by the relation $N'' = \varepsilon'' / (\varepsilon_0 - \varepsilon_\infty)$, and the adjustable parameter, $\Delta\varepsilon = (\varepsilon_0 - \varepsilon_\infty)$, varied until the N'' peak height matched the peak height of the tabulated data. Once the heights of the two peaks matched, the shape of the N'' peak was compared to the tabulated values for various values of β. Once the N'' peak was matched to the peak of the tabulated values the parameters τ_0, $\Delta\varepsilon$ and β, the ε' data was normalized by the equation, $N' = (\varepsilon' - \varepsilon_\infty) / (\varepsilon_0 - \varepsilon_\infty)$. ε_∞ was adjusted until N' matched the tabulated values. The four parameters thus obtained, τ_0, β, ε_∞ and ε_0, describe the mechanical spectrum measured at a fixed temperature. The filled circles are the measured dielectric data and the continuous lines are the fits to the tabulated values, with the resulting parameters shown in Tables 4.4, 4.5 and 4.6 for Tactix-AN, Tactix-3CA and Tactix-4CA. The average relaxation time, $\langle\tau\rangle$, was calculated from the characteristic relaxation time, τ_0, from Equation (4.15). The values of $\langle\tau\rangle$ obtained from the time-invariant analysis are plotted as solid triangles in Figures 4.20, 4.21 and 4.22. The agreement between the relaxation times determined from the time-variant data and the relaxation times determined from the time-invariant data confirms that the procedure for calculating $\tau_0(t)$ for a time-variant system is satisfactory (Johari and Pascheto 1995). It is noteworthy that the scatter of the $\langle\tau\rangle$ data is no more than that of the simulated data shown Figure 4.12.

Table 4.4: The parameters obtained from the fits of the constant N(t) dielectric spectra to Equation (2.36) for Tactix-AN.

time /ks	n(t)	$\Delta\epsilon$	ϵ_∞	β	τ_0 /μs	$<\tau>$ /ms	S_{conf} /J(Kmol)$^{-1}$
20.4	2.92	3.85	3.90	0.21	3.85	0.309	3.21
21.17	3.16	3.7	4.00	0.21	14.3	1.15	3.01
22.14	3.46	3.4	4.23	0.22	90	5.07	2.81
22.97	3.71	3.55	4.28	0.21	800	64.3	2.52

Table 4.5: The parameters obtained from the fits of the constant N(t) dielectric spectra to Equation (2.36) for Tactix-3CA.

time /ks	n(t)	$\Delta\varepsilon$	ε_∞	β	τ_o /μs	$\langle\tau\rangle$ /ms	S_{conf} /J(Kmol)$^{-1}$
16.37	3.46	4.88	3.65	0.25	0.62	0.015	4.08
17.16	3.71	4.7	3.7	0.25	1.65	0.040	3.82
17.74	3.89	4.6	3.8	0.25	3.8	0.091	3.62
18.30	4.06	4.6	3.8	0.24	8.1	0.25	3.40
18.94	4.25	4.35	3.96	0.25	21	0.50	3.27
19.50	4.41	4.15	4.1	0.26	50	0.95	3.15
20.10	4.58	4.05	4.15	0.26	120	2.29	3.01
20.70	4.74	4.02	4.17	0.26	280	5.34	2.88
21.30	4.90	3.82	4.26	0.27	650	10.1	2.80
21.95	5.06	3.75	4.29	0.27	1700	26.4	2.67
22.50	5.19	3.75	4.31	0.27	4000	62.1	2.57
23.30	5.38	3.75	4.35	0.27	15000	233	2.43

Table 4.6: The parameters obtained from the fits of the constant N(t) dielectric spectra to Equation (2.36) for Tactix-4CA.

time /ks	n(t)	$\Delta\varepsilon$	ε_∞	β	τ_o /μs	$\langle\tau\rangle$ /ms	S_{conf} /J(Kmol)$^{-1}$
18.21	3.46	4.80	4.75	0.33	1.9	0.012	3.67
19.04	3.71	4.78	4.70	0.33	6.0	0.037	3.43
19.66	3.89	4.78	4.72	0.33	18	0.11	3.23
20.25	4.06	4.61	4.68	0.33	41	0.26	3.09
20.94	4.25	4.62	4.65	0.33	130	0.81	2.92
21.54	4.41	4.76	4.59	0.32	500	3.52	2.72
22.21	4.58	4.56	4.50	0.32	1400	9.85	2.60
22.88	4.74	4.35	4.50	0.33	4800	29.9	2.48

4.2.5 The Bimodal Distribution in the Relaxation Times

The relaxation function that describes the dielectric properties of a monomeric mixture and of its different polymerized states is considered to be a distribution of times, which can be represented in different ways. Because several equally plausible representations are possible (Wagner 1913, Whitehead and Banos 1932, Yeager 1936, Fuoss and Kirkwood 1941, Cole and Cole 1941, Davidson and Cole 1950, Havriliak and Negami 1966, Williams and Watts 1970), it is difficult to determine which of them, if any, describes the true characteristics of the molecular dynamics. Therefore we avoid preference of a particular distribution function, and instead choose to use a generalized distribution for the purposes of this discussion.

When a single relaxation spectrum, whatever its shape, begins to evolve into two relaxation spectra, with two peaks or at least a minimum separating unresolveable peaks in the plot of ε'' against frequency, the molecular dynamics of the material acquires a bimodal distribution of relaxation times. The following discussion considers whether the time-variant data shows this evolution from unimodal to bimodal distribution. Time-invariant studies have already shown this evolution when polymerization leads to a network structure (Tombari and Johari 1992, Cassettari et al. 1993).

An enlargement of the time-variant ε'' near the end of the polymerization and the time-invariant spectra for large values of N(t) are shown in Figures 4.26(a,b) 4.27(a,b), and 4.28(a,b) for Tactix-AN, Tactix-3CA and Tactix-4CA, respectively. The time-variant curves show that in the upper limit of t (and N(t)), ε'' increased with increasing frequency

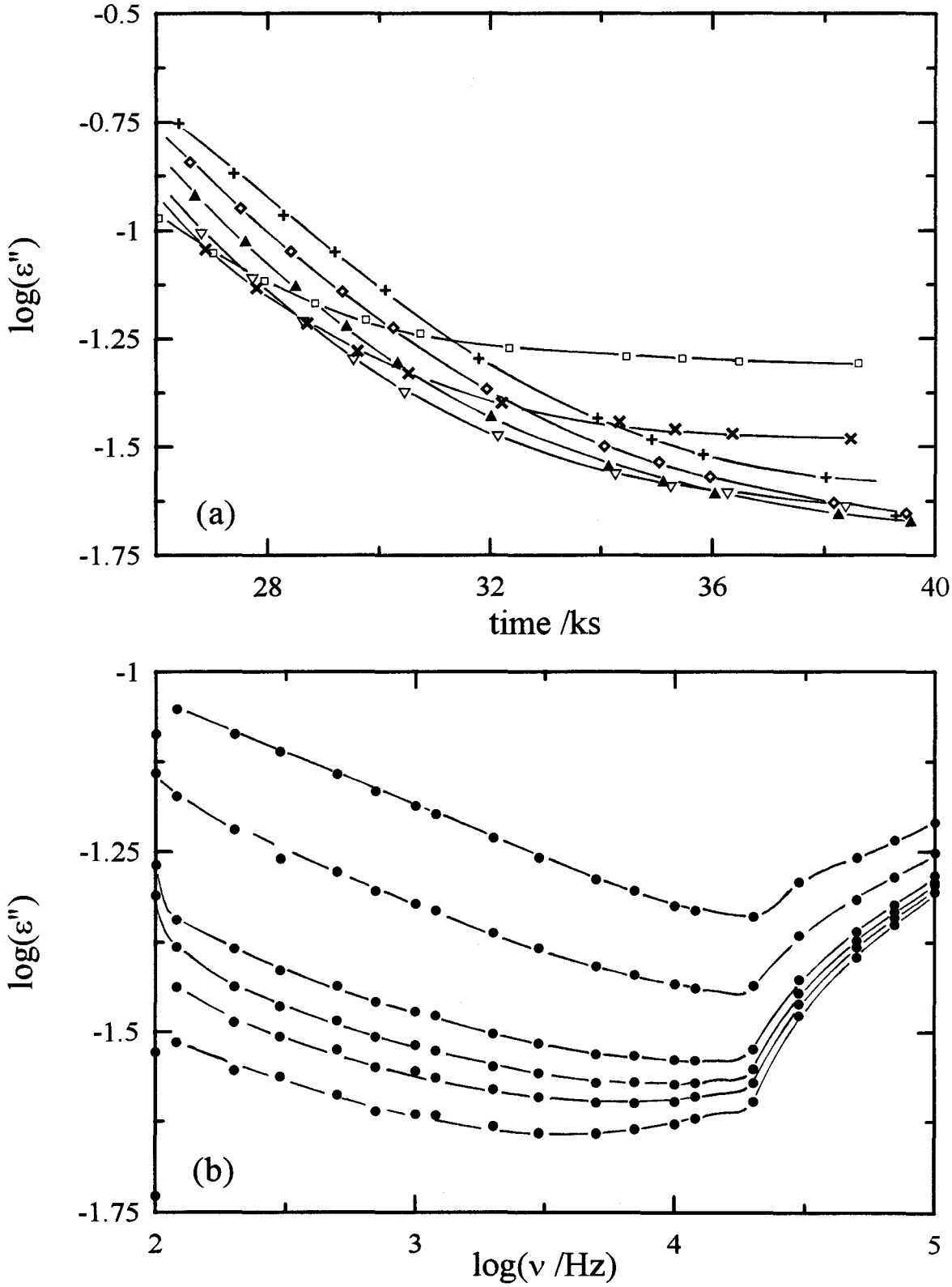

Figure 4.26: (a) The log of ε" plotted against reaction time showing the evolution of a second relaxation process, and, (b) The log of ε" plotted against the log of frequency for constant values of N(t) corresponding to long reaction times for the isothermal polymerization of Tactix-AN at 332.0K.

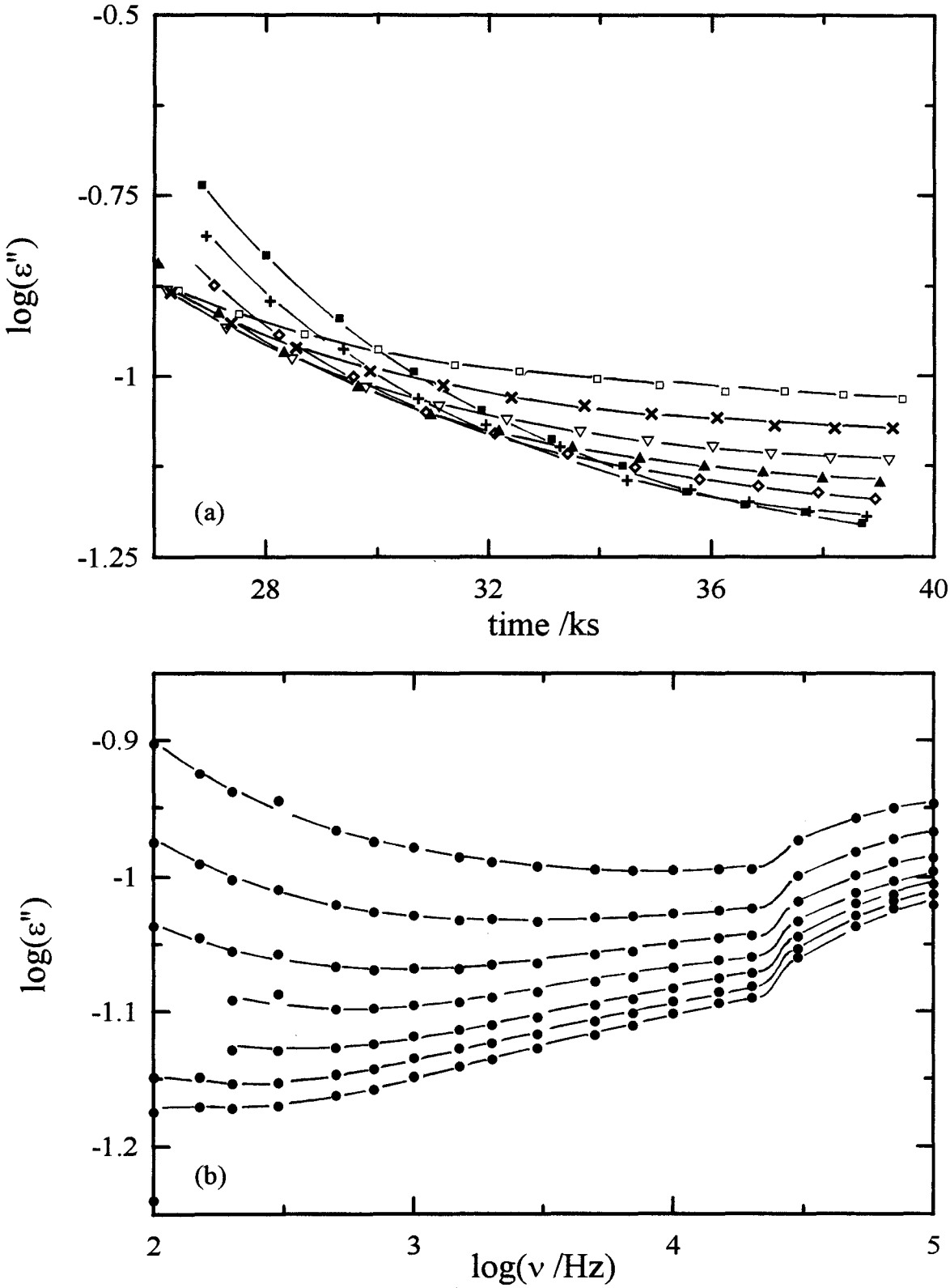

Figure 4.27: (a) The log of ε" plotted against reaction time showing the evolution of a second relaxation process, and, (b) The log of ε" plotted against the log of frequency for constant values of N(t) corresponding to long reaction times for the isothermal polymerization of Tactix-3CA at 360.6K.

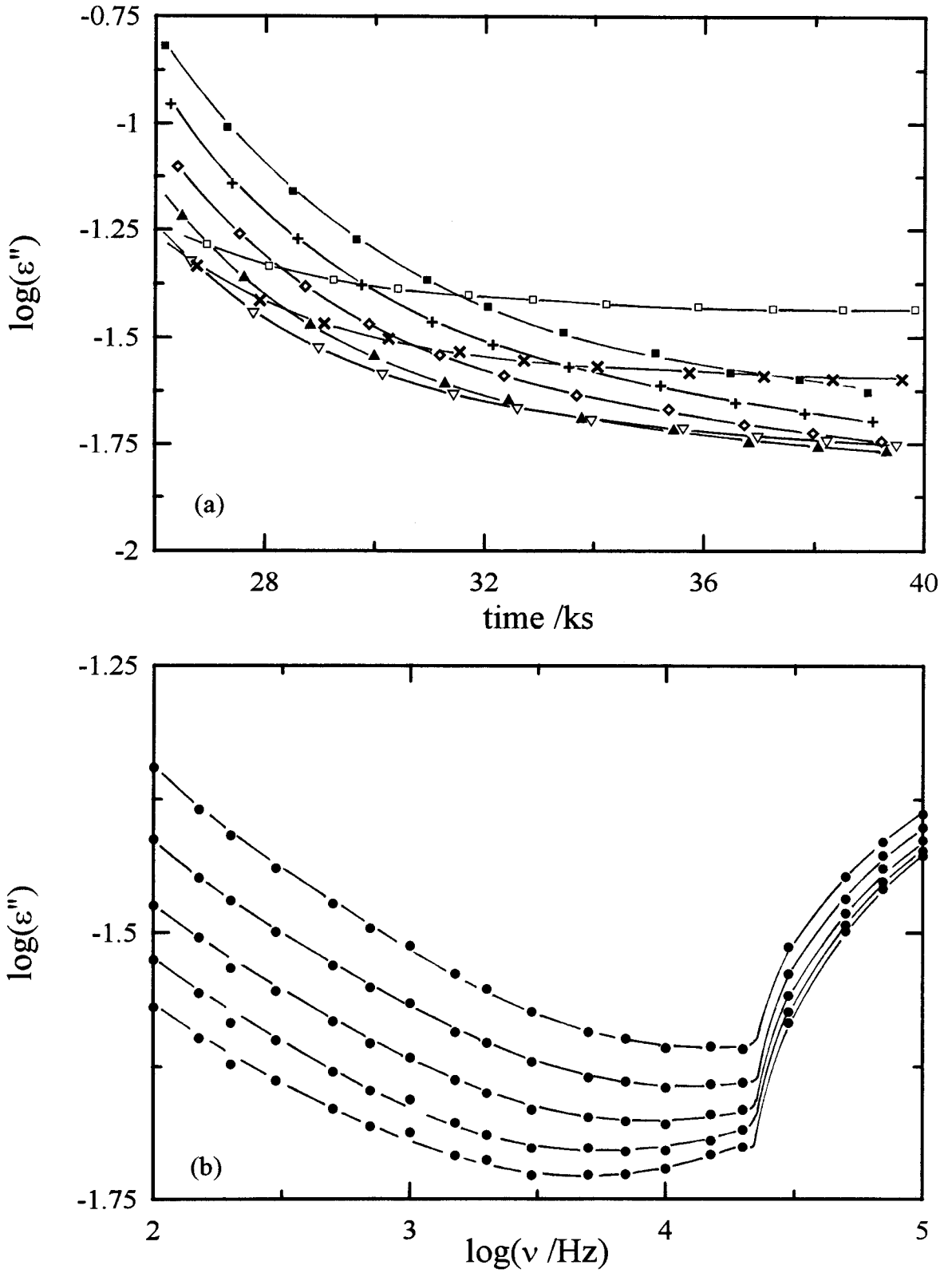

Figure 4.28: (a) The log of ε" plotted against reaction time showing the evolution of a second relaxation process, and, (b) The log of ε" plotted against the log of frequency for constant values of N(t) corresponding to long reaction times for the isothermal polymerization of Tactix-4CA at 349.5K.

for fixed values of t (and N(t)) such that ε" for a lower frequency increased more rapidly than for a higher frequency. Thus, the term 'cross-over' is used to described this observation of the time-dependent, fixed frequency dielectric properties. This can be expressed mathematically by writing the slope of these curves, $(\partial\varepsilon''/\partial\ln\omega)$ as a sum of two contributions:

$$d\varepsilon'' = \left(\frac{\partial\varepsilon''_{\alpha}}{\partial\ln\omega}\right)_N d\ln\omega + \left(\frac{\partial\varepsilon''_{\alpha}}{\partial N}\right)_\omega dN + \left(\frac{\partial\varepsilon''_{\beta}}{\partial\ln\omega}\right)_N d\ln\omega + \left(\frac{\partial\varepsilon''_{\beta}}{\partial N}\right)_\omega dN \qquad (4.45)$$

where α and β denote the low-frequency and high-frequency relaxation processes, respectively. The first two terms on the right hand side of Equation (4.45) are negative in our consideration of Figures 4.26(a), 4.27(a) and 4.28(a), because an increase in ω increases $\omega\tau_o$ beyond unity as does an increase in N (through an increase in $<\tau_\alpha>$). The last two terms corresponding to the β process are positive, because here an increase in both ω and N increase $\omega\tau_{o,\beta}$ towards unity as the ε" corresponds to the low-frequency side ($\omega\tau_o < 1$) of the relaxation peak. This is seen in the time-invariant plots for the mixtures for different values of N in Figures 4.26(b), 4.27(b) and 4.28(b). It appears that part of the β-relaxation process begins during the polymerization of the mixture to a polymeric material. Its occurrence would be completely revealed only by decreasing the temperature (or increasing the pressure) of the product at any stage of the polymerization, as has been observed earlier (Alig and Johari 1993).

CHAPTER V

THE DYNAMIC MECHANICAL PROPERTIES OF THE NEW POLYMERS

The dynamic mechanical properties of the new, three cross-linked polymers prepared in this study may be discussed in terms of the change in the limiting mechanical moduli with temperature and with polymer constituents, the shape of the spectra and the temperature dependence of the β- or Johari-Goldstein (Angell 1995, Frick and Richter 1995) relaxation process and the time-temperature superposition of the relaxation spectra. This is done in separate sections, as follows.

5.1 The Temperature Dependence of the Storage and Loss Shear Moduli

The glass transition temperature, T_g, was determined from the DSC scans made at a heating rate of 10K/min for the three ultimately formed polymers. The samples used were those which were used for the mechanical relaxation studies, and thereafter stored for 6 months at ambient temperature inside a desiccator. From their DSC scans, the T_g's obtained are 395K, 391K and 415K for Tactix-AN, Tactix-3CA and Tactix-4CA. The plots of $(dH/dT)_q$ against temperature are shown in Figure 5.1 for the mechanical samples. These T_g's roughly represent the temperatures above which the solid polymers behave like an elastomer or rubbery solid and below which they behave like a brittle solid. It should

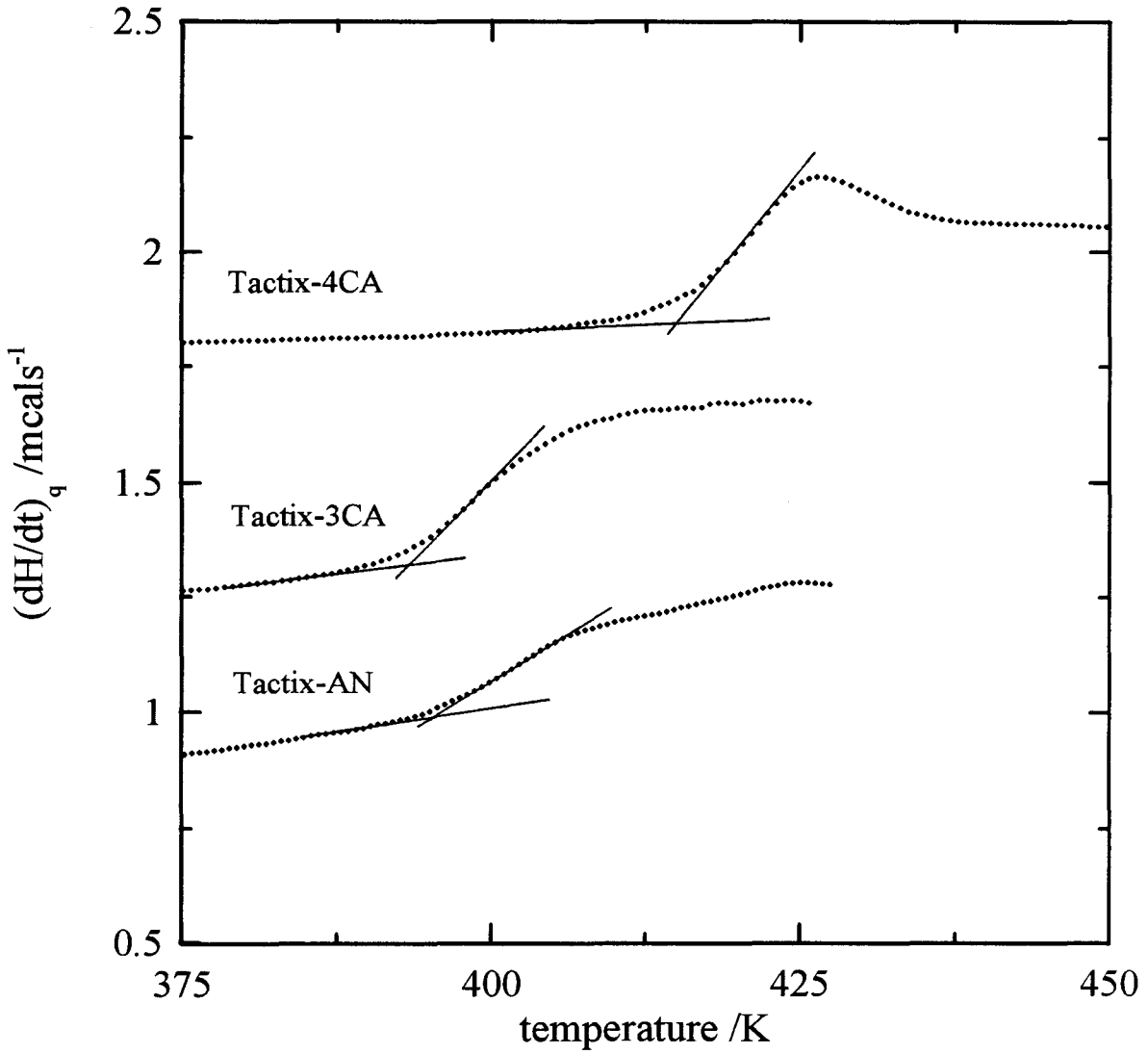

Figure 5.1: $(dH/dt)_q$ measured against temperature for the three fully polymerized mechanical samples.

be noted that the concept of brittle to ductile transition, as in the case with metals, is not applicable to polymers because the temperature range over which the property changes is large (30-60K), and because the properties are time-dependent. The values of the relaxed (or limiting zero-frequency) shear modulus, G_R, and the unrelaxed (or limiting high-frequency) shear modulus, G_U, were determined from the linear regions of the plot for log(G') against temperature for a measurement frequency of 1Hz. These are shown in Figures 5.2, 5.3 and 5.4 for Tactix-AN, Tactix-3CA and Tactix-4CA, respectively, where the linear regions are shown by dashed lines and the T_g's are marked. The values of G_R and G_U thus estimated for the three polymers linearly change with temperature according to the equations: $G_U(T')=G_U(T) - S_U(T'-T)$ and $G_R(T')=G_R(T) - S_R(T'-T)$, where T=350K for G_U and 440K for G_R, T' is the temperature above T, and S_U and S_R are the coefficients $(\partial G_U/\partial T)$ and $(\partial G_R/\partial T)$. For Tactix-AN, $S_U = -6.75\text{x}10^6$, and $S_R = 2.11\text{x}10^4$, for Tactix-3CA $S_U = -7.63\text{x}10^6$, and $S_R = 2.59\text{x}10^4$, and for Tactix-4CA $S_U = -708\text{x}10^6$, and $S_R = 2.82\text{x}10^4$, all in Pa/K. As the decrease in G' and the peak in G" appears in the temperature range of the glass transition, this decrease and the peak is to be associated with the α- or main-relaxation process.

In the dynamic mechanical behaviour of a cross-links polymer, the real component of the modulus, G', measured for a fixed frequency is expected to decrease with an increase in the temperature from one limiting value, G_U, to the other limiting value, G_R, according to the equation,

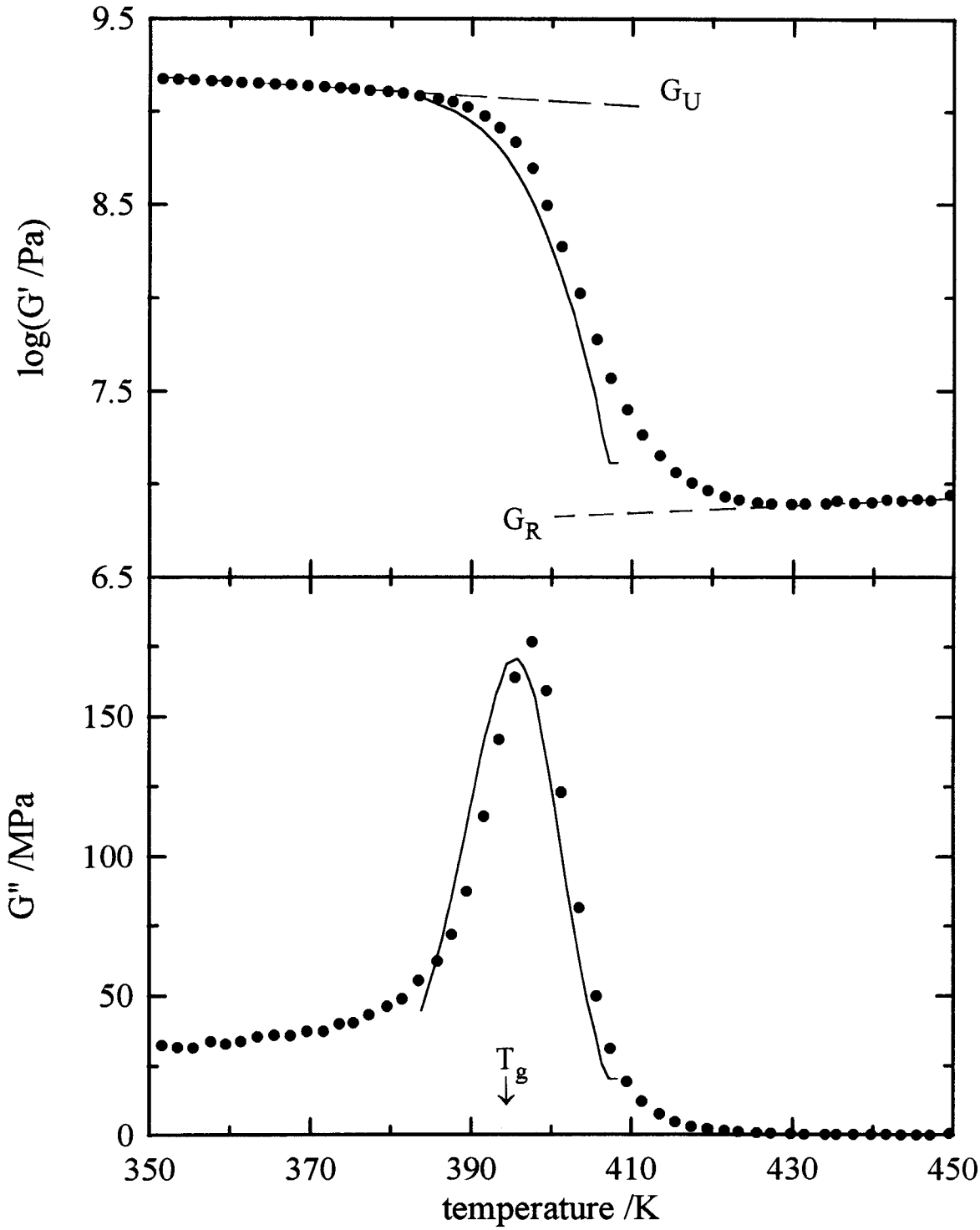

Figure 5.2: log(G') and G" plotted against temperature for the fully reacted Tactix-AN at a heating rate of 1K/min. The filled circles represent the experimental data and the calculation of the continuous lines is described in Section 5.4.

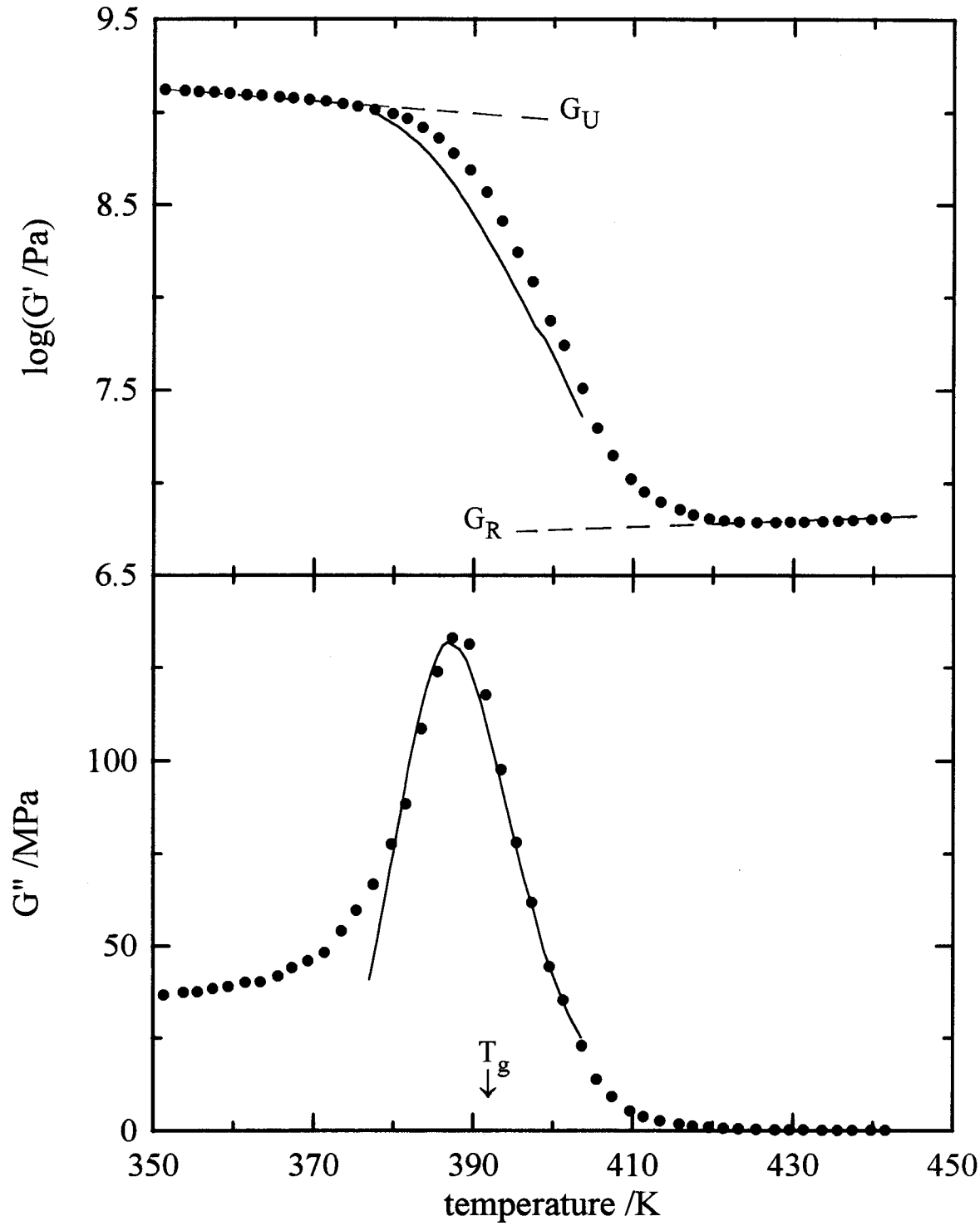

Figure 5.3: log(G') and G" plotted against temperature for the fully reacted Tactix-3CA at a heating rate of 1K/min. The filled circles represent the experimental data and the calculation of the continuous lines is described in Section 5.4.

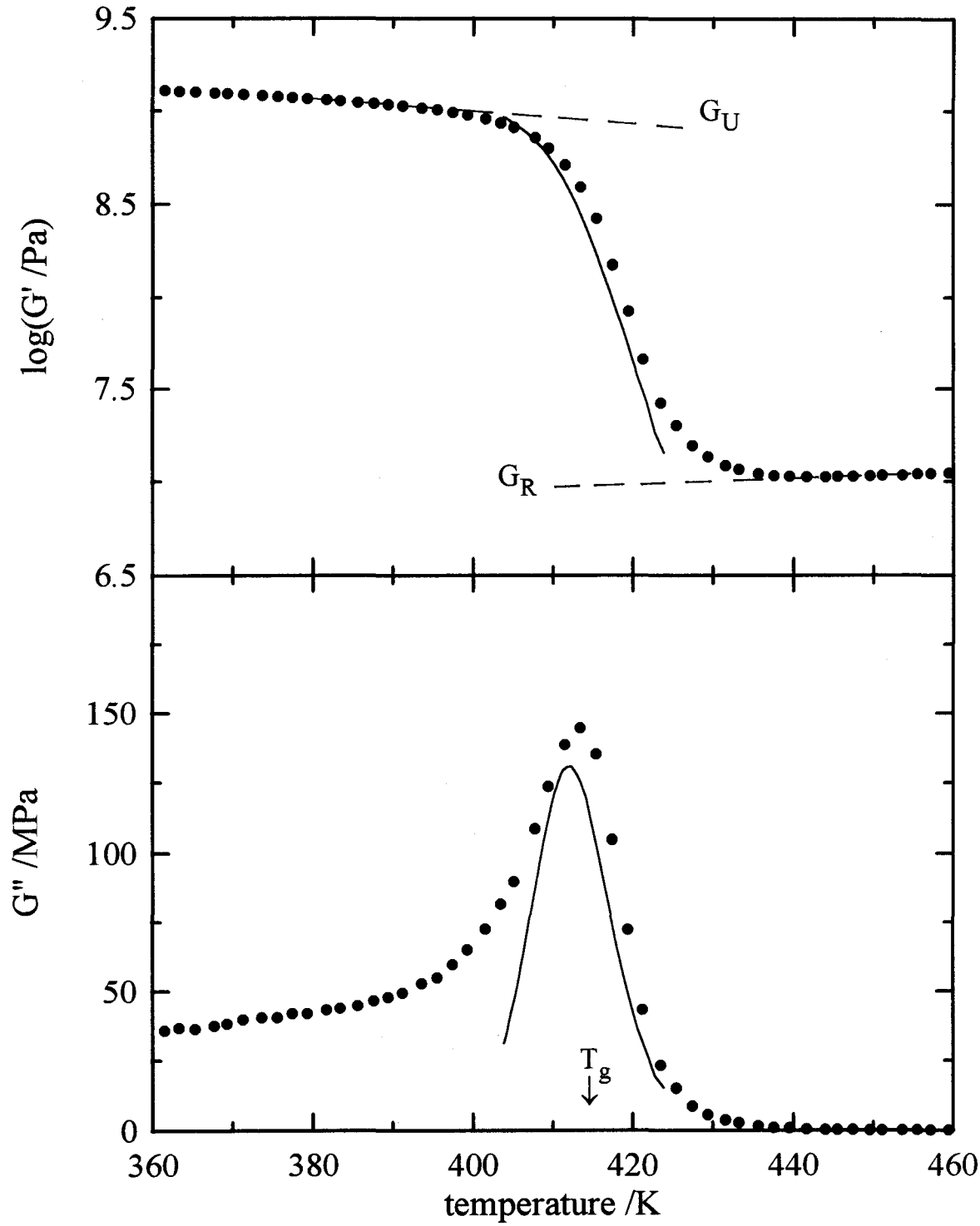

Figure 5.4: log(G') and G" plotted against temperature for the fully reacted Tactix-4CA at a heating rate of 1K/min. The filled circles represent the experimental data and the calculation of the continuous lines is described in Section 5.4.

$$G' = G_R + \frac{(G_U - G_R)\omega^2\tau^2}{1 + \omega^2\tau^2} \qquad \textbf{(5.1)}$$

where the relaxation time, τ, decreases with increasing temperature. When plotted against the temperature, G" is expected to show a peak at a temperature, T_m, where $\omega\tau = 1$, according to the expression,

$$G'' = \frac{(G_U - G_R)\omega\tau}{1 + \omega^2\tau^2} \qquad \textbf{(5.2)}$$

The results for Tactix-AN plotted in Figure 5.2 show that the α-relaxation process decreases G' from 1.51GPa to 8.0MPa, and a peak appears in G" at 397K. Similarly, Figure 5.3 shows that for Tactix-3CA, G' decreases from 1.35GPa to 6.6MPa and a peak appears in G" at 387K. For Tactix-4CA, G' decreases from 1.35GPa to 10.6MPa and a peak in G" appears at 413K, as shown in Figure 5.4. The shape of the G' and G" plots is determined by the magnitudes of G_U, G_R, τ, and the distribution parameter β, as described in Section 2.1.3, all for the α- or main-relaxation process.

In order to discuss the significance of the results in terms of the absolute shear moduli of the polymers, we first examine the temperature dependence of the limiting quantities as shown in Figures 5.2 to 5.4. The unrelaxed shear modulus, G_U, of the α-relaxation process observed here is equal to the relaxed shear modulus, G_R, of the secondary, low temperature or high-frequency β-relaxation process as discussed by Muzeau et al. (1991). So, any decrease in the G_R of the β-relaxation process with

increasing temperature would appear as a decrease in the G_U of the α-relaxation process. In addition, an increase in the temperature lowers the density of a polymer, which in turn results in a decrease in the intermolecular forces between the network's chain segments. This also causes a decrease in G_U with an increase in the temperature as less stress is now required to produce a given amount of strain. Thus the decrease of G_U of the three polymers with an increase in the temperature is to be seen as a combined effect of the decrease in the G_R of the β-relaxation process, whose magnitude, $(G_U - G_R)_\beta$, has been found to increase with the temperature (Muzeau et al. 1991) and the decrease in the intermolecular forces on decrease in the density. Without measurements of the absolute magnitudes of the β-relaxation process at each temperature and of the density of the polymers, it is not possible to determine quantitatively which of the two effects dominates. Nevertheless, qualitative information can still be obtained: Since the coefficient of thermal expansion of polymers at temperatures about 100K below T_g is typically less than $10^{-5}K^{-1}$ (Aklonis et al. 1973), a 1K increase in temperature will lower the density by $2x10^{-4}$g/ml, or by most 0.02%, if the density of the polymer was initially 1g/ml. The measured density of the polymers at 300K are 1.228g/ml for Tactix-AN, 1.174g/ml for Tactix-3CA, and 1.153g/ml for Tactix-4CA. Since the unrelaxed modulus is proportional to the density of a polymer (Ferry 1980), the 0.02% decrease in the density would decrease G_U by 0.02%, if nothing else changed. The actual decrease per Kelvin is: 0.45% for Tactix-AN, 0.56% for Tactix-3CA and 0.53% for Tactix-4CA, which are an order of magnitude greater than that expected from the decrease in density alone.

Hence we conclude that the main reason for the large decrease of G_U with an increase in the temperature, as seen from the equations of $G_U(T)$ and $G_R(T)$, a decrease in the G_R of the β-relaxation process. This relaxation process is expected to appear at temperatures below 350K and so has not been observed in the plots of Figures 5.2 to 5.4.

We now turn to a discussion of G_R and its temperature-dependence for the α-relaxation process in the three polymers. G_R is also referred to as the rubber modulus of the polymer, for which a number of statistical theories and empirical equations are available. Flory (1969) has discussed some of the theoretical equations and Charlesworth (1988b) has reviewed them before, discussing the absolute G_R values for the α-relaxation of diepoxide-monoamine-diamine network polymers. He has adequately summarized the relative importance of the various theoretical and empirical equations. For our purpose, we use the simplest of the equations for the rubbery modulus which applies to both entangled chain and network polymers (Stockmayer 1943, Treloar 1958, McCrum et al. 1967, Flory 1969, Ferry 1980), i.e.

$$G_{rubber} = \Phi N_x RT \qquad (5.3)$$

where G_{rubber} is the relaxed modulus of the α-relaxation process, Φ is a constant termed the "front factor", N_x is the number of moles of elastically active network strands per unit volume in the polymer's structure, R is the gas constant and T is the temperature. The constant Φ is introduced to account for changes in the chain dimensions caused by cross-linking. It represents the term $\overline{r}^2/\overline{r}_o^2$, where $\overline{r}^2$ is the mean square end-to-end distance of the strands in the network and $\overline{r}_o^2$ is the mean square end-to-end distance of the same

chains in the absence of network constraints. Graessley (1974) has deduced that Φ should be unity for most network polymers, and neutron scattering experiments (Benoit 1976) lends support to this conclusion. Charlesworth (1988b) has also discussed the relevance of other values for Φ and the use of yet more parameters. Whatever the value of Φ, Equation (5.3) indicates that the rubber modulus should be proportional to the number of cross-links per unit volume and the absolute temperature. Since an increase in temperature increases the specific volume and thus lowers N_x, the change in the rubber modulus with temperature is a result of two effects, namely, a decrease in N_x with increasing temperature, and an increase in the rubber modulus with temperature due to entropy itself. In Figures 5.2 to 5.4, G_R, nevertheless, is seen to increase with temperature, suggesting that the effect of the temperature alone must dominate the effect of the decrease in N_x due to thermal expansion alone. This may be shown quantitatively from the following consideration: A typical value for the coefficient of thermal expansion of network elastomers is about $10^{-4}K^{-1}$ (Aklonis et al. 1973, Plazek and Choy 1989), so $(\partial N_x/\partial T)$, is of the order of $-10^{-4}K^{-1}$, and the calculated cross-link density of the polymers from its molar volume is at most 0.006 moles/ml near 350K. So, the decrease in G_{rubber} due to the change in volume per K is by a factor of 1.0001, or that $\partial G_{rubber}/\partial T$ due to volume expansion alone is -1kPa/K (An analysis of the differential of Equation (5.3) would not yield this value). The observed $(\partial G_{rubber}/\partial T)$ is 21.1kPa/K for Tactix-AN, 25.9kPa/K for Tactix-3CA and 28.2kPa/K for Tactix-4CA, which are greater than expected from a decrease in the cross-link density alone. Thus our quantitative analysis shows that this increase in the rubber modulus is predominantly a result of the increase

in temperature, and therefore entropy, as discussed in the entropy theories of rubber modulus (Stockmayer 1943, Treloar 1958, Flory 1969, Ferry 1980). S_R represents the combined effect of the change in N_x and T.

The variation of G_U and the rubber modulus with the steric hindrance of the monoamine used for linking the triepoxide in this study are of some significance. For a constant temperature of 350K, G_U = 1.51GPa for Tactix-AN, 1.35GPa for Tactix-3CA and 1.35GPa for Tactix-4CA. The corresponding values of the rubber modulus are: 8.0MPa, 6.6MPa and 10.6MPa at 440K. This means that G_U remains virtually unaffected by the size and steric hindrance to motion of the cross-linking amine, but G_R increases when the chlorine atom is farther from the cross-linking nitrogen atom as in Tactix-4CA, and decreases when it is closer to the nitrogen atom as in Tactix-3CA.

5.2 The Distribution of Mechanical Relaxation Times

The G' and G" of the three polymers, which are shown in Figures 5.5 to 5.7, are now analyzed to determine whether or not the stretched exponential relaxation function, $\phi(t') = \exp(-(t'/\tau_o)^{\beta})$, as discussed in Section 2.1.3, may be useful in describing their spectral shape. The procedure for the analysis is similar to that for the dielectric spectra described in Chapter 4, and so will be only briefly given here.

Tables of normalized data calculated from the relaxation function given by Moynihan et al. (1973) and Dishon et al. (1985) were used to determine the distribution and are referred to as the tabulated values from here on. Firstly, the mechanical relaxation data were normalized along the frequency axis by the factor $\omega\tau_o$, such that the

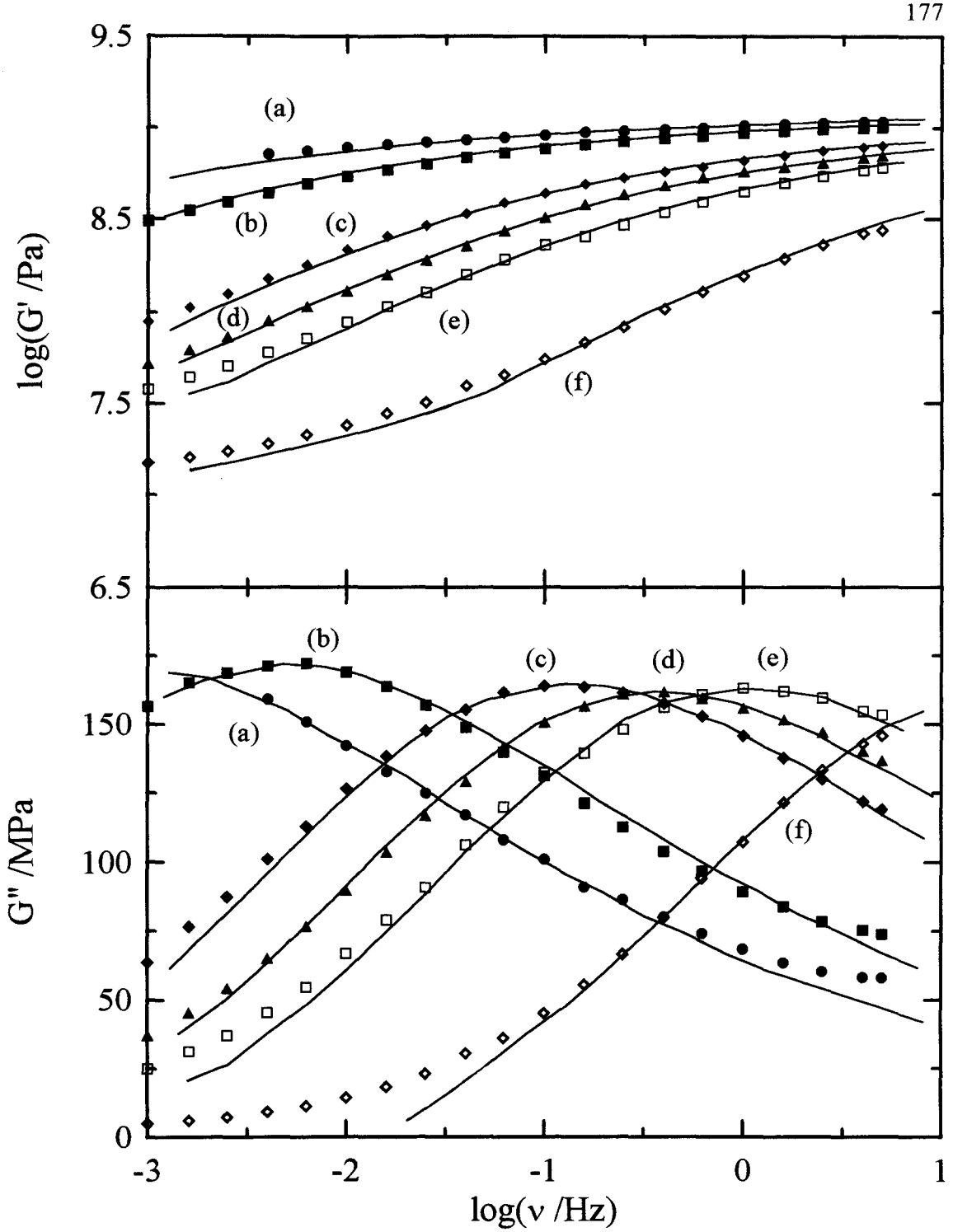

Figure 5.5: The log(G') and G" plotted against log(υ) for Tactix-AN at the following isothermal temperatures;(a) 386.1, (b) 389.8, (c) 393.4, (d) 395.2, (e) 396.2, (f) 401.2, (g) 406.4, (h) 412.0 and (i) 423.0K. The continuous lines are calculated from parameters in Table 5.1.

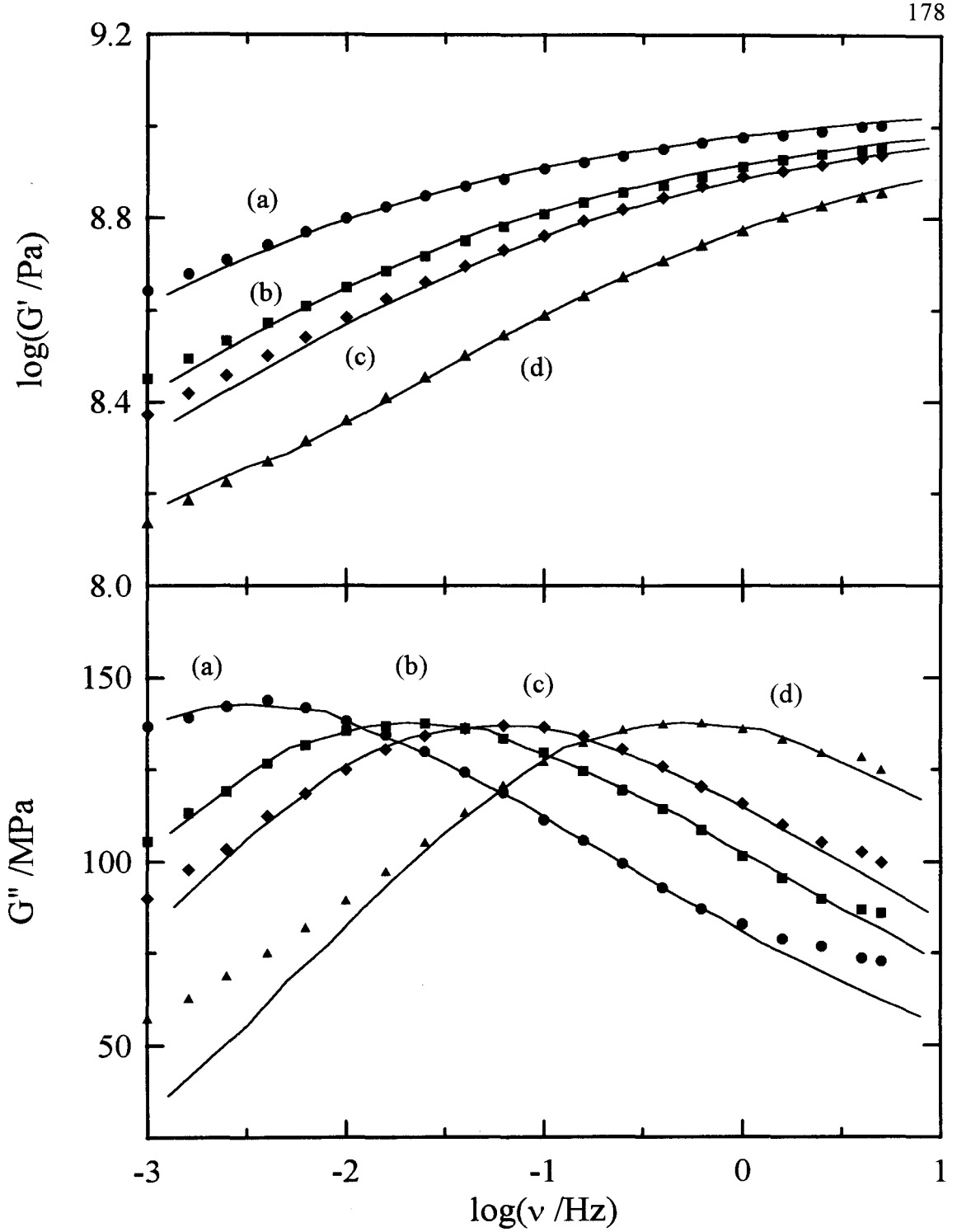

Figure 5.6: The log(G') and G" plotted against log(υ) for Tactix-3CA at the following isothermal temperatures;(a) 380.1, (b) 382.3, (c) 383.5 and (d) 386.2K. The continuous lines are calculated from parameters in Table 5.1.

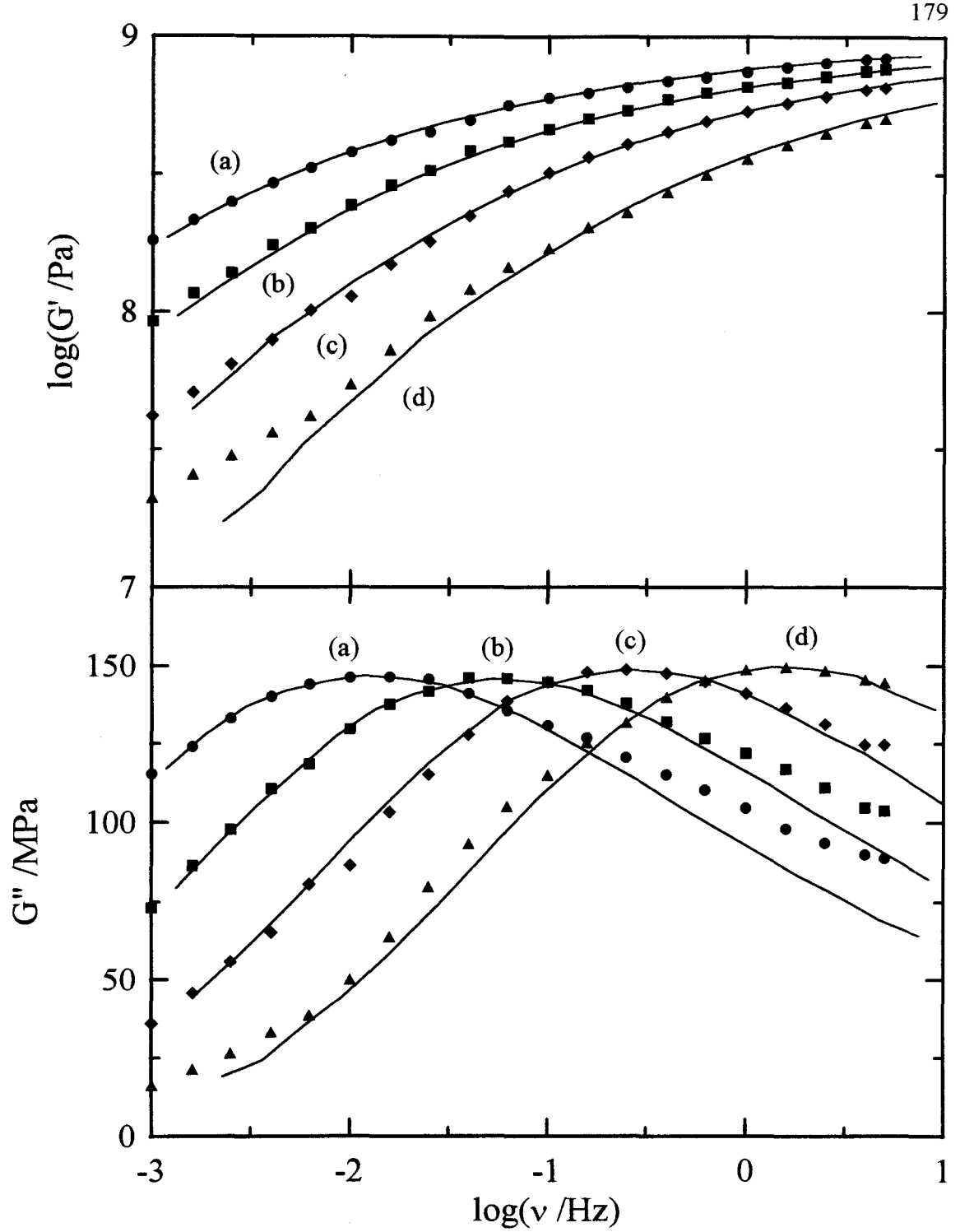

Figure 5.7: The log(G') and G" plotted against log(υ) for Tactix-4CA at the following isothermal temperatures;(a) 407.5, (b) 409.3, (c) 410.7 and (d) 412.6K. The continuous lines are calculated from parameters in Table 5.1.

G" peak in the normalized data corresponded with the peak of the tabulated values. Secondly, the height of the G" peak was normalized by the relation $N'' = G'' / (G_R - G_U)$, and the adjustable parameter, $\Delta G = (G_R - G_U)$, varied until the N" peak height matched the peak height of the tabulated data. Once the heights of the two peaks matched, the shape of the N" peak was compared to the tabulated values for various values of β. Once the N" peak was matched to the peak of the tabulated values the parameters τ_o, ΔG and β, the G' data was normalized by the equation, $N' = (G' - G_R) / (G_R - G_U)$. G_U was adjusted until N' matched the tabulated values. The four parameters thus obtained, τ_o, β, G_U and G_R, describe the mechanical spectrum measured at a fixed temperature. These parameters for the three polymers at various measurement temperatures are given in Table 5.1.

The continuous lines shown in Figures 5.5 to 5.7 were calculated by using the N' and N" values from the tables (Moynihan et al. 1973, Dishon et al. 1985) and the parameters τ_o, β, G_U and G_R. The calculated curves are limited to the frequency range that is provided by the tables, which covers $10^{-3} < \omega\tau_o < 10^4$. Furthermore, the absence of a peak in the G" data within the experimental spectral frequency range for some of the isothermal measurement made for Tactix-AN prevented the calculations of τ_o itself. Thus all the isothermal spectra in Figure 5.2 for Tactix-AN could not be analyzed to obtain values of τ_o, β, G_U and G_R.

As is evident in Figures 5.5 to 5.7, the stretched exponential equation fits the G' and G" data for the α-relaxation process satisfactorily at relatively low frequencies, but

Table 5.1: The parameters of the α-relaxation spectrum of the three polymers at different temperatures and their T_g's.

Temp /K	ΔG /GPa	G_U /GPa	G_R /MPa	β	τ_o /s	$\langle\tau\rangle$ /s
Tactix-AN T_g = 395K						
386.1	1.20	1.23	25	0.25	125	3000
389.8	1.21	1.24	25	0.25	21	504.0
393.4	1.16	1.19	28	0.25	0.78	18.72
395.2	1.14	1.17	30	0.25	0.28	6.72
396.2	1.15	1.18	30	0.25	0.1	2.4
401.2	1.13	1.16	25	0.25	0.005	0.12
Tactix-3CA T_g = 391K						
380.1	1.14	1.23	90	0.22	32	1802.6
382.3	1.099	1.20	100	0.22	4.9	276.0
383.5	1.095	1.20	110	0.22	1.85	104.2
386.2	1.1	1.22	120	0.22	0.2	11.3
Tactix-4CA T_g = 415K						
407.5	1.038	1.05	10	0.25	8.5	204.0
409.3	1.03	1.04	9.0	0.25	1.9	45.6
410.7	1.05	1.06	12	0.25	0.4	9.6
412.6	1.055	1.07	12	0.25	0.07	1.68

underestimates the G" and overestimates G' at frequencies beyond the G" peak. The deviations at the high frequency end of the α-relaxation spectrum become more prominent as the temperature is decreased and the α-relaxation peak shifts to a lower frequency.

The complex plots of normalized G' and G" are shown in Figures 5.8, 5.9 and 5.10 for Tactix-AN, Tactix-3CA and Tactix-4CA, respectively. Here, the mechanical oscillation frequency increases from left to right. The continuous lines represent the values calculated from the parameters listed in Table 5.1, and the plots indicate the combined manner in which calculated G' and G" data agree with the experiment. The values of G_U in Table 5.1 are about 25% less than the values plotted in Figures 5.2 to 5.4, but G_R in the figures deviates by up to a factor of three since the linear approximation of G_R is only accurate for temperatures near 450K, the reference temperature used. The calculated curve again deviates from the experimental data at the high-frequency end of the plots, and these deviations are more clear here than in the G' and G" spectra given in Figures 5.5 to 5.7.

A more informative analysis of the data is done by plotting the normalized quantities, $G''/\Delta G$ and $(G' - G_R)/\Delta G$, against the frequency normalized with respect to ω_0 $(= 1/\tau_0)$, i.e. against $\omega\tau_0$. These plots are shown in Figures 5.11, 5.12 and 5.13 for the Tactix-AN, Tactix-3CA and Tactix-4CA polymers, respectively. The plots show the data points measured at different temperatures, which are denoted by the different symbols given in the figures, and their comparison with the calculated data obtained by using the stretched exponential relaxation function with the values listed in Table 5.1. Here, the

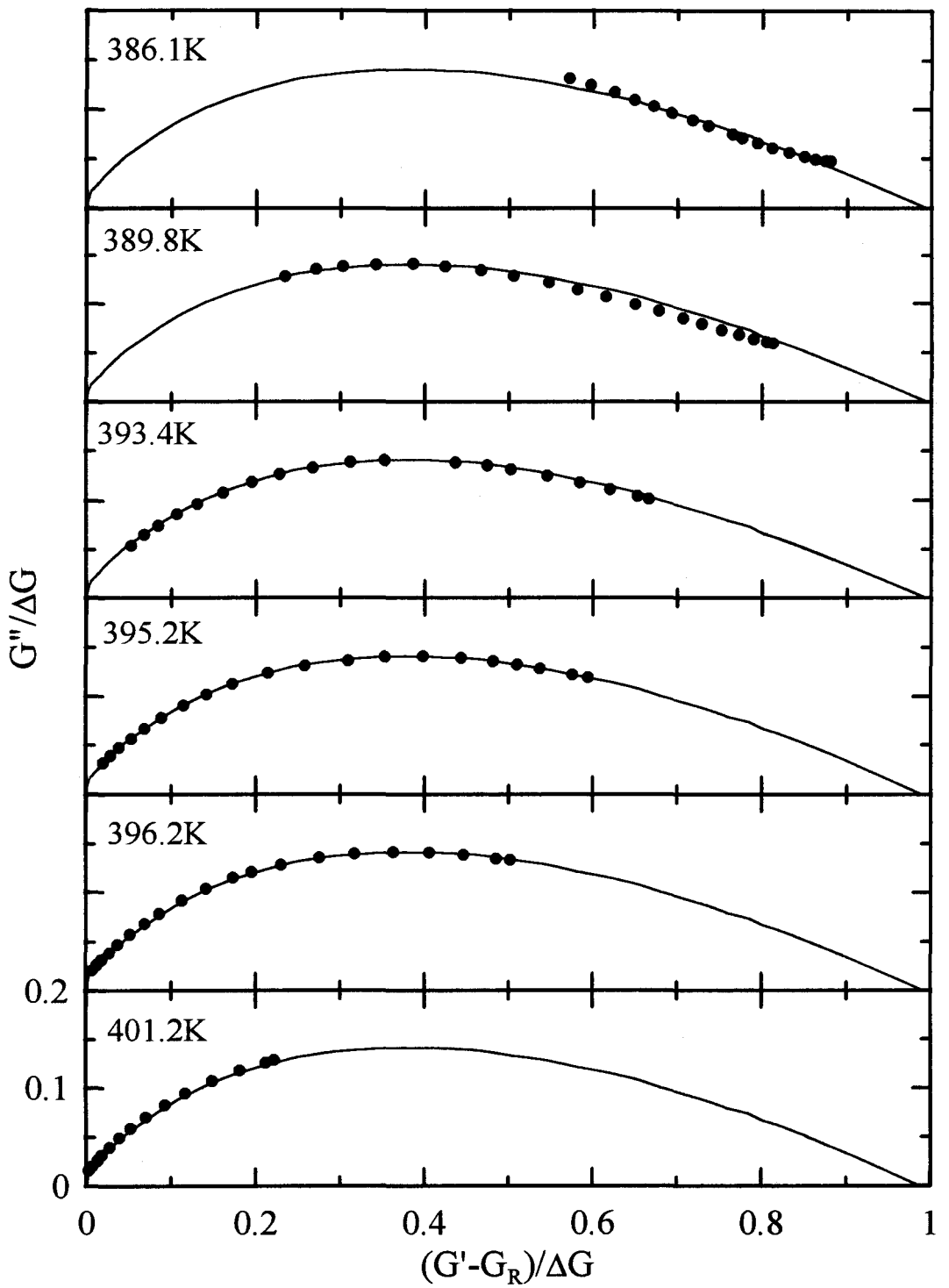

Figure 5.8: Complex plane plots of normalized G'' against normalized G' at various isothermal measurement temperatures for Tactix-AN.

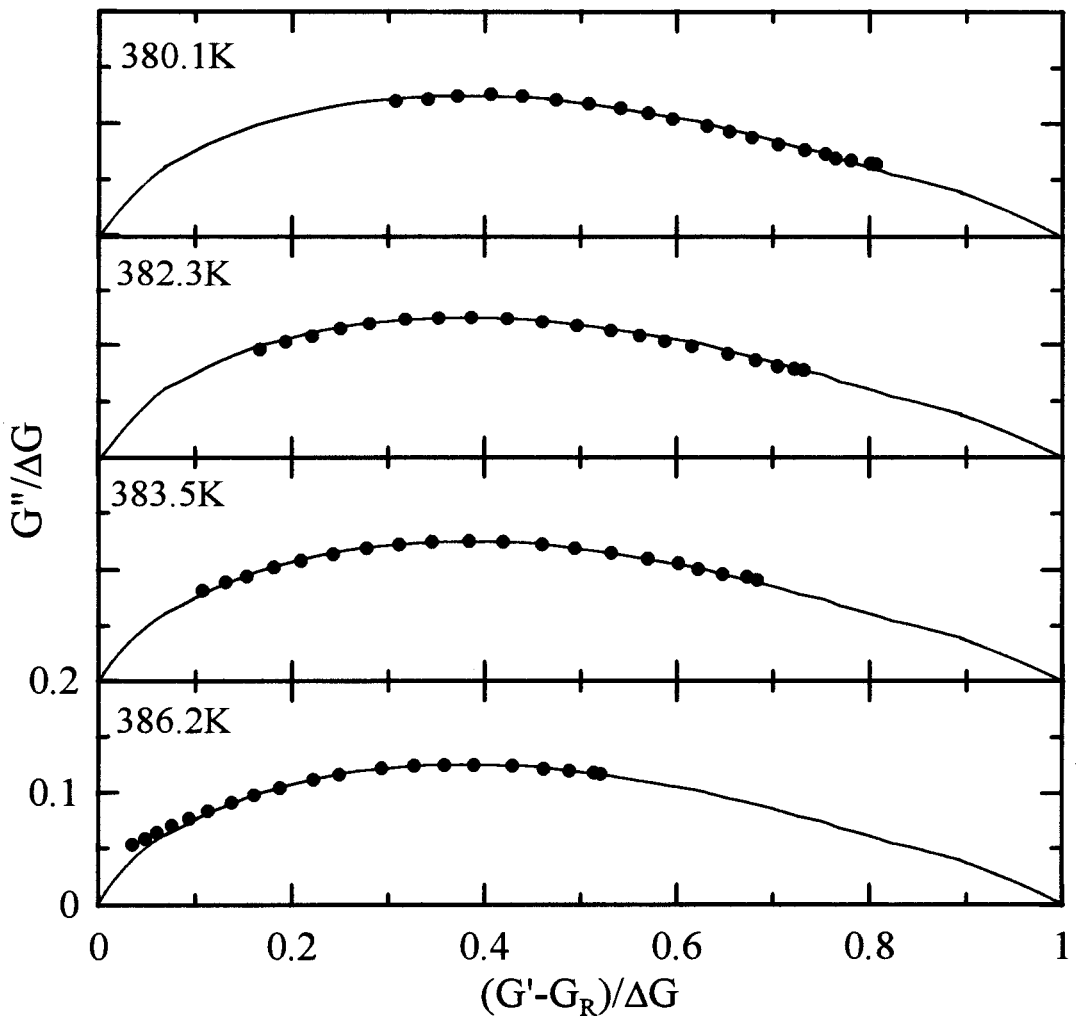

Figure 5.9: Complex plane plots of normalized G" against normalized G' at various isothermal measurement temperatures for Tactix-3CA.

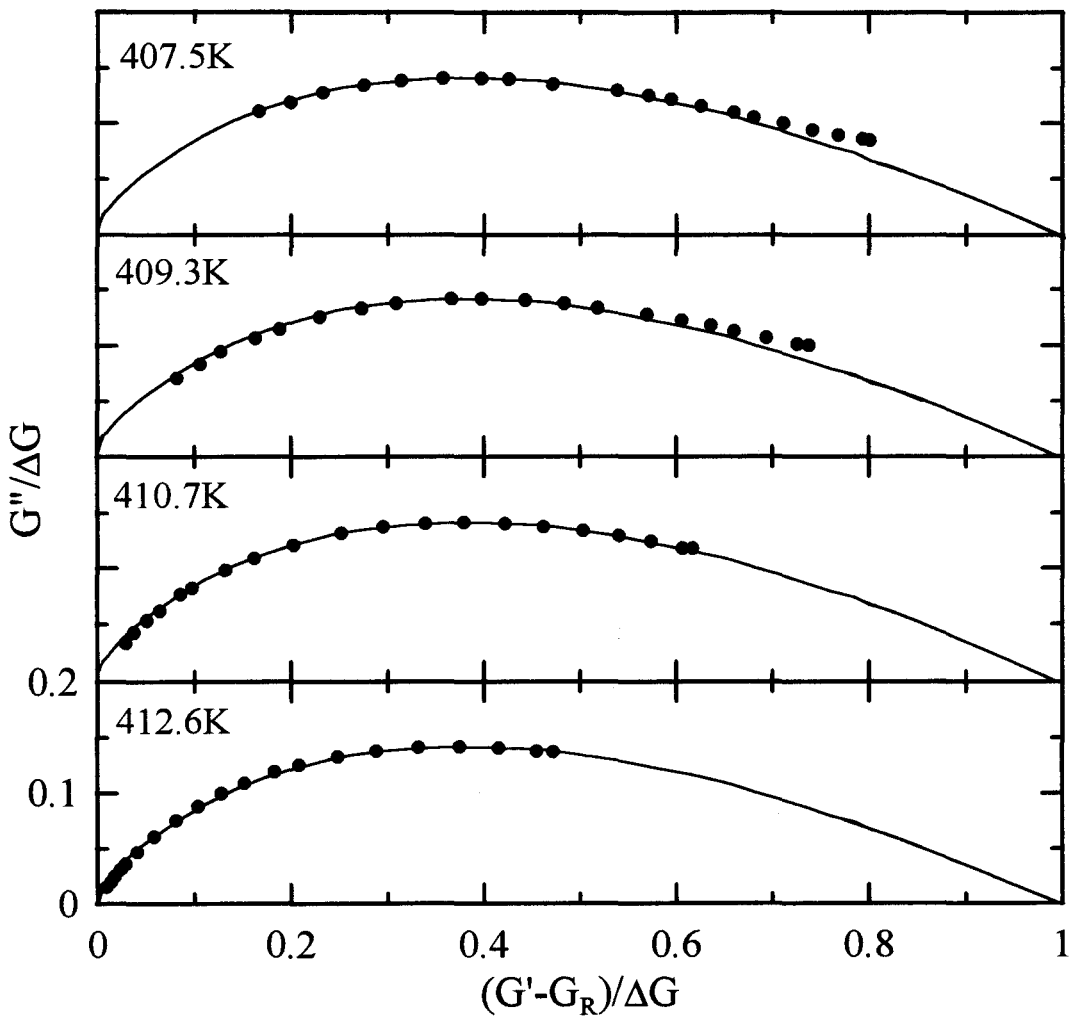

Figure 5.10: Complex plane plots of normalized G'' against normalized G' at various isothermal measurement temperatures for Tactix-4CA.

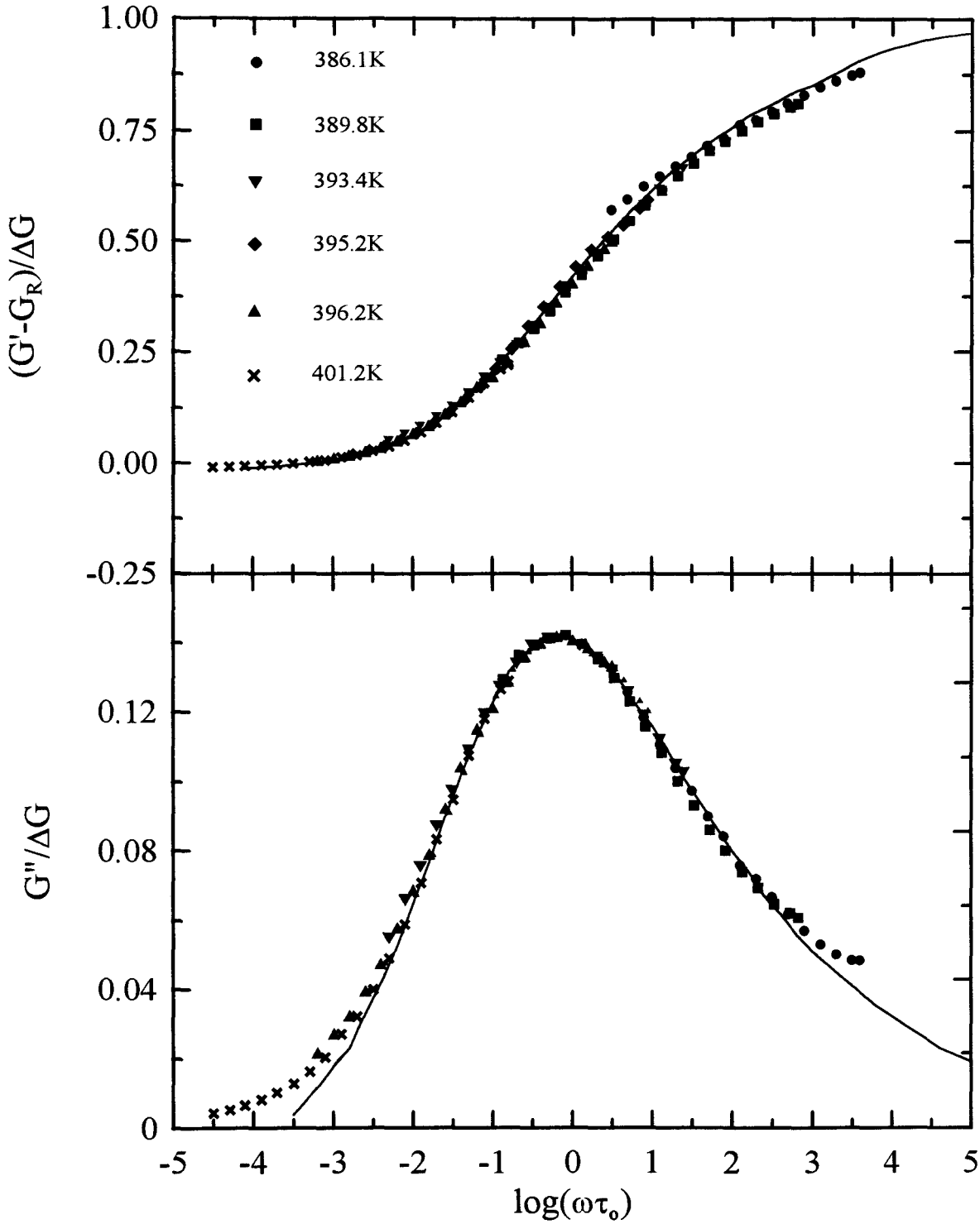

Figure 5.11: Normalized G' and G" plotted against the normalized frequency for measurements at various isothermal temperatures for Tactix-AN. The continuous line was calculated with β=0.25.

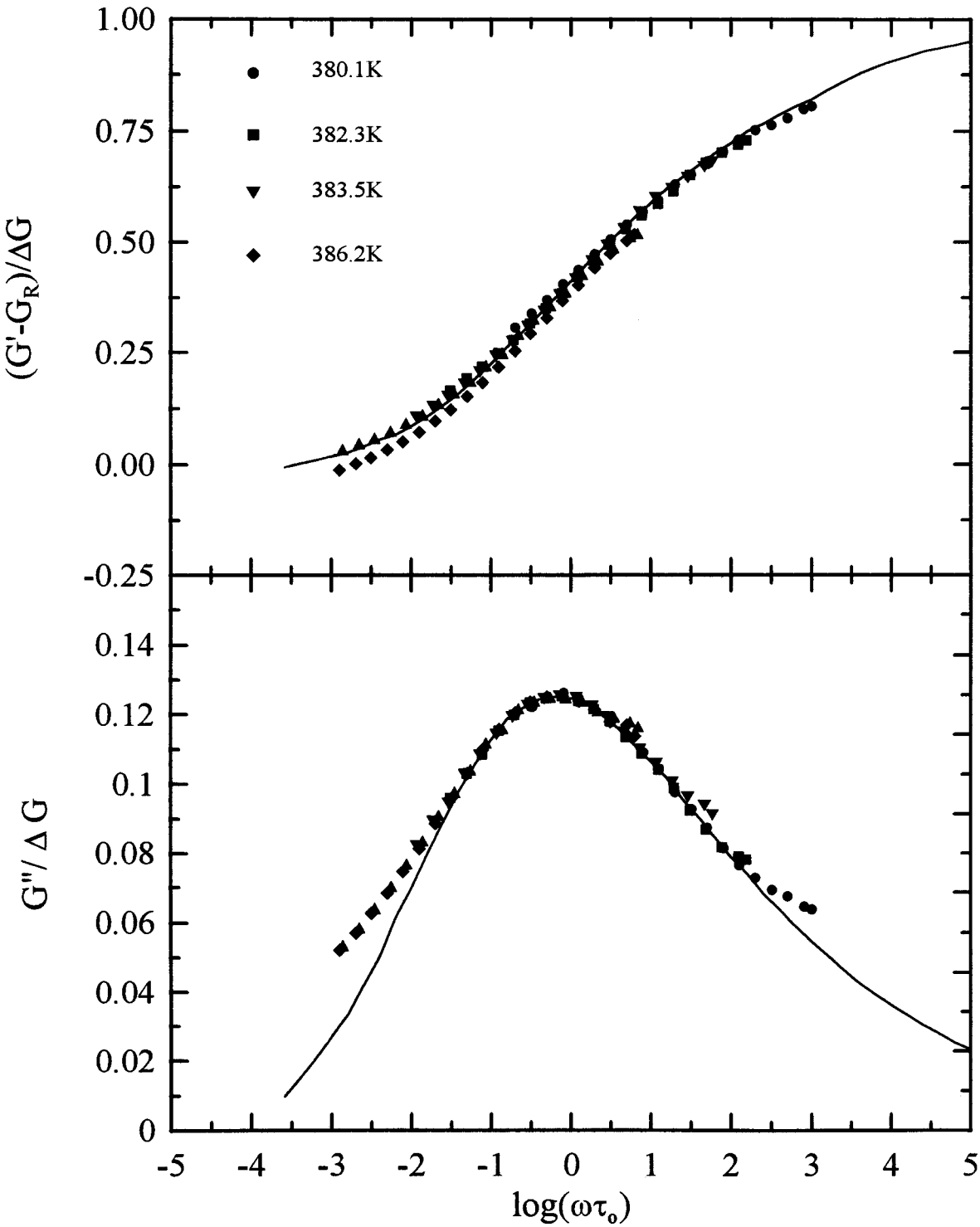

Figure 5.12: Normalized G' and G" plotted against the normalized frequency for measurements at various isothermal temperatures for Tactix-3CA. The continuous line was calculated with β=0.22.

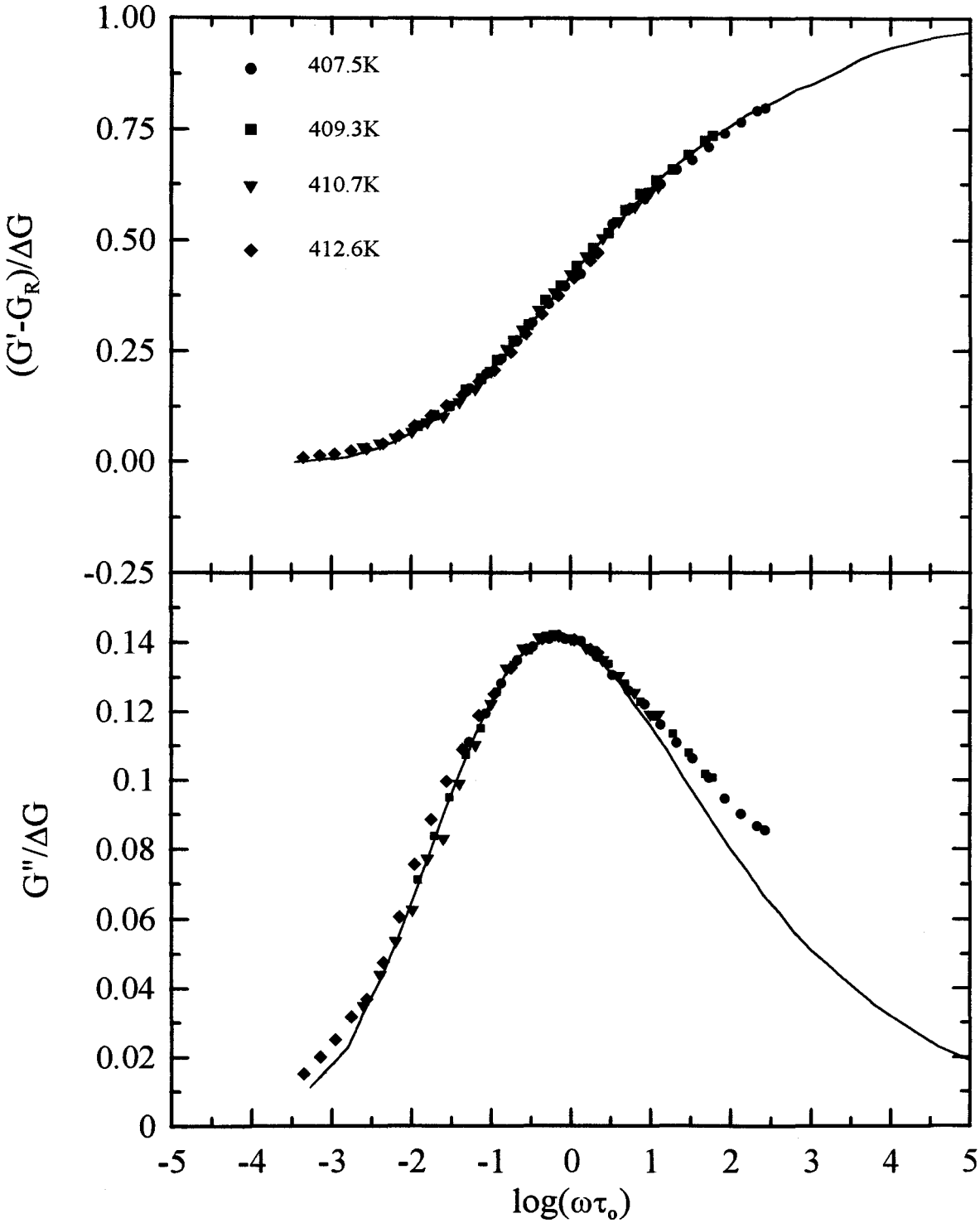

Figure 5.13: Normalized G' and G" plotted against the normalized frequency for measurements at various isothermal temperatures for Tactix-4CA. The continuous line was calculated with β=0.25.

deviations between the calculated and measured values occur at both the low- and the high- frequency sides of the normalized peak, and these deviations, particularly on the low-frequency side of the peaks, are most prominent for Tactix-3CA in Figure 5.12.

5.3 The High-Frequency, Low-Temperature or β-Relaxation Process

One of the important aspects of the analysis given in Sections 5.1 and 5.2 is that it has brought into evidence contributions from a high-frequency, or low-temperature, β-relaxation process. This is clear from the fitting of the distribution function to the isothermal spectra of Figures 5.5 to 5.7, which gives the calculated G" lower than the G" values measured at the high-frequency end of the spectrum. It is also clear from the calculated G" at a fixed frequency plotted against the temperature (Figures 5.2 to 5.4), which shows that the measured values at $T < T_g$ are substantially greater than the calculated values.

The increase of the mechanical loss owing to the presence of the β-relaxation process in a polymer near room temperature is technologically important, because its magnitude indicates absorption of energy into heat prior to fracture (McCrum et al. 1967 pp. 7-11). For this reason, polymers like polycarbonates are widely used for constructing objects that are subjected to mechanical impact. The mechanical loss tangent, $\tan\phi$, of polycarbonate of molecular weight 28600 is 10^{-2} in the range 290-350K (G'Sell et al. 1989) and for other molecular weight polycarbonates, the value remains nearly the same (Bauwens-Crowet and Bauwens 1979, Yee and Smith 1981, Cavaillé 1987). For the three

new polymers prepared in this study, tanϕ in this temperature range is from $2.0x10^{-2}$ to $2.6x10^{-2}$, as shown in Figure 5.14, which is greater than that of polycarbonate. We therefore conclude that the new polymers studied here absorb more mechanical energy at 1Hz than polycarbonates, and their toughness to fracture, we suggest, will be found to be comparable to that of polycarbonate. As tanϕ for Tactix-3CA is the highest at temperatures between 300-360K, this polymer is expected to be most suitable for construction of objects that are designed to absorb more energy before fracturing, than the linear chain polymers.

5.4 The Relaxation Time and Fixed Frequency Moduli

The self-consistency of the analysis given here may be examined by calculating G', G" and tanϕ at a fixed frequency of 1Hz measured at different temperatures for each of the three polymers. This may be done by using the relaxation time distribution function of Equation (2.36) discussed in Section 5.2, the temperature variation of G_U and G_R discussed in Section 5.1, the fixed frequency G" against temperature plots of Figures 5.2 to 5.4, and the relaxation time, τ_o, determined from the isothermal spectrum of G" shown in Figures 5.5 to 5.7. The values of τ_o obtained from the spectrum of G" and the corresponding average relaxation times, $<\tau>$, calculated from Equation (2.37) are also listed in Table 5.1. $\log(<\tau>)$ is plotted against the reciprocal temperature in Figure 5.15, where the T_g determined for each of the mechanical samples is marked by an arrow.

To calculate the G', G" and tanϕ data over the temperature range of measurements,

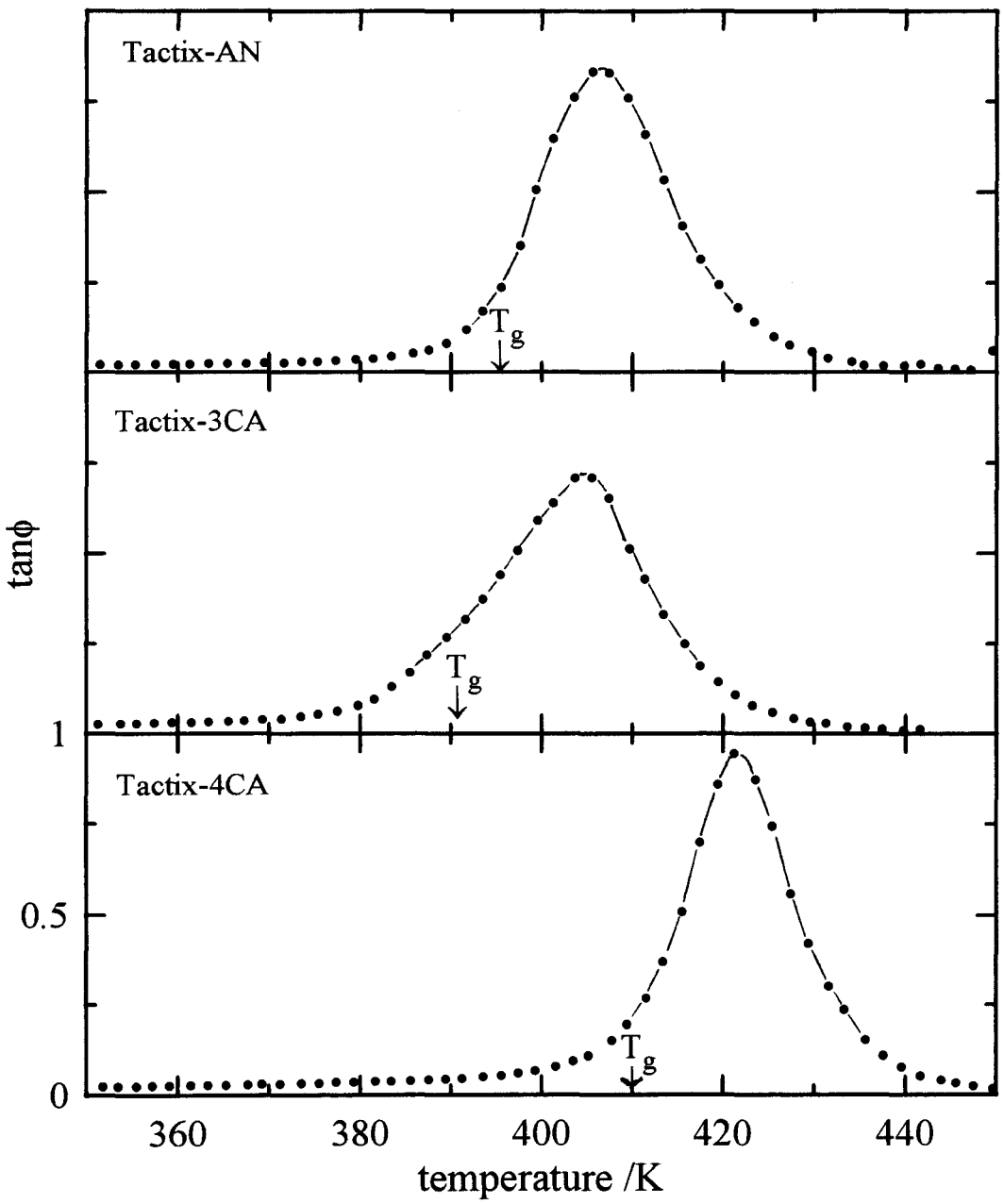

Figure 5.14: The mechanical loss, tanϕ, plotted against the temperature for a heating rate of 1K/min for the three polymers.

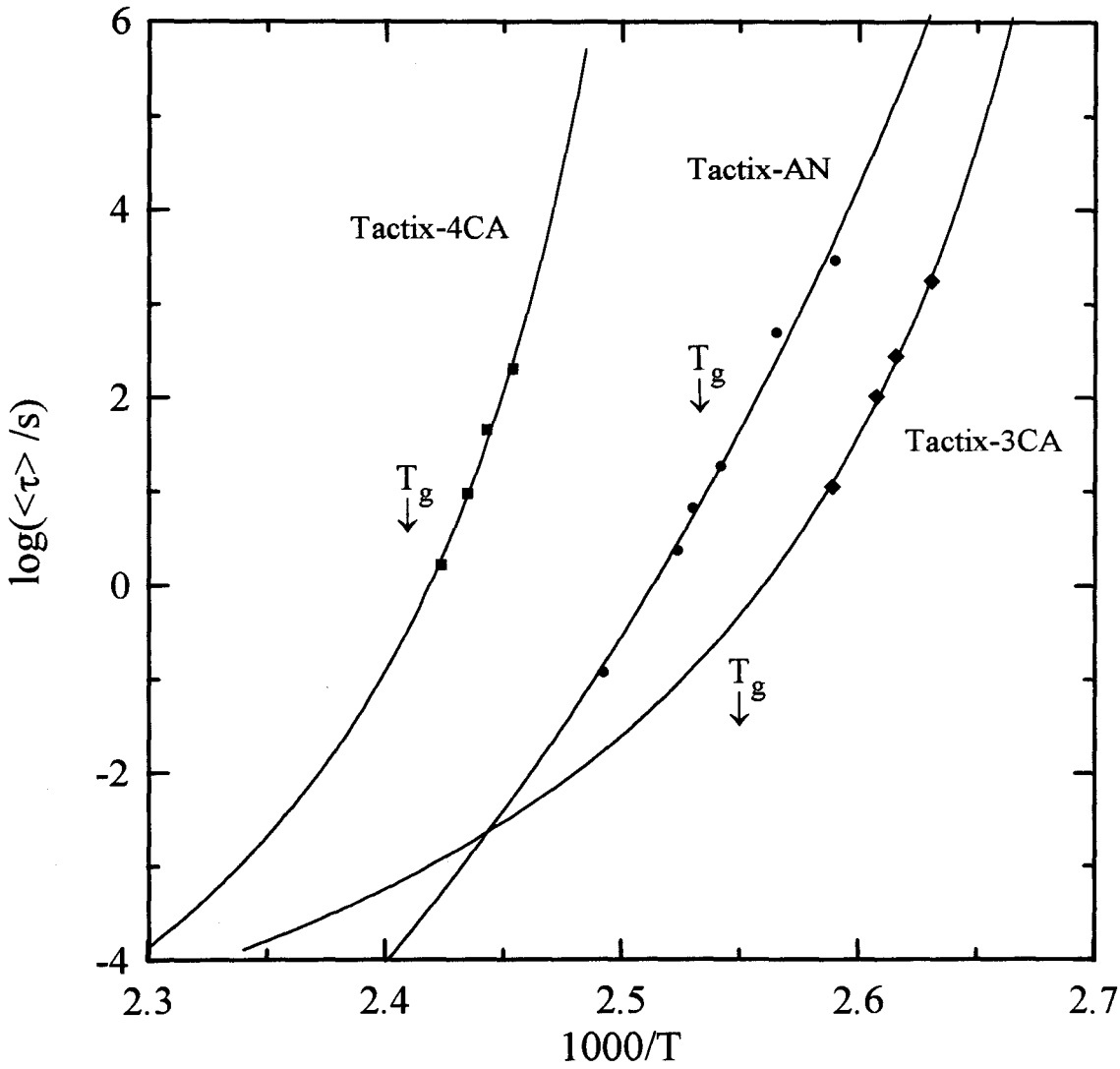

Figure 5.15: log(<τ>) plotted against the reciprocal of temperature for the three polymers.

one requires β, G_U, G_R and τ_o at different temperatures. In Table 5.1, we have already seen that β remains constant with the changing temperature over a range of about 15K, and this β, we assume, remains constant over the entire temperature range of our study. The temperature dependence of G_U and G_R is obtained from an extrapolation of the measured G' against temperature data as in Figures 5.2 to 5.4. The τ_o data were then fitted to the Vogel-Fulcher-Tamman (VTF) empirical equation (McCrum et al. 1967, pp.169-174),

$$<\tau> = A_{VTF} \exp\left(\frac{B_{VTF}}{T - T_o}\right) \qquad \textbf{(5.4)}$$

where A_{VTF}, B_{VTF} and T_o are empirical parameters characteristic of a polymer. According to Equation (5.4), when $T \to T_o$, $<\tau> \to \infty$ and when $T \to \infty$, $<\tau> \to A_{VTF}$. As well, a plot of $\ln(<\tau>)$ against $1/(T-T_o)$ is a straight line with slope B_{VTF} and intercept $\ln A_{VTF}$. In this way, T_o was adjusted until a straight line was obtained using the $<\tau>$ data, thus giving A_{VTF} and B_{VTF}. The three parameters calculated from the $<\tau>$ - temperature data were used to calculate $<\tau>$ over the temperature range 340-450K along with the values of β, G_U and G_R. If the fit to the data in Figures 5.2 to 5.4 was not adequate, then T_o was adjusted further and the calculated values were again compared to the data in Figures 5.2 to 5.4. The three parameters which best fit both the $<\tau>$ and the G', G" data are given in Table 5.2.

Table 5.2: The parameters for the temperature-dependence of the relaxation time and the distribution parameters used for calculating the fixed-frequency G' and G" data at different temperatures.

polymer	$\ln(A_{VTF})$	B_{VTF}	T_o /K	β
Tactix-AN	-47.66	3713.10	320	0.25
Tactix-3CA	-17.36	601.78	356	0.22
Tactix-4CA	-20.71	589.50	385	0.25

The calculated curve for G' and G" are shown in Figures 5.2 to 5.4 as continuous lines, where its agreement with the measured data is evident within the experimental and analytical uncertainties, particularly in the temperature range of the α-relaxation peak in G". The calculated curve has a limited range for the same reasons stated in Section 5.2, namely, the tabulated values (Moynihan et al. 1973, Dishon et al. 1985) available for $\omega\tau_o$ range from $10^{-3} < \omega\tau_o < 10^4$, and for lower values of $\omega\tau_o$, the data calculated for the normalized function does not converge unless more than several hundred terms are included (Moynihan et al. 1973, Dishon et al. 1985, Muzeau et al. 1991). The deviations from the measured values seen at low temperatures indicates a contribution from the β-relaxation process which has been excluded from the calculations. The deviations noted at high temperatures are likely to be due to our assumption of a temperature-independent distribution function and errors in our estimates of $G_U(T)$ and $G_R(T)$.

5.5 The Time-Temperature Superposition

The most widely used procedure for obtaining information of practical interest from the mechanical relaxation and creep data of amorphous polymers is the construction of plots from time-temperature superposition (Ferry 1980, Aklonis et al. 1973, Cavaillé et al. 1987) of the G' and G" data. In this procedure, isothermal spectra of G' and G" measured at different temperatures and over a narrow frequency or time range are superposed by shifting each point of the spectra at a given temperature by the same amount horizontally along the frequency or time axis. From a set of measurements made over a relatively limited frequency or time, the procedure thus leads to a 'master' or reduced curve which covers an apparently much wider frequency or time range. The master curve is then used to extrapolate the behaviour of the material to frequencies and times otherwise unaccessible for an experiment and thus becomes useful in the engineering application of the polymer. The assumption that the time temperature superposition is valid has served also as a basis for mathematical models and phenomenological descriptions in the rheology and the physical ageing effects in the amorphous solids within the temperature range of their viscoelasticity or glass transition (Ferry 1980, Aklonis et al. 1973).

Master curves of G' and G" are thus constructed, over a much wider frequency than used in the experiments, by superposition of spectra obtained at different temperatures. These curves are used in the prediction of long-term mechanical behaviour of polymers in engineering applications. If the mechanisms involved in the viscoelastic

deformation of the polymer have the same temperature dependence, and if the shape of the spectra remains unchanged with changing temperature, the master curve provides an adequate basis for mathematical modelling and for both the short-time and long-time extrapolations of the polymer's mechanical behaviour.

For linear chain polymers the equations deduced by Rouse (1953) had shown that the limiting moduli, G_U and G_R should vary not only with temperature, but also with $T\rho$, the product of the temperature, T, and the density, ρ. Since ρ of polymers, as of most solids, decreases with an increase in the temperature, the product $T\rho$ may remain constant with changing temperature or may decrease if the decrease in ρ overcompensates the increase in T. Ferry had stressed the point that the hypothesis of $T\rho$ remaining constant, which is used in the construction of master curves of mechanical modulus, be examined whenever the master curves are constructed. The isothermal spectra of G' and G" for Tactix-AN in Figures 5.5, for Tactix-3CA in Figure 5.6 and for Tactix-4CA in Figure 5.7, which were obtained over a wide range of temperature, are in a frequency range sufficiently wide to cover the modulus from the rubbery plateau to the glass region, and, therefore, an attempt was made to superpose part of the spectrum on another using only a horizontal displacement. The master curves obtained are shown in Figure 5.16 for G' and Figure 5.17 for G". In each figure, the plots for all three polymers are given. The logarithmic shift factors are: 2.2 for 386.1K, 1.4 for 389.8K, -0.56 for 395.2K, -1.0 for 396.2K, -2.3 for 401.2K, -3.7 for 406.5K, -4.2 for 412.0K and -4.4 for 423.1K, with the reference temperature as 393.4K for Tactix-AN, 1.2 for 380.1, 0.40 for 382.3K, and -1.0

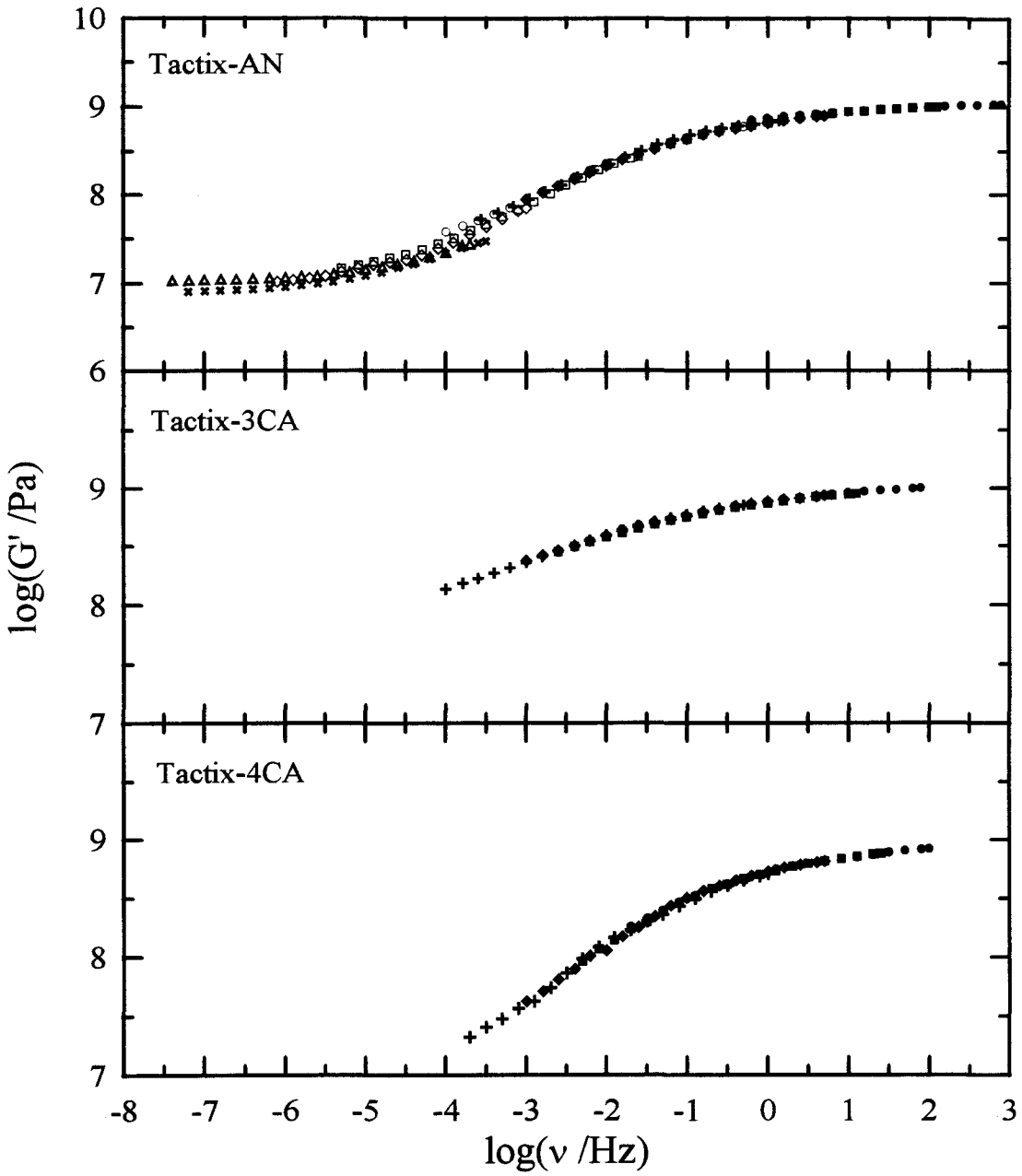

Figure 5.16: The time-temperature superposition of the G' isothermal spectra plotted against frequency for the three polymers.

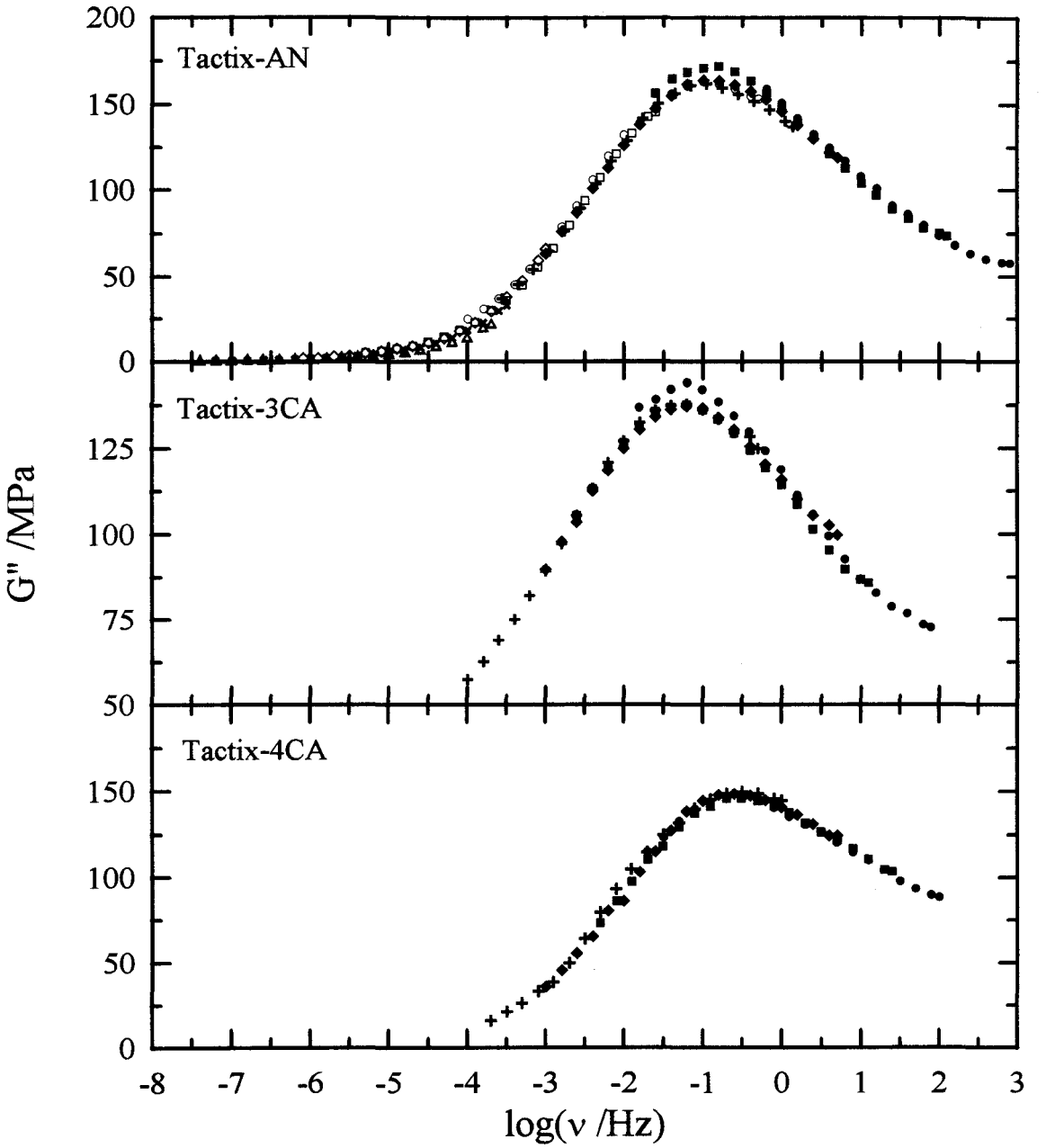

Figure 5.17: The time-temperature superposition of the G" isothermal spectra plotted against frequency for the three polymers.

for 386.2K, with the reference temperature as 382.3K for Tactix-3CA, 1.3 for 407.5K, 0.7 for 409.3K and -0.7 for 412.6K, with the reference temperature as 410.7K for Tactix-4CA.

It is evident from these two figures that the scatter of the G' and G" data in the master curves obtained by superposing the isotherms is considerable, and that this scatter cannot be improved upon by merely a vertical displacement of the spectrum for any of the three polymers. There is also further evidence that the master curve cannot be constructed. This evidence comes from the examination of the magnitudes of the G" peaks in the isothermal spectra of the three polymers given in Figures 5.5 to 5.7.

When both G' and G" data could be shifted along the frequency axis to produce a satisfactory master curve, with the same shift factors, then the ratio G"/G', or tanϕ, should also produce a master curve with the same shift factors. Since tanϕ is plotted on a linear scale -in contrast to the logarithmic scale plots of G'- the tanϕ plots are more sensitive as an indication for the satisfactory or otherwise construction of the master curve than are the G' and G". Figure 5.18 shows the results of the tanϕ master curves, for which it is clear that the height of the tanϕ peak increases and its half-width changes as the temperature is decreased, and that a horizontal shift of frequency alone could not produce a master curve for tanϕ. Although the tanϕ peak for Tactix-3CA is not observed in the limited data available, it is clear that even at frequencies higher than the anticipated tanϕ peak the isothermal spectra do not superpose. Thus in addition to a large vertical displacement of the peak that is necessary to construct a master curve, one needs also to change the half-width and the shape of the spectra measured at different temperatures.

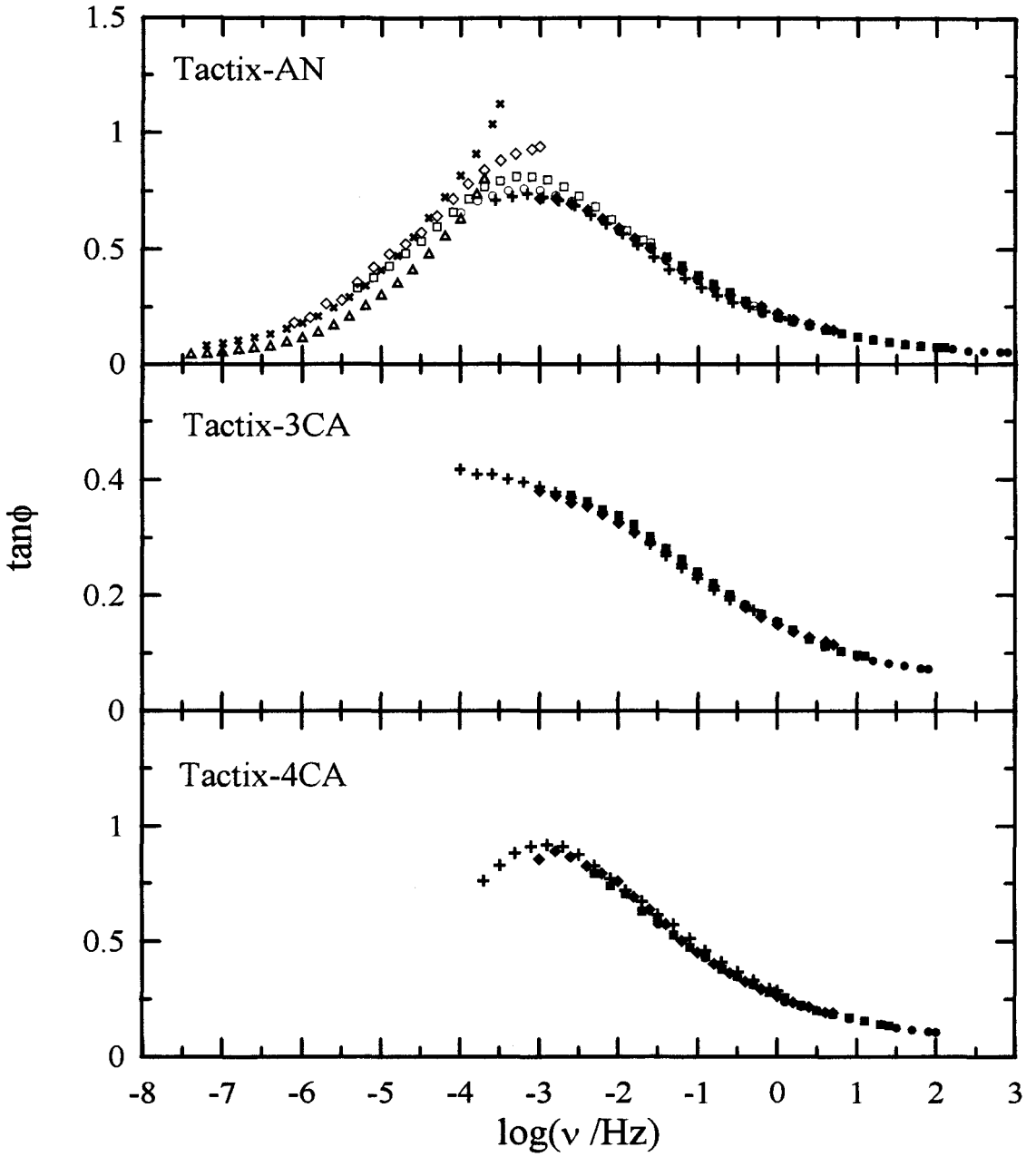

Figure 5.18: The time-temperature superposition of the tanϕ isothermal spectra plotted against frequency for the three polymers.

For the construction of a master curve by a time-temperature superposition procedure, it is also assumed that different energy absorption or relaxation processes in a polymer respond with different sensitivity to the temperature and mechanical stress (Plazek 1985). Thus any departure from the time-temperature superposition would be a reflection of the possibility that the relaxation of different parts of the polymer's chain or network structure respond differently to changes in the temperature. The relative importance of these relaxations will be discussed in Section 5.6, but it should be stressed here that although the master curves of G' and G" in Figures 5.16 and 5.17 seem satisfactory at first sight, the evidence in Figure 5.18 makes it clear that this is an artefact of the logarithmic scale of the plots. Thus, we conclude that it is necessary to analyze the G' and G" data in terms of their ratio, $G''/G' = \tan\phi$, before extrapolations made from the master curves can be seen as reliable. $\tan\phi$ spectra show combined deviations of G' and G" from superposability, and the deviations become more pronounced in $\tan\phi$ because of a relatively larger change in G' rather than G". This is so because the increase in the height of the $\tan\phi$ peak in Figure 5.18 is dominated by a relatively larger decrease in G' and not by the increase in the height of the G" peaks for Tactix-AN and Tactix-3CA in Figures 5.5 and 5.6. Of course, the G" peak height for Tactix-4CA in Figure 5.7 is found to decrease on decreasing the temperature, and for $\tan\phi$ to increase, it is necessary that G' at that frequency decrease more than G".

5.6 Reasons for the Failure of the Time-Temperature Superposition

We first consider how a change in G_U and G_R with changing temperature can affect the superposition. Tanϕ is given by G"/G', or from Equations (5.1) and (5.2), it is given by,

$$\tan\phi = \frac{(G_U - G_R)\omega\tau}{(G_R + G_U\omega^2\tau^2)} \qquad (5.5)$$

when the process involved occurs with a single relaxation time, τ. For most polymers, as for the network polymers here, G_U is in the range of 1GPa and G_R is in the range of 1MPa. Tanϕ shows a peak when $\omega^2\tau^2 = (G_U/G_R)$, and its value is given by $\tan\phi_{max} \approx \frac{1}{2}(G_U/G_R)^{1/2}$. In this simplified consideration, if G_U and G_R do not change with temperature, the value of $\tan\phi_{max}$ also does not change with temperature; only its position on the frequency axis changes because τ changes with the temperature according to $\tau = \tau_o\exp(E/RT)$, where E is the activation energy and τ_o is the limiting value of τ for $T\rightarrow\infty$, or according to the Vogel-Fulcher-Tamman Equation (5.4). So, any deviations from the time-temperature superposition would be due partly to the temperature variations of G_U and G_R as described in the following: In Section 5.1, we have determined the temperature dependence of G_U and G_R by extrapolation of the G' curves. For the three polymers this variation deduced from Figures 5.2 to 5.4 is 0.45% K^{-1}, 0.56% K^{-1} and 0.53% K^{-1} for G_U of Tactix-AN, Tactix-3CA and Tactix-4CA polymers and 0.26% K^{-1}, 0.39% K^{-1} and 0.27% K^{-1} for G_R of the same polymers. For G_U, this change is less than

0.6%, and since G_U is two orders of magnitude greater than G_R for the three polymers, tanϕ is dominated by G_U, according to Equation (5.5), and should therefore vary by at most 0.6% K^{-1} with the temperature. The observed change is 8.5% K^{-1} for Tactix-AN, 2.6% K^{-1} for Tactix-3CA and 1.9% K^{-1} for Tactix-4CA. Thus the deviations from the time-temperature superposition cannot be attributed to changes in G' and G" with changing temperature.

The second reason may be associated with the temperature-dependent and frequency-independent background mechanical loss, G" and tanϕ. This loss is said to arise from anharmonic coupling of the various vibrational modes (Smith 1966, Amrhein and Muller 1968) to the frequency of the alternating stress field. It is also deduced that the background loss, or tanϕ increases with temperature, usually according to T^n, where $1.5 < n < 3$. Muzeau et al. (1991) have discussed the influence of this increase on the spectra of shear relaxation of poly(methyl methacrylate) where they have also suggested various methods for the analysis of the spectrum. For the Tactix-AN polymer, studied over the temperature range 386K to 423K, and assuming a value of 0.001 for the background loss at 386.1K and n=3, the maximum increase in the background tanϕ is from 0.001 to 0.0013 over the temperature range 386K to 423K. This increase is much less than that observed for the tanϕ peak for Tactix-AN shown in Figure 5.18. Similarly, the anticipated increase in the background tanϕ is from 0.001 to 0.0011 for the temperature range 380K to 386K for Tactix-3CA and is 0.001 to 0.0011 for the temperature range 407K to 412K for Tactix-4CA. These are about 1/100 of the observed

increase in the tanϕ peak for the polymers, as shown in Figure 5.18. Therefore, we conclude that the failure of the time-temperature superposition is not due to the presence of the frequency-independent background loss which increases G" and not G' and thus raises tanϕ.

The third consideration is in terms of the influence of secondary or β-relaxations. Referred to as Johari-Goldstein relaxations (Angell 1995, Frick and Richter 1995), these relaxations represent thermally excited molecular configurational or conformational motions which occur in amorphous materials at temperatures below, near and slightly above their T_g (Johari and Goldstein 1970, Johari 1973, 1985, Cavaillé et al. 1987). The relaxations contribute to both the thermodynamic and kinetics of supercooled liquids and polymers (Johari 1980, 1982). Accordingly, an isothermal relaxation spectrum represents the sum of contributions from the main- or α-relaxation and the secondary- or β-relaxation. Since the temperature dependence of the β-relaxation is much weaker than that of the α-relaxation and the strength of the β-relaxation much stronger than that of the α-relaxation (Johari 1973, 1982), a change in the shape of the spectrum occurs on cooling an amorphous solid as the two spectrum separate in the frequency plane. In this study the β-relaxation peak is not observed at temperatures as low as 330K. If this peak has remained unresolved its tanϕ magnitude is less than 0.02, which is the value at 350K, as seen in Figure 5.18. The deviations of the measured spectrum of G" from that of the calculated spectrum at the high-frequency end of the spectrum do indicate contributions from the β-relaxation process, but this contribution becomes negligibly small near the

tanϕ peak in the spectrum. Thus, we conclude that the failure of the time-temperature superposition is not attributable to the contributions from a secondary- or β- relaxation.

It seems sufficiently clear that none of the three effects, namely the change in G_U and G_R, the change in the frequency-independent background loss, and the β-relaxation process, contribute substantially to the changes in the height of the tanϕ peak, and for this reason, the principle of time-temperature superposition does not apply for the three new polymers.

Linear chain polymers and lightly cross-linked polymers, and even some highly cross-linked polymers, for which the time-temperature superposition of the isothermal spectra is used to construct the master curves, are often said to be thermorheologically simple, because their viscoelastic functions do not, by implication, change with temperature. Mikolajczak et al.'s (1987) study of the dynamic mechanical spectra of the network polymer formed from the reaction of diglycidyl ether of bisphenol-A and 4,4'-di-aminodiphenylmethane show a pronounced departure from the thermorheological simplicity in the same manner as given in Figures 5.4 to 5.7 here. Since network polymers, and even cross-linked linear chain polymers, do not show a terminal zone of viscous flow, it seems that the difference between the assumed temperature dependence of the viscoelastic and viscosity behaviour may not be the reason for the thermorheologically complex behaviour observed here.

CHAPTER VI

CONCLUSIONS

Cross-linked network polymerization of three different substances was studied by measuring the dielectric spectroscopy as the reaction progressed towards completion. The three, new, polymers ultimately formed were also studied by dynamic mechanical spectrometry. Differential scanning calorimetry was used to monitor the heat evolved from the isothermal polymerization, from which the number of covalent bonds (N(t)) formed at any instant of reaction was determined. This enabled us to examine the reaction kinetics as well as to relate the time-variant properties, such as the average relaxation time and the gelation time, to the number of bonds formed.

The calorimetric studies showed that the extent of reaction increased with time in a manner different from that given by the empirical equations used in the literature. A mathematical procedure which directly reveals this disagreement has been used, and it is concluded that the failure of the empirical equation for describing the reaction kinetics is due to the difference between the reaction kinetics of the primary and secondary amine. The latter forms after one proton of the $-NH_2$ group of the amine has been exchanged for a covalent bond.

The activation energies for each of the polymerization reactions are in the range 88.8 to 116.7kJ/mol.

The dielectric permittivity and loss measured at different instances of reaction under isothermal conditions could thus be related to the number of bonds formed at that instant. The permittivity and loss spectra showed an asymmetric distribution of relaxation which remained constant as the size of the macromolecule grew, or N(t) increased. The equilibrium and high-frequency permittivities decreased as N(t) increased. The permittivity decreased in an almost linear manner with an increase in N(t). Both the characteristic and average relaxation times of the empirical stretched exponential function increased progressively more rapidly as N(t) increased at a constant temperature. An unimodal relaxation spectrum at the temperature of polymerization evolved into a bimodal relaxation spectra as N(t) approached its maximum value, so that the total contribution to the dielectric permittivity was from two processes, namely the α-, or main-, and the β-relaxations.

Dielectric data simulated from various parameters and then analyzed showed that the more convenient method of single-ac-frequency monitoring of the polymerization process yielded the same parameters as the more tedious procedure of measuring the dielectric spectra at fixed values of N(t). The analysis also showed that the time-dependence of the relaxation time can be obtained from a few fixed frequency measurements during the course of the polymerization reaction and that the various parameters obtained by this procedure agreed well with the original parameters used to generate the simulated data. Measurements on the three substances studied here confirmed the essential correctness of the procedure used with the single-frequency measurements.

The extent of reaction at the gelation time was calculated from the irreversible decrease in the dc conductivity during the polymerization of the mixtures. The extent of reaction at the gelation time calculated from the power-law equation for dc conductivity was 50% less than that obtained from the Flory-Stockmayer theory, but the extent of gelation calculated from the singularity equation for conductivity agreed well with the theory. The deviation from the Flory-Stockmayer theory are attributed to: (i) the unrealistic assumptions that Flory made to simplify the statistics, (ii) the different probabilities of reaction between unreacted groups and unreacted groups of reacted molecules, such as unreacted functional groups at the free ends of polymer chains, (iii) the formation of intramolecular loops which do not contribute to the network structure but increase the extent of reaction required for gelation, and (iv) the long cross-links that exist between the Tactix-742 molecules linked by the anilines as compared to epoxies cross-linked with diamines. As the number of bonds increased, the high-frequency, or low-temperature, β-relaxation process emerged, and was observed for both the time-invariant and time-variant dielectric data.

Thus, the number of bonds formed, N(t), during the reaction of the monomeric liquid to the ultimately polymerized solid is a fundamental measure of the dielectric state of the system compared to the duration of the reaction itself. The experiments also suggest that a given dielectric state can be reached by increasing N(t), as in this study, or by decreasing N(t) from a state of complete reaction, by irradiation from high-energy x-rays, γ-rays or uv-rays, or by changing the temperature of the monomeric liquid. Only the last of these can be carried out reversibly, the other two remain irreversible, isothermal processes. Comparisons between systems can be made more appropriately when they contain equal number of bonds during polymerization,

since equilibrium properties are independent of the time required to reach that state.

The unrelaxed modulus, G_U, for the three new polymers, measured from dynamic mechanical spectrometry, decreased linearly with increasing temperature, which was attributed to the decrease in the relaxed modulus, G_R, of the β-relaxation process. G_R of the main-relaxation increased linearly with increasing temperature, which is caused by the increase of the configurational entropy of the polymer network segments with temperature, as discussed in the theories for rubber elasticity. The time-temperature superposition of the mechanical spectra was found to be inadequate for all the three polymers studied. Several reasons for this lack of time-temperature superposition were discussed, namely, (i) the change of G_U and G_R with temperature, which causes differences between the strength of each of the isothermal spectra measured, (ii) the presence of a temperature-dependent, frequency-independent background mechanical loss which changes the magnitude of each of the mechanical loss peaks, and (iii) the influence of a secondary-, or Johari-Goldstein relaxation process which alters the shape at the high-frequency end of the main-relaxation spectrum. As none of the three reasons discussed could account for the failure of the time-temperature superposition, it was concluded that the principle of time-temperature superposition did not apply to the three polymers because their viscoelastic functions for each segment change with temperature in different manners. The three new polymers produced have a mechanical loss peak at room temperature which is attributable to the β-relaxation process, whose magnitude is greater than that of polycarbonates. This implies that the polymers produced here can absorb more energy at room temperature than the polycarbonates prior to fracture.

REFERENCES

Adolf, D., Martin, J.E. and Wilcoxon, J.P. (1990), *Macromolecules*, **23**, 527.

Aklonis, J.J., MacKnight, W.J. and Shen. M. (1973), Introduction to Polymer Viscoelasticity, John Wiley & Sons, Inc., New York.

Alig, I., Lellinger, D. and Johari, G.P. (1992), *J. Polym. Sci. B. Polym. Phys.*, **30**, 791.

Alig, I. and Johari, G.P. (1993), *J. Polym. Sci. B. Polym. Phys.*, **31**, 299.

Alig, I., Nanke, K. and Johari, G.P. (1993), *J. Polym. Sci. B. Polym. Phys.*, **31**, 299.

Amrhein, E.M. and Muller, F.H. (1968), *J. Am. Chem. Soc.*, **90**, 3146.

Angell, C.A. (1995), *Science*, **267**, 1928.

Aronhime, M.T. and Gillham, J.K. (1986), *J. Appl. Polym. Sci.*, **78**, 83.

Arridge, R.G.C. (1985), An Introduction to Polymer Mechanics, Taylor and Francis, London.

Aukward, J.A., Warfield, R.W. and Petree, M.C. (1958), *J. Polym. Sci.*, **27**, 199.

Barret, K.E.J. (1967), *J. Appl. Polym. Sci.*, **11**, 1617.

Barton, J.M. (1985), *Adv. Polym. Sci.*, **72**, 111.

Bauwens-Crowet, C. and Bauwens, J.C. (1979), *J. Mater. Sci.*, **14**, 1817.

Benoit, H. (1976), *J. Macromol. Sci. Phys.*, **B12**, 27.

Carrozzino, S. Levita, G., Rolla, P. and Tombari, E. (1990), *Polym. Eng. Sci.*, **30**, 366.

Cassettari, M., Salvetti, G., Tombari, E. and Johari, G.P. (1993), *J. Mol. Liquids*, **56**, 141.

Cassettari, M., Salvetti, G., Tombari, E., Veronsi, S. and Johari, G.P. (1993), *J. Polym.*

Sci. B Polym. Phys., **31**, 199.
Cavaillé, J.Y. (1987), Thesis Docteur d'Etat es Sciences Physique.

Cavaillé, J.Y., Jourdan, C., Perez, J., Monnerie, L. and Johari, G.P. (1987), *J. Polym. Sci. B. Polym. Phys.*, **25**, 1235.

Cavaillé, J.Y., Johari, G.P. and Mikolajczak, G.(1987), *Polymer*, **28**, 1841.

Charlesworth, S. (1980), *J. Polym. Sci. Polym. Chem. Ed.*, **18**, 1621.

Charlesworth, J.M. (1988a), *Polym. Eng. Sci.*, **28**, 214.

Charlesworth, J.M. (1988b), *Polym. Eng. Sci.*, **28**, 221.

Choy, I.C. and Plazek, D.J. (1986), *J. Polym. Sci. B. Polym. Phys.*, **24**, 1303.

Cifferri, A. (1961), *J. Polym. Sci.*, **54**, 149.

Cole, K.S. and Cole, R.H. (1941), *J. Chem. Phys.*, **9**, 341.

Cole, R.H. and Tombari, E. (1991), *J. Noncryst. Solids*, **131-133**, 969.

Curie, P.J. (1888), *Ann. Chim. Phys.*, **17**, 385.

Davidson, D.W. and Cole, R.H. (1950), *J. Chem. Phys.*, **18**, 1417.

Davidson, D.W. and Cole, R.H. (1951), *J. Chem. Phys.*, **19**, 1484.

Davies, C.W. (1962), Ion Association , Butterworths, London.

Debye, P. (1929), Polar Molecules , Chem. Catalog., New York.

DeGennes, P.G. (1979), Scaling Concepts in Polymer Physics, Cornell University Press, Ithaca, New York.

Delmonte, J. (1959), *J. Appl. Polm. Sci.*, **2**, 108.

DiMarzio, E.A. (1964), *J. Res. N.B.S.*, **68A**, 611.

Dishon, M., Weiss, G.H. and Bendler, J.T. (1985), *J. Res. N.B.S.*, **90**, 27.

Djabourov, M. (1988), *Contemp. Phys.*, **29**, 273.

Douglas, R.W. (1963), *Proc. 4th Int. Conf. on Rheology, Providence*, R.I., PartI, eds. E.H. Lee and A.L. Copley, Wiley, New York.

Douglas, R.W. (1966), *Br. J. Appl. Phys.*, **17**, 435.

Dušek, K. (1985), *Adv. Polym. Sci.*, **78**, 1.

Ellis, B. (ed.) (1993), Chemistry and Technology of Epoxy, Chapman and Hall, London.

Enns, J.B. and Gillham, J.K. (1983), *J. Appl. Polym. Sci.*, **28**, 2567.

Ferrari, C., Salvetti, G., Tombari, E. and Johari, G.P. (1995), accepted for Publication in *Phys. Rev. Letters*.

Ferry, J.D. (1980), Viscoelastic Properties of Polymers, Wiley, New York.

Flammersheim, H.J., Harold, H.H., Bellsted, K and Klee, J. (1983), *Makromol. Chem.*, **184**, 113.

Flory, P.J. (1941), *J. Amer. Chem. Soc.*, **63**, 3083, 3091, 3096.

Flory, P.J. (1942), *J. Chem. Phys.*, **46**, 132.

Flory, P.J. (1953), Principles of Polymer Chemistry , Cornell University Press, New York.

Foun, C.C., Moroni, A., Pearce, E.M. and Mijovic, J. (1984), *J. Polym. Mater. Sci. Eng.*, **51**, 411.

Fox, T.G. and Loshaek, S. (1955), *J. Polym. Sci.*, **15**, 371.

Frick, B. and Richter, D. (1995), *Science*, **267**, 1940.

Fröhlich, H. (1949), Theory of Dielectrics , Oxford University Press, Oxford.

Fuoss, R.M. and Kirkwood, J.G. (1941), *J. Amer. Chem. Soc.*, **63**, 369.

Fuoss, R.M. (1958), *J. Am. Chem. Soc.*, **80**, 5059.

Gibbs, J.H. (1960), Modern Aspects of Vitreous State vol.2 , ed. J.D. Mackenzie,

Butterworths, London, p.152.

Glover, D.J., Duffy, J.V. and Hartmann, B. (1988), *J. Polym. Sci. A. Polym. Chem.*, **26**, 79.

Graessley, W.W. (1974) *Adv. Polym. Sci.*, **16**, 1.

Grenier-Loustalot, M.F. and Grenier, P. (1987), Crosslinked Epoxies , eds. B. Sedlacek and J. Kahovec, Walter de Gruyter, Berlin.

Grenier-Loustalot, M.F., Orozco, L. and Grenier, P. (1987), *Makromol. Chem.*, **188**, 2559.

Grenier-Loustalot, M.F., Grenier, P., Horny, P. and Chenard, J.Y. (1988), *Br. Polym. J.*, **20**, 463.

G'See, C.G., El Bari, H., Perez, J., Cavaillé, J.Y. and Johari, G.P. (1989), *Mater. Sci. and Eng.*, **A110**, 223.

Hallbrucker, A. and Johari, G.P. (1990), *Phys. Chem. Glasses*, **30**, 211.

Hamon, G.V. (1952), *Proc. Inst. Elec. Engrs.*, **99**, Pt.IV, 27.

Haran, E.N., Gringras, H. and Katz, D., (1963), *J. Appl. Polym. Sci.*, **9**, 3505.

Havriliak, S. and Negami, S. (1966) *J. Polym. Sci. C Polym. Symp.*, **14**, 99.

Hopkinson, J. (1877), *Phil. Trans. Roy. Soc.*, **167**, 599.

Horie, K., Hiura, H., Sawada, M., Mita, I and Kambe, H. (1970), *J. Polym. Sci. A-1*, **8**, 1357.

Johari, G.P. and Goldstein, M. (1970), *J. Chem. Phys.*, **53**, 2372.

Johari, G.P. (1973), *J. Chem. Phys.*, **58**, 17.

Johari, G.P. (1982), *J. Chem. Phys.*, **77**, 4619.

Johari, G.P. (1985), *J. Chim. Phys.*, **58**, 17.

Johari, G.P. and Mangion, M.B.M. (1991), *J. Noncryst. Solids*, **131-133**, 921.

Johari, G.P. (1993a), Chemistry and Technology of Epoxy Resins, ed. B. Ellis, Chapman and Hall, London, ch.6 and references therein.

Johari, G.P. (1993b), *J. Mol. Liquids*, **56**, 153.

Johari, G.P. (1994a), Disorder Effects on Relaxation Processes, eds. R. Richert and A. Blumen, Springer Verlag, Berlin, p.627.

Johari, G.P. (1994b), *J. Chem. Soc. Faraday Trans.*, **90**, 883.

Johari, G.P., Wasylyshyn, D.A. and Jain, S.K. (1994), *J. Chem. Soc. Faraday Trans.*, **90**, 2065.

Johari, G.P. and Pascheto, W. (1995), *J. Chem. Soc. Faraday Trans.*, **91**, 343.

Johnson, J.F. and Cole, R.H. (1951), *J. Am. Chem. Soc.*, **73**, 4536.

Katz, D. and Tobolsky, V. (1962), *Polymer*, **4**, 417.

Kienle, R.H. and Race, H.H. (1934), *Trans. Electrochem. Soc.*, **65**, 87.

Kim, D.H. and Kim, S.H. (1987), *Polym. Bull.*, **18**, 533.

Kohlrausch, R. (1847), *Ann. Phys. (Leipzig)*, **91**, 179.

Lindsey, C.P. and Patterson, G.D. (1980), *J. Chem. Phys.*, **73**, 3348.

MacDonald, J.R. (ed.) (1987), Impedance Spectroscopy-Empasizing Solid Materials and Systems , Wiley-InterScience, New York, p.90-95.

Majumdar, C.K. (1971), *Sol. State Comm.*, **9**, 1087.

Mangion, M.B.M. and Johari, G.P. (1990a), *Macromolecules*, **23**, 3687.

Mangion, M.B.M. and Johari, G.P. (1990b), *J. Polym. Sci. B. Polym. Phys.*, **28**, 1621.

Mangion, M.B.M. and Johari, G.P. (1991a), *Polymer*, **32**, 2747.

Mangion, M.B.M., Vandelwal, J.J., Walton, D. and Johari, G.P. (1991), *J. Polym. Sci. B. Polym. Phys.*, **29**, 723.

Mangion, M.B.M. and Johari, G.P. (1991b), *J. Polym. Sci. B. Polym. Phys.*, **29**, 1117.

Mangion, M.B.M. and Johari, G.P. (1991c), *J. Polym. Sci. B. Polym. Phys.*, **29**, 1127.

Manning, M.F. and Bell, M.E. (1940), *Rev. Mod. Phys.*, **12**, 215.

Maroni, A., Mijovic, J., Pearce, E.M. and Foun, C.M. (1986), *J. Appl. Polym. Sci.*, **32**, 3761.

May, C.A. (ed.) (1988), Epoxy Resins: Chemistry and Technology , Marcel Dekker, New York.

McMrum, N.G., Read, B.E. and Williams, G. (1967), "Anelastic and Dielectric Effects in Polymeric Solids", Dover Publications, Inc., New York.

Mijovic, J., Kim, J. and Slaby, J. (1984), *J. Appl. Polym. Sci.*, **29**, 1449.

Mijovic, J. (1986), *J. Appl. Polym. Sci.*, **31**, 1177.

Mikolajczak, G., Cavaillé, J.Y. and Johari, G.P. (1987), *Polymer*, **28**, 2023.

Moynihan, C.T., Boeach, L.P. and Labarge, N.L. (1973), *Phys. Chem. Glasses*, **14**, 122.

Murayama, T. and Bell, J.P. (1970), *J. Polymer Sci. A-2*, **8**, 437.

Muzeau, E., Perez, J. and Johari, G.P. (1991), *Macromolecules*, **24**, 4713.

Neilsen, L.E. (1974), Mechanical Properties of Polymers and Composites , vol.1, New York, Marcel Dekker.

Parthun, M.G. (1991), Master's Thesis, McMaster University, Canada,

Parthun, M.G. and Johari, G.P. (1992a), *Macromolecules*, **25**, 3149.

Parthun, M.G. and Johari, G.P. (1992b), *Macromolecules*, **25**, 3254.

Parthun, M.G. and Johari, G.P. (1992c), *J. Polym. Sci., B. Polym. Phys.*, **30**, 665

Parthun, M.G. and Johari, G.P. (1995a), accepted for publication in *J. Chem Phys.*

Parthun, M.G. and Johari, G.P. (1995b), accepted for publication in *J. Chem. Phys.*

Parthun, M.G., Wasylyshyn, D.A. and Johari, G.P. (1995), accepted for publication in *J. Mol. Liquids.*

Pascheto, W. (1991), Master's Thesis, McMaster University, Canada.

Plazek, D.J. and Choy, I.C. (1989), *J. Polym. Sci. B. Polym. Phys.*, **27**, 307.

Plazek, D.J. and Frund, Z.N., Jr. (1990), *J. Polym. Sci. B. Polym. Phys.*, **28**, 431.

Prime, R.B. (1973), *Polym. Eng. Sci.*, **13**, 365.

Riccardi, C.C., Adabbo, H.E. and Williams, R.J.J. (1984), *J. Appl. Polym. Sci.*, **29**, 2481.

Riccardi, C.C. and Williams, R.J.J. (1986), *J. Appl. Polym. Sci.*, **32**, 3445.

Rouse, P.E. (1953), *J. Chem. Phys.*, **21**, 1272.

Ryan, C.M. and Dutta, A. (1979), *Polymer*, **20**, 203.

Scherer, G.W. (1986), Relaxation in Glass and Composites , Wiley, New York.

Sidebottom, D.L. and Johari, G.P. (1990), *Chemical Physics*, **147**, 205.

Smith, G.C. (1966), *Kolloid Z*, **212**, 15.

Souror, S and Kamal, M.R. (1976), *Thermochim. Acta*, **14**, 41.

Spacek, V., Pouchly, J. and Biros, J. (1987), *J. Eur. Polym. J.*, **23**, 377.

Stauffer, D., Coniglio, A., and Adam, M. (1982), *Adv. Polym. Sci.*, **44**, 105.

Stockmayer, W.H. (1943), *J. Chem. Phys.* **11**, 45.

Tombari, E. and Johari, G.P. (1992), *J. Chem. Phys.*, **97**, 6677.

Tombari, E. and Johari, G.P. (1993), *J. Chem. Soc. Faraday Trans.*, **89**, 3477.

Treloar, L.R.G. (1958), The Physics of Rubber Elasicity , Oxford University Press, Oxford.

Wagner, K.W. (1913), *Ann. der Physik*, **40**, 817.

Wasserman, S. and Johari, G.P. (1993), *J. Appl. Polym. Sci.* **48**, 905.

Wasserman, S. and Johari, G.P. (1994), *J. Appl. Polym. Sci.* **53**, 331.

Wasylyshyn, D.A., Parthun, M.G. and Johari, G.P. (1995), accepted for publication in *J. Mol. Liquids.*

Whitehead, J.B. and Banos, A. (1932), *Trans. AIEEE*, **51**, 392.

Williams, G. and Watts, D.C. (1970), *Trans. Faraday Soc.*, **66**, 80.

Wisanrakkit, G., Gillham, J.K. and Enns, J.B. (1987), *Polym. Mater. Sci. Eng.*, **57**, 87.

Wisanrakkit, G. and Gillham, J.K. (1990), *J. Appl. Polym. Sci.*, **41**, 2885.

Yeager, W.A. (1936), *Physica*, **7**, 434.

Yee, A.F. and Smith, S.A. (1981), *Macromolecules*, **14**, 54.